Desiccant Cooling with Solar Energy

Gerrit Höfker

A thesis submitted in partial fulfilment
of the requirements of De Montfort University
for the degree of Doctor of Philosophy

December 2001

Institute of Energy and Sustainable Development
De Montfort University Leicester

Department of Building Physics
Fachhochschule Stuttgart – Hochschule für Technik

Abstract

Desiccant cooling systems combine sorptive dehumidification, heat recovery, evaporation and heating to create a cooling process which can offer energy savings compared to conventional air conditioning systems. Waste heat or solar energy can be used for the required regeneration of the sorbens in the dehumidifier, leading to further energy savings.

A desiccant cooling plant with solar air collectors has been installed and parametric studies, particularly of the dehumidifier, have been undertaken. These show that it is possible to reduce the regeneration air flow with only a small reduction in the dehumidification efficiency, enabling desiccant cooling systems to run with high COPs. The results of the measurements were used as input parameters to a new dynamic simulation program, which was specifically developed for the purpose of assessing the potential for desiccant cooling under different climatic conditions. The program predicts the hourly performance of a desiccant cooling system and the associated building. With this new simulation tool it is possible to optimise desiccant cooling systems with solar components.

The simulations were executed for a desiccant cooling system with solar air collectors connected to a test building and using climatic data of Stuttgart, Phoenix(Arizona), Seville and Djakarta. The use of solar air collectors signifies that no energy storage is available either in the desiccant cooling system or in the solar system. Thermal inertia is only provided by the mass of the building. The simulations show that it is almost possible in climates like Stuttgart to ensure thermal comfort with a desiccant cooling system driven only by solar air collectors nearly all the time. In the investigated climates of Seville, Phoenix and Djakarta additional cooling and dehumidification are required. For the requirements of deep dehumidification in tropical climates, a double stage desiccant cooling cycle with a second rotating dehumidifier and a second heat recovery device is suggested.

The mean COP of desiccant cooling systems increases by using a variable regeneration air flow. When using solar energy, the control of desiccant cooling systems must be adapted to solar operation to achieve high solar fractions.

Acknowledgements

This research was carried out at the Institute of Energy and Sustainable Development at De Montfort University Leicester working in collaboration with the Department of Building Physics at the Hochschule für Technik Stuttgart. This work could not have been completed without the support and help of many people in both institutions.

I am grateful to Prof. Dr. Ursula Eicker, Prof. Dr. Kevin J. Lomas, Prof. Dr. Vic Hanby and Herbert Eppel for their encouragement and enthusiastic support and for their critical review of the thesis. Furthermore, I am grateful to the members of the Department of Building Physics for their assistance. Finally, I would like to thank my familiy who always stand by my side.

I declare that the content of the submission represents my own work. The contents of the work have not been submitted for any other academic or professional award. I acknowledge that the thesis is submitted according to the conditions set down in the regulations. Furthermore, I declare that the work was carried out as part of the course for which I was registered. I draw attention to any relevant considerations of rights of third parties or of the security which might merit a restriction on loan or access.

Contents

1 Introduction **18**

2 State–of–the–Art Cooling Technologies **23**

2.1 Passive Cooling 23

2.2 Compressor Cooling 24

2.3 Thermomechanical Cooling 26

2.4 Absorption Cooling 27

2.5 Adsorption Cooling 32

2.6 Desiccant Cooling 34

2.7 Application of Solar Energy in Cooling Processes 40

2.8 Comparison of Cooling Technologies 42

3 Theory of Sorption in Desiccant Cooling Systems **44**

3.1 Theory of Adsorption and Desorption 44

3.2 Theory of Rotating Dehumidifiers 52

4 Measurements at Desiccant Cooling Test Plant **59**

4.1 Desiccant Cooling Test Plant with Solar Air Collectors 59

4.2 Measurement Results 64

4.3 Analysis of Measurement Results 66

5 Modelling of Desiccant Cooling Systems, Solar Collectors and Buildings 80

5.1 Desiccant Cooling System 81

5.2 Solar Collectors 86

5.3 Building 93

5.4 Simulation Basic Model 100

5.5 Simulation Case Studies 102

5.6 Discussion of Simulation Results 117

6 Suggestions for the Design of Desiccant Cooling Systems 128

6.1 General Suggestions for Desiccant Cooling with Solar Energy 128

6.2 Control of Desiccant Cooling Systems with Solar Energy 130

6.3 Desiccant Cooling in Different Climates 133

6.4 Current Economical Aspects of Desiccant Cooling Systems 137

7 Conclusions 140

A 151

List of Tables

2.1 Comparison of different cooling technologies 43

4.1 Components of the desiccant cooling test plant 61

4.2 Sensors and monitoring equipment of the desiccant cooling test plant . . 61

5.1 Transmission and absorption of clear single glazing 97

5.2 Transmission and absorption of clear double glazing 97

5.3 Transmission and absorption of low–ϵ double glazing 97

5.4 BESTEST cases used for validity checks of ESIMA and for simulations . 98

5.5 BESTEST constructions used for simulations 98

5.6 Description of the climates used in the simulations 101

5.7 Control of the desiccant cooling system in the simulations 103

5.8 Simulation results of case study 1 (heavyweight building, hygienic ventilation during occupation time) 107

5.9 Simulation results of case study 2 (heavyweight building, hygienic ventilation during occupation time, enhanced night ventilation with 4 air changes per hour) 108

5.10 Simulation results of case study 3 (heavyweight building, ventilation with maximum 4 air changes per hour, night ventilation) 109

5.11 Simulation results of case study 4 (heavyweight building, hygienic ventilation during occupation time, half collector area as in case study 1) 110

5.12 Simulation results of case study 5 (lightweight building, hygienic ventilation during occupation time) 111

5.13 Simulation results of case study 6 (heavyweight building, hygienic ventilation during occupation time, DCS with ambient air regeneration) 112

5.14 Simulation results of case study 7 (heavyweight building, hygienic ventilation during occupation time, controlled to reach an inlet temperature close to 17 °C) 113

5.15 Simulation results of case study 8 (heavyweight building, ventilation with maximum 4 air changes per hour, night ventilation, regeneration air flow controlled) 114

5.16 Simulation results of case study 9 and 10 (double stage desiccant cooling system) 116

6.1 Examples of pressure losses in different air conditioning systems 139

List of Figures

1.1 Temperature requirements according to DIN 1946 21

1.2 Thermal comfort field according to ASHRAE 21

1.3 Energy demand in office buildings 22

1.4 Cooling loads in office buildings 22

2.1 Cooling and dehumidification process of a surface cooler 26

2.2 Compression chiller and single–effect absorption chiller 30

2.3 Double–effect and single–effect/double–lift absorption chiller 31

2.4 Schematic of an adsorption chiller 33

2.5 Example of air conditions in a desiccant cooling ventilation cycle 38

2.6 Example of air conditions in a desiccant cooling recirculation cycle 39

2.7 Solar cooling systems 40

3.1 Chemical sorption on the surface of silica gel 45

3.2 Sorption isotherms of silica gel 49

3.3 Bond enthalpy and evaporation enthalpy 50

3.4 Adsorption after a change of concentration 51

3.5 Schematic of a rotating dehumidifier 52

3.6 Determination of the maximal possible ΔX in a psychrometric chart . . 54

3.7 Relationships between the heat transfer coefficient h_c, the Reynolds number Re, the Nusselt number Nu and the air velocity 58

4.1 Control and monitoring equipment of the test plant 62

4.2 Concentric adapters used in the test plant for precise air flow measurements 62

4.3 Sketch and photograph of the exhibition room 63

4.4 Photograph of the building with the test plant and the exhibition room . 64

4.5 Measured ΔX in a DCS ventilation cycle 69

4.6 Measured ΔX in a DCS ventilation cycle (ambient air regeneration) . . . 70

4.7 Comparison of calculated ΔX using mean η_{sorp} and measurements 71

4.8 Comparison of calculated ΔX using mean η_{sorp} and measurements (ambient air regeneration) 72

4.9 Calculated η_{sorp} of the measured ΔX 73

4.10 Calculated η_{sorp} of the measured ΔX (ambient air regeneration) 74

4.11 Calculated course of the COP in a DCS ventilation cycle 75

4.12 Calculated COP from the test plant measurements 76

4.13 Calculated COP from the test plant measurements (ambient air regeneration) 77

4.14 Further measurement results of the dehumidifier 78

4.15 Measurement results of test plant components 79

5.1 Flow chart of the calculation procedure for a DCS ventilation cycle with solar air collectors 85

5.2 Schematic of an air collector 91

5.3 Efficiencies of different collectors 92

5.4 Efficiencies of different air collectors 92

5.5 BESTEST building 96

5.6 Results of ESIMA compared with BESTEST results 99

5.7 Psychrometric chart of Seville's climate 104

5.8 Psychrometric chart of Stuttgart's climate 104

5.9 Psychrometric chart of Phoenix' climate 105

5.10 Psychrometric chart of Djakarta's climate 105

5.11 Desiccant cooling cycle used for the simulations 106

5.12 Desiccant cooling cycle (ambient air regeneration) used for the simulations 106

5.13 Double stage ventilation cycle used for the simulations 106

5.14 Double stage desiccant cooling ventilation cycle with solar air collectors . 115

6.1 Control of rotation fluctuating regeneration temperatures 132

6.2 Combination of a desiccant cooling system with a compression chiller without using solar energy 135

6.3 Combination of a desiccant cooling system with a compression chiller without using solar energy 135

6.4 Solar assisted desiccant cooling system with a compression chiller 136

6.5 Solar assisted desiccant cooling system with a compression chiller 136

A.1 Seville: Simulation results of case study 1 (heavyweight building, hygienic ventilation during occupation time) 152

A.2 Seville: Simulation results of case study 3 (heavyweight building, ventilation with maximum 4 air changes per hour, night ventilation) 153

A.3 Seville: Simulation results of case study 7 (heavyweight building, hygienic ventilation during occupation time, controlled to reach an inlet temperature close to 17 °C) 154

A.4 Seville: Simulation results of case study 8 (heavyweight building, ventilation with maximum 4 air changes per hour, night ventilation, regeneration air flow controlled) 155

A.5 Seville: Simulation results of case study 8 (heavyweight building, ventilation with maximum 4 air changes per hour, night ventilation, regeneration air flow controlled) 156

A.6 Stuttgart: Simulation results of case study 1 (heavyweight building, hygienic ventilation during occupation time) 157

A.7 Stuttgart: Simulation results of case study 3 (heavyweight building, ventilation with maximum 4 air changes per hour, night ventilation) 158

A.8 Stuttgart: Simulation results of case study 7 (heavyweight building, hygienic ventilation during occupation time, controlled to reach an inlet temperature close to 17 °C) 159

A.9 Stuttgart: Simulation results of case study 8 (heavyweight building, ventilation with maximum 4 air changes per hour, night ventilation, regeneration air flow controlled) 160

A.10 Stuttgart: Simulation results of case study 8 (heavyweight building, ventilation with maximum 4 air changes per hour, night ventilation, regeneration air flow controlled) 161

A.11 Phoenix: Simulation results of case study 1 (heavyweight building, hygienic ventilation during occupation time) 162

A.12 Phoenix: Simulation results of case study 3 (heavyweight building, ventilation with maximum 4 air changes per hour, night ventilation) 163

A.13 Phoenix: Simulation results of case study 7 (heavyweight building, hygienic ventilation during occupation time, controlled to reach an inlet temperature close to 17 °C) 164

A.14 Phoenix: Simulation results of case study 8 (heavyweight building, ventilation with maximum 4 air changes per hour, night ventilation, regeneration air flow controlled) 165

A.15 Phoenix: Simulation results of case study 8 (heavyweight building, ventilation with maximum 4 air changes per hour, night ventilation, regeneration air flow controlled) 166

Nomenclature

a	diffusivity	m^2/s
A	area	m^2
A_{coll}	collector area	m^2
Bi^*	special Biot number	–
c	coefficient in Langmuirs equation	–
c_{p}	heat capacity of fluid	$kJ/(kgK)$
C_{bypass}	content of flow through bypass	–
COP	coefficient of performance	–
D	diffusion coefficient	m^2/s
D	diameter	m
D_{i}	interior diameter	m
d_{h}	hydraulic diameter	m
F'	collector efficiency factor	–
F''	collector flow factor	–
F_{fin}	standard fin efficiency	–
F_{R}	heat removal factor	–
G	irradiation	kWh/m^2
h	heat transfer coefficient	$W/(m^2K)$
h	enthalpy	kJ/kg
h_{c}	convective heat transfer coefficient	$W/(m^2K)$
h_{fi}	heat transfer coefficient	$W/(m^2K)$
h_{r}	radiative heat transfer coefficient	$W/(m^2K)$
h_{W}	wind heat transfer coefficient	$W/(m^2K)$
h_{B}	bond enthalpy	kJ/kg
h_{E}	evaporation enthalpy	kJ/kg
h_{S}	sorption enthalpy	kJ/kg
I	irradiance	W/m^2
l	length	m
Lc	Lewis number	–
$\dot{m}$	mass flow	kg/s
n	available spaces in a monomolecular layer	–
Nu	Nusselt number	–

Pr	Prandtl number	–
P	pressure	Pa
P_{tot}	total atmospheric pressure	Pa
P_{S}	vapour pressure at saturation	Pa
P	Fourier number	–
Q	energy	kWh
Q_{U}	energy gain	kWh/m^2
r	radius	m
r	adaptation parameter for virtual layers	–
rh	relative humidity	–
rh_{i}	indoor relative humidity	–
R_{A}	gas constant of air	$J/(kgK)$
R_{V}	gas constant of vapour	$J/(kgK)$
$R_{\mathrm{L,h}}$	heat transfer resistance	m^2K/W
$R_{\mathrm{L,m}}$	mass transfer resistance	m^2K/W
Re	Reynolds number	–
t	time	s
T	absolute temperature	K
U	overall heat transfer coefficient	$W/(m^2K)$
v	velocity	m/s
$\dot{V}_{\mathrm{P}}$	air flow process	m^3/s
$\dot{V}_{\mathrm{R}}$	air flow regeneration	m^3/s
W	width between collector fins or tubes	m
W	electrical energy	kWh
x	length	m
X	absolute humidity	g/kg
X_{P}	absolute humidity of process air	g/kg
X_{R}	absolute humidity of regeneration air	g/kg
X_{S}	water content of sorbent	g/kg
X_{s}	absolute humidity at saturation	g/kg

α	absorption coefficient	–
δ	mass transfer coefficient	$kg/(m^2s)$
Δx	length	m
ΔX	dehumidification	g/kg
ϵ	emissivity coefficient	–
ϵ_{abs}	emissivity coefficient of absorber	–
ϵ_{glass}	emissivity coefficient of glass	–
η_{coll}	efficiency of collector	–
η_{h}	efficiency of enthalpy exchanger	–
η_{hum}	efficiency of humidifier	–
η_{HR}	efficiency of heat recovery	–
η_{sorp}	efficiency of dehumidifier	–
ϑ	temperature	°C
ϑ_{abs}	absorber temperature	°C
ϑ_{amb}	ambient temperature	°C
ϑ_{ext}	external temperature	°C
$\vartheta_{\text{f,in}}$	inlet temperature of a collector	°C
$\vartheta_{\text{f,m}}$	mean fluid temperature in a collector	°C
ϑ_{i}	indoor temperature	°C
ϑ_{int}	internal temperature	°C
ϑ_{p}	percepted temperature	°C
ϑ_{P}	process air temperature	°C
ϑ_{R}	regeneration air temperature	°C
λ	heat conductivity	$W/(mK)$
ρ	density	kg/m^3
ρ_{A}	density of air	kg/m^3
ρ_{sorp}	density of sorbent	kg/m^3
σ	radiation constant of Stefan and Boltzmann	$W/(m^2K^4)$
τ	transmission coefficient	–
Ψ	porosity	–
ω	specific surface of a regenerator	m^2/m^3

Glossary

absorption	The mass transfer of a gas into the bulk of a liquid.
adsorbate	Substance in gas or liquid phase picked up by the solid adsorbent.
absorbent	The solid substance providing the interface.
adsorption	Enrichment of one or more components in an interfacial layer on solid surfaces.
bond enthalpy	Heat of desorption.
condensation enthalpy	Heat of condensation.
cooled sorption	A sorption process in which the sorption enthalpy is removed by a heat exchanger thus increasing the dehumidification potential. A cooled sorption is not possible with a rotary dehumidifier.
enthalpy exchanger	Combined heat and mass recovery in which both mass and heat transfer are involved, employing an adsorbent matrix with a large moisture and heat capacity.
evaporation enthalpy	Heat of evaporation.
heat regenerator	Rotating heat recovery which consist of a revolving porous matrix through which two physically separated air streams pass in counterflow. Heat regenerators require a non–hygroscopic matrix with a large heat capacity.

mass regenerator	Rotating mass recovery which consist of a revolving porous matrix through which two physically separated air streams pass in counterflow. Mass regenerators require an adsorbent matrix with a large moisture but a small heat capacity.
matrix	A solid structure with distributed void space in its interior as well as its surface.
porosity	Ratio of void volume to total volume.
regeneration temperature	Temperature required to enable desorption in a sorption process
sorption	Sorption is the comprehensive term for all processes in which a substance is selectively bound by another substance.
sorption enthalpy	The sorption enthalpy is the sum of the evaporation enthalpy and the bond enthalpy.

Chapter 1

Introduction

Cooling is important for space conditioning of most buildings in warm climates and in non–residential buildings with high internal cooling loads in cooler climates. Along with the growth of cooling loads in modern buildings with low thermal inertia, the peak electricity demand increases during the day. This causes some problems concerning the energy supply in some countries, because the demand for air conditioning occurs simultaneously with the maximum demand of industry and households. The inertia of energy plants leads to a high consumption of coal, oil, gas and nuclear energy by energy companies to ensure the provision of electricity. To depress the swing of energy demand during the day, solar energy for cooling purposes could make a significant contribution to lowering the energy consumption. Using solar energy for cooling purposes is an attractive idea with good prospects for conventional air conditioning systems. The replacement of compressor cooling systems by solar thermal cooling systems could make an important contribution to environmental protection. The main argument for the applicability of solar energy is that cooling loads and solar availability are approximately in phase. Due to the combination of solar cooling and heating, solar collectors which are now used only for heating purposes would become more economical.

According to Figure 1.1 from the german standard DIN 1946, thermal comfort can only be provided if the perceived temperature does not exceed 25 °C to 27 °C depending on the ambient temperature and does not fall below 22 °C to 20 °C depending on the type of ventilation system. Furthermore, the absolute humidity should be in the range of 5 g/kg to 12 g/kg. In Figure 1.2 the ASHRAE requirements for comfort are shown in a psychrometric chart. Thermal comfort is given when a human being is satisfied with the

temperature, the humidity and the air movements in his environment and does not wish to have air which is warmer, colder, dryer or more humid. To provide these thermal comfort requirements FRANZKE 1995 gives a specific end energy demand of 50 kWh/m^2a for cooling and 75 kWh/m^2a for heating in non–domestic buildings in Germany. Considering that the majority of the air conditioning systems are electrically driven and assuming an efficiency of 0.33 for the production of electricity, the amount of primary energy required for cooling is 150 kWh/m^2a, which is nearly double the primary energy demand required for heating. Figure 1.3 shows this comparison. A total replacement of the cooling provision by solar energy would reduce Germany's annual CO_2 emissions by 150000 t per year. Assuming a more realistic solar fraction of 2/3, the saving potential is in the range of 100000 t per year. This exemplifies the potential of energy savings, the importance of heat protection in summer and the need of air conditioning systems that take care of the environment. The reduction of cooling loads (typical values are shown in Figure 1.4) through well–advised building design will certainly be more convenient, as it is often less expensive than providing additional cooling. Good building design minimizes loads on any air conditioning and heating system.

A main argument for solar cooling is that the cooling demand is often correlated with the irradiation, for example in buildings with large glazing areas. Furthermore, the cooling demand often occurs during hours of high irradiation, for example in non–domestic buildings like offices. Conventional compressor cooling machines can run on energy which is gained by using photovoltaics. The costs of these solutions, however, are currently very high. Solar cooling can however be accomplished by absorption cycles, adsorption cycles or desiccant cooling cycles. Within these classes, there are many variations, using continuous or intermittent cycles, hot or cold side storage, various control strategies, various temperature ranges of operation and the use of different solar collector types. However, these cooling cycles are connected to district heating systems or cogeneration plants until now.

The research on solar cooling was mainly established by investigations in the 70th and 80th in the United States. Significant improvements in the absorption chiller technology and the desiccant cooling technology were the outcome of these investigations. The main focus was on components rather than on systems. In Germany there is ongoing research in the field of desiccant cooling systems. Particularly the performance of different dehumidifier technologies is being investigated in detail. Furthermore, investigations are conducted on the economics of desiccant cooling systems. Desiccant cooling systems

seem to be one of the most promising technologies for solar cooling considering energy efficiency and economics.

Hence, the aim of this work is the detailed investigation of the performance of solar driven desiccant cooling systems. Solar air collectors, which have not been part of investigations to date, seem to be appropriate for the implementation of solar energy, because desiccant cooling systems are air handling units requiring warm air for the regeneration process. Therefore, a test plant has been installed to analyse a desiccant cooling system's performance with solar air collectors. A simulation program has been developed to evaluate the performance of a desiccant cooling system with solar air collectors interacting with a building. Parametric studies with annual simulations for four different climates have been conducted to calculate mean COPs, the occurrence of the possible control modes and the amount of cooling energy achieved with the desiccant cooling system driven only by solar energy. On the basis of the measurement results, the experience gained with the test system and the results of the annual simulations, design suggestions are formulated which also take other cooling technologies into account.

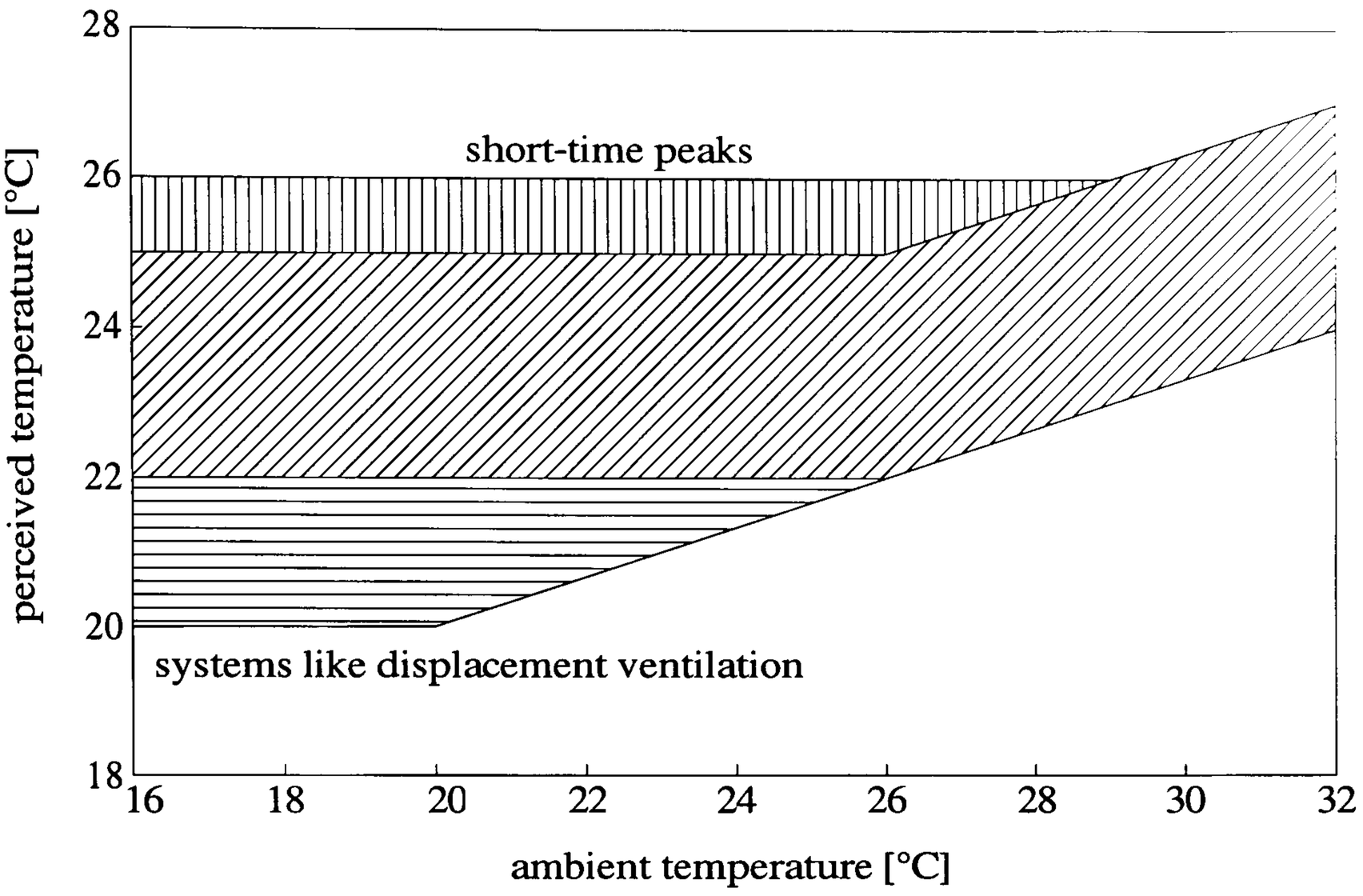

Figure 1.1: Temperature requirements according to DIN 1946

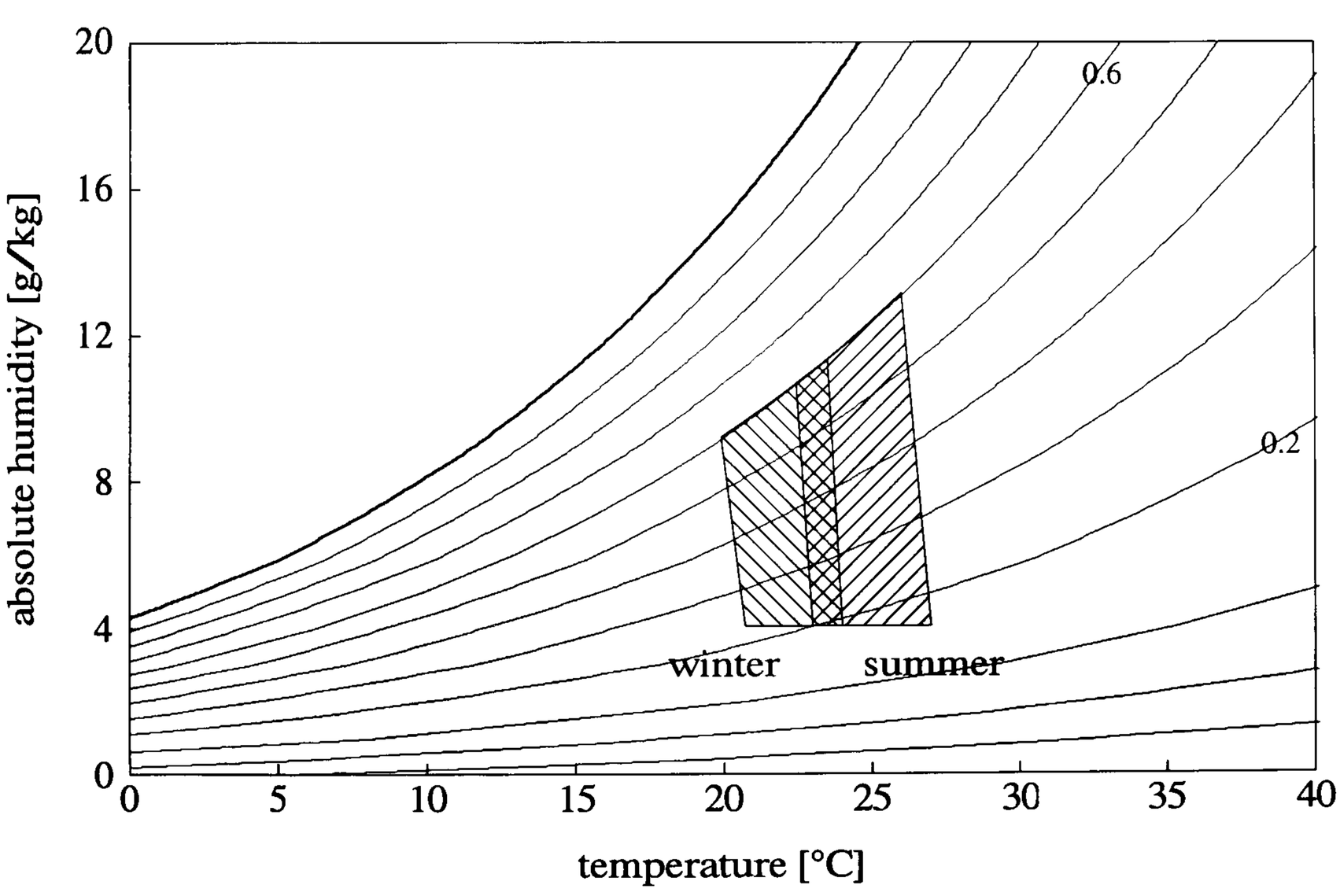

Figure 1.2: Thermal comfort field according to ASHRAE

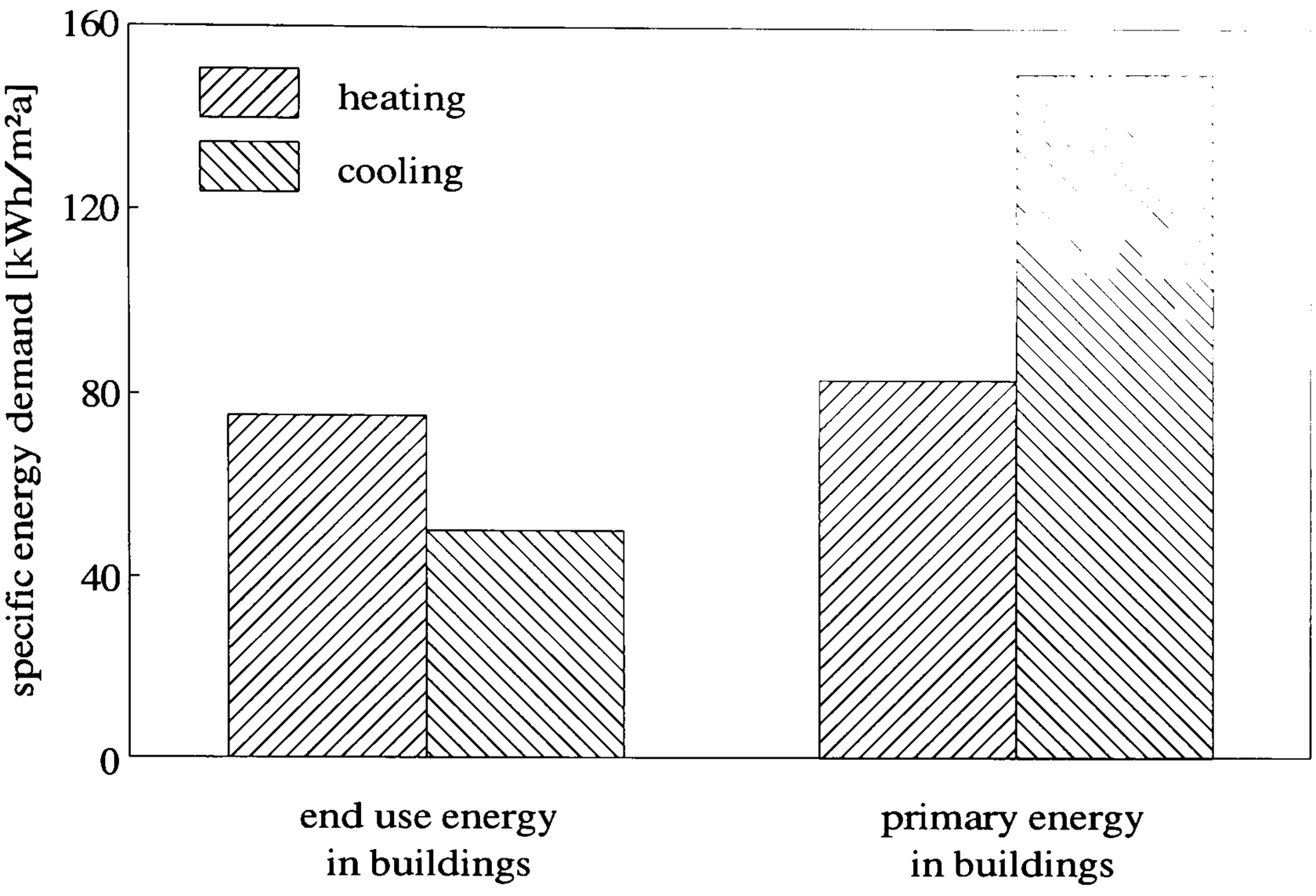

Figure 1.3: Energy demand in office buildings

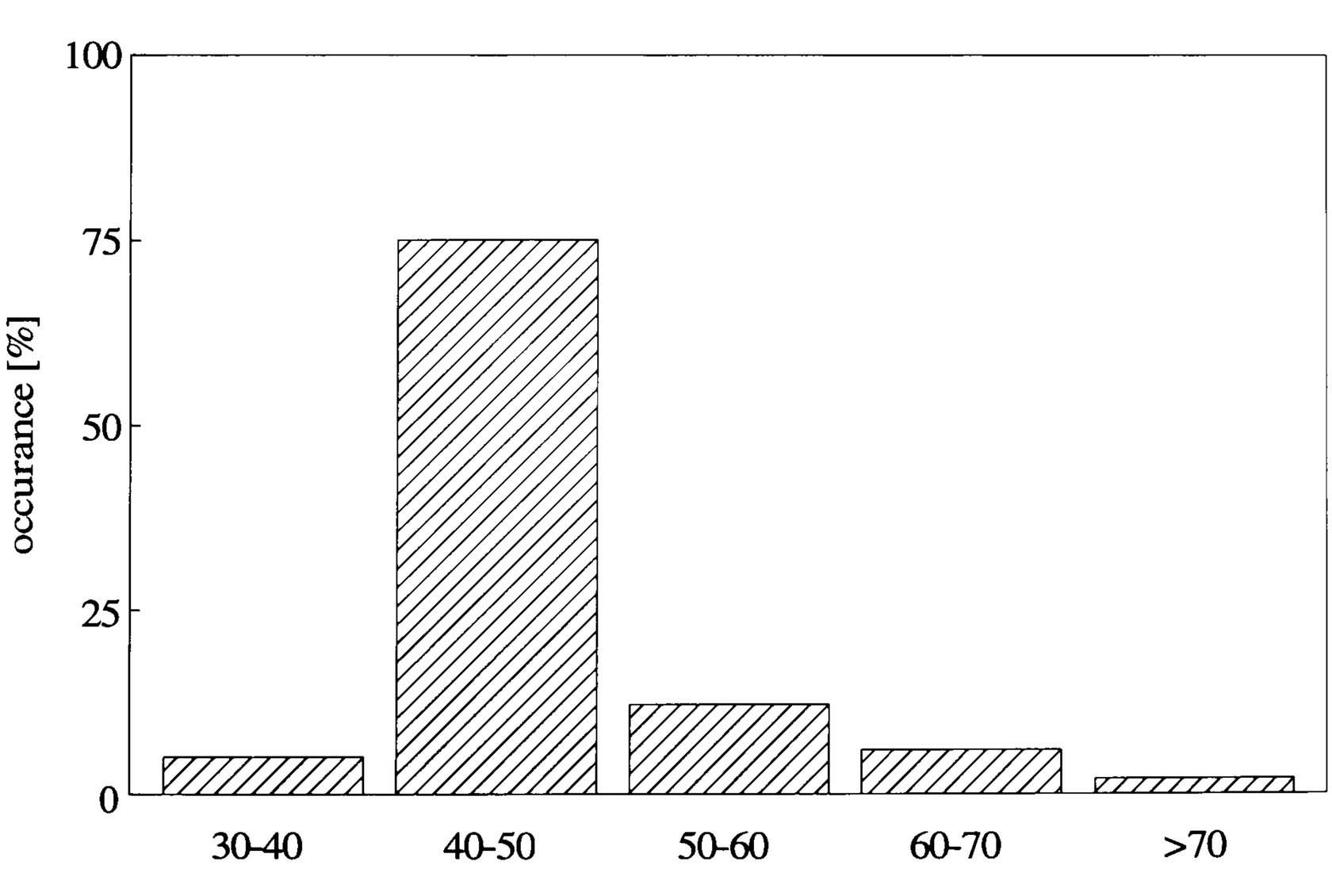

Figure 1.4: Cooling loads in office buildings according to IHLE 1996

Chapter 2

State–of–the–Art Cooling Technologies

2.1 Passive Cooling

The microclimate and the site design can significantly influence the thermal performance of a building. All aspects of site design can interfere with the design of a building with regard to the incident irradiance and the available wind. Vegetation can also improve the microclimate around a building, and therefore decrease the cooling load. MOFFAT and SCHILLER 1981 estimated that a large tree evaporates around 1460 kg of water on a sunny day, which equals a cooling capacity of 242 kWh. Areas with a great deal of vegetation may decrease the air temperature by 2 K to 3 K.

Shading is the primary design measure of heat gain protection. External shading devices or the shade of surrounding vegetation or buildings can result in satisfactory thermal performances of the building. Internal shading devices or special glazings can also reduce the heat gain, but they should always be the second choice.

The thermal mass of a building absorbs heat in the course of a day and determines the magnitude of indoor temperature swings, reduces peak cooling loads and transfers a part of the absorbed heat into the night. In non–tropical climates a building can be pre–cooled by night ventilation, and the cooling effect of the night can be transferred into

the early hours of the following day. BROWN 1990 calculated an average reduction in energy consumption for cooling close to 20% if night ventilation is used. According to SZOKOLAY 1984 an efficient thermal storage is acceptable where the diurnal swing of ambient temperature exceeds 10 K. Caused by the phase–shift between the air temperature swing and the surface temperature swing, the operational temperature variations are much lower than in lightweight buildings. In this case, higher air temperatures are more acceptable than in lightweight buildings.

Ventilation is necessary in all indoor spaces to introduce the required level of fresh air. The required air change in buildings can be achieved by natural ventilation, mechanical ventilation systems or a combination of both. Natural ventilation is caused by pressure differences at the inlets and outlets, which are results of wind and buoyancy. Night ventilation, wind towers and solar chimneys are the main natural ventilation techniques. They should be used in buildings with high cooling loads and in climates where ambient temperatures could be a heat sink.

In climates with a high magnitude of temperature swing between summer and winter, ground cooling by buried pipes could make a major contribution to lowering the cooling loads. Ground temperatures remain almost constant during the day at depths exceeding 1 m. In depths of around 10 m the magnitude of seasonal temperature swings is negligible. This shows that a seasonal storage can be achieved with pipes buried at a depths of approximately 5 m. This technique is not appropriate to cool buildings in tropical climates because the temperature gradient with the ground depth is very low.

Evaporative cooling by vegetation or mechanical humidifiers could make a major contribution to decrease cooling loads in climates with low humidity. The potential of evaporative cooling must be estimated for different climates with regard to the respective comfort conditions.

2.2 Compressor Cooling

Compression chillers are closed systems for energy transformation which are assigned to transport heat between different temperature reservoirs. The compression chiller, a cold

vapour heat pump, is the most widely used cooling technology today. In those machines the working medium, called refrigerant, evaporates by taking up heat from outside and condenses by giving off heat to the outside. To achieve a heat transformation at different temperatures the heat supply and the heat removal takes place at different pressures. and the pressure dependence of the boiling point is used. The main components of a compression chiller are the evaporator, the condenser, the compressor and an expansion valve. Figure 2.2 shows a schematic in a pressure–temperature chart. In the evaporator the liquid refrigerant evaporates at a low pressure and takes up heat from outside via a heat exchanger. The vapour of the refrigerant will be sucked in from the compressor and compressed. At a higher temperature and pressure level the vapour condenses in the condenser and gives off the heat. The condensate will be expanded down to the evaporation pressure in the expansion valve and the circuit is closed. The characteristic parameter for describing the efficiency is the coefficient of performance COP, which is the ratio of the expended compression work to the supplied heat to the evaporator.

$$\mathrm{COP} = \frac{Q}{W} \tag{2.1}$$

A typical COP is, according to ZIEGLER 1997, in the range of 2 to 3 for the generation of cold with temperatures of -10 °C , and for the purpose of air conditioning with temperatures of 5 °C , in the range of 4 to 5. The refrigerants mainly used are chlorofluorocarbons abbreviated as CFC. Because of their effects on the ozone layer of the atmosphere they must now be replaced with alternative refrigerants.

In air conditioning systems in which, in addition to the cooling effect, a desired dehumidification is required, the surfaces of the heat exchanger must be cooled down below the dew point temperature of the passing process air. In this case dehumidification occurs by condensation. To achieve the desired absolute humidity, it is therefore often necessary to cool down the process air below the initial desired temperature. Hence a heating device must be installed after the cooling device. This process of dehumidification is shown in a psychrometric chart in Figure 2.1a. In addition to the use of heat exchangers with low surfaces temperatures, it is possible to dehumidify the air at cold water surfaces. Therefore, water droplets with a temperature below the dew point temperature can be sprayed into the process air flow. These dehumidification processes described above are applied in all air conditioning systems in which only closed cooling cycles are used.

The heat produced in the condenser must be removed from the system. Therefore, cooling towers are required to carry the heat to the outside. Closed cooling towers consist of a water/air heat exchanger in which the cooling water flows from the condenser. In these towers a fan increases the surface heat transfer coefficient. To achieve a high cooling efficiency, water can be sprayed, if required, onto the heat exchanger to increase the heat transfer by evaporation. To reduce the investments and the required space for the cooling tower it is additionally possible to use open cooling towers. Here the warm water from the condenser is sprayed in counter flow in an air stream. A small part of the heat removal is of sensible nature and largely of a latent nature. The disadvantages of the open cooling towers are the dirt retention and the amount of fresh water required for the system which is, according to RECKNAGEL ET AL. 1994, around 6 $kg/(h\,kW)$.

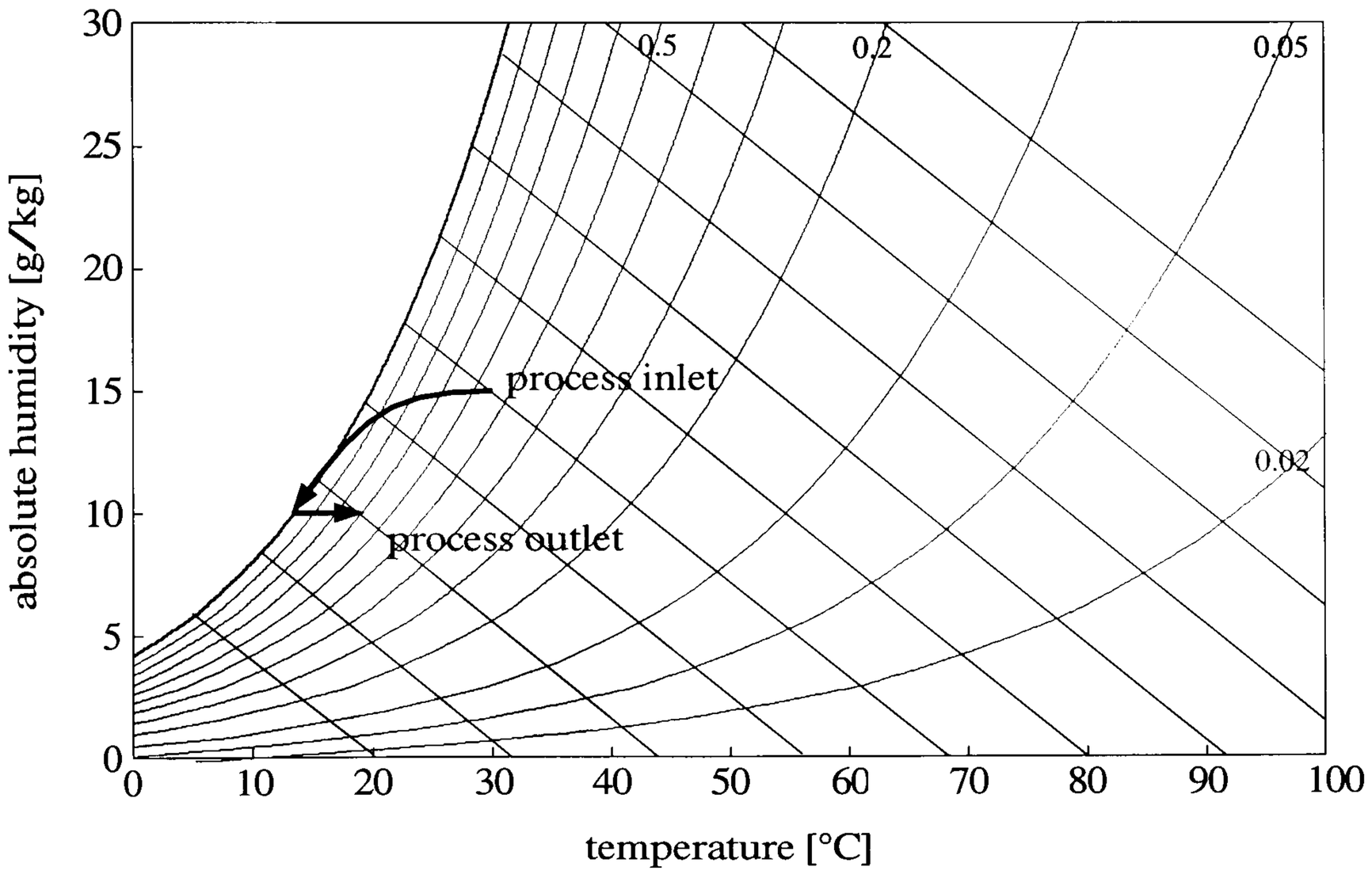

Figure 2.1: Cooling and dehumidification process of a surface cooler with additional heating to the desired process condition

2.3 Thermomechanical Cooling

In these processes compression chillers are used, and only the driving mechanism for the compressor is provided thermally. In the thermomechanical Rankine process thermally generated steam is used in an engine. This engine drives the compressor of the com-

pression chiller. When comparing this system with other systems, the advantage is the flexibility of the energy supply. If the Rankine machine is connected to the grid and no cooling demand exists, generated electric energy can be supplied to the grid. On the other hand, this system can also be driven by electric energy if thermal energy is not available. However, the main disadvantage of this process is the two–step conversion of energy. CURRAN 1993 presents the results of the research in this regard which occurred in the United States in the 80th investigation.

2.4 Absorption Cooling

Heat transformation processes like the absorption cooling process have, in contrast to the compressor cooling processes, a sorption system that functions like a thermal compressor and replaces the mechanical compressor. In the following, the basics of closed absorption systems will be presented. These investigations were presented by LAMP, ZIEGLER 1997 and ASUE 1996. A closed absorption process exchanges only heat with the surroundings and no fluid such as air or refrigerant. As in a compression chiller, a refrigerant evaporates at low temperature and low pressure while taking up heat from outside. At a higher temperature and pressure level the refrigerant condenses while giving off heat to the outside. The evaporated refrigerant is absorbed in a sorption fluid in the absorber at low pressure while the sorption heat is conveyed to the outside. The solution rich in refrigerant must be regenerated on a high pressure and temperature level. After regeneration the refrigerant vapour flows first to the condenser, afterwards the condensate to the evaporator and the poor solution to the absorber and the process starts again. Thus both, the refrigerant and the sorbens, are kept in a closed loop. An absorption system as described can be realised using different kinds of sorption couples. Common sorption couples are lithiumbromide/water and water/ammonia, where the first substance is the solvent and the second the refrigerant.

Figure 2.2b shows the simplest realisation of such a machine which is called single–effect absorption cycle. It mainly consists of four heat exchangers for the heat transfer from and to the surroundings. The efficiency of this cycle represented by the coefficient of performance COP is theoretically 1.0 and in realised plants around 0.7, and can be defined by the ratio of the gained cooling energy to the supplied heating energy. The COP of a single–effect absorption cycle can be calculated with

$$\mathrm{COP_{SE}} = \frac{\frac{1}{T_1} - \frac{1}{T_2}}{\frac{1}{T_0} - \frac{1}{T_1}} \tag{2.2}$$

where T_0 is the temperature of the evaporator, T_1 the temperature of the condenser. which is usually the same as the absorber temperature, and T_2 the temperature of the generator, where the heat from outside is supplied to the system. The COP of an absorption cycle depends primarily on the temperature levels at which the heat is coupled in the system and out of the system. The choice of the specific sorption system with different sorption couples does not considerably influence the COP. The COP can only be increased by increasing the generator temperature. However, in single–effect cycles the generator temperature is given by the physical properties of the sorption couple and hence the maximum COP is fixed. This limitation can only be overcome with multistage cycles. The increase in the COP with regard to a higher driving temperature can be achieved by double–effect absorption cycles in which a second generator and condenser are implemented at a higher temperature and pressure level. Figure 2.3a shows this cycle. The heat of condensation of the second condenser is used to regenerate the sorbens of the first generator at the middle pressure and temperature level. In the double–effect cycle a COP of 2.0 can be theoretically achieved, in practice 1.2. It must be calculated with

$$\mathrm{COP_{DE}} = \frac{\frac{1}{T_1} - \frac{1}{T_3}}{\frac{1}{T_1} - \frac{1}{T_2}} \cdot \frac{\frac{1}{T_1} - \frac{1}{T_2}}{\frac{1}{T_0} - \frac{1}{T_1}} \tag{2.3}$$

where T_3 represents the highest temperature at the second generator. The double–effect cycle can be further improved by a third generator and condenser leading to a triple–effect cycle. The problem with these highly efficient absorption cycles is that the driving temperatures cannot be reached by efficiently operating solar collectors. As a result, it is necessary to find an efficient absorption cycle working with low temperatures which can be reached with efficiently operating solar collectors. Therefore LAMP and ZIEGLER 1997 suggested a double–lift cycle in which a second generator and absorber is introduced at an intermediate pressure level resulting in a decrease of COP down to theoretically 0.5, and in practice to 0.4. It must be calculated with

$$\mathrm{COP_{DL}} = \frac{\frac{1}{T_1} - \frac{1}{T_2'}}{\frac{1}{T_1} - \frac{1}{T_2}} \cdot \frac{\frac{1}{T_1} - \frac{1}{T_2}}{\frac{1}{T_0} - \frac{1}{T_1}} \tag{2.4}$$

where T_2' is the temperature of the generator which is placed at the intermediate pressure and temperature level. SCHWEIGLER ET AL. 1997 developed on the basis of the

ideas of Alefeld a single–effect/double–lift absorption cycle shown in Figure 2.3b which is appropriate for the use of solar energy. The heat is used in three generators which were configured in sequence and the temperature of the fluid decreases more than in the other cycles. This property is very important for the use of solar collectors because of the higher efficiency at low temperatures. The COP of this cycle is between the COP of the single–effect cycle with 0.7 and the COP of the double–lift cycle with 0.4 and depends on the distribution of heat to the three generators. It must be calculated with

$$\mathrm{COP}_{\mathrm{SE/DL}} = \frac{\mathrm{COP}_{\mathrm{SE}} \cdot \mathrm{COP}_{\mathrm{DL}}}{\sigma \cdot \mathrm{COP}_{\mathrm{DL}} + (1-\sigma) \cdot \mathrm{COP}_{\mathrm{SE}}} \tag{2.5}$$

with

$$\sigma = \frac{Q_{\mathrm{SE,evap}}}{Q_{\mathrm{SE,evap}} + Q_{\mathrm{DL,evap}}} \tag{2.6}$$

Up to now, all of the described absorption cycles have required a pump to transport the solution from the absorber to the generator. Van Platen and Munters developed a diffusion–absorption heat pump in which the pump is replaced by a vapour–bubble pump. This process is described by BÄCKSTRÖM and EMBLIK 1965. In this cycle, in which the sorption couple of water/ammonia is used, an additional inert gas like helium is required to keep the process running. The main advantage of this machine is that there are no moving parts. This cooling principle is mainly used in small refrigerators.

As also described on page 25, the heat removal from the condenser must be achieved by cooling towers. If the absorption chillers must be used for the purpose of air conditioning with the necessity of dehumidification, the dehumidification process described on page 25 must also be considered.

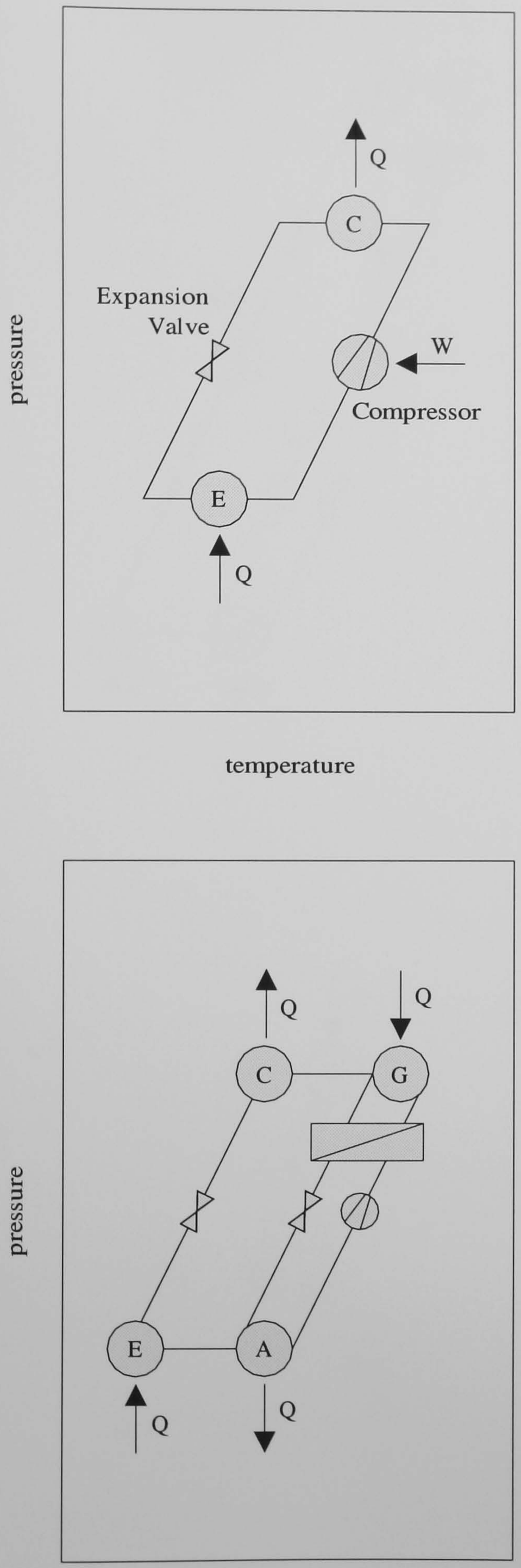

Figure 2.2a: Compression chiller

C: condensor
E: evaporator

Q: thermal energy
W: electrical energy

Figure 2.2b: Single–effect absorption chiller

C: condensor
E: evaporator
A: absorber
G: generator

Q: thermal energy

Figure 2.2: Compression chiller and single–effect absorption chiller

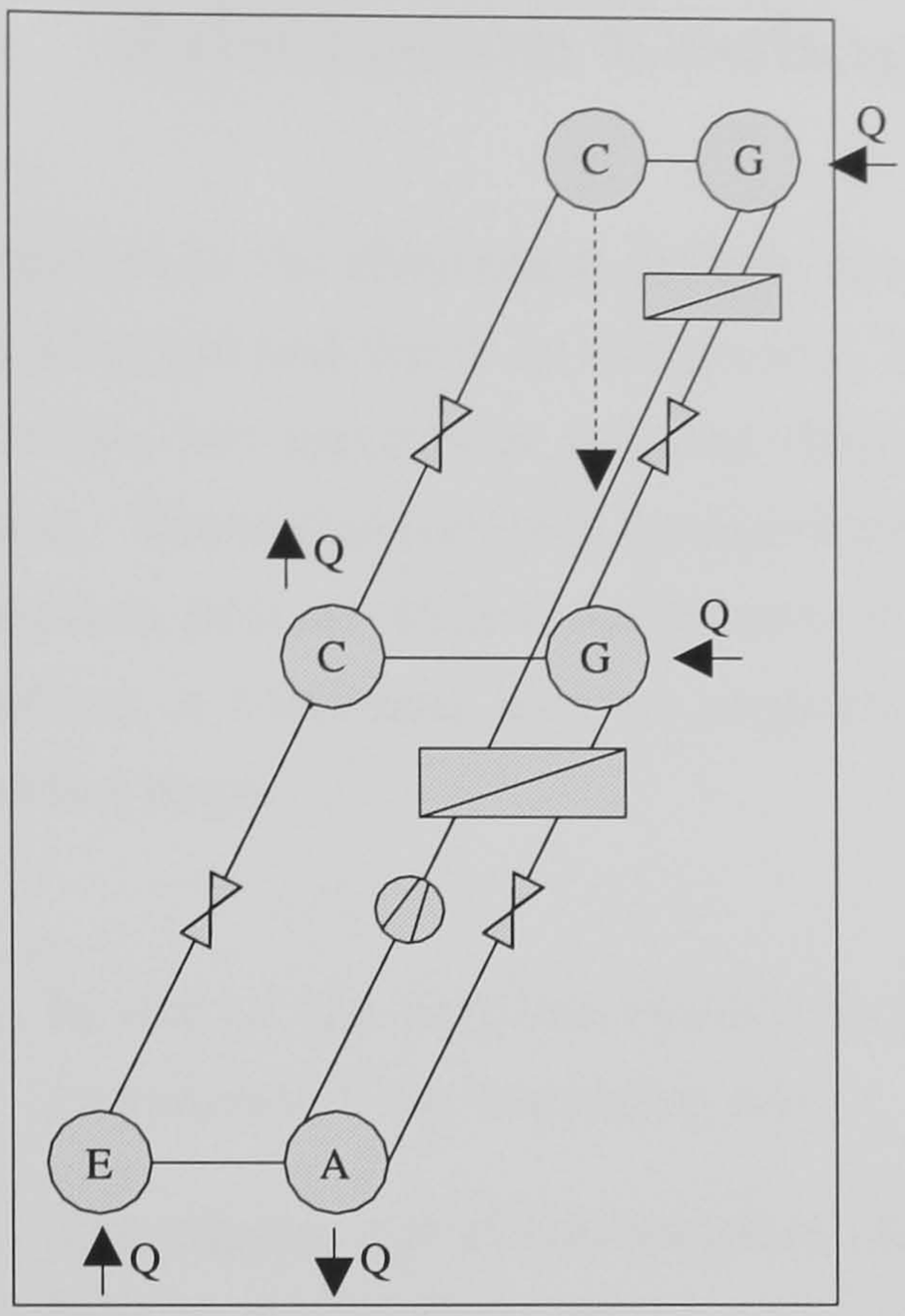

Figure 2.3a: Double–effect absorption chiller

C: condensor

E: evaporator

A: absorber

G: generator

Q: thermal energy

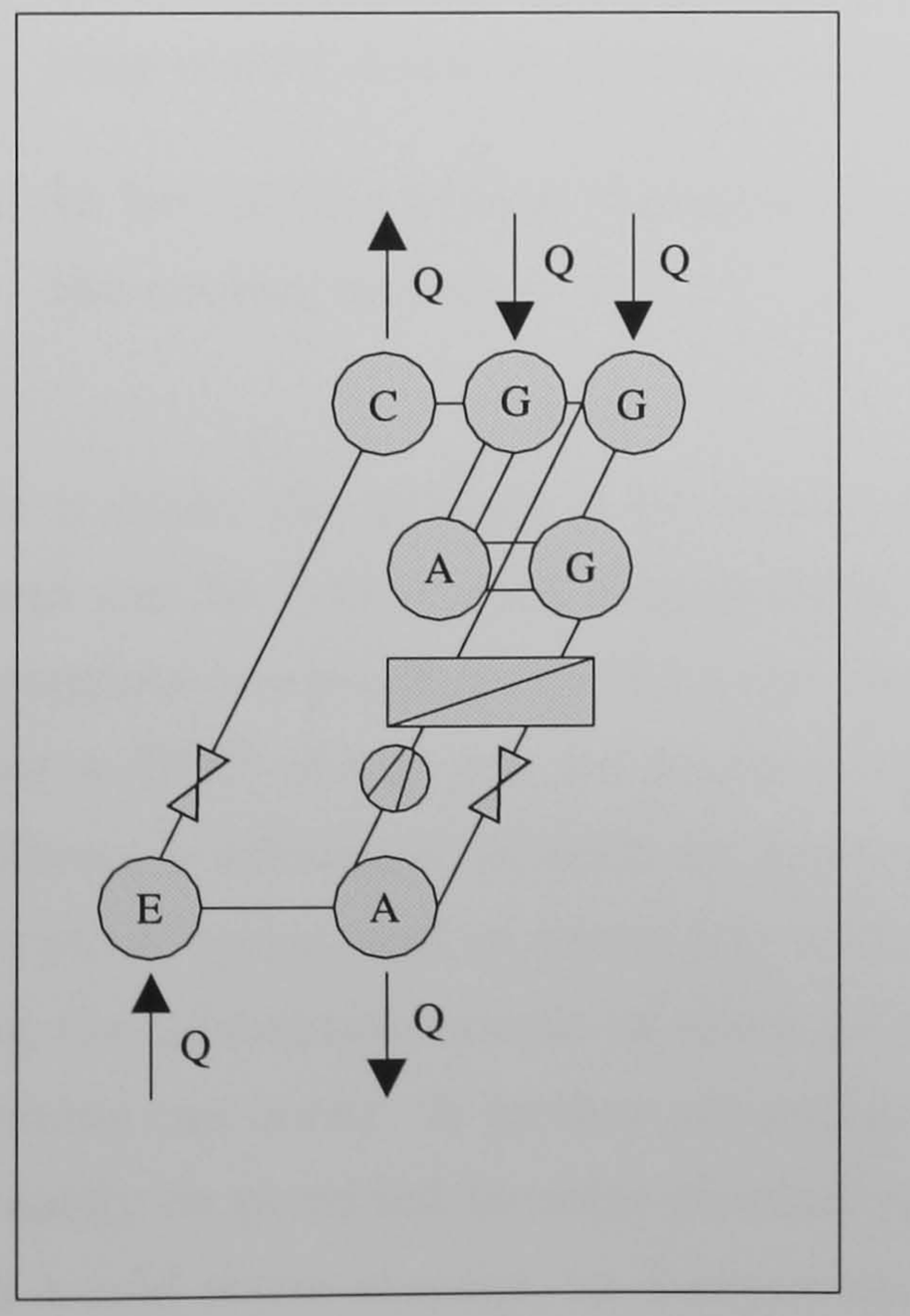

Figure 2.3b: Single–effect/double–lift absorption chiller

C: condensor

E: evaporator

A: absorber

G: generator

Q: thermal energy

Figure 2.3: Double–effect and single–effect/double–lift absorption chiller

2.5 Adsorption Cooling

In contrast to the absorption chillers, closed adsorption chillers work with the solid adsorbens silica gel and water as refrigerant. The silica gel is not movable in the closed system. Therefore, two reactors or sorption chambers are necessary to achieve a quasi–continuous process. These reactors will be alternately activated for the adsorption process and the desorption process with a cycle time of around 7 minutes. In addition to the sorption chambers, a condenser and an evaporator are necessary. The process proceeds in the following steps:

1. In one of the sorption chambers the water adsorbed at the silica gel is desorbed (regenerated) by supplying heat.
2. The vapour out of this sorption chamber is condensed in the condenser, giving off heat to the cooling water.
3. The condensed water is sprayed into the evaporator which is typically at a near vacuum condition. In this way heat is removed from the cooling circuit which is thus cooled down to the desired temperature.
4. In the other sorption chamber the vapour is adsorbed and the heat is given up to the cooling water.

After a cycle, the process is be repeated achieving a quasi–continuous operation. This system can be driven with regeneration temperatures of 55 °C to 95 °C, which is a very appropriate temperature level for the use of solar thermal energy. With these adsorption cycles a COP of 0.6 can be reached at a regeneration temperature of 70 °C. Figure 2.4 shows a schematic of such an adsorption chiller. Comparing adsorption cycles with absorption cycles, and in particular with the absorption couple of lithiumbromide/water, using the adsorption couple of silica gel/water has the advantage that no crystallisation problems can occur. A further advantage is the low regeneration temperature level which can easily be provided by solar thermal energy. Adsorption chillers should always be used with a cold water storage, to dampen the fluctuation of the cold water temperatures out of the discontinuous process in the adsorption chiller. Gassel 2000 suggests a storage volume of at least 1/40 of the hourly cold water flow.

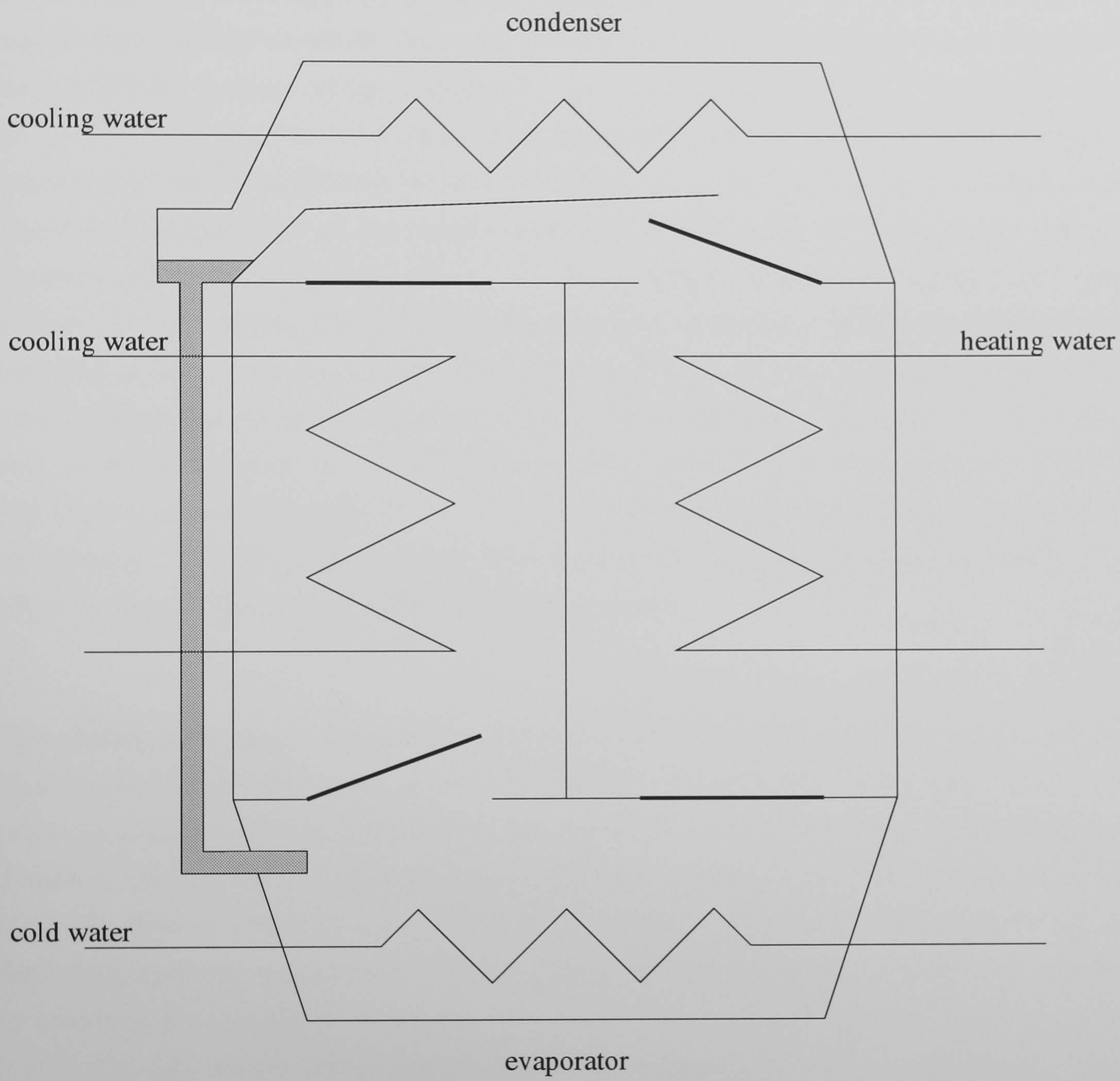

Figure 2.4: Schematic of an adsorption chiller

2.6 Desiccant Cooling

In contrast to the cooling processes described up to now, desiccant cooling systems use no closed cooling devices. The entering humid air streams from outside and inside are used as refrigerants. Desiccant cooling systems are complete air handling units in which the cooling effect of evaporating water is used. In contrast to the evaporation process in compression chillers in which the total pressure acting on the refrigerant is decreased to start a boiling process of the refrigerant, the evaporation process in humidifiers occurs below the boiling point. The removal of energetic water molecules occurs through the passing inert air. The driving force is the difference of the partial vapour pressure of the liquid surface and that of the unsaturated air. Particularly in dry climates where the vapour pressure is not close to the saturation pressure, noticeable cooling effects can be gained. If appropriate for the particular climatic conditions, direct humidifiers can be installed in the supply air stream. If an increase of the absolute humidity is not desired, a cooling effect can be gained by using indirect humidification. Here, the outlet air stream will be humidified and the cooling effect will be utilised by a heat recovery. If the partial vapour pressure is close to the saturation pressure, only a limited cooling effect can be achieved. In this situation prior dehumidification could increase the possible cooling effect by humidification and allow moisture control.

The cooling technology presented here is based on a process combining sorptive dehumidification, heat recovery, evaporation and heating. The so–called desiccant cooling system takes air from outside or from within the building (or a combination), and dehumidifies it with a solid or liquid desiccant, cools it by heat exchange and then evaporatively cools it to the desired state at a maximum 100% relative humidity in the supply air. The desiccant must be regenerated by heat. The dehumidification is mainly accomplished by rotating dehumidifiers which are heat and mass regenerators comprised of a porous matrix through which two physically separated air streams pass in counterflow. For the application in desiccant cooling systems it is usual for a carrier material to be coated or soaked with the desiccant. Common desiccants are silica gel and lithium chloride.

The example in Figure 2.5 shows a desiccant cooling process under usual design conditions for Central Europe ($\vartheta_{\text{amb}} = 32\,°\text{C}$, $rh_{\text{amb}} = 40\%$; $\vartheta_{\text{in}} = 26\,°\text{C}$, $rh_{\text{in}} = 55\%$). Ambient air is dried by a dehumidifier from 1 to 2, regeneratively cooled by exhaust air from 2 to 3, evaporatively cooled from 3 to 4 and then brought into the building. The inlet humidifier allows control of the temperature and humidity. Returning air at state 5 from the inside

of the building moves in the opposite direction and is evaporatively cooled to 6 up to saturation. At 7 the air is heated by the energy removed from the process air stream by the heat recovery. From 7 to 8 solar or other heat must increase the temperature up to the level for the particular desiccant required to regenerate it for subsequent dehumidification. From 8 to 9 the regeneration air takes up water from the desiccant and cools down. This common cycle of a desiccant cooling system shown in Figure 2.5 is called the Pennington cycle or ventilation cycle. In addition to the ventilation cycle, in which only fresh air enters the adsorbing part of the dehumidifier, a recirculation cycle is possible as shown in Figure 2.6. The same components are used, however building air is recirculated and ambient air is only used for regeneration. The advantage of a recirculation cycle compared with the ventilation cycle is that the cooling capacity of the desiccant cooling system can be designed to be equal to the cooling load of the building. In ventilation cycles, the cooling capacity of the system must be higher than the cooling load because the intake air is often warmer and more humid. The disadvantage is that there is no fresh air supply in recirculation cycles. Furthermore, combinations with partial recirculation are possible.

The energetic performance of a desiccant cooling system can be improved if a part of the regeneration air flow is bypassed around the desorption part of the rotating dehumidifier. Typical values for the bypass air flow are around 25% of the process air flow. To classify the process it is necessary to define a coefficient of performance. For the calculation of the COP it is usual to use enthalpy differences instead of temperature differences to show the influence of dehumidification. The thermal COP neglecting the electrical power needed to run the whole system is be calculated using

$$\mathrm{COP} = \frac{h_{\mathrm{amb}} - h_{\mathrm{in}}}{(1 - C_{\mathrm{bypass}}) \cdot \Delta h_{\mathrm{heater}}} \tag{2.7}$$

where C_{bypass} represents the content of air bypassing around the desorption part of the dehumidifier and $\Delta h_{\mathrm{heater}}$ the enthalpy differences caused by the heater or solar collectors.

In the 70th and 80th investigations, solar desiccant cooling systems were covered in the United States which were surveyed by HENNING 1998. The outcome of the research was the development of mainly solid dehumidifiers with silica gel which showed the best performance and the development of several cycles like the ventilation cycle and the recirculation cycle. Hybrid systems with conventional chillers have not been investigated in detail. JURINAK 1882 investigated the performance of different rotating dehumidifiers in

desiccant cooling systems configured in the ventilation and the recirculation cycle. With the use of dehumidifiers with a small thermal capacity, he estimated mean thermal COPs in ventilation cycles which are about 25% higher than in recirculation cycles. The basis for this statement was the long–term consideration of different climates in the United States.

BUSWEILER 1995 compared different cooling technologies with regard to their primary energy demand. He discovered that in principle the primary energy demand of desiccant cooling systems is smaller than in a comparable compressor cooling system for air conditioning. HEINRICH and FRANZKE 1997 give an overview on desiccant cooling systems and the components needed. They compare different adsorbens materials like lithium chloride and silica gel for rotating dehumidifiers and give qualitative statements concerning their sorption properties. Lithium chloride soaked cellulose is a material combination with a high sorption capacity, high adsorption and desorption velocities and a low bond enthalpy. The bond enthalpy is in the range of 6% of the evaporation enthalpy of water. The disadvantage of rotating dehumidifiers with lithium chloride soaked cellulose is that they should not be left in air conditions with $rh > 0.9$ over a long time. A further material combination for rotating dehumidifiers is silica gel on mineral fibres. The bond enthalpy is, according to BUSWEILER 1984, in the range of 10% of the evaporation enthalpy of water. The adsorption and the desorption velocity is in the middle range. Compared with the lithium chloride soaked cellulose the sorption capacity is lower. The advantage of this material combination is the insensitivity to all humidities. WEISCHEDEL 1996 conducted investigations with a desiccant cooling system with a rotating silica gel dehumidifier and showed that the desorption process starts above a regeneration temperature level of 45 °C. Hence he conducted that solar air collectors could be a useful possibility for implementing solar energy in desiccant cooling systems. ERPENBECK 1999 made long–term measurements on a desiccant cooling system with solar liquid collectors and a storage system connected to a conference hall. Expect for the liquid collectors and the required heat exchanger, he used system components comparable to those used for the measurements described later on. He identified a mean COP of 0.45 over the entire measurement period.

An advantage of the described desiccant cooling systems compared with the closed systems of compression chillers or the absorption and adsorption technologies is that no cooling towers are required. The heat of adsorption is regained and used for the prewarming of the regeneration air. The disadvantage of these systems is that the sorption

heat increases the temperature of the sorbens and limits the possible dehumidification. A cooled dehumidification process resulting in a possible deep dehumidification can be achieved with desiccant bed systems. They contain at least two silica gel beds, which are alternately activated for the adsorption and the desorption process. In these systems the condensation enthalpy and the bond enthalpy can be directly removed from the bed by a cold water circuit. In contrast to desiccant cooling systems with rotating dehumidifiers, cooling towers are required. KHELIFA 1984 made investigations with two silica gel bed reactors, where the adsorption process was cooled. Furthermore, he used a heat recovery for pre–cooling the air after the adsorption process with the outlet air of the room in this test system. For a regeneration temperature of 70 °C thermal COPs in the range of 0.15 to 0.33 were achieved depending on the temperature of the cold water circuit for the cooled adsorption process. To increase the thermal COP, a second heat recovery was used for pre–warming the fluid upstream of the heater with the exhaust air of the desorption reactor. For this improved design, the COP reached values between 0.33 and 0.50 under the same conditions.

Another type of desiccant cooling system with a cooled sorption process uses liquid desiccants. This idea, described, for example, in DUFFIE and BECKMAN 1991, was developed in the 50th investigations by Loef, who used liquid triethylene glycol as the drying agent. This type of desiccant cooling system was marketed commercially and was used in large installations in the United States. In Europe, research is currently be conducted on liquid desiccant cooling systems. Detailed information is provided in publications of LÄVEMANN and SIZMANN 1992, KESSLING and LÄVEMANN 1995 and KESSLING 1997. In these systems with liquid sorbens the process air will be dehumidified by a cooled absorption process in which a small stream of a hygroscopic salt solution runs over a cooled plate and passes the air. The salt solution is diluted by dehumidifying the air and runs to a tank. If heat is available, the diluted solution can be concentrated by desorbing the water and will be stored in another tank. The main advantage of this desiccant cooling technology is the possibility of energy storage. With this dehumidification technology, energy can be stored in the concentrated salt solution. The density of energy storage can reach values of 1000 MJ/m^3, which is 3 times greater than the density of energy storage in an ice storage system. KESSLING and LÄVEMANN 1995 describe that a storage of 1 m^3 can provide a dehumidification capacity of 10 kW over an entire day. The regeneration of the diluted salt solution can be achieved at temperatures over 60 °C. The disadvantage of the liquid desiccant cooling systems is the difficult handling of the corrosive salt solution.

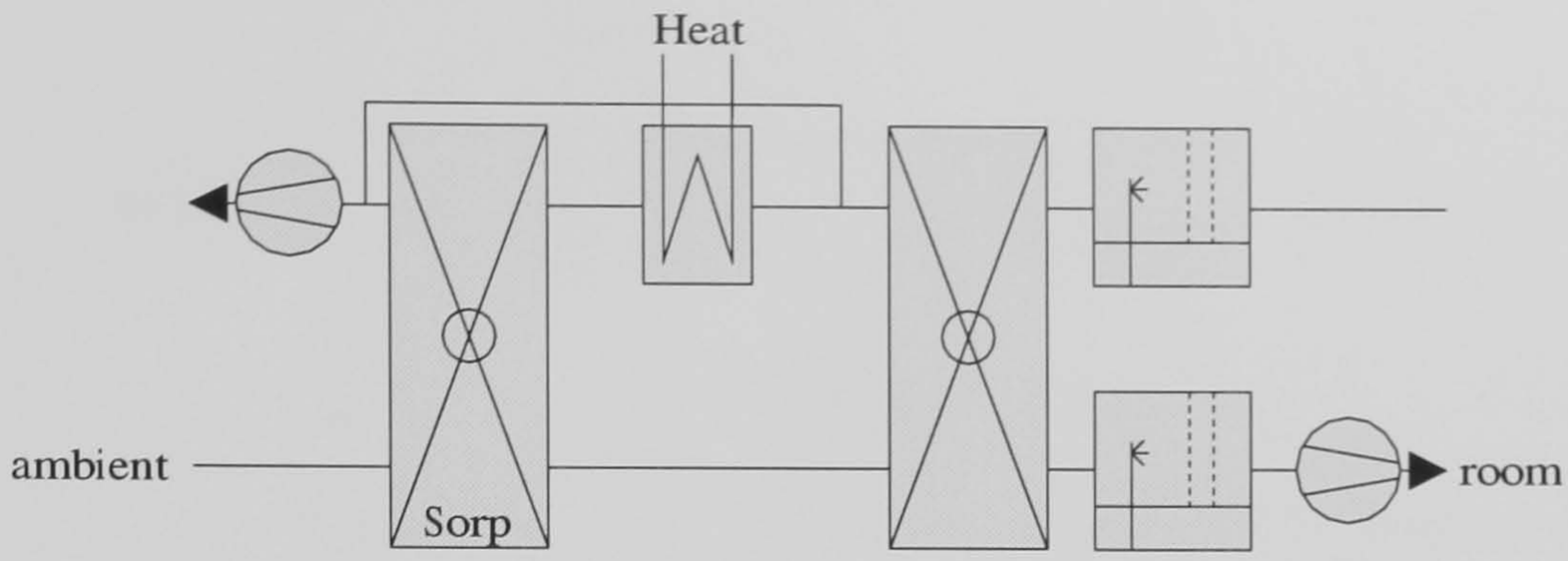

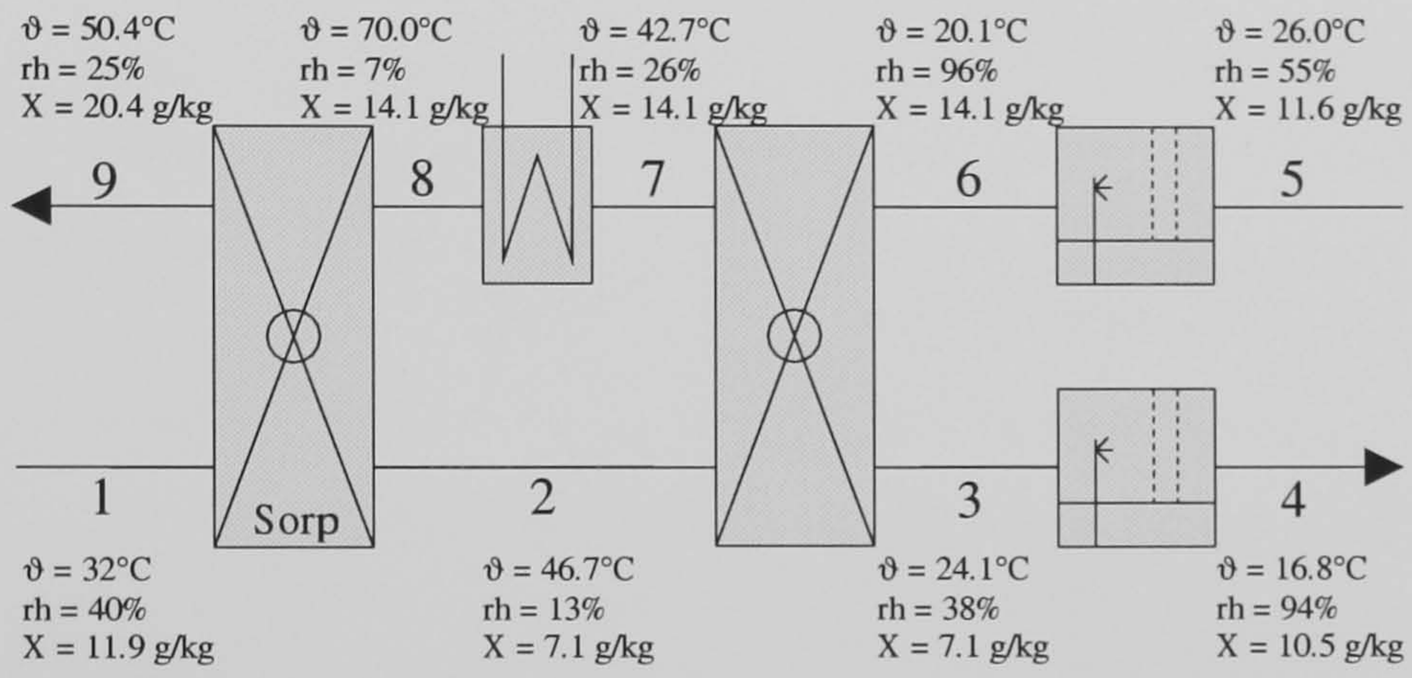

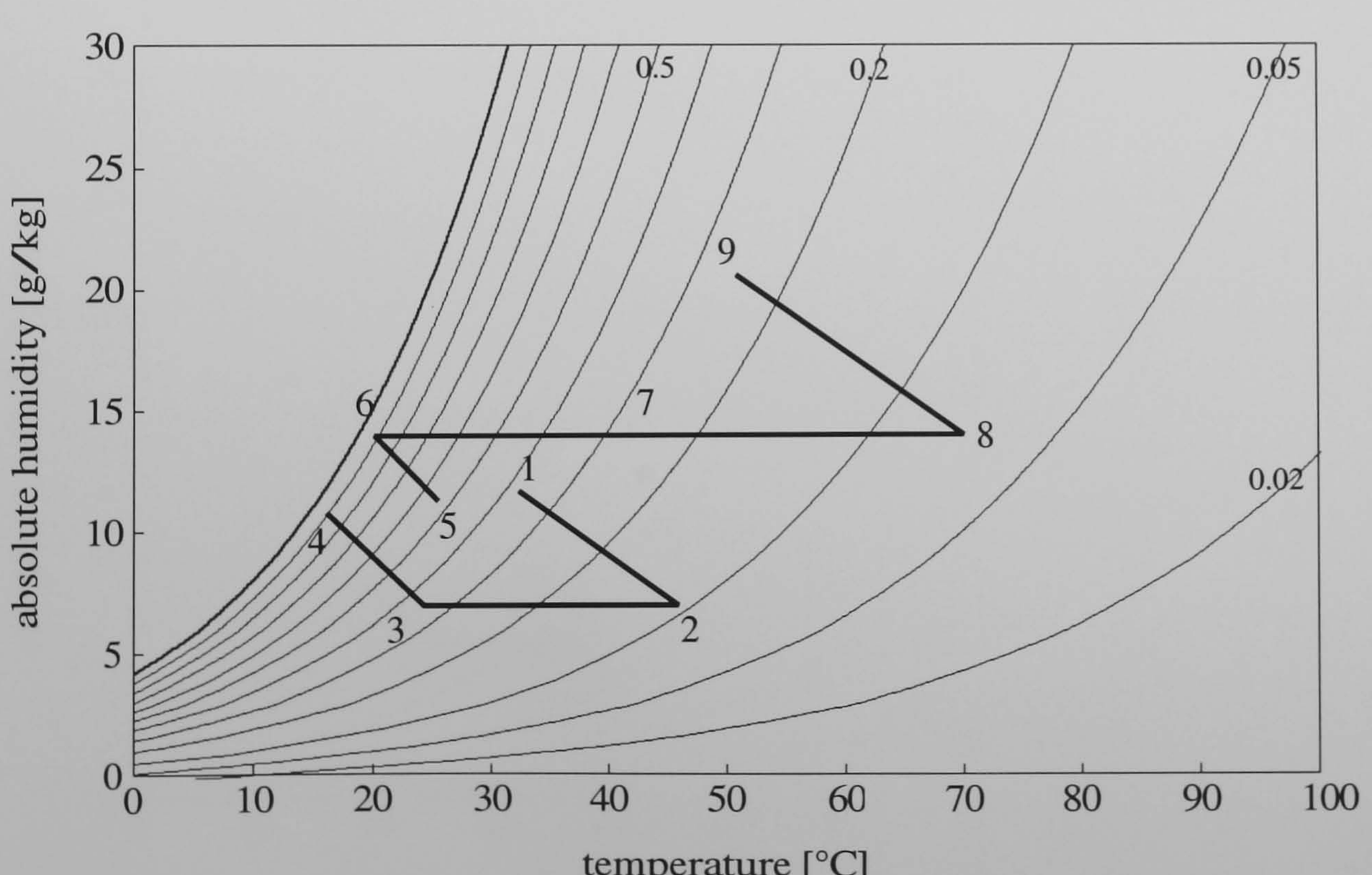

Figure 2.5: Example of air conditions in a desiccant cooling ventilation cycle for normative conditions of Germany and a regeneration temperature of 70 °C

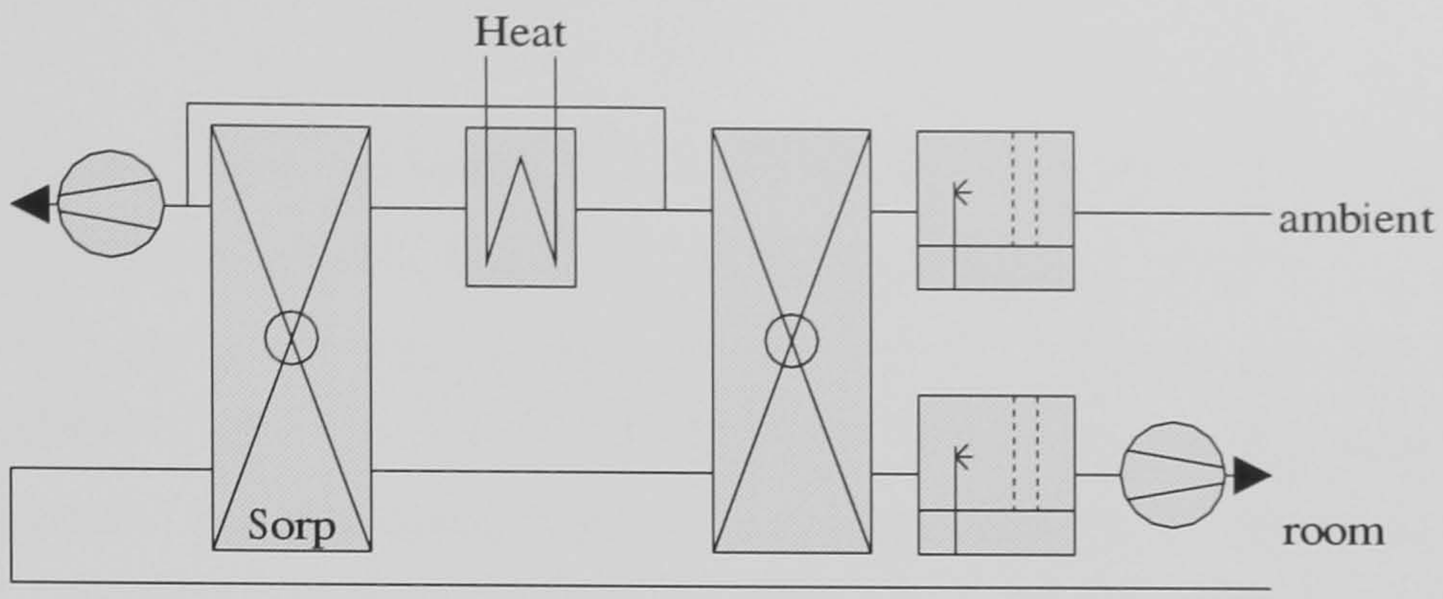

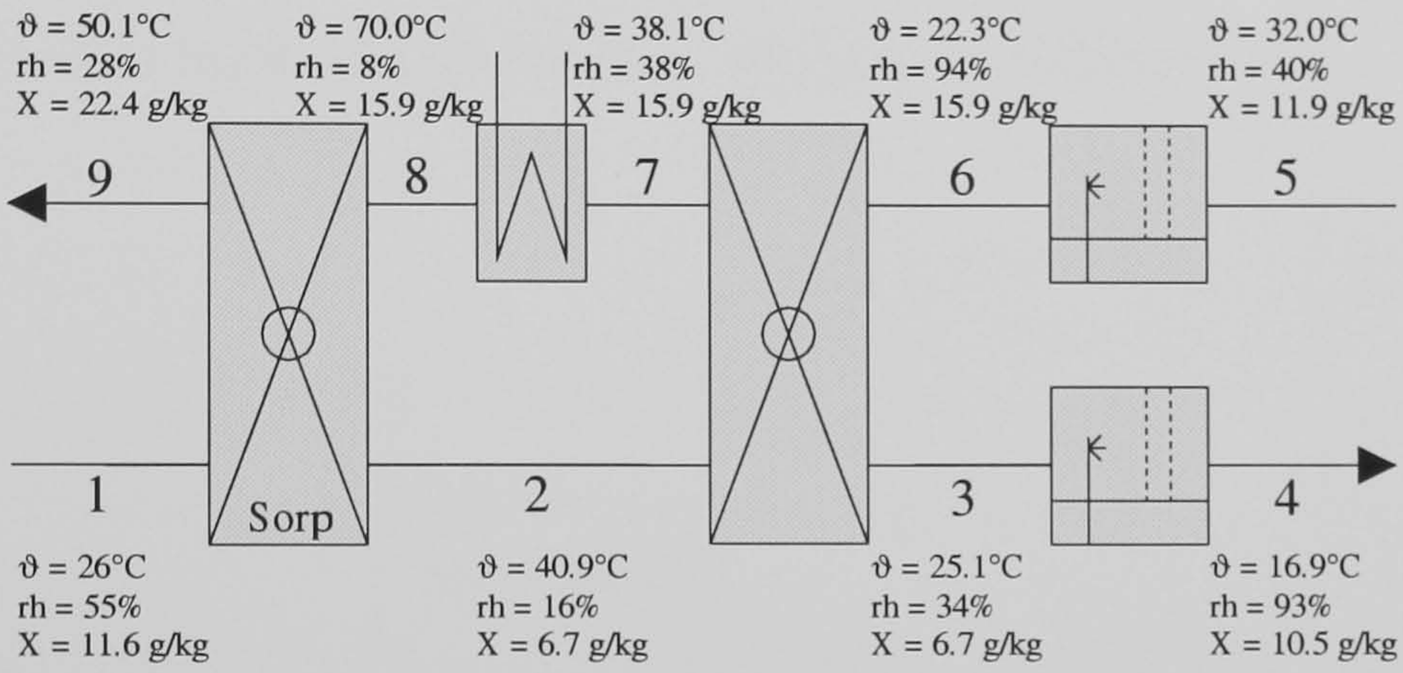

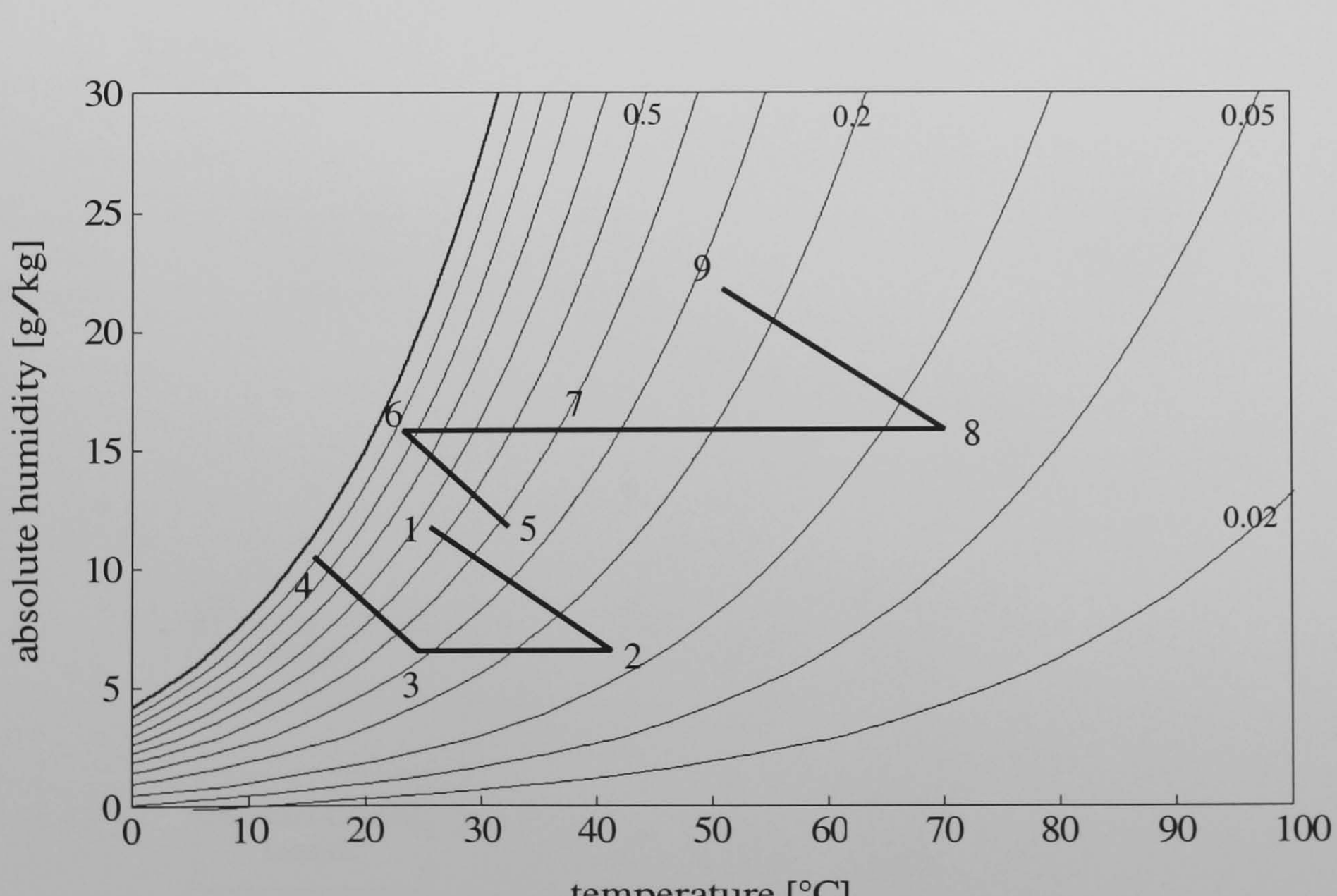

Figure 2.6: Example of air conditions in a desiccant cooling recirculation cycle for normative conditions of Germany and a regeneration temperature of 70 °C

2.7 Application of Solar Energy in Cooling Processes

A main argument for solar cooling is that the cooling demand is often correlated with the irradiation, for example in buildings with large glazing areas. Furthermore, the peak cooling demand often occurs during hours of high irradiation, for example in non–domestic buildings like offices. Hence it is sensible that the use of solar energy should be considered for cooling purposes. All the cooling processes described above can be classified as electrically driven processes, heat transformation processes or thermomechanical processes. Each of these can be supplied with solar energy. Figure 2.7 gives an overview made by ERPENBECK 1999. In the following the electrically powered cooling systems using photovoltaic and thermomechanical systems will not be considered.

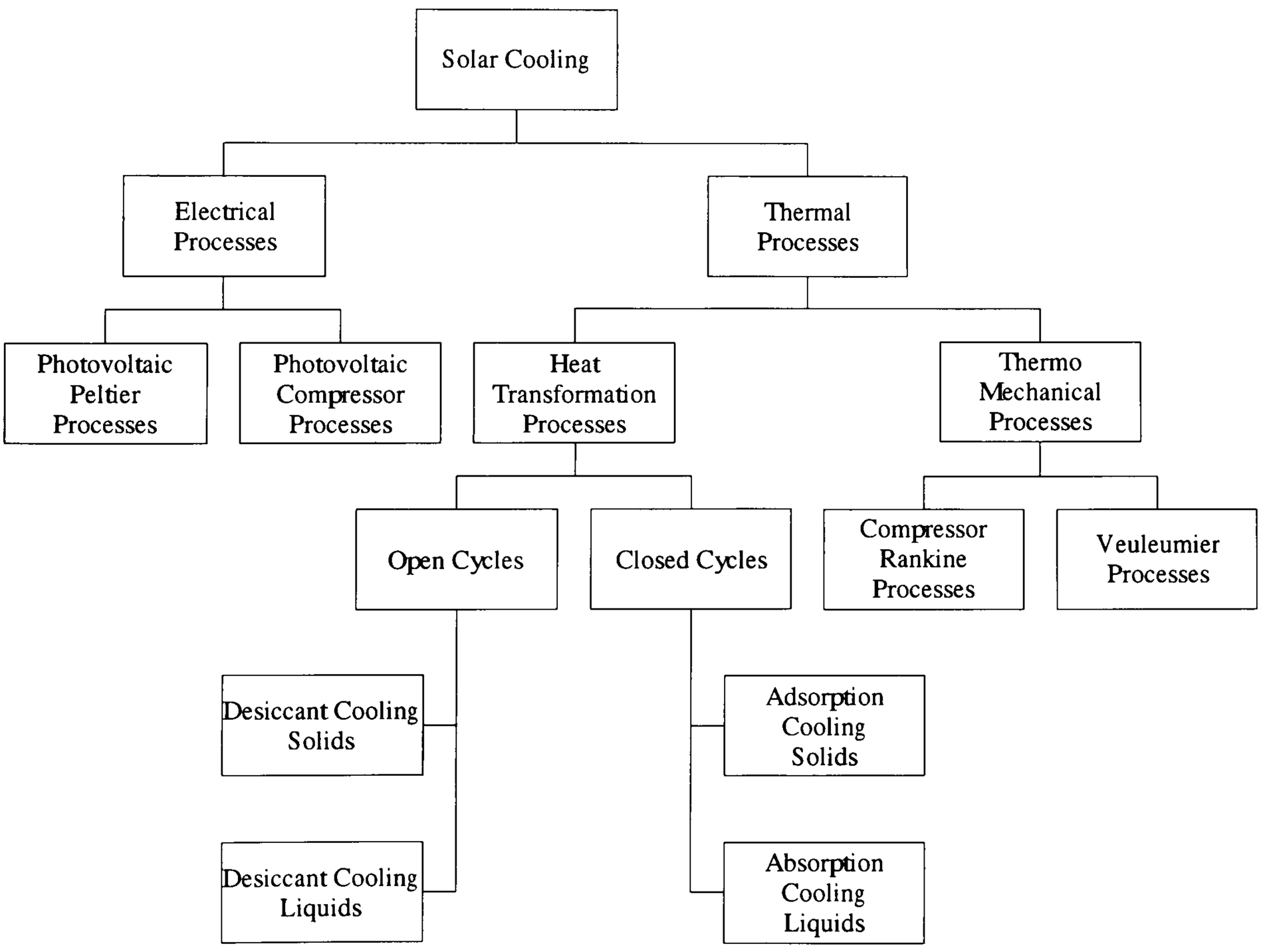

Figure 2.7: A survey of solar cooling systems by ERPENBECK 1999

Collectors appropriate for solar cooling and solar air conditioning are available. The main differences compared to the use in warm water systems are the higher temperature requirements. In principle it is necessary to strive for low collector temperatures to obtain high efficiencies. Desiccant cooling systems require the lowest driving temperatures. These temperatures, which are in the range of 45 °C to 95°C, can be obtained with flat–plate collectors. Because the desiccant cooling system is a complete air handling unit. it is also possible to use solar air collectors. They can reach a regeneration temperature comparable to that of liquid flat–plate collectors in which an additional heat exchanger is necessary to heat the regeneration air. In adsorption cooling systems the same liquid collector technology can be used as in desiccant cooling systems. Absorption cooling systems require higher temperatures in the range of 110 °C to 150 °C, which can only be provided by sophisticated collector technology such as vacuum–tube collectors. When using solar driven absorption systems, it is necessary to optimise the desired cooling system and the solar system together. This is indispensable, because high COPs can only be reached with high temperatures and, on the other hand, the efficiencies of solar collectors decrease with increasing fluid temperatures.

Large collector areas are necessary to cover the heat requirement of solar cooling systems. Hence it is useful to replace walls and roofs by active solar components to decrease costs for the additional solar installations. With the construction of collector facades or collector roofs, large areas could be used to gain heat for the solar cooling processes. Particularly for the desiccant cooling systems and the adsorption cooling systems, where the lowest regeneration temperatures are needed, the building integration of flat–plate solar collectors seems to be realisable. By using solar air collectors such facades and roofs should be easy to realise. These collector facades could be constructed with common double facade technology. A sophisticated technology is the construction of glazed double facades with photovoltaic systems. Using the gap as an air collector, the photovoltaic elements are cooled and their electrical efficiency increases. Furthermore, the cooling load of the building decreases, as the surface temperature on the inside of the glazing is lower than in the case of a stagnant air layer. One such pilot project is the Mataro library near Barcelona. A description of the building integration and the calculation of the thermal performance is provided in EICKER ET AL. 1998.

2.8 Comparison of Cooling Technologies

BEHNE 1997 investigated alternatives to compressor cooling systems in office buildings in different climates. Absorption cooling systems and desiccant cooling systems (Figure 2.5) driven by gas or district heating were considered. He showed that for each climate an economical and an energy saving alternative to compressor cooling systems can be found. BEGGS and WARWICKER 1998 give values of 14% to 50% of energy cost savings and savings of CO_2–emissions under climatic conditions representative for Central Europe for the use of desiccant cooling systems instead of compressor cooling systems. BUSWEILER and GÖBEL 1997 describe that the investments for desiccant cooling systems are in the same range as for conventional cooling systems with compression chillers. Furthermore, the main economic advantage occurs in the reduction of running costs.

HEINRICH and FRANZKE 1997 compared different cooling technologies concerning their energetic performance. In Table 2.1 the results of the investigation are listed. HENNING ET AL. 1998 considered the use of solar energy in desiccant cooling systems, absorption cooling systems and adsorption cooling systems. They calculated for the climatic conditions of Freiburg in Germany that above a solar fraction of 20%, single–effect absorption cycles and desiccant cooling systems lead to savings of primary energy compared to conventional air conditioning systems with compression chillers and heat recovery. Adsorption chillers lead to an energy saving potential above a solar fraction of 30%. Having solar fractions of 90%, savings of 60% with desiccant cooling systems and 70% with absorption and adsorption cycles can be achieved.

Considering all these aspects, the desiccant cooling systems seem to be the most attractive for the application of solar thermal energy. Under ecological aspects they are easy to handle, because they contain no toxic substances. Furthermore, they are economically attractive, because the investment costs are already close to those of conventional air conditioning systems providing dehumidification, heat recovery and humidification.

Table 2.1: Comparison of different cooling technologies by HEINRICH and FRANZKE 1997

	driving mechanism	COP	COP_p primary energy
compression chiller for cooling, dehumidification and postheating	electric	3 – 4	≈ 0.6
compression chiller for cooling, dehumidification in co–generation	electric	3 – 4	≈ 1.2
single–effect absorption chiller for cooling, dehumidification and postheating	heat 85 °C – 180 °C solar thermal energy [1]	0.7	≈ 0.4
adsorption chiller for cooling, dehumidification and postheating	heat 55 °C – 95 °C solar thermal energy [1]	0.6	≈ 0.35 [2]
desiccant cooling system	heat 45 °C – 95 °C solar thermal energy [1]	≈ 0.8	≈ 0.75
desiccant cooling system in co–generation with compression chiller	heat, electric 45 °C – 95 °C solar thermal energy [1]	4 – 5	>1.6

[1] Solar thermal energy not considered in the calculation of the primary energy COP_p

[2] estimated value

Chapter 3

Theory of Sorption in Desiccant Cooling Systems

In the following chapter the theory of adsorption on solid desiccants will be described in general. In particular the effect of a temperature increase during the adsorption process and the influence on the potential of dehumidification will be discussed. Furthermore, models of rotating dehumidifiers will be presented.

3.1 Theory of Adsorption and Desorption

Sorption is the comprehensive term for all processes in which a substance is selectively bound by another substance. The substance picked up is called sorbat (usually in gas or liquid phase) and the substance picking it up is called sorbent (usually in liquid or solid phase). Gas molecules can be adsorbed to a surface due to the interaction between the gas and the molecular forces of the solid. This surface absorption is called adsorption and leads to an enrichment of one or more components in an interfacial layer on solid surfaces. In contrast to the adsorption, the absorption always results in a dilution of the absorbing substance. Due to this terminology the terms of absorbent and absorbate, adsorbent and adsorbate are used respectively in this thesis.

When adsorbed molecules gain enough energy, they can leave the surface by overcoming the activation energy. This activation energy can be reached by increasing the tempera-

ture of the adsorbed molecules.

A common adsorbent is silica gel, which gives in an unsaturated condition according to WILLMES 1992, a partial vapour pressure for water of only 0.001 $Torr$ or 0.13 Pa. This corresponds to the drying potential of a concentrated sulphuric acid. As, for example, described in HOLLEMANN, WIBERG 1995 and ATKINS 1988, silica gel is an amorphous substance consisting of an irregular three–dimensional network of SiO_2 tetrahedrons carrying hydroxyl groups. Pores arise by connections of the polysilica gel particles via oxygen. The dimensions depend on the size of the particles and of its packing density. According to JOKISCH 1975 the pores have a large active surface in the range of 500 m^2/g. The bonding of water onto the hydroxyl groups of silica gel (chemical sorption) is shown in the schematic in Figure 3.1. The further adsorption in additional layers occurs by van der Waal's forces (physical sorption) which are the decisive driving force for decreasing the vapour pressure.

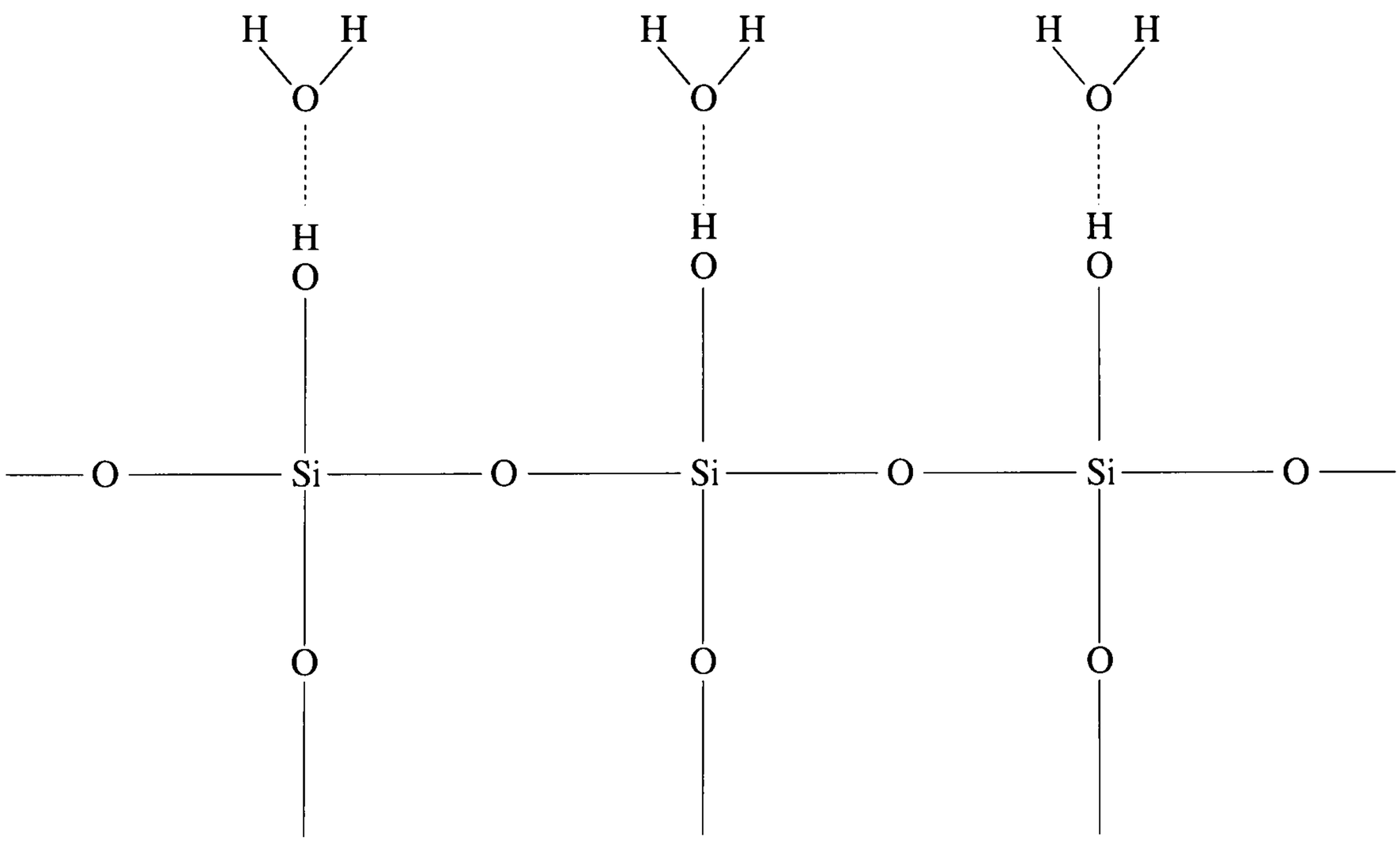

Figure 3.1: Schematic of the chemical sorption on the surface of silica gel

The most common way to characterise adsorption systems is the use of sorption isotherms as shown in Figure 3.2 for the example of the sorption pair water and silica gel. By plotting the sorption isotherms against the absolute humidity the dependence on temperature

is shown (Figure 3.2a). Using the relative humidity for the abscissa leads to a merging of all plots (Figure 3.2b).

For the analytical description lying behind these curves some theoretical models such as based on Langmuir and BET theory are available; these are described in KRISCHER and KAST 1978. Langmuir developed a model in which a monomolecular allocation is considered on smooth surfaces up to the densest allocation of molecules in one layer. Instead of the number of molecules, it is possible to use the water content X_S and the Langmuir equation can be written as

$$X_S = \frac{X_{S,max} \cdot c \cdot X}{1 + c \cdot X} \tag{3.1}$$

where c is a material dependent dimensionless constant describing the bond energy of the first layer and $X_{S,max}$ the maximum adsorbate content of the monomolecular layer. This constant c can be calculated from the general gas constant R, the bond enthalpy h_B and the absolute temperature

$$c = v \cdot \exp\left(\frac{h_B}{R \cdot T}\right). \tag{3.2}$$

BUSWEILER 1984 uses a value of 1 for the parameter v. After filling all the free spaces in the first monomolecular layer, additional layers n will be adsorbed at higher vapour pressures. The BET theory of BRUNAUER, EMMET and TELLER 1938 results in

$$X_S = X_{S,max} \cdot \frac{c \cdot X}{1 - X} \cdot \frac{1 - (n+1) \cdot X^n + n \cdot X^{n+1}}{1 + (c-1) \cdot X - c \cdot X^{n+1}}. \tag{3.3}$$

At low vapour pressures the sorbent isotherms have a shape which is equal to the Langmuir isotherm and give the impression that saturation exists. At higher vapour pressures the curvature changes and the water content increases. This can be interpreted as multi–layer adsorption.

The adsorption of gas molecules on solid surfaces causes the evaporation enthalpy to be released which leads to a temperature increase. In addition to the evaporation enthalpy, which depends on the properties of the adsorbed gas, the bond enthalpy, which depends on

the properties of the adsorbent, is also released. This bond enthalpy obviously depends on the number of gas molecules already adsorbed, so it is necessary to have a concentration dependant bond enthalpy. KAVIANY 1991 gives an overview of the phenomena. The differential bond enthalpy can be calculated using the Clausius–Clapeyron equation

$$h_{\mathrm{B}} = -R \cdot \frac{\partial \ln P}{\partial \frac{1}{T}} \tag{3.4}$$

which shows the interrelation between the vapour pressure function P and the bond enthalpy h_{B}. The relation of bond enthalpy as a function of water content is shown in Figure 3.3a after GUTERMUTH 1980. For the application of water adsorption, which is part of this work, the evaporation enthalpy is given in Figure 3.3b. According to POLANYI 1916 and KAST and JOKISCH 1972 the bond enthalpy for higher water contents is given by

$$h_{\mathrm{B}} = -R \cdot T \cdot \ln(rh) \tag{3.5}$$

where rh is the relative humidity. This equation is a special case of the Clausius–Clapeyron equation and is not valid for very low water contents, because the adsorbed molecules do not cover the surfaces of the adsorbens uniformly. The sorption enthalpy h_{S}, which is the heat released by the sorption process, is the sum of the evaporation enthalpy h_{E} and the integral bond enthalpy h_{B}.

$$h_{\mathrm{S}} = h_{\mathrm{E}} \cdot (X_0 - X_1) + \int_{X_1}^{X_0} h_{\mathrm{B}}(X) dX \tag{3.6}$$

For the calculation of the kinetics of adsorption a knowledge of the exact value of the differential adsorption enthalpy is not decisive in most cases. The evaporation enthalpy

$$h_{\mathrm{E}} = 2501 \frac{kJ}{kg} - 2.4 \cdot \vartheta \tag{3.7}$$

shown in Figure 3.3b is approximately ten times greater then the bond enthalpy also shown in Figure 3.3a. Hence it is appropriate to use, according to BUSWEILER 1984, a mean value of around $h_{\mathrm{B}} = 250 kJ/kg$.

After a change in the vapour pressure concentration in the environment of an adsorbens. the adsorption can be described with the following steps (Figure 3.4):

1. Overcoming the mass transfer resistance of the interfacial layer
2. Mass transfer within the adsorbent
3. Adsorption on the inner surfaces resulting in a temperature increase
4. Heat conduction to the surface
5. Heat transfer from the surface to the environment

Desorption tests by EICHENGRÜN 1993 with zeolithe and by UHLMANN 1976 and BUSWEILER 1984 with silica gel have shown that the velocity of desorption is higher than the velocity of adsorption. Two theories are available to explain this sorption hysteresis. The first theory describes the hysteresis by assuming different angles of contact in pores with capillary condensation. In the second theory, also described by DREHER 1979 , the assumption is that capillary condensation takes place in micropores which are placed in front of macropores while these are still filled with vapour. This phenomena is called the ink–bottle–effect. So the adsorption process will be slowed down. During desorption the macropores are filled with liquid water at the same vapour pressure and the desorption process will not be delayed. However, neither theory is able to provide a quantitative prediction.

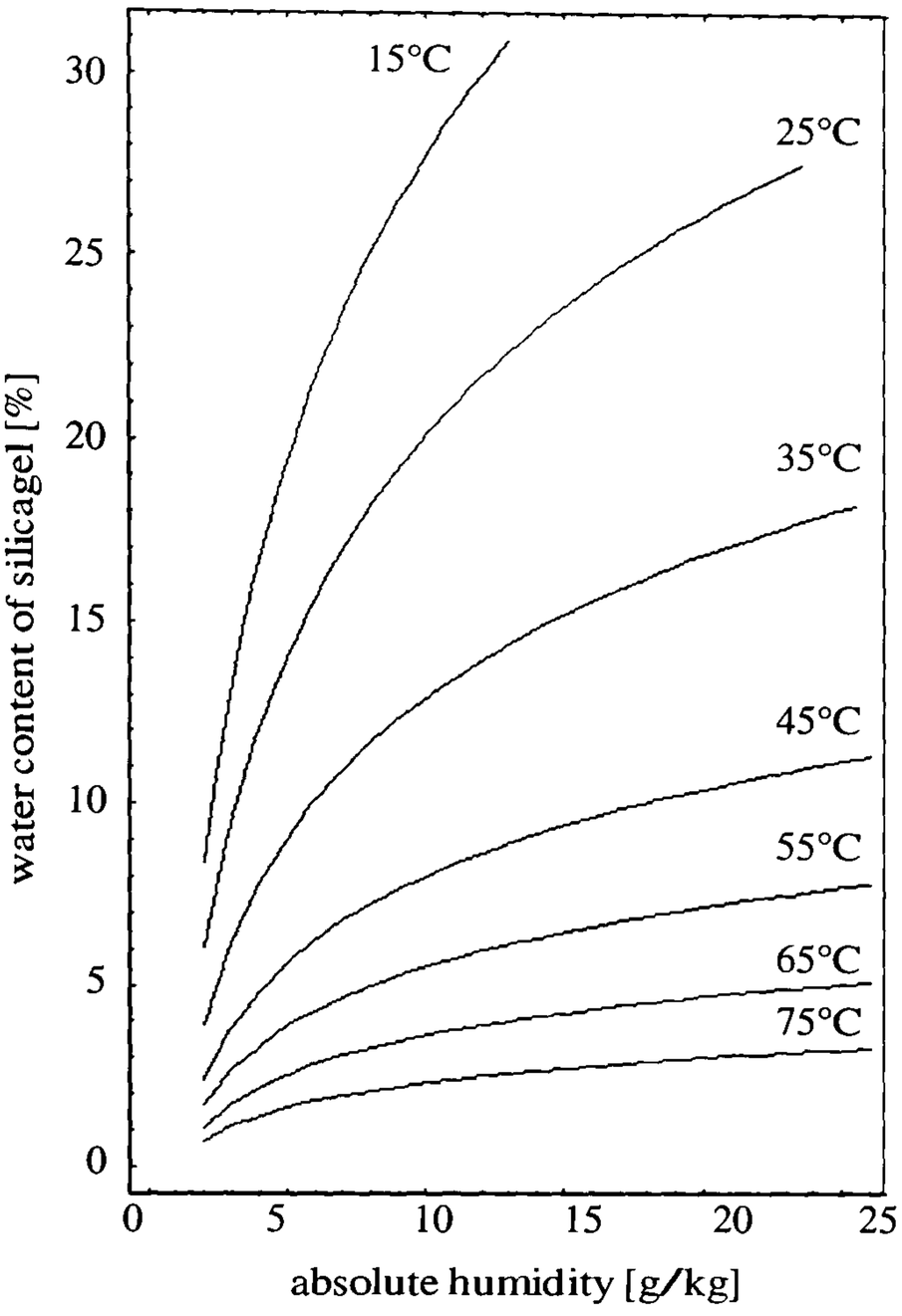

Figure 3.2a: Sorption isotherms of silica gel dependent on absolute humidity and temperature after KRISCHER and KAST 1978

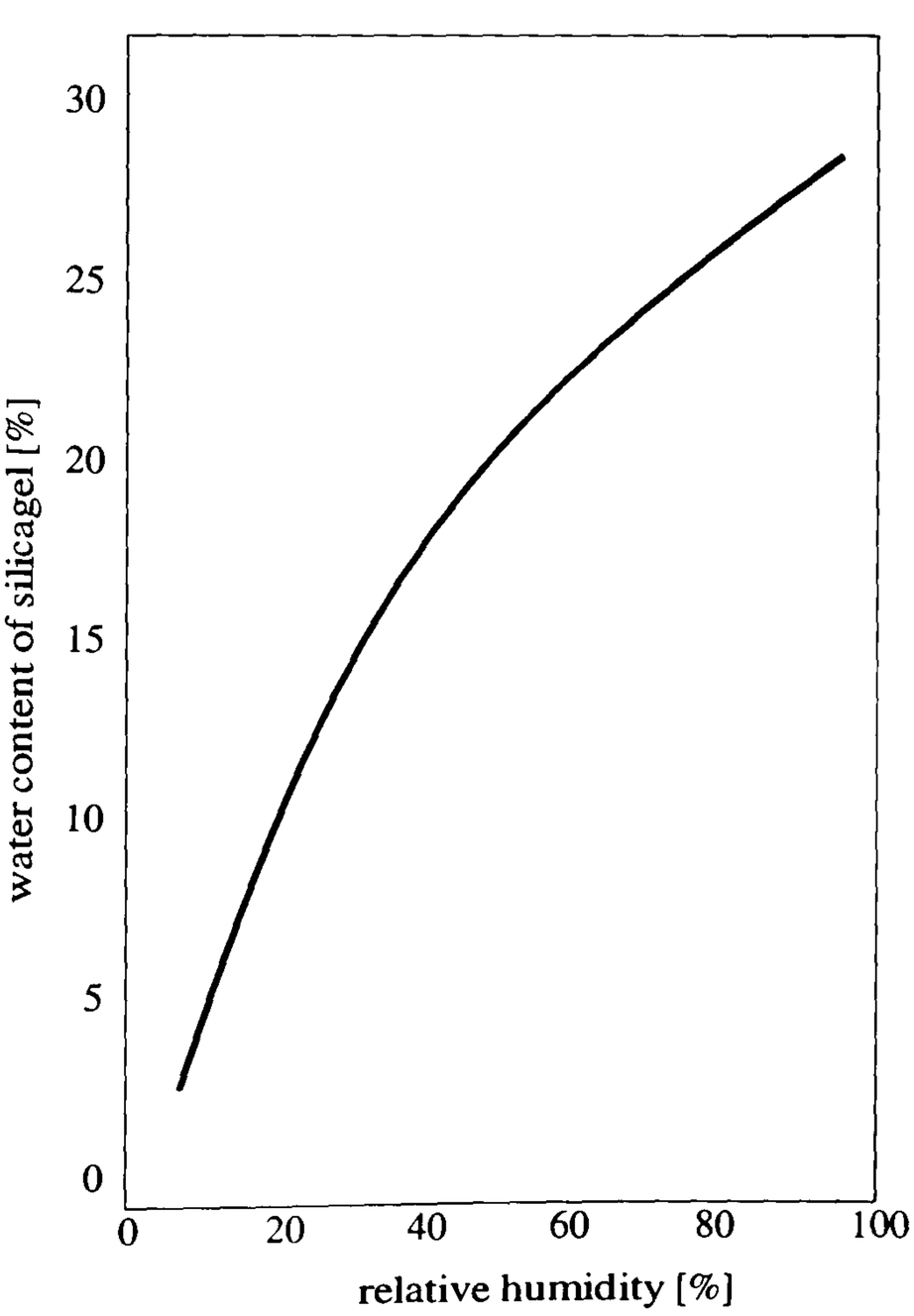

Figure 3.2b: Sorption isotherms of silica gel dependent on relative humidity

Figure 3.2: Sorption isotherms of the Langmuir type of silica gel

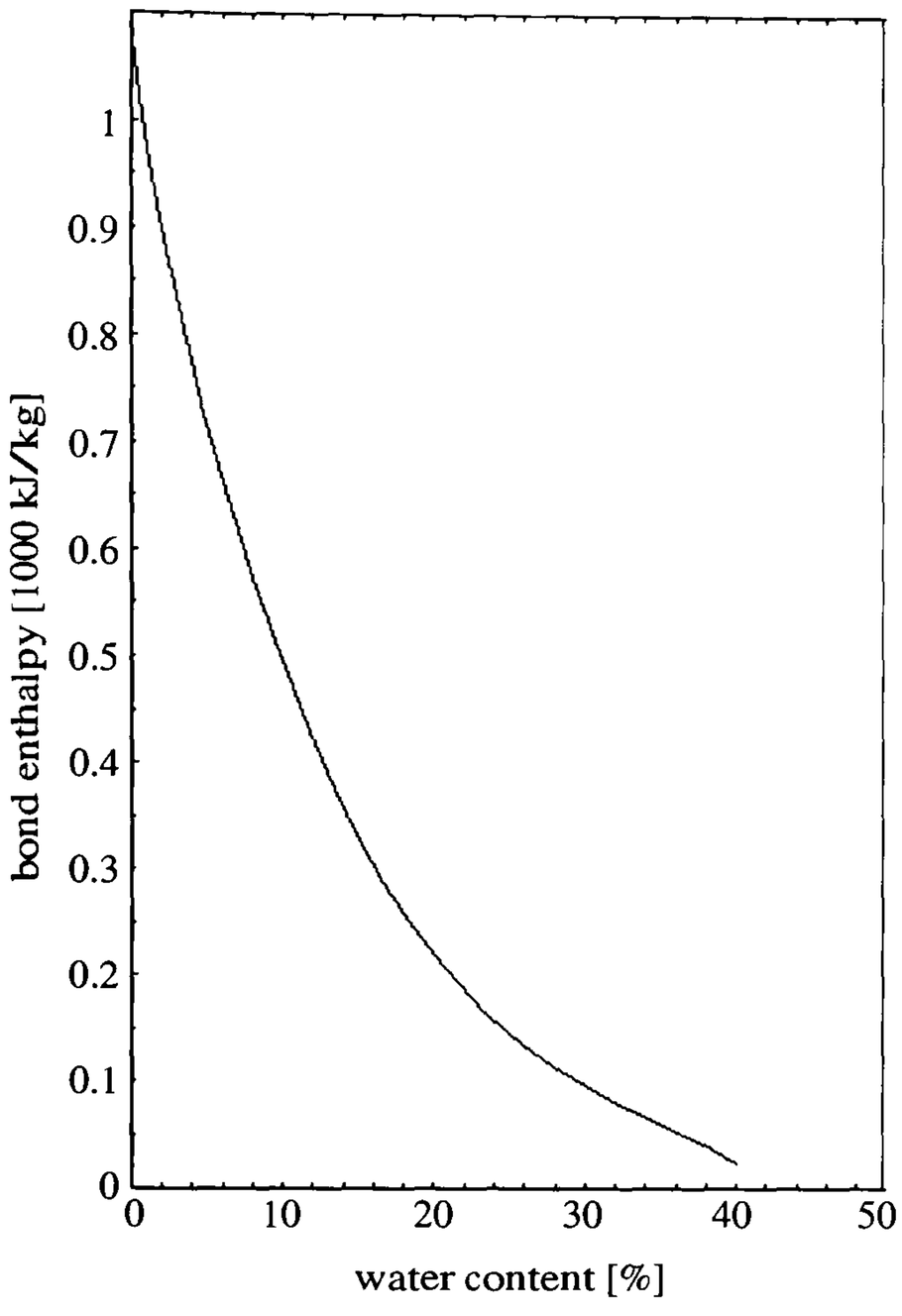

Figure 3.3a: Bond enthalpy dependent on water content after GUTERMUTH 1980

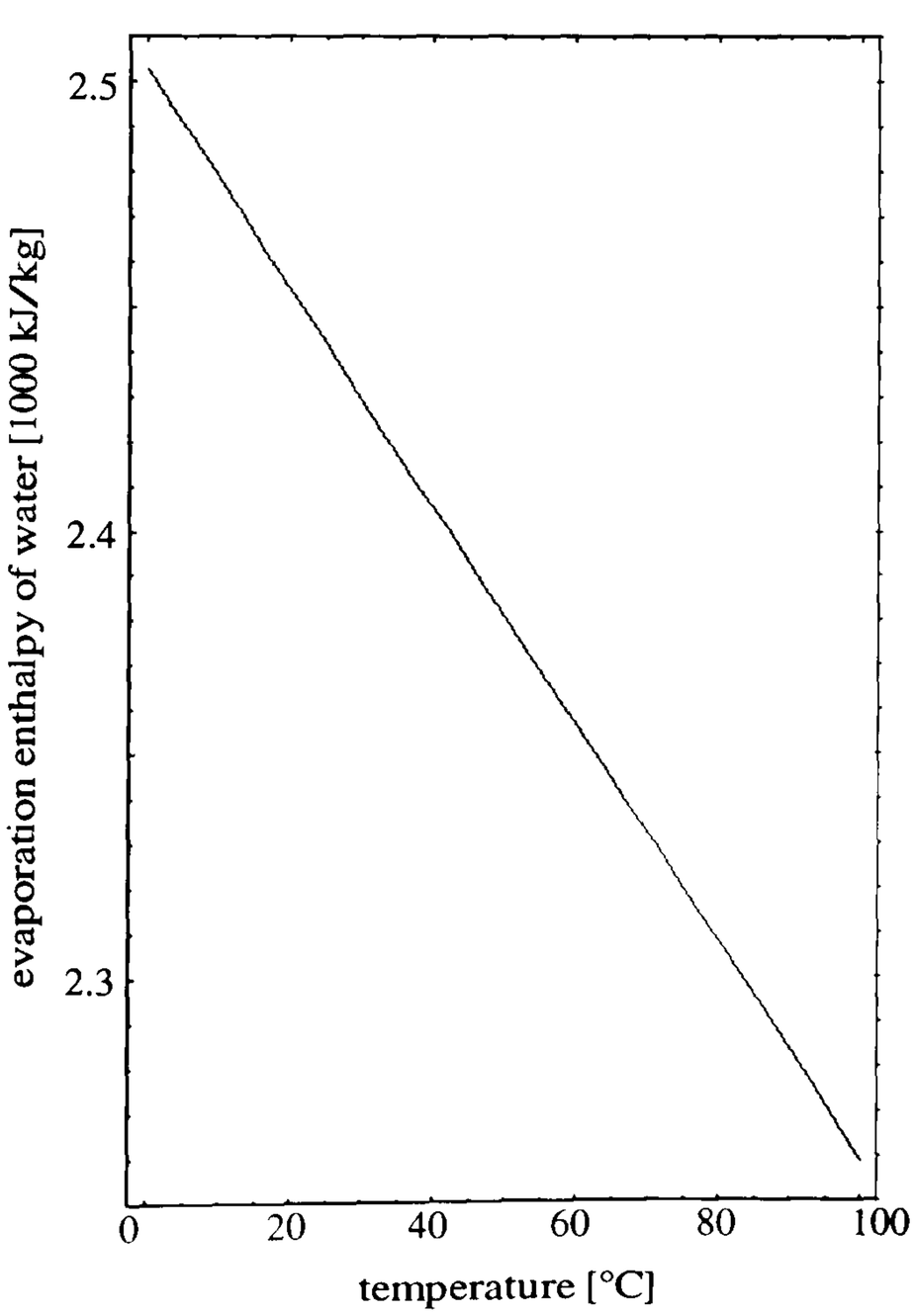

Figure 3.3b: Evaporation enthalpy of water dependent on temperature after KRISCHER and KAST 1978

Figure 3.3: Bond enthalpy and evaporation enthalpy

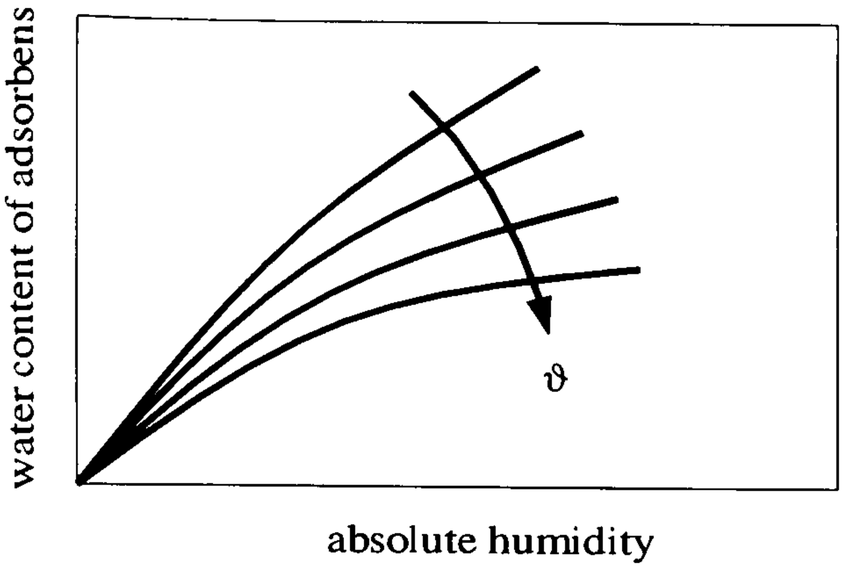

Figure 3.4a: Sorption isothermes of an adsorbent

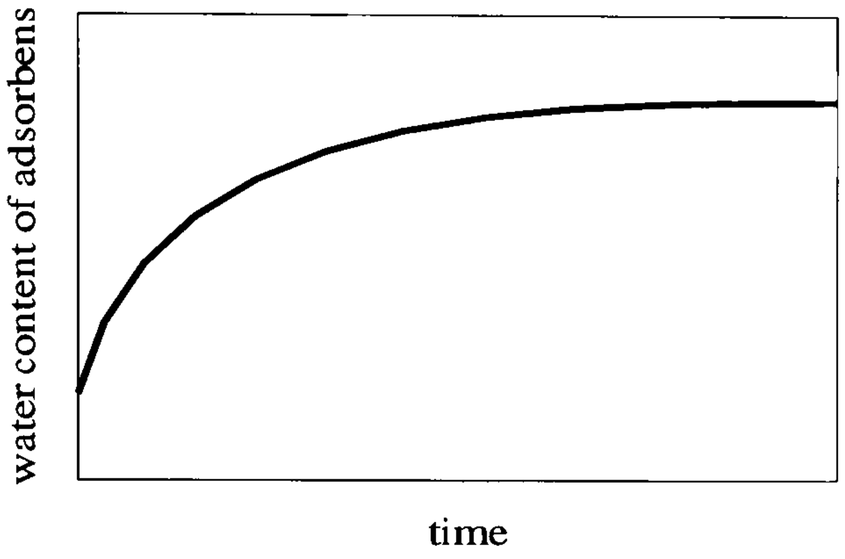

Figure 3.4b: Progress of water content in the adsorbent

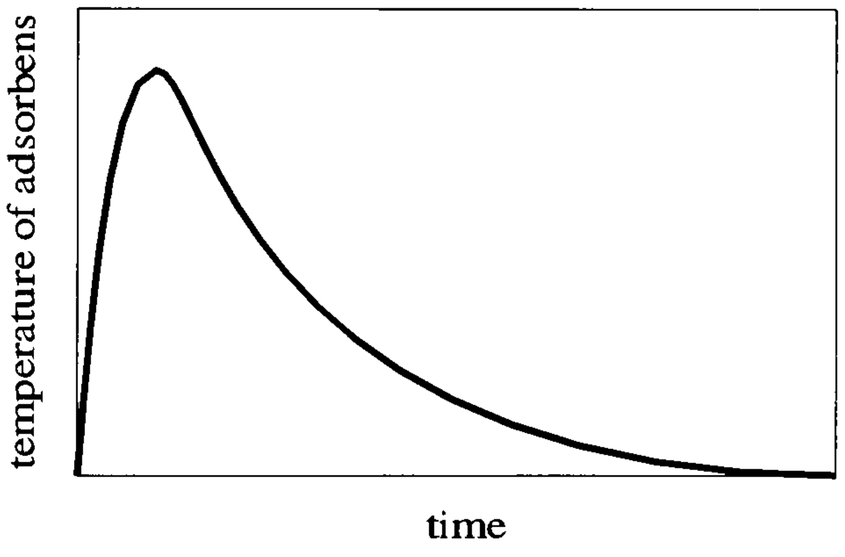

Figure 3.4c: Progress of temperature in the adsorbent

Figure 3.4: Adsorption after a change of concentration in the environment of an adsorbent

3.2 Theory of Rotating Dehumidifiers

Rotating heat and mass regenerators consist of a revolving porous matrix through which two physically separated air streams pass in counterflow (Figure 3.5). The porous matrix is usually made by winding a thin sheet or ribbon of a material on a hub. In general, rotating heat and mass regenerators may be asymmetrical with different flow areas for each air stream and with unequal air flows in each air stream. A rotating heat and mass regenerator can be designed as a sensible heat regenerator, as an enthalpy exchanger for sensible and latent heat recovery, or as a dehumidifier. The physical properties of the porous matrix largely determine the performance characteristics of the regenerator. Sensible heat regenerators require a non–hygroscopic matrix with a large heat capacity. Dehumidifiers, in which maximum moisture transfer is to be gained, utilise an adsorbent matrix with a large moisture but a small heat capacity. Enthalpy exchangers, in which both mass and heat transfer are desired, employ an adsorbent matrix with a large moisture and heat capacity. In desiccant cooling systems, rotating dehumidifiers are used in which a carrier material is coated or soaked with a desiccant.

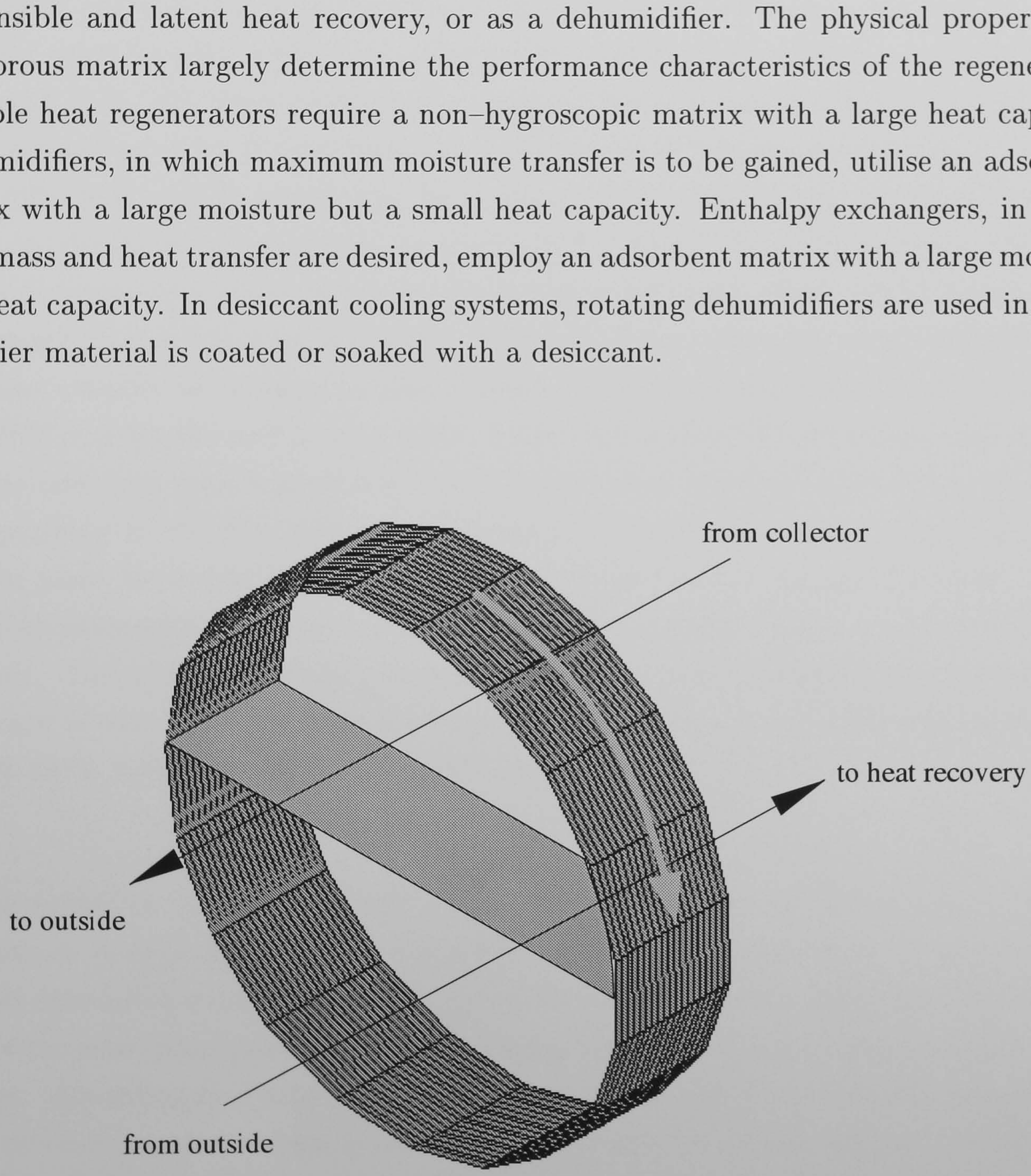

Figure 3.5: Schematic of a rotating dehumidifier

In the case of equal air flows in the process and the regeneration section of the regenerator with a hygroscopic matrix rotating at a high speed (around 10 revolutions per minute)SPAHN and GNIELINSKI 1971 provide an equation to calculate the maximum possible enthalpy exchange

$$\eta_{\mathrm{h}} = \frac{1}{1 + \frac{2 \cdot \Psi \cdot v \cdot \rho_{\mathrm{A}}}{\delta \cdot \omega \cdot l}}. \tag{3.8}$$

where Ψ is the porosity of the matrix, v the velocity of the air, ρ_{A} the density of the air, δ the mass transfer coefficient, ω the specific surface of the enthalpy exchanger and l the length of it. The main function of a dehumidifier is to reduce the absolute humidity of the process air flow. To calculate the performance of rotating dehumidifiers, detailed finite difference models considering heat and mass transfer in the hygroscopic matrix have been developed, for example, by MACLAINE–CROSS 1974. These models, which are further developments of the theory of adsorption bed systems, describe the mass transfer via convection and the inner resistance of the adsorbens. An analysis of combined heat and mass transfer by analogy to heat transfer alone has been developed by BANKS ET AL. 1970 and BANKS and CLOSE 1972. They showed that the governing equations for a rotary heat and mass regenerator can be transformed into two independent potentials corresponding to the heat transfer calculation. The potentials for the heat and mass transfer must be derived from the properties of the applied storage materials. These potentials determine the outlet conditions with characteristic curves on the psychrometric chart. The advantage is the calculation of heat recovery, dehumidifier and enthalpy exchanger in one model. In these investigations of BANKS ET AL. 1970 and BANKS and CLOSE 1972, silica gel was mainly used as adsorbent.

For the modelling of whole desiccant cooling systems in which the dehumidifiers are only elements, it is appropriate to use simplified models. The calculation of the maximum possible dehumidification will depend only on the thermodynamic properties. The driving force of the adsorption process is the difference of vapour pressure between the air and the sorbens. According to PFEIFFER 1986 the process air can be maximally dehumidified down to rh = constant which is marked by the condition of the regeneration air. The derivation is given in the following implicit equation considering the ratio of the saturation vapour pressures in the regeneration and process part and must be solved numerically with

$$\Delta X_{\mathrm{P}} = X_{\mathrm{P}} - X_{\mathrm{R}} \cdot \left(\frac{P_{\mathrm{S}} \left(\vartheta_{\mathrm{R}} + \Delta X_{\mathrm{P}} \cdot \frac{h_{\mathrm{S}}}{c_{\mathrm{p}}} \right)}{P_{\mathrm{S}} \left(\vartheta_{\mathrm{P}} \right)} \right)^{\frac{h_{\mathrm{S}}}{h_{\mathrm{E}}}} . \tag{3.9}$$

In this equation of Pfeiffer, X_{P} represents the absolute humidity in kg/kg of the process air, X_{R} the absolute humidity of the regeneration air and ΔX_{P} the dehumidification. P_{S} is the saturation pressure, h_{S} the sorption enthalpy and h_{E} the evaporation enthalpy. HENNING 1993 and ERPENBECK 1999 suggested a model on the basis of the considerations of LÄVEMANN and SIZMANN 1992 and KAST 1988 in which the calculation must be solved along the sorption path. This method illustrated in Figure 3.6 is known as the intersection method and was first presented by JURINAK 1982. Here it is necessary to evaluate the changes of enthalpy of the air passing through the dehumidifier. The sorption path can be written as

$$h_{\mathrm{out}} = h_{\mathrm{in}} + \int_{rh_0}^{rh_1} h_{\mathrm{S}}(X) dX = h_{\mathrm{in}} + h_{\mathrm{E}} \cdot (X_1 - X_0) + \int_{rh_0}^{rh_1} h_{\mathrm{B}}(X) dX \tag{3.10}$$

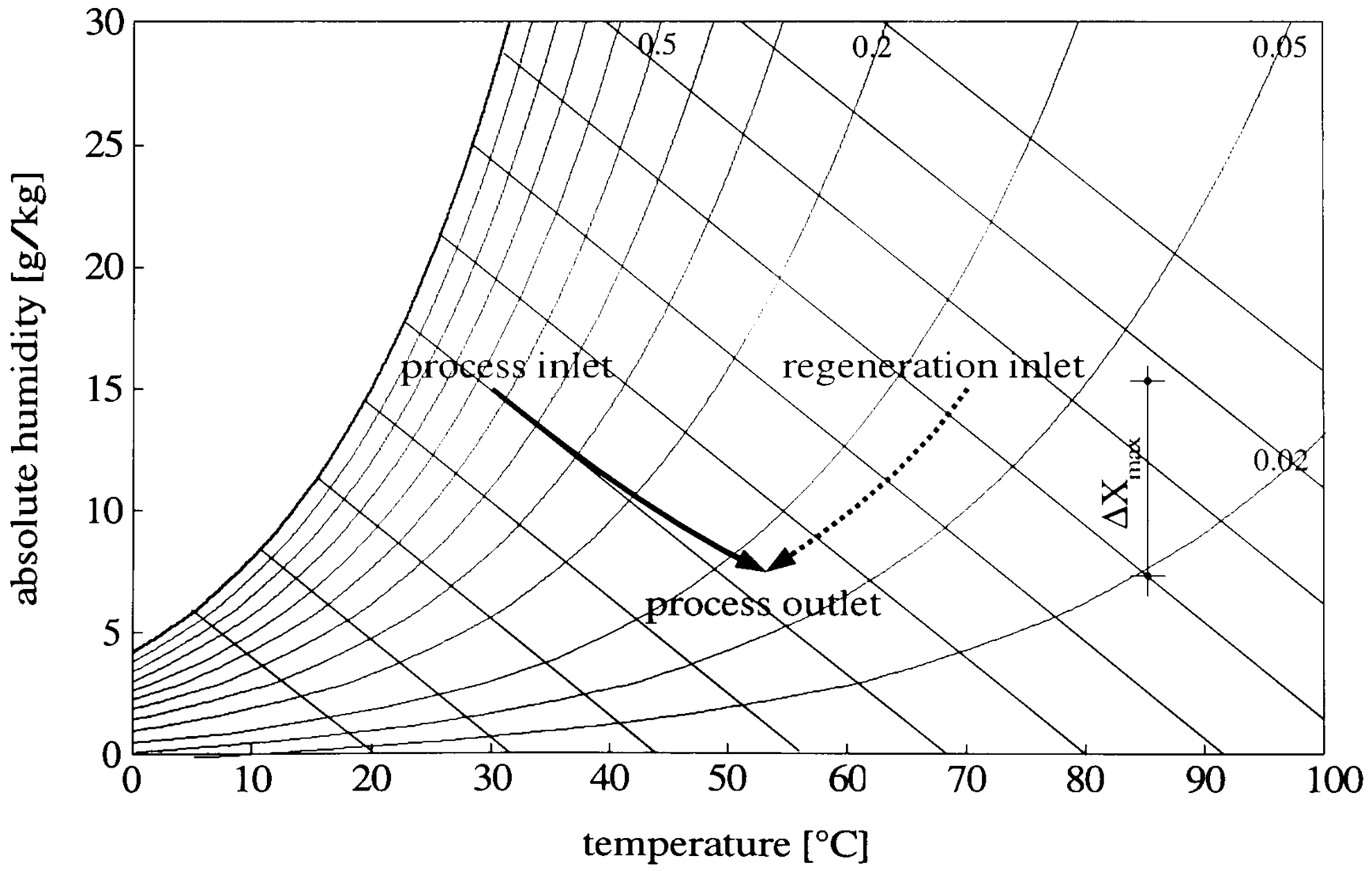

Figure 3.6: Determination of the maximal possible dehumidification of a rotating dehumidifier in a psychrometric chart with the intersection method

The sorption path in equation 3.10 can only be specified by the material–dependent differential bond enthalpy h_B. This sorption path is ideal because all the irreversibilities of a real process are ignored. Irreversibilities are, for example, the transfer of heat. The dehumidification efficiency η_{sorp} defined by HENNING 1993 and ERPENBECK 1999 describes the ratio of the real dehumidification to the maximum possible dehumidification. The maximum possible dehumidification must be calculated from the inlet conditions of both the process and regeneration air stream. With the equations 3.9 and 3.10 the maximum possible dehumidification can be calculated. For the technical application a dehumidification efficiency η_{sorp} must be introduced to consider all irreversibilities of the dehumidification process in real dehumidifiers. This dehumidification efficiency defined in 3.11 depends on the rotation speed of the dehumidifier and on the speed of the air passing the process and the regeneration section of the wheel.

$$\eta_{\text{sorp}} = \frac{X_{\text{P,in}} - X_{\text{P,out}}}{\Delta X_{\text{max}}} \tag{3.11}$$

FRANZKE 1989 asserts that the mass transfer is 87% determined by convection and the heat transfer is completely dependent on convection. The radiative heat transfer can be ignored because the adsorbens is only in a radiative exchange with an adsorbens of the same temperature. Based on this, only the convective part of heat and mass transfer need to be considered. Because the heat and mass transfer in rotating dehumidifiers is mainly influenced by heat transfer, the heat transfer mechanism is investigated in greater detail below.

Starting from the heat balance in a tube, the length–dependent heat transfer resistance $R_{\text{L,h}}$ can be calculated from

$$R_{\text{L,h}} = \frac{\frac{1}{r_1 \cdot h} + \frac{1}{\lambda} \cdot \ln \frac{r_2}{r_1}}{2\pi} \tag{3.12}$$

where r_1 is the inside radius of the tube and r_2 the outside radius, h the surface heat transfer coefficient and λ the heat conductivity. The mass transfer resistance $R_{\text{L,m}}$ is analogous to the heat transfer resistance using the diffusion coefficient D and can be calculated with

$$R_{\text{L,m}} = \frac{\frac{1}{r_1 \cdot \delta} + \frac{1}{D \cdot \rho} \cdot \ln \frac{r_2}{r_1}}{2\pi}. \tag{3.13}$$

The surface mass transfer coefficient δ must be derived using the term a/D. which is the Lewis number, from

$$\delta = \frac{\dot{} \quad h}{c_{\mathrm{p}} \left(\frac{a}{D}\right)^{0.66}} \tag{3.14}$$

where a is the diffusivity and D the diffusion coefficient. For the mixture of air and vapour the quotient a/D is close to 1. It is possible to estimate the Nusselt number for the mass transfer (equal to the Nusselt number for the heat transfer), which is an indication of steady–state convective surface heat transfer, from

$$Nu_{\mathrm{mass}} \approx Nu_{\mathrm{heat}}. \tag{3.15}$$

Using the convective surface heat transfer coefficient, the hydraulic diameter d_{h} of a tube and the heat conductivity of the fluid, the Nusselt number can be calculated as

$$Nu = \frac{h_{\mathrm{c}} \cdot d_{\mathrm{h}}}{\lambda}. \tag{3.16}$$

To calculate the Nusselt number, and from this the convective surface heat transfer coefficient, a knowledge of the Reynolds number Re, which describes the kind of flow, is necessary

$$Re = \frac{v \cdot d_{\mathrm{h}}}{\nu}. \tag{3.17}$$

Here the kinematic viscosity must be considered. At 0 °C the kinematic viscosity has a value of $\nu_0 = 13.28 \cdot 10^{-6} m^2/s$ and is given for other temperatures by

$$\nu = \nu_0 \cdot \left(\frac{T}{273.15\,K}\right)^{1.76}. \tag{3.18}$$

When the Reynolds number reaches a value of 2300 the flow changes from laminar to turbulent. The description of the heat transfer properties in a fluid is specified by the Prandtl number

$$Pr = \frac{\nu \cdot \rho \cdot c_{\mathrm{p}}}{\lambda} \tag{3.19}$$

which has a value of around 0.80 for the considered processes. By applying these equations to the calculation of the convective surface heat transfer coefficient in rotating dehumidifiers the Nusselt number can be calculated for a tube with laminar flow according to WAGNER 1998 by

$$Nu = 0.664 \cdot \sqrt{Re \cdot \frac{d_{\mathrm{h}}}{l}} \cdot \sqrt[3]{Pr}. \tag{3.20}$$

This equation is valid, because the Reynolds numbers in the thin tubes of a rotating dehumidifier are generally in the range from 100 to 500, and the flow is therefore laminar. Using equation 3.16, the calculation of the convective surface heat transfer coefficient is possible. The values are within the range of 6 to 18 $W/(m^2K)$ corresponding to velocities of 0.5 to 4 m/s in the tubes of the dehumidifier. Some relationships between the heat transfer coefficient h_c, the Reynolds number Re, the Nusselt number Nu and the air velocity are shown in Figure 3.7.

Despite the described phenomena of a higher desorption velocity versus the adsorption velocity, FRANZKE 1989 recommends to use the same cross–sectional area for the regeneration section as for the process or adsorption section of a rotating dehumidifier. Hence it is necessary to reduce the velocity in the regeneration section for optimum dehumidification. If this is not done the desorption will be completed before the wheel enters the adsorption section and the adsorbent will be heated unnecessarily which would lead to a heat retention. This reduction of the air velocity in the regeneration section leads to possible energy savings, because a smaller air volume must be heated up to the required regeneration temperature.

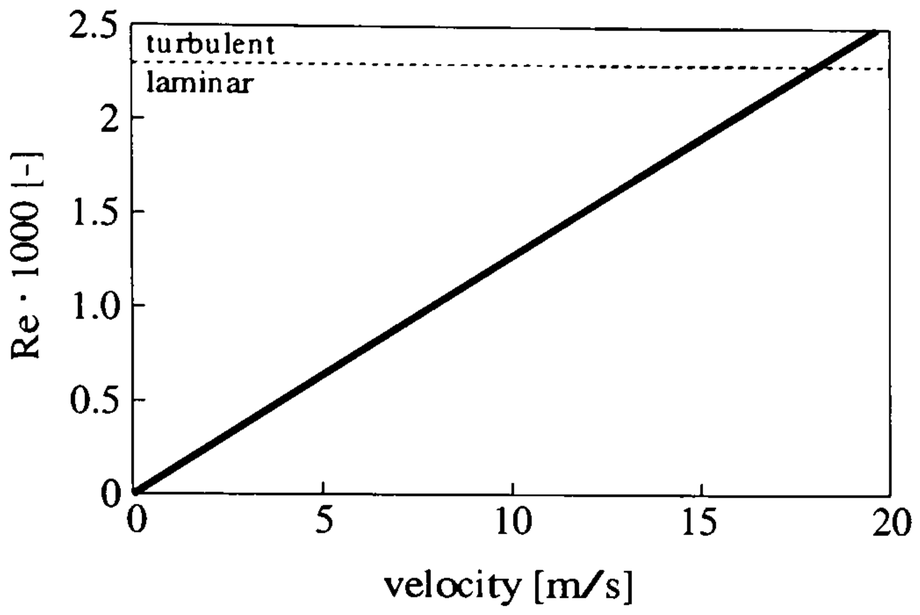

Figure 3.7a: Reynolds number dependent on velocity

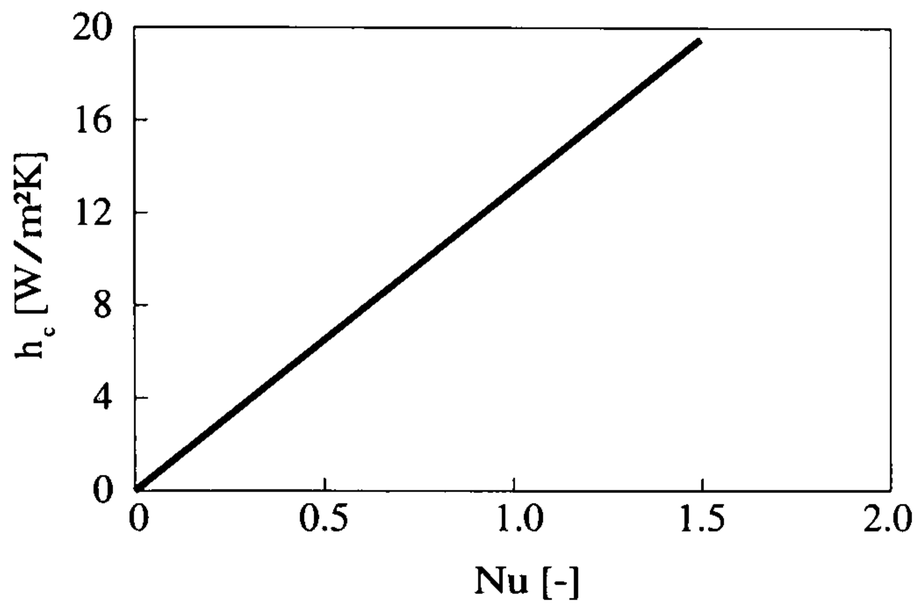

Figure 3.7b: Convective heat transfer coefficient dependent on Nusselt number

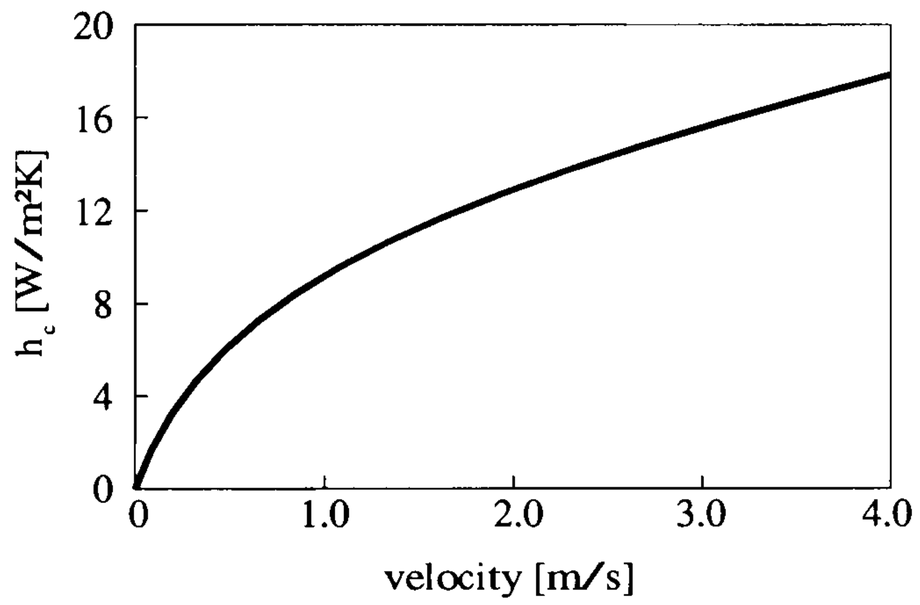

Figure 3.7c: Convective heat transfer coefficient dependent on velocity

Figure 3.7: Relationships between the heat transfer coefficient h_c, the Reynolds number Re, the Nusselt number Nu and the air velocity in a dehumidifier with a hydraulic diameter of $d_h = 2\ mm$.

Chapter 4

Measurements at Desiccant Cooling Test Plant

In this chapter the experimental plant installed for this work will be described and the measurements will be presented and discussed. The performance of the rotating dehumidifier was measured in detail.

4.1 Desiccant Cooling Test Plant with Solar Air Collectors

The world's first test plant for an open cycle desiccant cooling system with solar air collectors has been installed at the Fachhochschule Stuttgart – Hochschule für Technik (Figures 4.1, 4.2, 4.3 and 4.4). The test plant is connected to an exhibition room with a high cooling load during the summer months. With the modular setup, a quick change of components is possible. By doing so, parameter studies can easily be conducted. The test plant was developed to make very precise measurement possible. Figure 4.1 shows a schematic with the measurement and control parameters.

With regard to the choice of sensors, the measurement of temperatures and relative humidity causes no problems. However, measuring air flow in a compact plant is very complicated. A fully developed symmetrical flow profile is only possible in very long ductwork. Turbulence appears at bends and expansions of ducts which make the mea-

surement difficult. For this reason long ducts were used to connect the components of the system. Each component was connected to the ducts by special concentric adapters as shown in Figure 4.2. In Table 4.1 the installed components are listed. Table 4.2 shows the used sensors.

While designing the test plant at the beginning of this work, three options for the control system were discussed:

1. a control system operated by a microprocessor
2. a PC control system with common interfaces
3. a Building Management System (BMS)

Based on the costs of the hardware, the option with the microprocessor is the most attractive solution. The complexity of the test plant with the control of dehumidifier, heat recovery, two humidifiers, two fans and several dampers, however, and the desired visualisation cause this solution to exceed the available memory. Another factor working against the microprocessor solution was that programming of a controller for a test plant would be very time consuming. A PC control system has the advantage of a more flexible programming environment, but the required application in building techniques with continuously writing and reading of data without any communication problems could only be achieved with sophisticated PC operating systems. Furthermore, all control and measurement cables must be connected at one point, which is only feasible in a small plant. Therefore, a Building Management System was chosen, which has the advantage of decentralised control of DDC sub–stations (direct digital control), which can carry out control procedures on their own. A data communication server can be used to connect the sub–stations and to visualise the data.

Table 4.1: Components of the desiccant cooling test plant with solar air collectors

Components	Specifications
dehumidifier	Munters MCC-1 0870 Si diameter 870 mm, depth 200 mm, 90 W
heat recovery	Kraftanl. Heidelb. Rototherm PT 10W–0950–200V 70 diameter 950 mm, depth 200 mm, 200 W
2 humidifiers	Munters FA 4-95 090-060-C1-0-R one–step control, circulating water, 80 W
2 fans	Gebhardt REMF 18-0315-2 radial continuous control, 1.5 kW
electric heater	Helios EHR-K24/50/25-30 continuous control, 24 kW
10 m air collectors black	Grammer GLK3 schwarz
10 m air collectors selective	Grammer GLK3 selektiv
20 m cpc water collectors	Ritter Paradigma CPC 21
2 stratification storage	Solvis Stratos 1000 l

Table 4.2: Sensors and monitoring equipment of the desiccant cooling test plant

Components	Specifications
BMS system	Landis & Staefa Landis & Staefa UNIGYR
temperature ϑ	Landis & Staefa QAM 21 PTC resistance sensor Ni 1000 W QFM 66 PTC resistance sensor, 0–10 V, 0–50 C
relative humidity rh	Landis & Staefa QFM 66 capacitive humidity sensor, 0–10 V, 0–100 C
air flow V	L-Tec SVP 315 R averaging Prandtl tube, 2–25 m/s

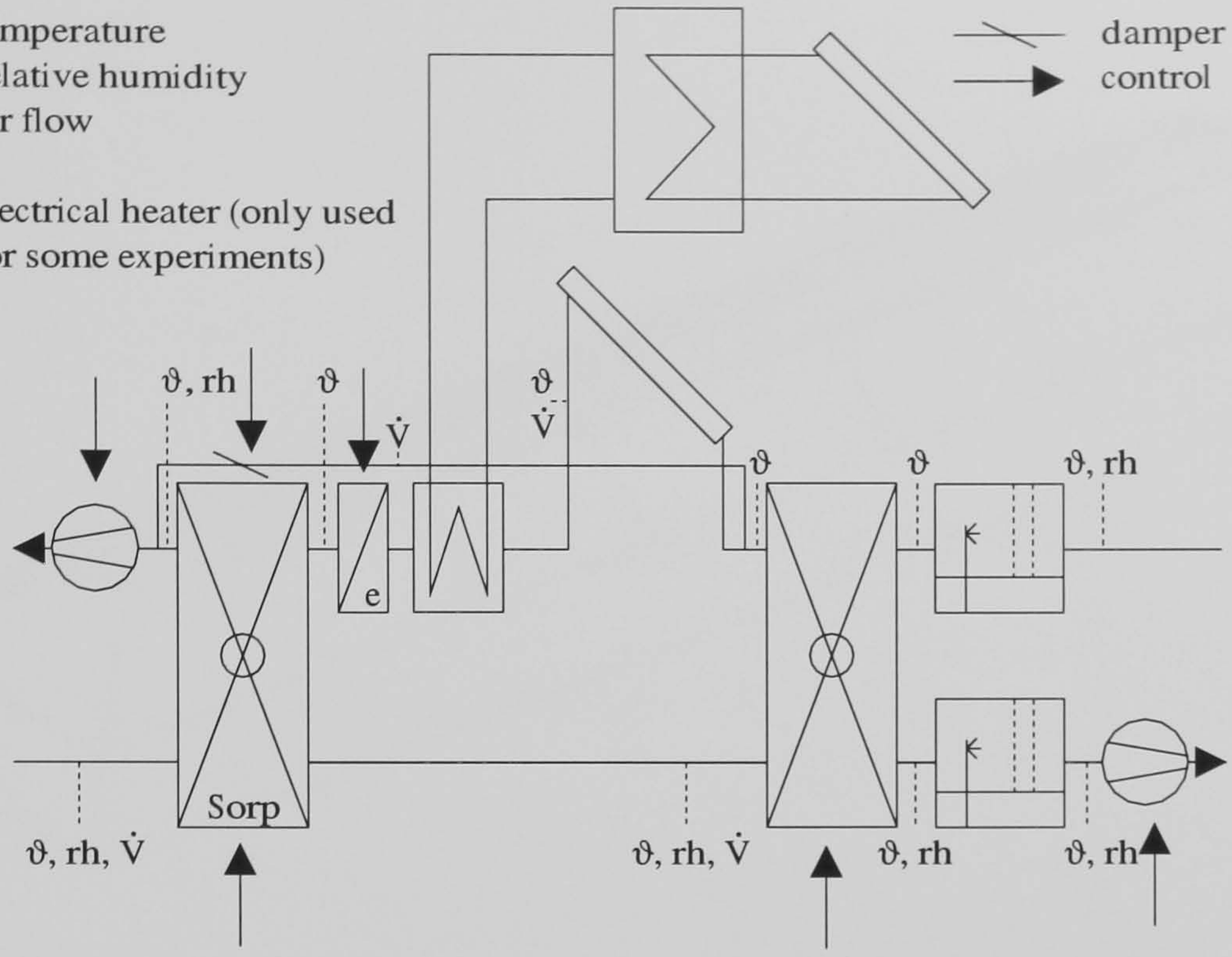

Figure 4.1: Control and monitoring equipment of the desiccant cooling test plant

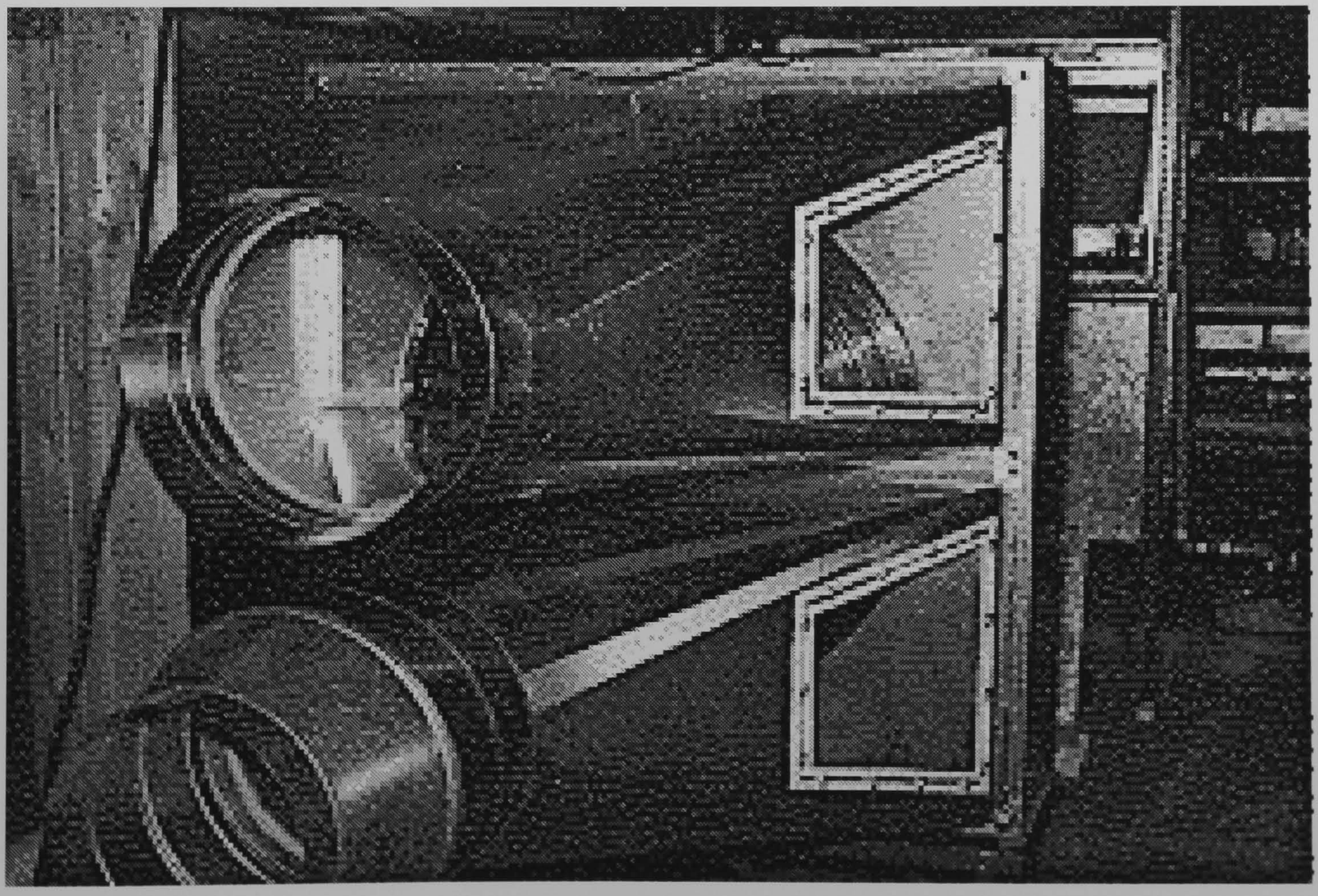

Figure 4.2: Concentric adapters used in the test plant for precise air flow measurements

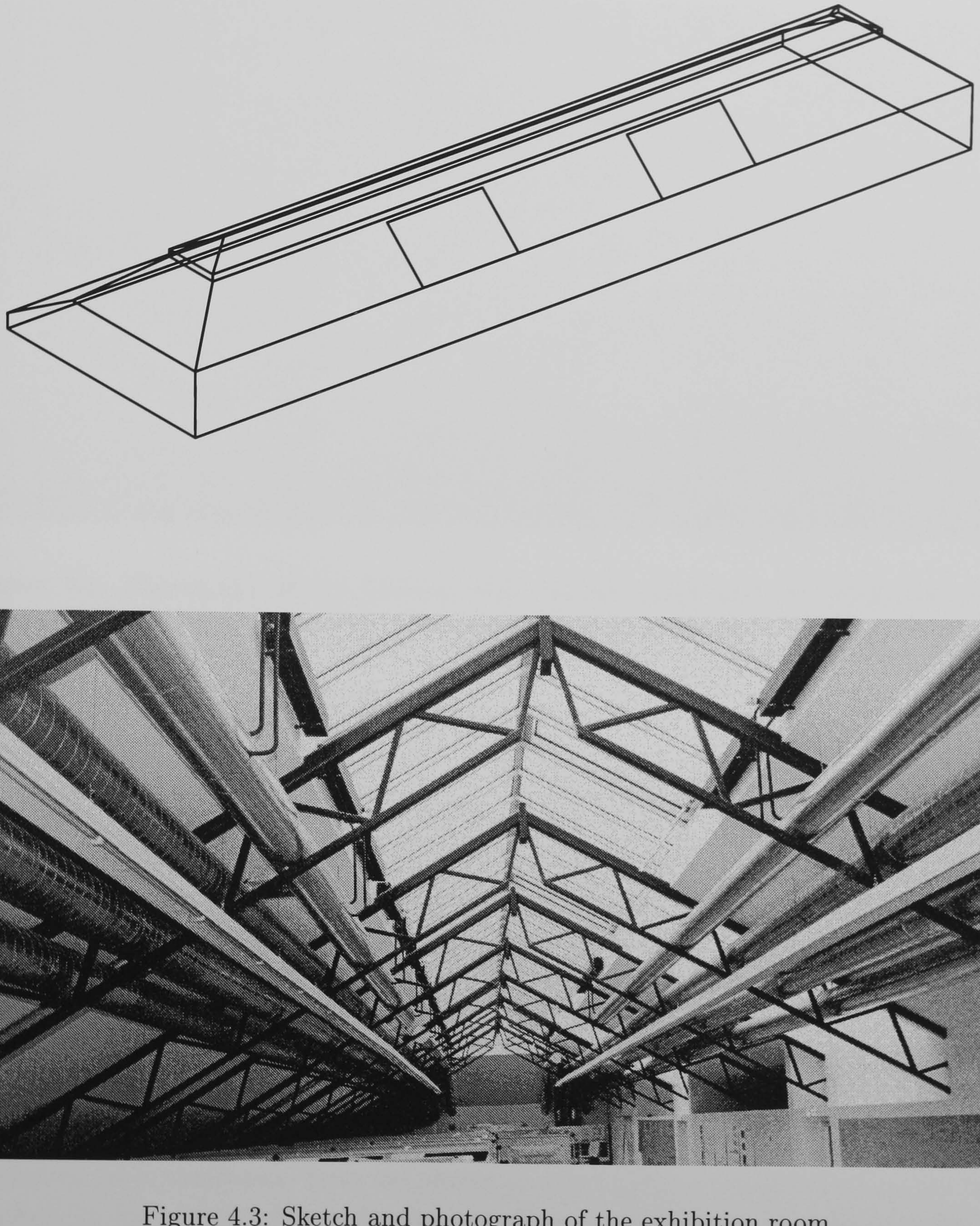

Figure 4.3: Sketch and photograph of the exhibition room

Figure 4.4: Photograph of the building with the test plant and the exhibition room (connection pieces for the solar air collectors jut out of the roof)

4.2 Measurement Results

Because of the lack of a possibility to condition the inlet air streams in the desiccant cooling plant, it was sometimes difficult to carry out parameter studies without uncontrolled changes in the boundary conditions. Hence large steps were chosen to run through the whole range of interesting regeneration temperatures. Furthermore, it was impossible to take measurements under extreme conditions of temperature and humidity, and therefore results are only available with Stuttgart's climatic conditions.

The measurement results of the achieved dehumidification in a desiccant cooling system configured as a ventilation cycle are shown in Figure 4.5. The process air flow was constant at $\dot{V}_{\mathrm{P}} = 2530\,m^3/h$ while the regeneration air flow was changed from $\dot{V}_{\mathrm{R}} = 2530\,m^3/h$ down to $\dot{V}_{\mathrm{P}} = 890\,m^3/h$. This corresponds to a ratio of $\dot{V}_{\mathrm{R}}/\dot{V}_{\mathrm{P}} = 1.00$ down to $\dot{V}_{\mathrm{R}}/\dot{V}_{\mathrm{P}} = 0.35$. Maximum dehumidification was reached at a rotation speed of 15 revolutions per hour. The measurements for the evaluation of an optimum rotation speed are shown in Figure 4.14. To obtain reliable results for the performance of the dehumidification with low regeneration air flows, it was necessary to improve the seals of

the dehumidifier. With the non–improved seals noticeable leakage air flows appeared due to the pressure difference in the different flow sections and valid measurement results were not achievable. The calculated dehumidification efficiencies from the dehumidification measurements according to equation 3.11 are shown in Figure 4.9. The results are

$$\begin{aligned}
\dot{V}_{\mathrm{R}}/\dot{V}_{\mathrm{P}} = 0.35 \quad &: \quad \eta_{\mathrm{sorp}} = 0.62 \pm 0.03 \\
\dot{V}_{\mathrm{R}}/\dot{V}_{\mathrm{P}} = 0.50 \quad &: \quad \eta_{\mathrm{sorp}} = 0.75 \pm 0.05 \\
\dot{V}_{\mathrm{R}}/\dot{V}_{\mathrm{P}} = 0.75 \quad &: \quad \eta_{\mathrm{sorp}} = 0.82 \pm 0.04 \\
\dot{V}_{\mathrm{R}}/\dot{V}_{\mathrm{P}} = 1.00 \quad &: \quad \eta_{\mathrm{sorp}} = 0.87 \pm 0.03
\end{aligned}$$

The next parameter study of the dehumidification performance of the dehumidifier used was for a ventilation cycle with ambient air regeneration shown in Figure 5.12. The measurement results are shown in Figure 4.6. The calculated dehumidification efficiencies from the dehumidification measurements according to equation 3.11 are shown in Figure 4.10.

$$\begin{aligned}
\dot{V}_{\mathrm{R}}/\dot{V}_{\mathrm{P}} = 0.35 \quad &: \quad \eta_{\mathrm{sorp}} = 0.64 \pm 0.02 \\
\dot{V}_{\mathrm{R}}/\dot{V}_{\mathrm{P}} = 0.50 \quad &: \quad \eta_{\mathrm{sorp}} = 0.77 \pm 0.04 \\
\dot{V}_{\mathrm{R}}/\dot{V}_{\mathrm{P}} = 0.75 \quad &: \quad \eta_{\mathrm{sorp}} = 0.84 \pm 0.02 \\
\dot{V}_{\mathrm{R}}/\dot{V}_{\mathrm{P}} = 1.00 \quad &: \quad \eta_{\mathrm{sorp}} = 0.83 \pm 0.03
\end{aligned}$$

In addition to the dehumidification performance which was of main interest, the performance of the other components of the test plant were investigated. Figures 4.14c shows that an increase in the rotation speed of the dehumidifier leads to a moisture recovery of in excess of 1.7 revs/min. Here the performance of the wheel changes and the dehumidifier becomes an enthalpy exchanger. At a rotation speed greater than 5 revs/min an enthalpy recovery efficiency of

$$\eta_{\mathrm{h}} = 0.85$$

was evaluated. Calculating the heat recovery efficiency from the same data, the heat recovery efficiency of the enthalpy exchanger with a rotation speed greater than 2 revs/min was

$$\eta_{\mathrm{HR}} = 0.82.$$

In contrast to the measured heat recovery efficiency of the dehumidifier, the measured efficiency of the used heat recovery was

$$\eta_{\mathrm{HR}} = 0.74.$$

The humidification efficiencies of the applied humidifiers were also included in the investigations. At an air flow of $\dot{V} = 1850\,m^3/h$ a humidification efficiency of 0.76 was achieved and dropped to

$$\eta_{\mathrm{hum}} = 0.66$$

at $\dot{V} = 2750\,m^3/h$, which is near the humidifier design point of $\dot{V} = 3000\,m^3/h$. While measuring the performance of the system the COPs of the entire test plant were investigated. For the desiccant cooling cycle the courses of the measured COPs are presented in Figure 4.12 and for the desiccant cooling cycle with ambient air regeneration in Figure 4.13.

4.3 Analysis of Measurement Results

The measurements of the rotating dehumidifier were of greatest interest and hence the investigations made in detail. The dehumidification achieved depends on the inlet conditions of the entering air, of the velocities in the process and the regeneration section and the regeneration temperature and humidity. In addition, the rotation speed influences the performance significantly. 15 revolutions per hour were determined as the optimum for dehumidification. A faster rotation speed leads to incomplete regeneration and dehumidification. Lower rotation speeds lead to a lower dehumidification because the maximum possible water content in the adsorbens is reached some time before entering the regeneration section. In the regeneration section the water is removed before entering the process section resulting in an unfavorable increase in the adsorbens temperature. This effects a reduced adsorption in the process part; the adsorbens must first be cooled down by the inlet air until the adsorption process can restart. While running the dehumidifier at optimum rotation speed, the actual dehumidification efficiency is $\eta_{\mathrm{sorp}} = 0.82$ at $\dot{V}_{\mathrm{R}}/\dot{V}_{\mathrm{P}} = 0.75$, which is a common bypass fraction. Particularly interesting is the fact that the dehumidification efficiency decreases only by 20% to $\eta_{\mathrm{sorp}} = 0.62$ while the air flow is

reduced by 40%, which is directly coupled with the energy input for regeneration. This can be explained by the faster desorption velocity compared with the adsorption velocity and the fact that the heat and mass transfer coefficients only change with the square root of the air velocity (equations 3.16, 3.17 and 3.20). Using the dehumidifier as an enthalpy exchanger with a high rotation speed yields to $\eta_{\mathrm{h}} = 0.85$ and $\eta_{\mathrm{HR}} = 0.82$, which are quite high values considering that the dehumidifier is not optimal for the purpose of an enthalpy exchanger. For this purpose a higher thermal capacity of the matrix is desirable.

For a comparison of the measured dehumidifier performance with the introduced models for the maximum dehumidification, calculations have been undertaken, shown in Figure 4.7 and Figure 4.8. The calculated maximum dehumidification is multiplied with the dehumidification efficiency identified above. All plotted curves have been calculated with the intersection method (see equation 3.10) and fit well. In contrast, the application of Pfeiffer's model, introduced in equation 3.9, leads to an overprediction of the achievable dehumidification of approximately 10%.

With the rotating heat recovery optimum efficiencies of $\eta_{\mathrm{HR}} = 0.74$ were reached with rotation speeds in the range between 4 and 10 revolutions per minute. Lower rotation speeds decrease the efficiency, as the thermal mass has delivered their stored energy before entering the other part, and hence only a fraction of the wheel is effective. The performance of the humidifiers used yields lower humidification efficiencies than indicated by the manufacturer. Because their performance does not influence the performance of the whole system significantly, no further attention was paid to this operating region.

Figure 4.11 shows the influence of the performance of the dehumidifier and the heat recovery to the COP of the entire desiccant cooling system. Furthermore, the dependence of the COP on the regeneration temperature is plotted. The COPs measured of the desiccant cooling cycle are shown in Figure 4.12 and for the desiccant cooling cycle with ambient air regeneration in Figure 4.13. The results are lower than estimated because the measured heat recovery efficiency with 0.74 and the outlet humidifier efficiency with 0.66 in the test plant are too low to achieve a very good overall system performance. Furthermore, the COPs of the DCS ventilation cycle do not rise as expected by decreasing the regeneration temperature. Comparing the COP results of the DCS ventilation cycle with the COP results of the DCS ventilation cycle with ambient air regeneration show that especially at low regeneration temperatures higher COPs can be reached if ambient

air is used for regeneration. This can be explained with the lower ambient air humidity (in Stuttgart) compared with the absolute humidity after the outlet humidifier which significantly influences the COP at low regeneration temperatures.

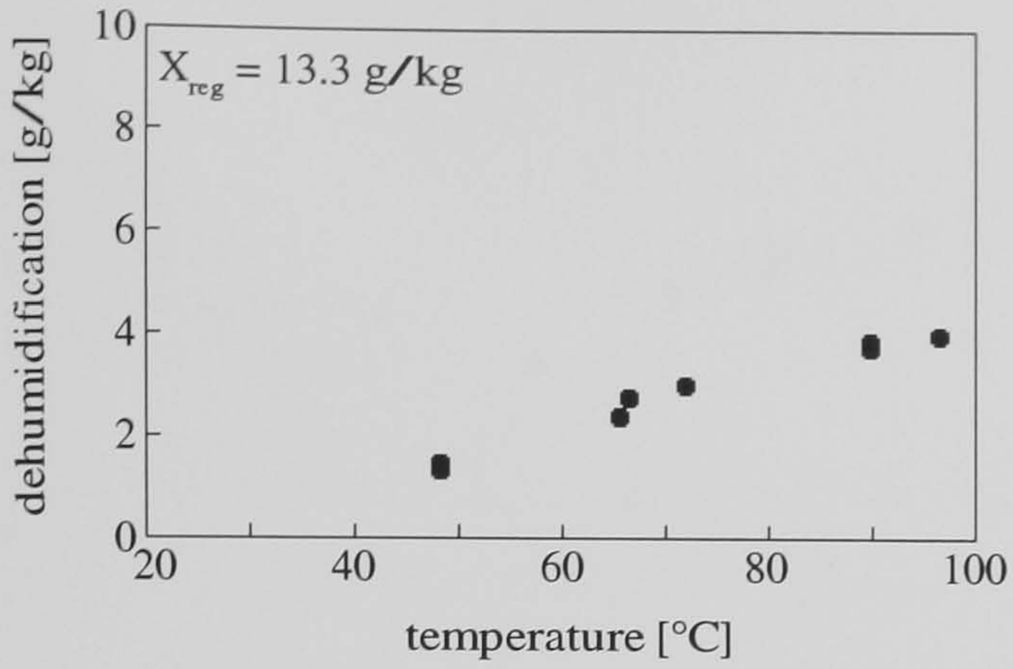

$\dot{V}_{\mathrm{R}}/\dot{V}_{\mathrm{P}} = 0.35,\ \dot{V}_{\mathrm{P}} = 2530m^3/h$

- ϑ_{amb}= 29 °C , $rh_{\mathrm{amb}} = 0.36$

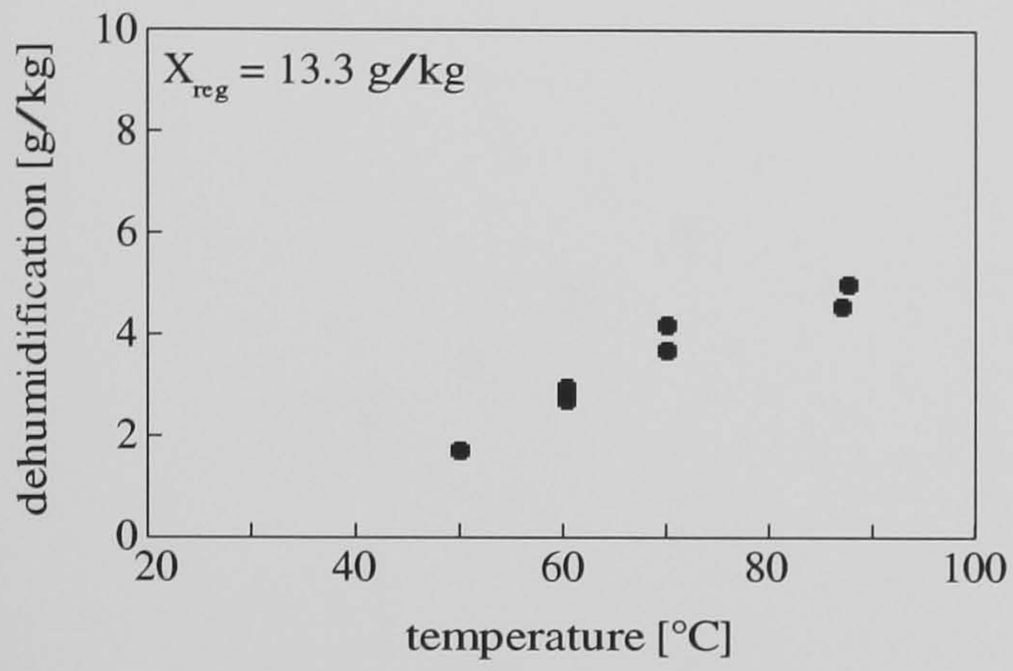

$\dot{V}_{\mathrm{R}}/\dot{V}_{\mathrm{P}} = 0.50,\ \dot{V}_{\mathrm{P}} = 2530m^3/h$

- ϑ_{amb}= 29 °C , $rh_{\mathrm{amb}} = 0.35$

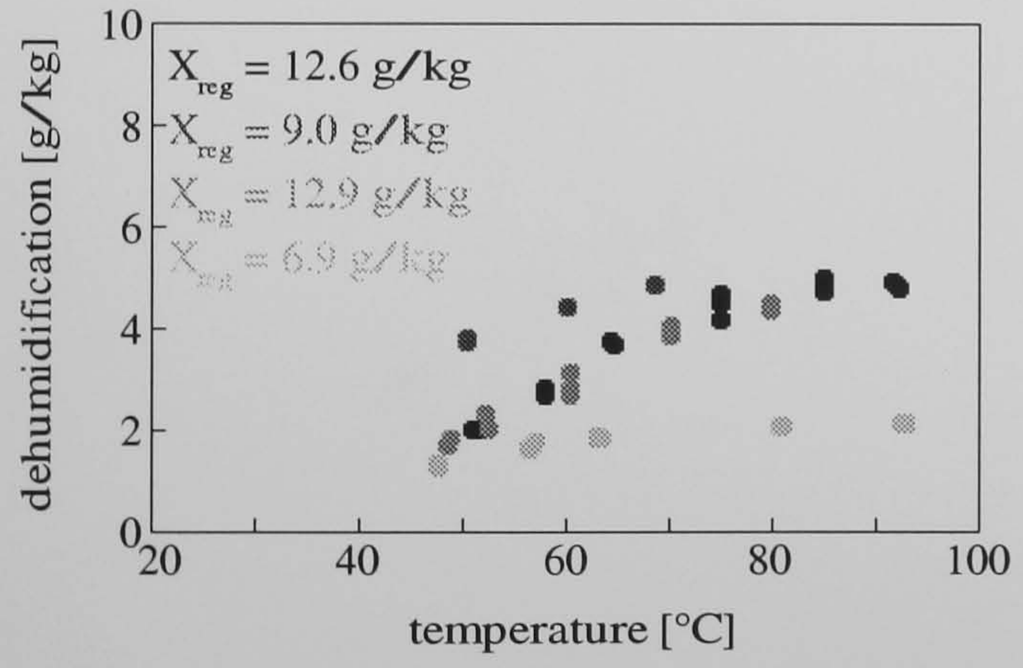

$\dot{V}_{\mathrm{R}}/\dot{V}_{\mathrm{P}} = 0.75,\ \dot{V}_{\mathrm{P}} = 2530m^3/h$

- ϑ_{amb}= 28 °C , $rh_{\mathrm{amb}} = 0.38$
- ϑ_{amb}= 12 °C , $rh_{\mathrm{amb}} = 0.83$
- ϑ_{amb}= 29 °C , $rh_{\mathrm{amb}} = 0.34$
- ϑ_{amb}= 12 °C , $rh_{\mathrm{amb}} = 0.35$

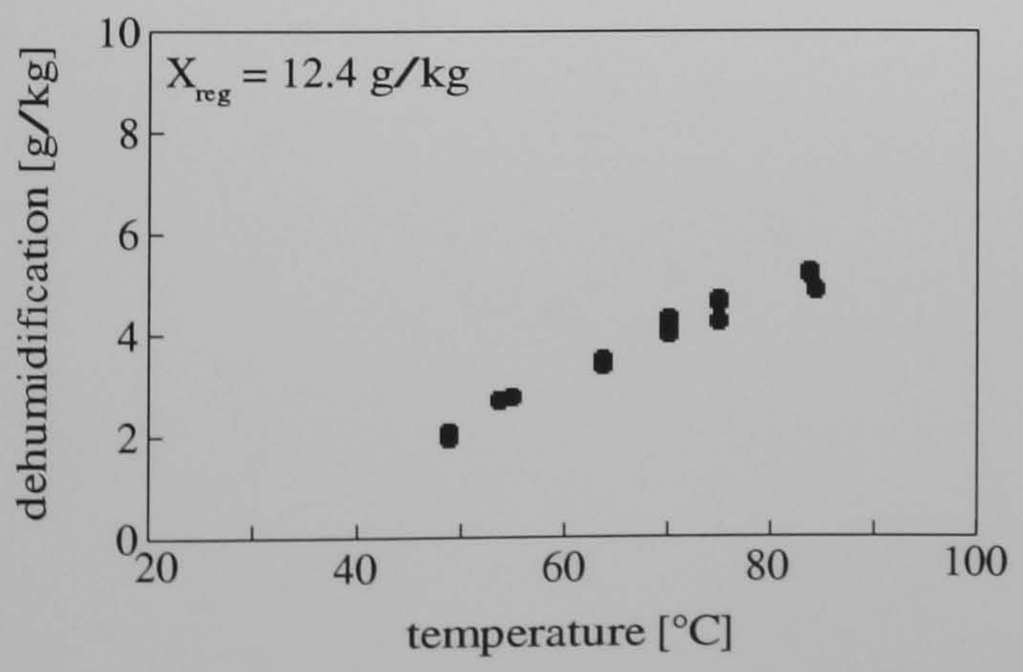

$\dot{V}_{\mathrm{R}}/\dot{V}_{\mathrm{P}} = 1.00,\ \dot{V}_{\mathrm{P}} = 2530m^3/h$

- ϑ_{amb}= 28 °C , $rh_{\mathrm{amb}} = 0.34$

Figure 4.5: Measured ΔX in a DCS ventilation cycle

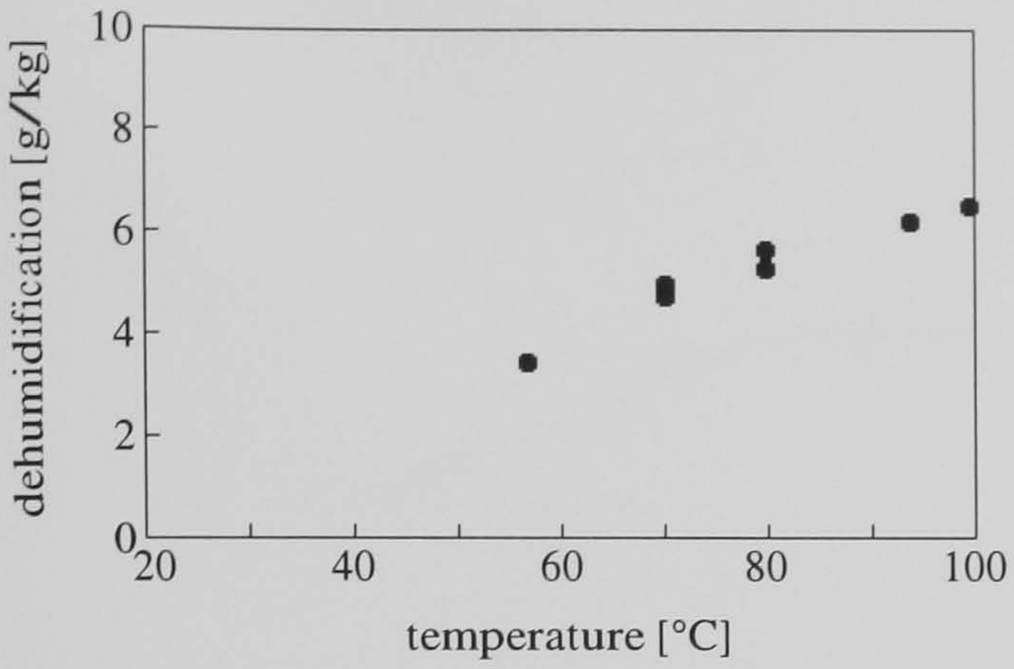

$\dot{V}_{\mathrm{R}}/\dot{V}_{\mathrm{P}} = 0.35,\ \dot{V}_{\mathrm{P}} = 2530m^3/h$

- ϑ_{amb}= 29 °C , $rh_{\mathrm{amb}} = 0.50$

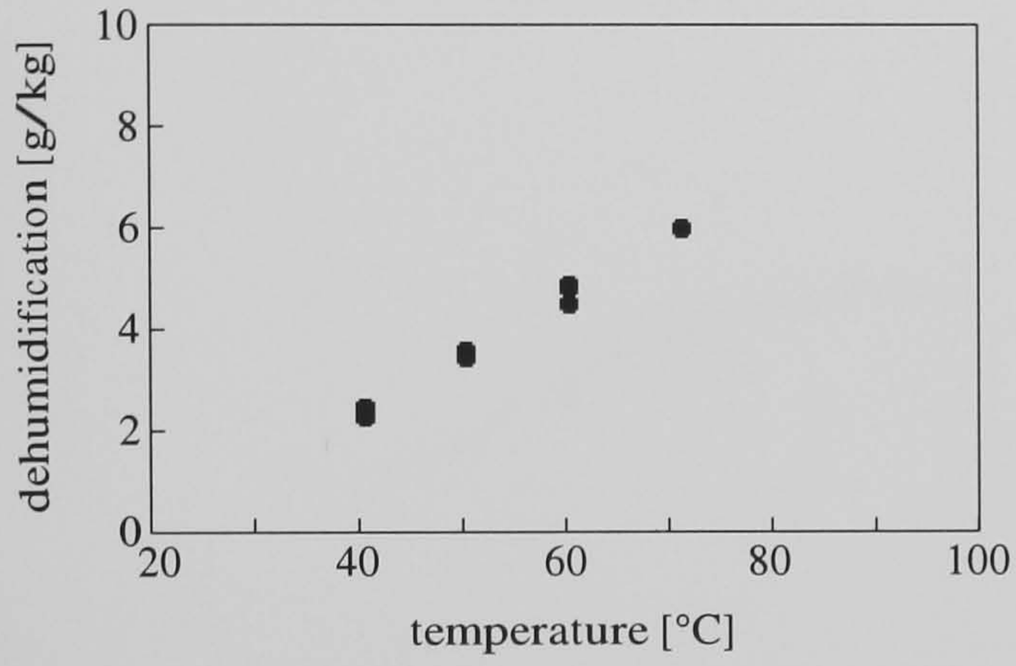

$\dot{V}_{\mathrm{R}}/\dot{V}_{\mathrm{P}} = 0.50,\ \dot{V}_{\mathrm{P}} = 2530m^3/h$

- ϑ_{amb}= 27 °C , $rh_{\mathrm{amb}} = 0.52$

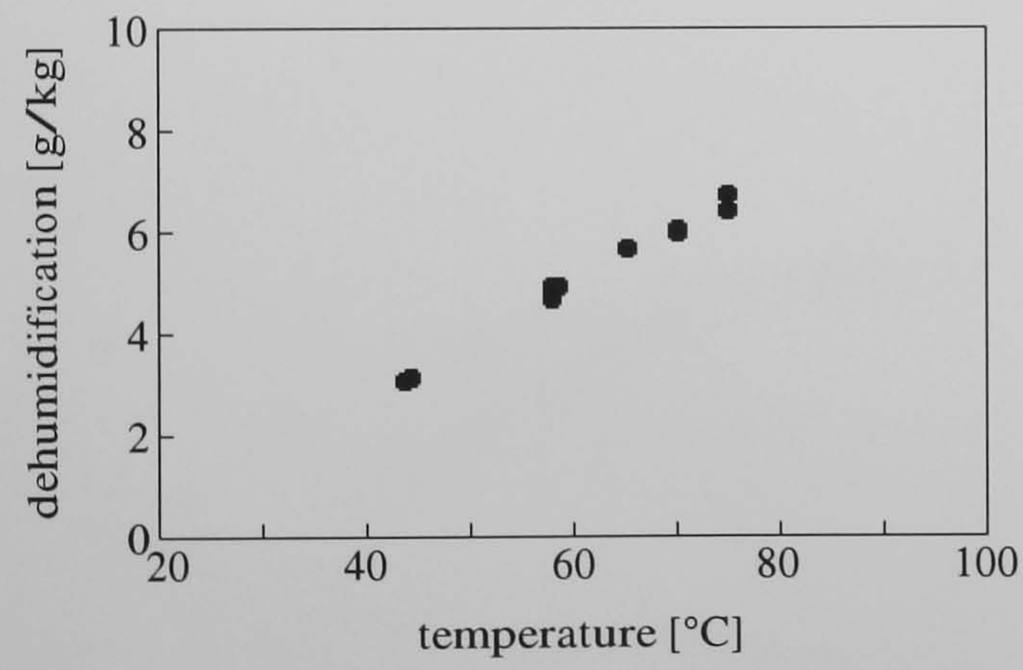

$\dot{V}_{\mathrm{R}}/\dot{V}_{\mathrm{P}} = 0.75,\ \dot{V}_{\mathrm{P}} = 2530m^3/h$

- ϑ_{amb}= 26 °C , $rh_{\mathrm{amb}} = 0.50$

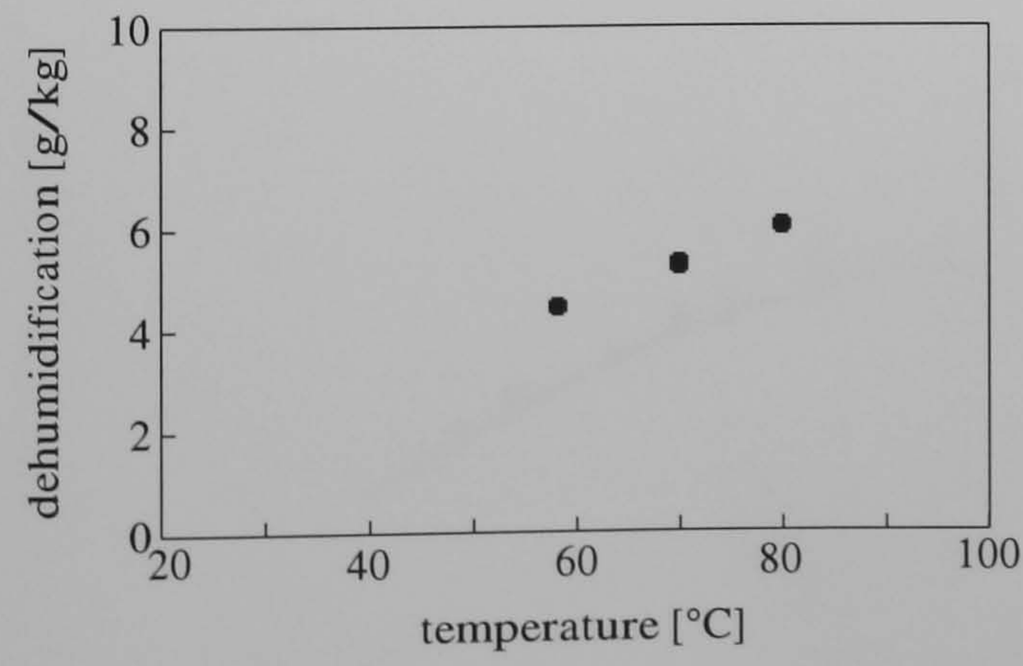

$\dot{V}_{\mathrm{R}}/\dot{V}_{\mathrm{P}} = 1.00,\ \dot{V}_{\mathrm{P}} = 2530m^3/h$

- ϑ_{amb}= 29 °C , $rh_{\mathrm{amb}} = 0.39$

Figure 4.6: Measured ΔX in a DCS ventilation cycle (ambient air regeneration)

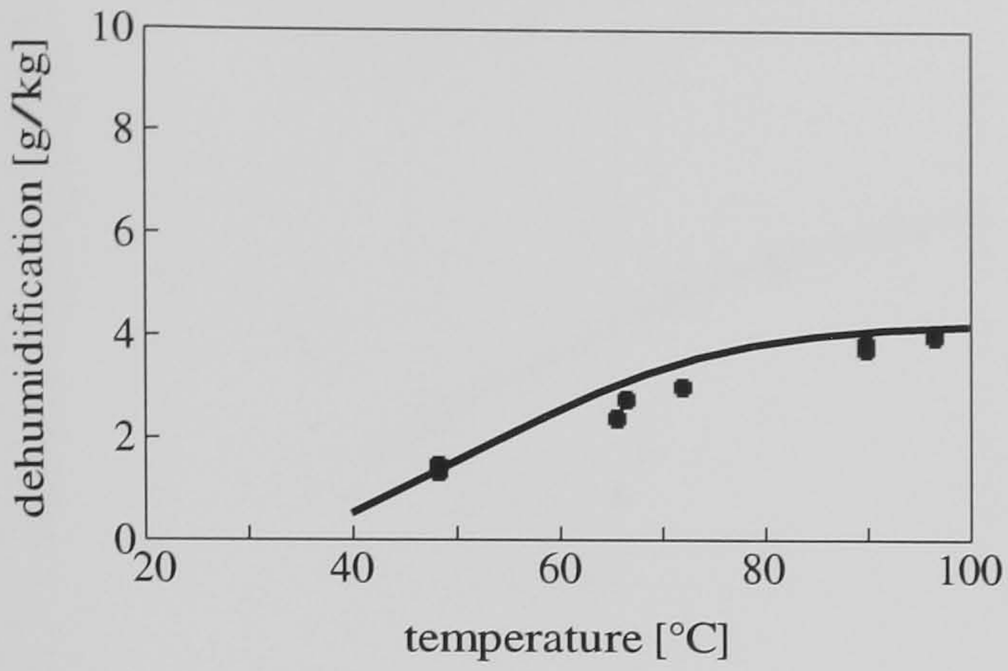

$\dot{V}_{\mathrm{R}}/\dot{V}_{\mathrm{P}} = 0.35,\ \dot{V}_{\mathrm{P}} = 2530m^3/h$

- ϑ_{amb}= 29 °C , $rh_{\mathrm{amb}} = 0.36$

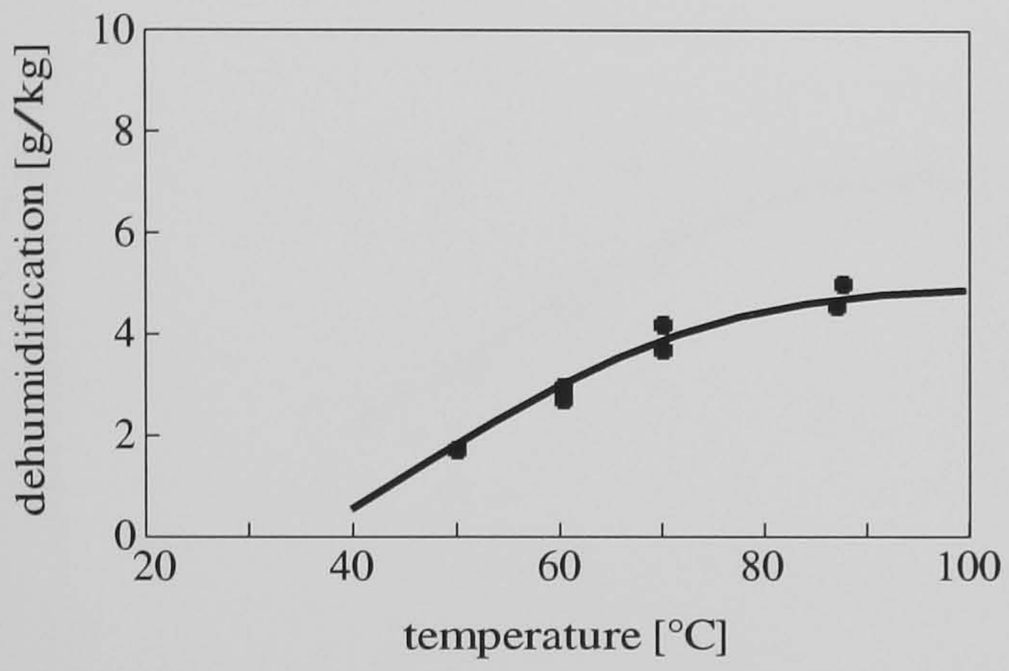

$\dot{V}_{\mathrm{R}}/\dot{V}_{\mathrm{P}} = 0.50,\ \dot{V}_{\mathrm{P}} = 2530m^3/h$

- ϑ_{amb}= 29 °C , $rh_{\mathrm{amb}} = 0.35$

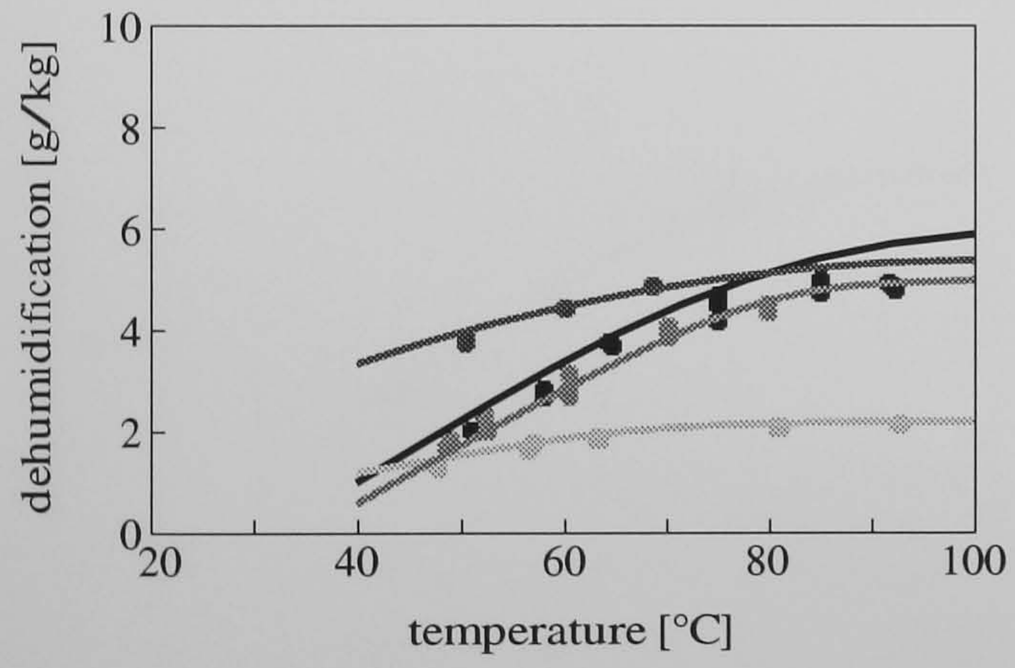

$\dot{V}_{\mathrm{R}}/\dot{V}_{\mathrm{P}} = 0.75,\ \dot{V}_{\mathrm{P}} = 2530m^3/h$

- ϑ_{amb}= 28 °C , $rh_{\mathrm{amb}} = 0.38$
- ϑ_{amb}= 12 °C , $rh_{\mathrm{amb}} = 0.83$
- ϑ_{amb}= 29 °C , $rh_{\mathrm{amb}} = 0.34$
- ϑ_{amb}= 12 °C , $rh_{\mathrm{amb}} = 0.35$

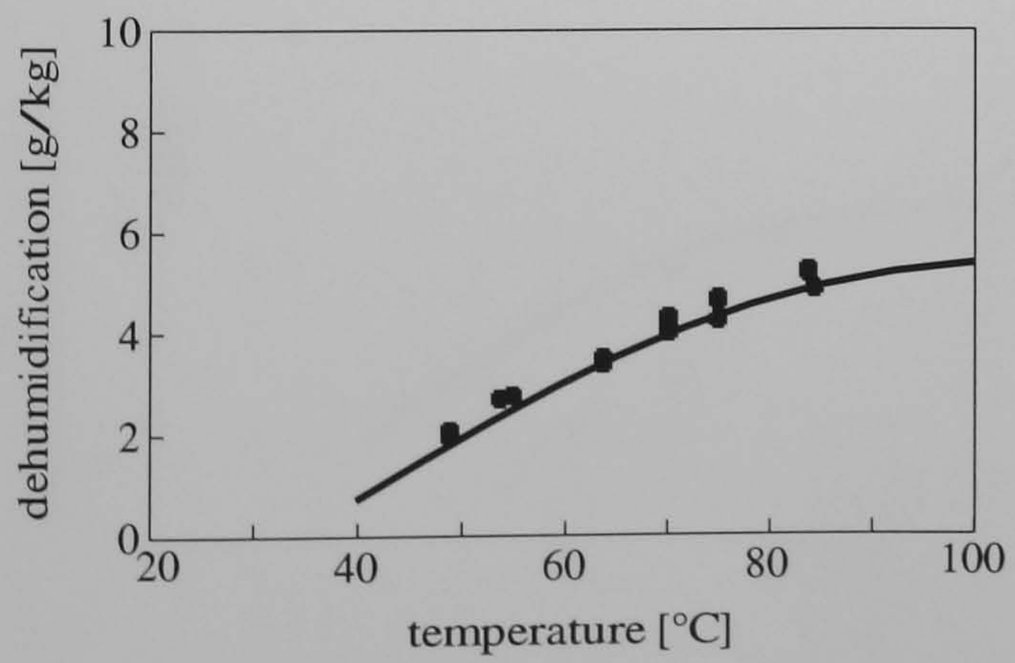

$\dot{V}_{\mathrm{R}}/\dot{V}_{\mathrm{P}} = 1.00,\ \dot{V}_{\mathrm{P}} = 2530m^3/h$

- ϑ_{amb}= 28 °C , $rh_{\mathrm{amb}} = 0.34$

Figure 4.7: Comparison of calculated ΔX using mean η_{sorp} and measurements

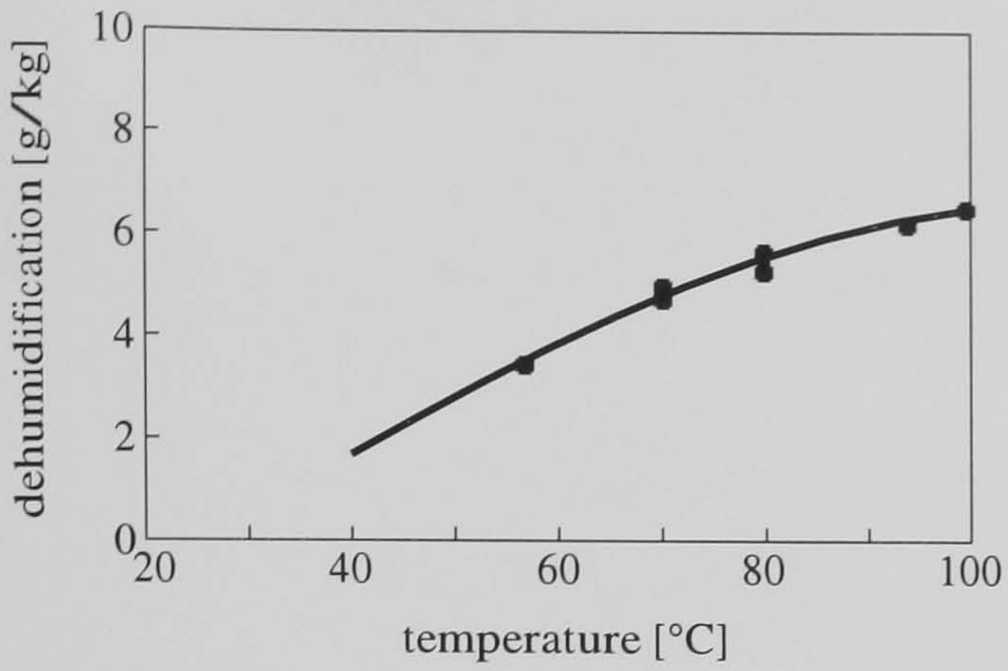

$\dot{V}_{\mathrm{R}}/\dot{V}_{\mathrm{P}} = 0.35,\ \dot{V}_{\mathrm{P}} = 2530m^3/h$

- ϑ_{amb}= 29 °C , $rh_{\mathrm{amb}} = 0.50$

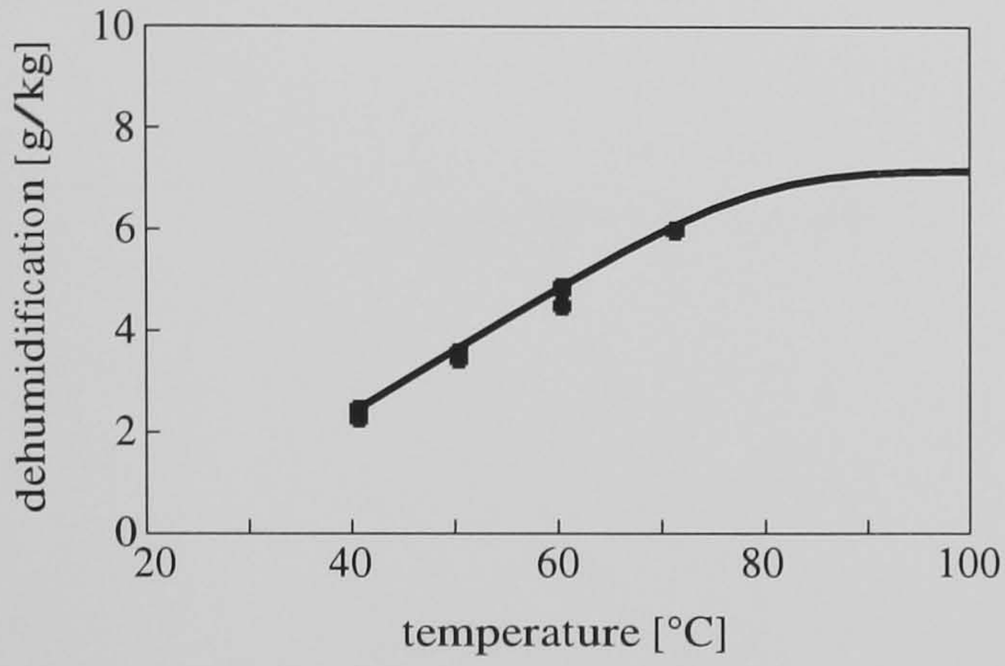

$\dot{V}_{\mathrm{R}}/\dot{V}_{\mathrm{P}} = 0.50,\ \dot{V}_{\mathrm{P}} = 2530m^3/h$

- ϑ_{amb}= 27 °C , $rh_{\mathrm{amb}} = 0.52$

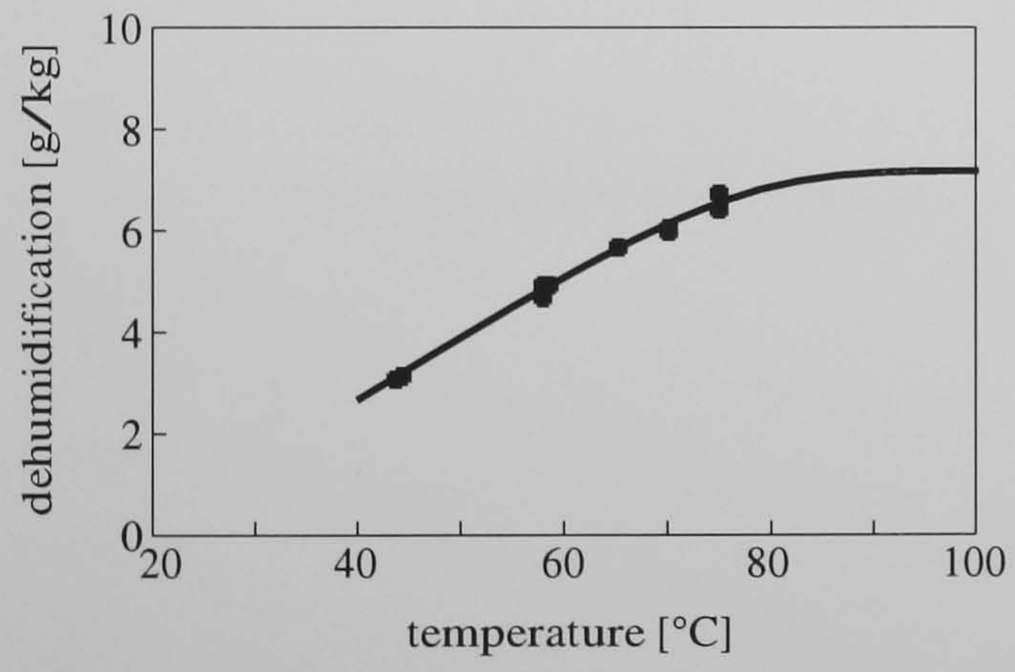

$\dot{V}_{\mathrm{R}}/\dot{V}_{\mathrm{P}} = 0.75,\ \dot{V}_{\mathrm{P}} = 2530m^3/h$

- ϑ_{amb}= 26 °C , $rh_{\mathrm{amb}} = 0.50$

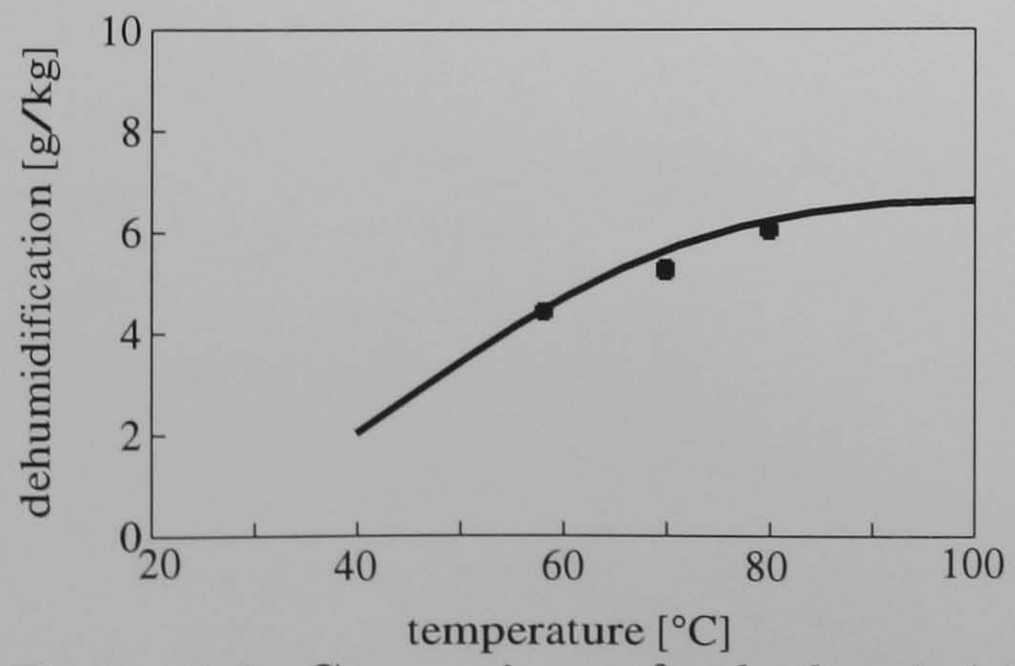

$\dot{V}_{\mathrm{R}}/\dot{V}_{\mathrm{P}} = 1.00,\ \dot{V}_{\mathrm{P}} = 2530m^3/h$

- ϑ_{amb}= 29 °C , $rh_{\mathrm{amb}} = 0.39$

Figure 4.8: Comparison of calculated ΔX using mean η_{sorp} and measurements (ambient air regeneration)

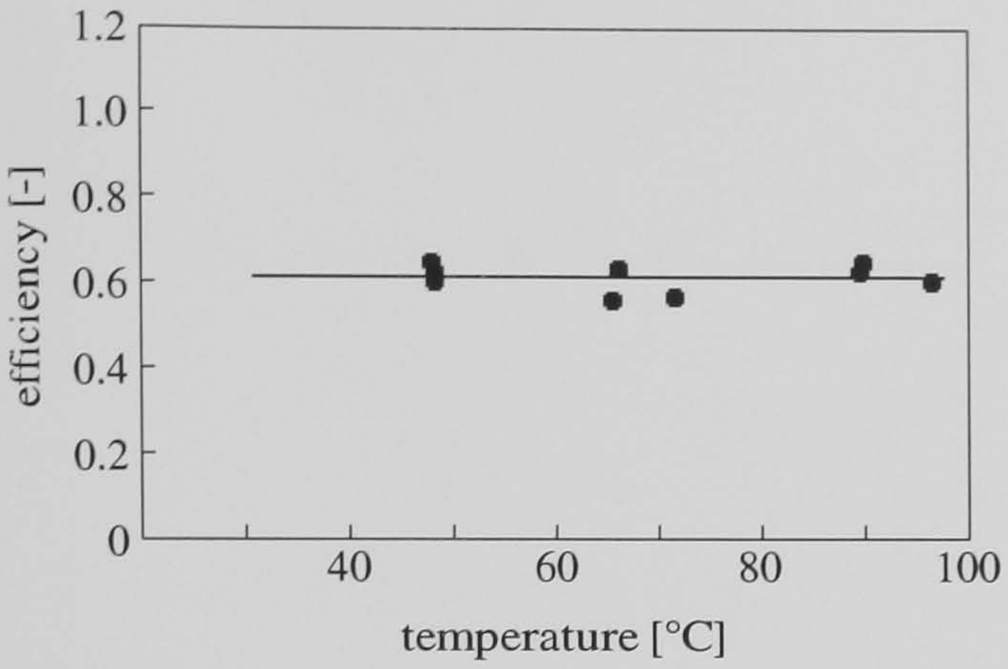

$\dot{V}_\mathrm{R}/\dot{V}_\mathrm{P} = 0.35,\ \dot{V}_\mathrm{P} = 2530 m^3/h$

- $\eta_\mathrm{sorp} = 0.62 \pm 0.03$

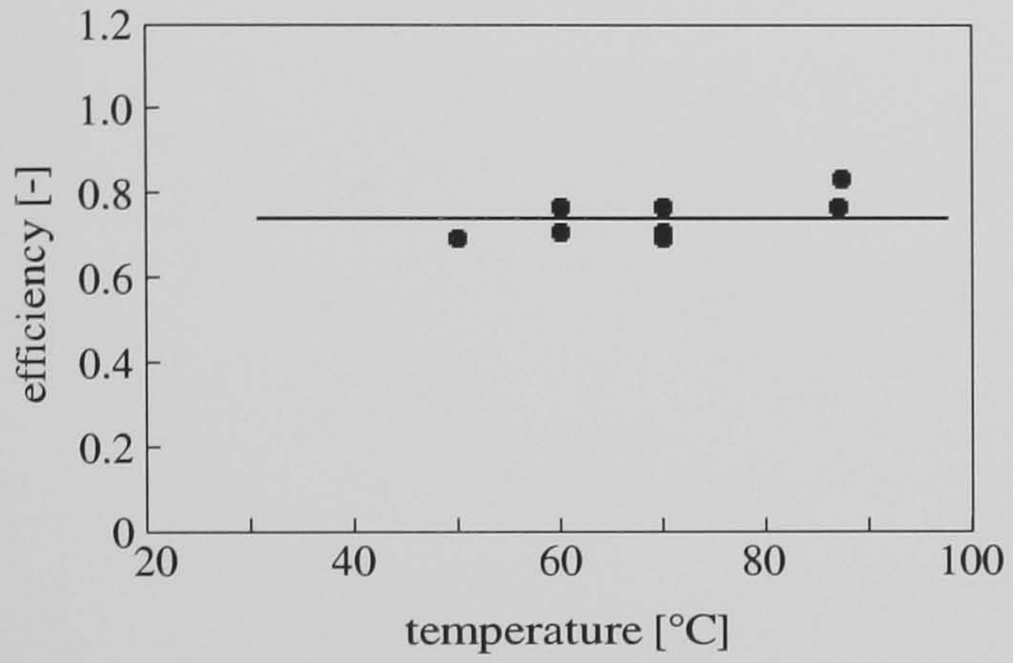

$\dot{V}_\mathrm{R}/\dot{V}_\mathrm{P} = 0.50,\ \dot{V}_\mathrm{P} = 2530 m^3/h$

- $\eta_\mathrm{sorp} = 0.75 \pm 0.05$

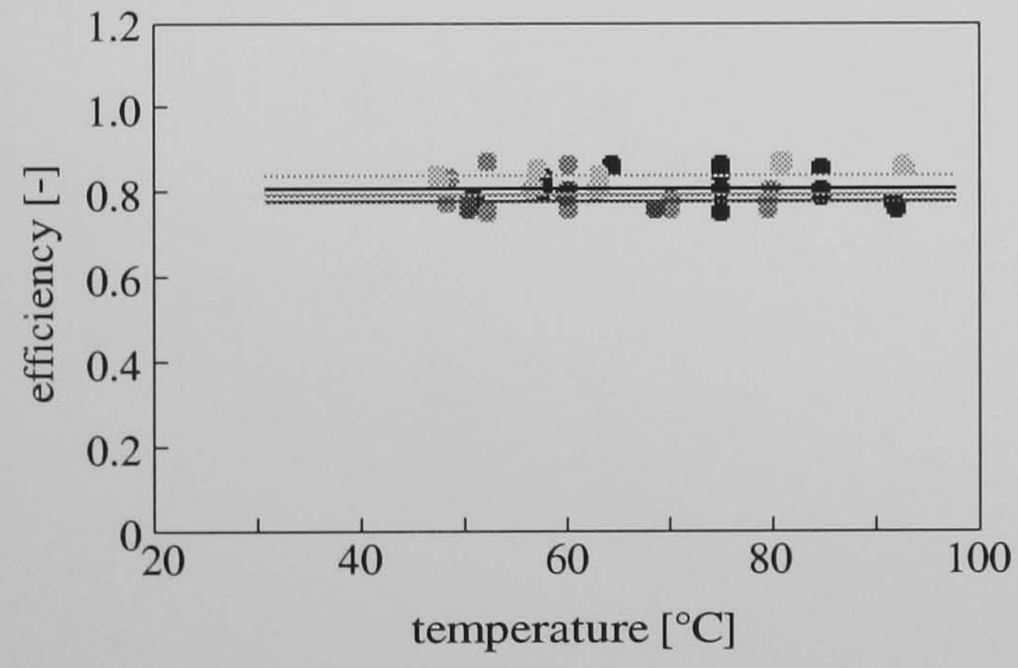

$\dot{V}_\mathrm{R}/\dot{V}_\mathrm{P} = 0.75,\ \dot{V}_\mathrm{P} = 2530 m^3/h$

- $\eta_\mathrm{sorp} = 0.82 \pm 0.04$
- $\eta_\mathrm{sorp} = 0.79 \pm 0.02$
- $\eta_\mathrm{sorp} = 0.80 \pm 0.04$
- $\eta_\mathrm{sorp} = 0.85 \pm 0.02$

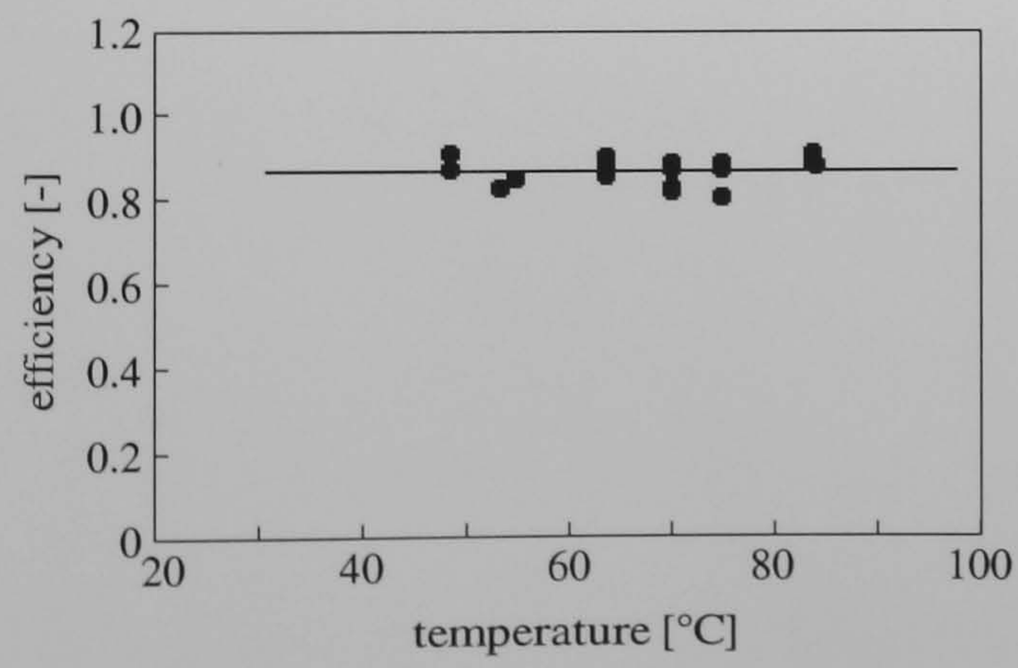

$\dot{V}_\mathrm{R}/\dot{V}_\mathrm{P} = 1.00,\ \dot{V}_\mathrm{P} = 2530 m^3/h$

- $\eta_\mathrm{sorp} = 0.87 \pm 0.03$

Figure 4.9: Calculated η_sorp of the measured ΔX

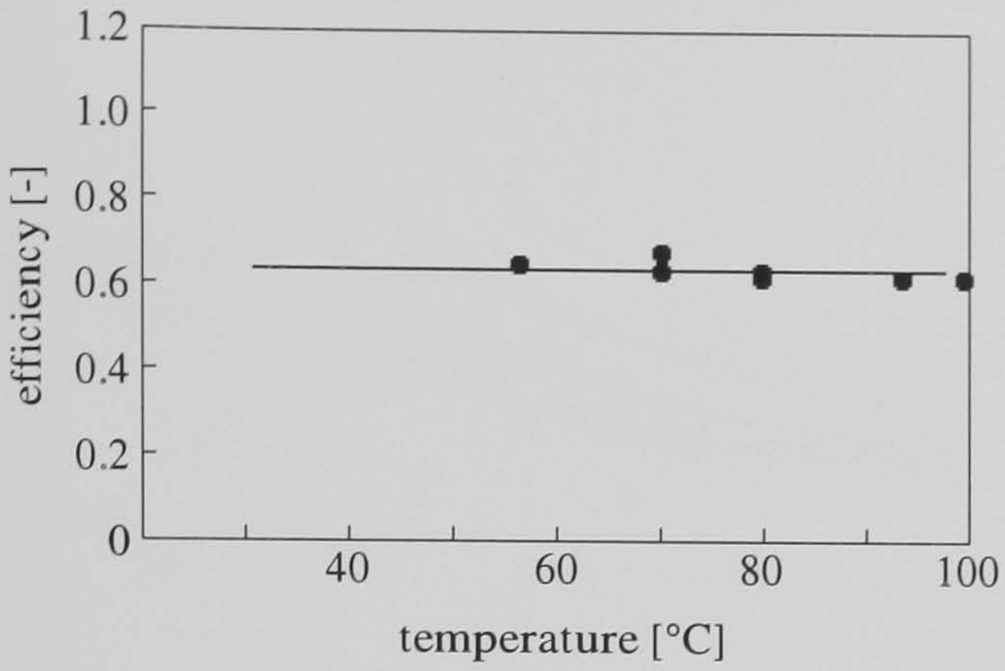

$\dot{V}_{\mathrm{R}}/\dot{V}_{\mathrm{P}} = 0.35,\ \dot{V}_{\mathrm{P}} = 2530m^3/h$

- $\eta_{\mathrm{sorp}} = 0.64 \pm 0.02$

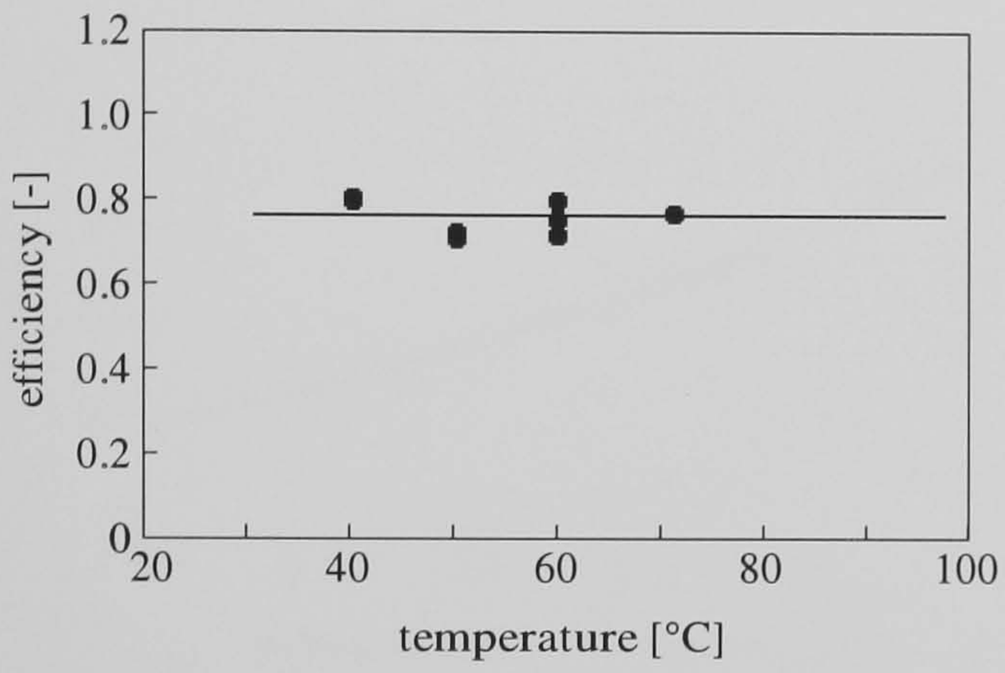

$\dot{V}_{\mathrm{R}}/\dot{V}_{\mathrm{P}} = 0.50,\ \dot{V}_{\mathrm{P}} = 2530m^3/h$

- $\eta_{\mathrm{sorp}} = 0.77 \pm 0.04$

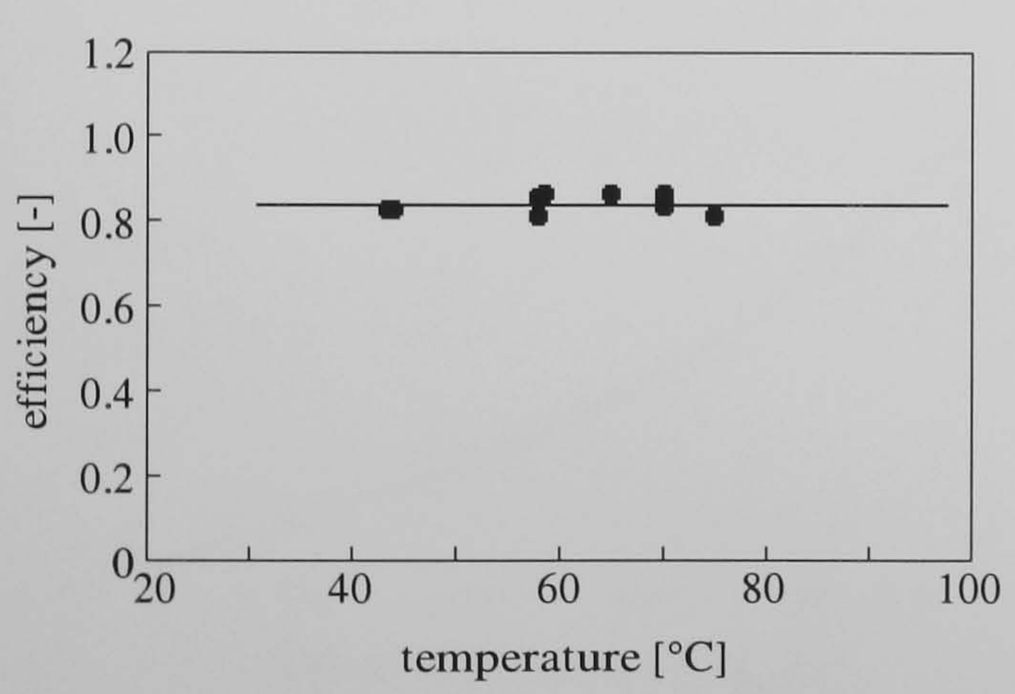

$\dot{V}_{\mathrm{R}}/\dot{V}_{\mathrm{P}} = 0.75,\ \dot{V}_{\mathrm{P}} = 2530m^3/h$

- $\eta_{\mathrm{sorp}} = 0.84 \pm 0.02$

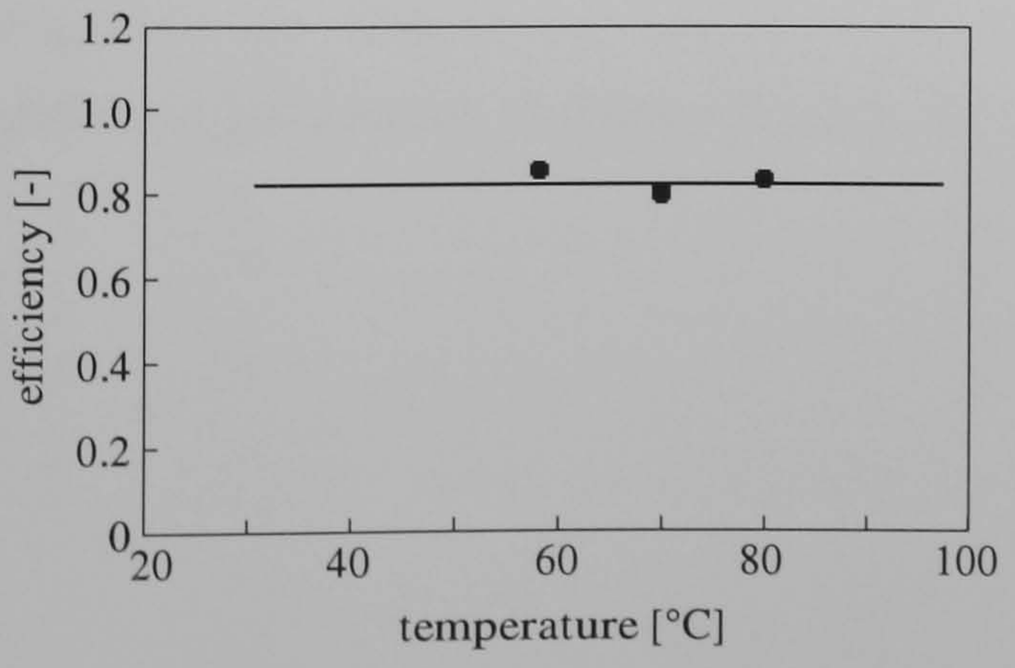

$\dot{V}_{\mathrm{R}}/\dot{V}_{\mathrm{P}} = 1.00,\ \dot{V}_{\mathrm{P}} = 2530m^3/h$

- $\eta_{\mathrm{sorp}} = 0.83 \pm 0.03$

Figure 4.10: Calculated η_{sorp} of the measured ΔX (ambient air regeneration)

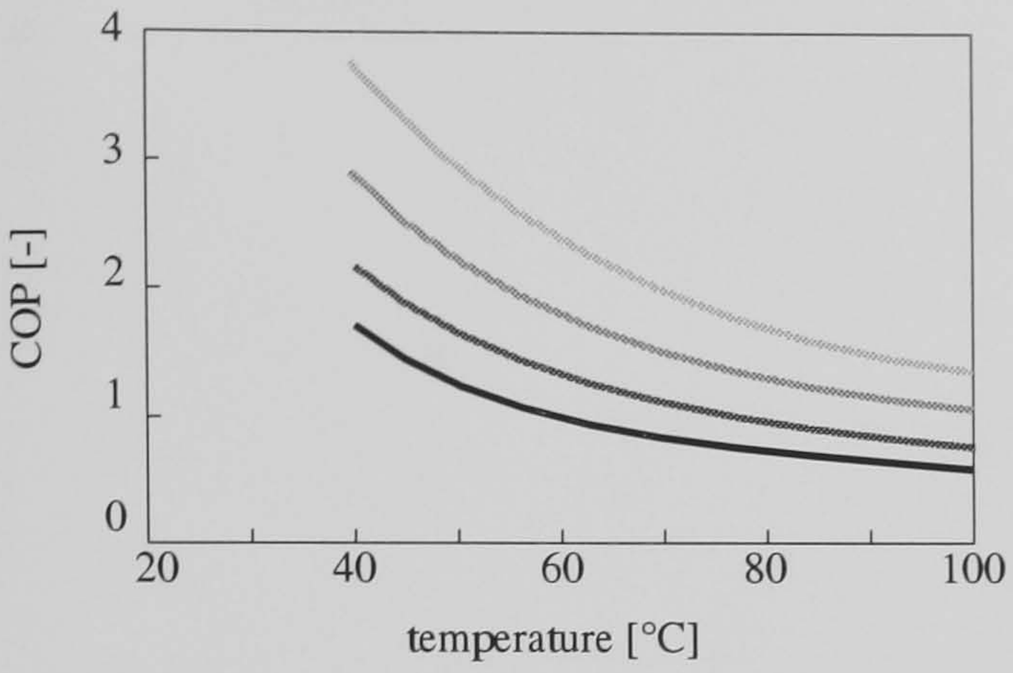

Figure 4.11a: COP dependent on regeneration temperature

- $\dot{V}_{\mathrm{R}}/\dot{V}_{\mathrm{P}} = 0.35$, $\eta_{\mathrm{sorp}} = 0.62$
- $\dot{V}_{\mathrm{R}}/\dot{V}_{\mathrm{P}} = 0.50$, $\eta_{\mathrm{sorp}} = 0.76$
- $\dot{V}_{\mathrm{R}}/\dot{V}_{\mathrm{P}} = 0.75$, $\eta_{\mathrm{sorp}} = 0.82$
- $\dot{V}_{\mathrm{R}}/\dot{V}_{\mathrm{P}} = 1.00$, $\eta_{\mathrm{sorp}} = 0.86$

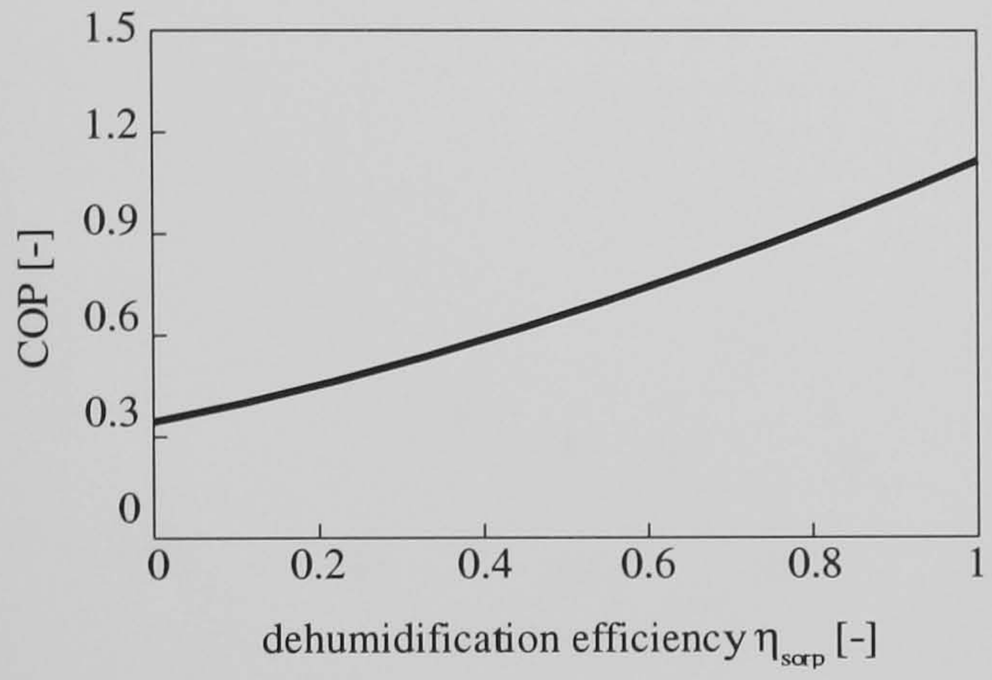

Figure 4.11b: COP of desiccant cooling system dependent on dehumidification efficiency
$\vartheta_{\mathrm{reg}} = 70\,^{\circ}\mathrm{C}$, $\eta_{\mathrm{HR}} = 0.85$, $\eta_{\mathrm{hum}} = 0.90$

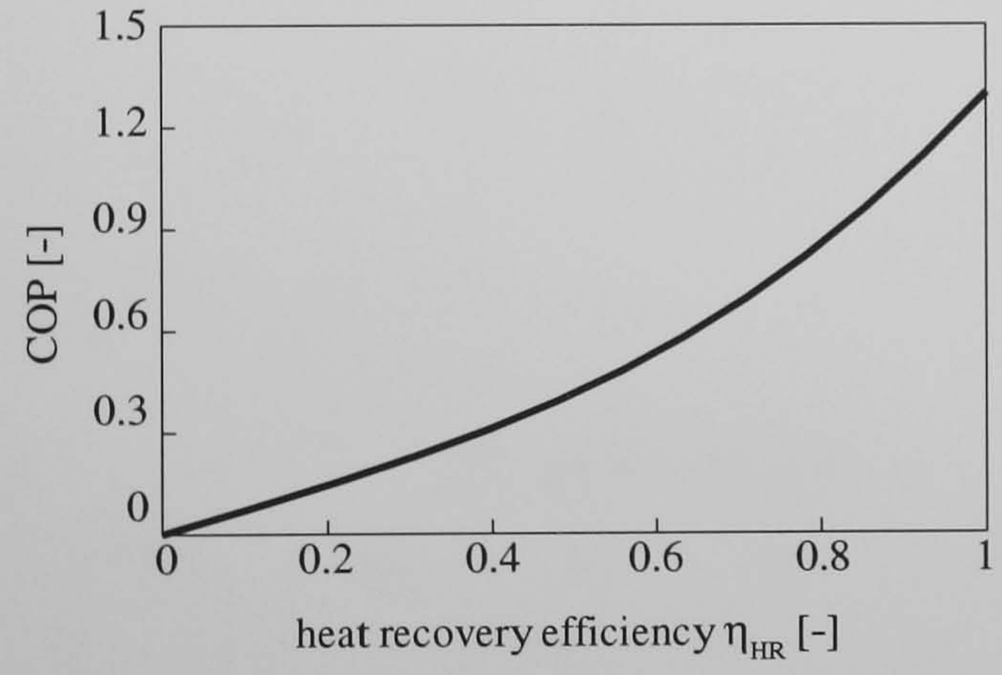

Figure 4.11c: COP of desiccant cooling system dependent on heat recovery efficiency
$\vartheta_{\mathrm{reg}} = 70\,^{\circ}\mathrm{C}$, $\eta_{\mathrm{sorp}} = 0.82$, $\eta_{\mathrm{hum}} = 0.90$

Figure 4.11: Calculated course of the COP in a DCS ventilation cycle depending on different parameter studies ($\vartheta_{\mathrm{amb}} = 32\,^{\circ}\mathrm{C}$, $rh_{\mathrm{amb}} = 0.40$, $\vartheta_{\mathrm{in}} = 26\,^{\circ}\mathrm{C}$, $rh_{\mathrm{in}} = 0.55$)

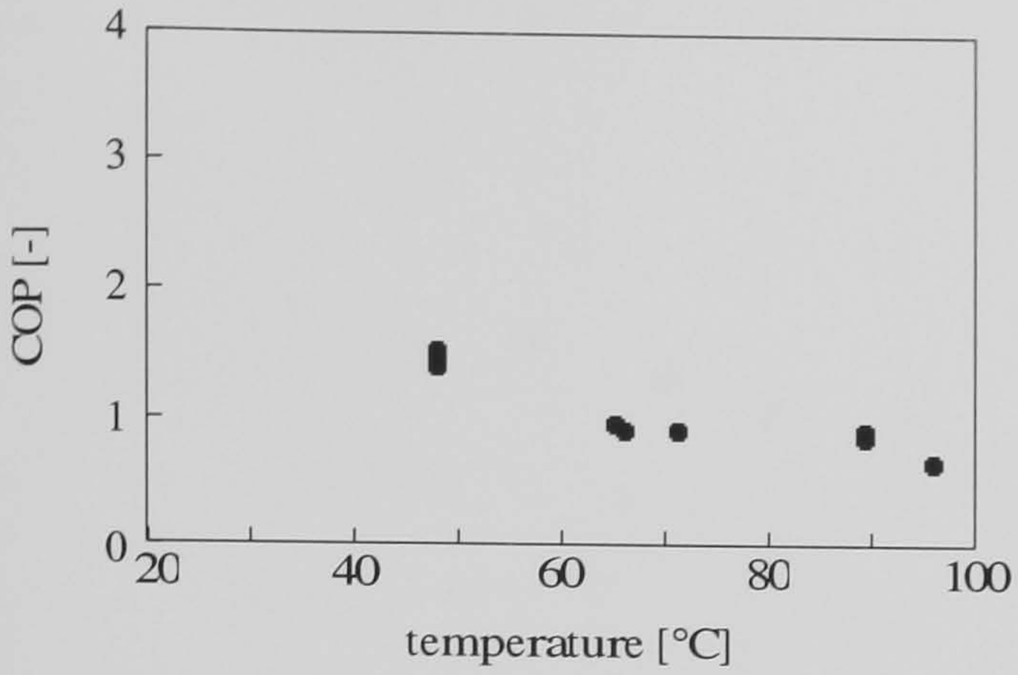

$\dot{V}_{\mathrm{R}}/\dot{V}_{\mathrm{P}} = 0.35,\ \dot{V}_{\mathrm{P}} = 2530m^3/h$

- $\eta_{\mathrm{sorp}} = 0.62 \pm 0.03$

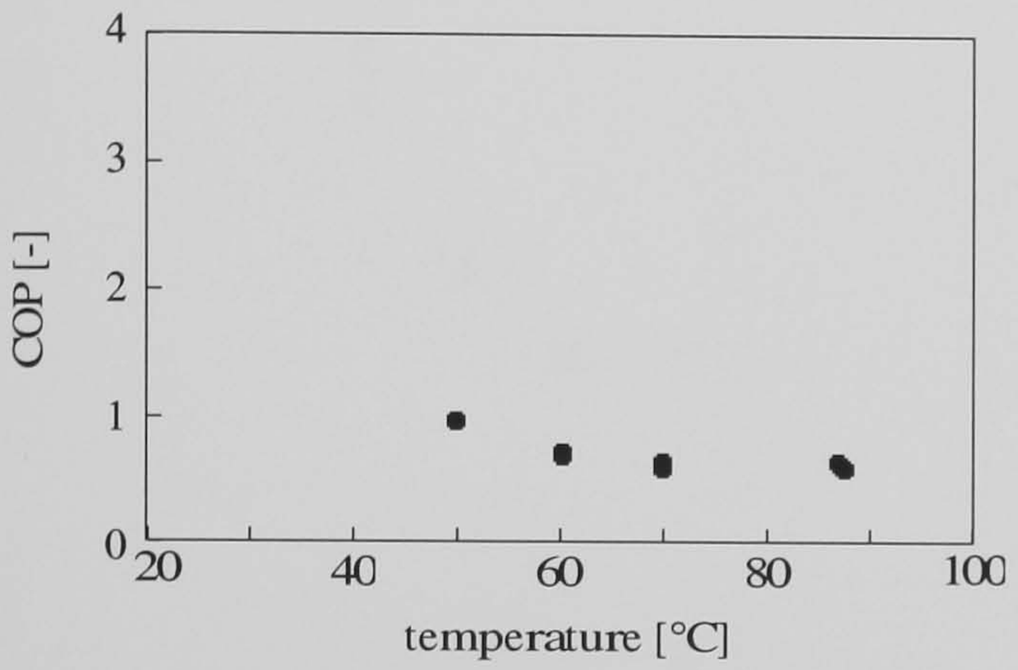

$\dot{V}_{\mathrm{R}}/\dot{V}_{\mathrm{P}} = 0.50,\ \dot{V}_{\mathrm{P}} = 2530m^3/h$

- $\eta_{\mathrm{sorp}} = 0.75 \pm 0.05$

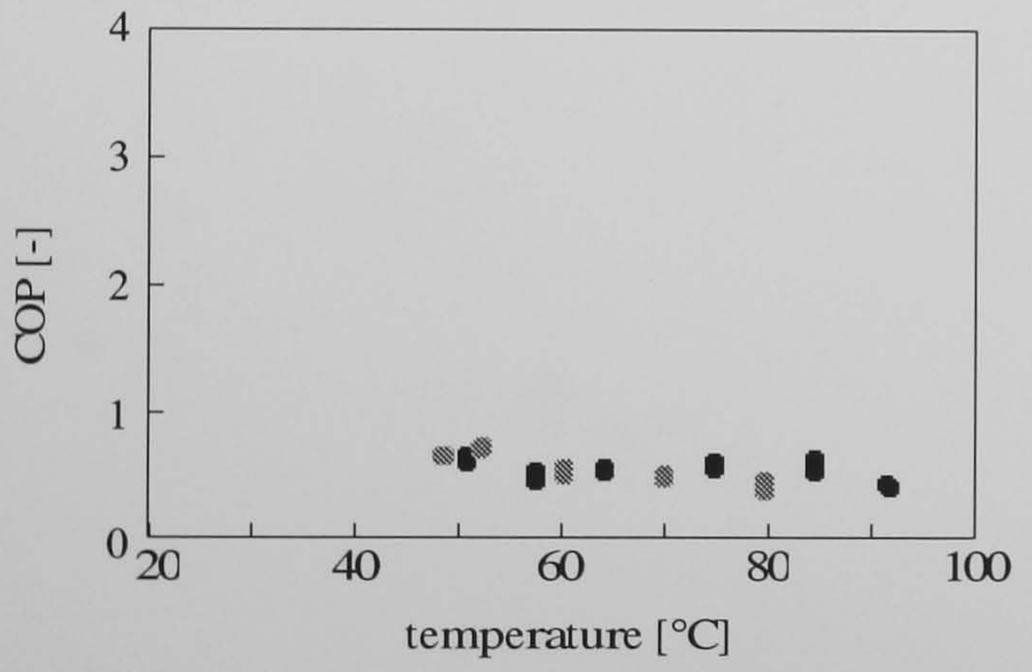

$\dot{V}_{\mathrm{R}}/\dot{V}_{\mathrm{P}} = 0.75,\ \dot{V}_{\mathrm{P}} = 2530m^3/h$

- $\eta_{\mathrm{sorp}} = 0.82 \pm 0.04$
- $\eta_{\mathrm{sorp}} = 0.79 \pm 0.02$
- $\eta_{\mathrm{sorp}} = 0.80 \pm 0.04$
- $\eta_{\mathrm{sorp}} = 0.85 \pm 0.02$

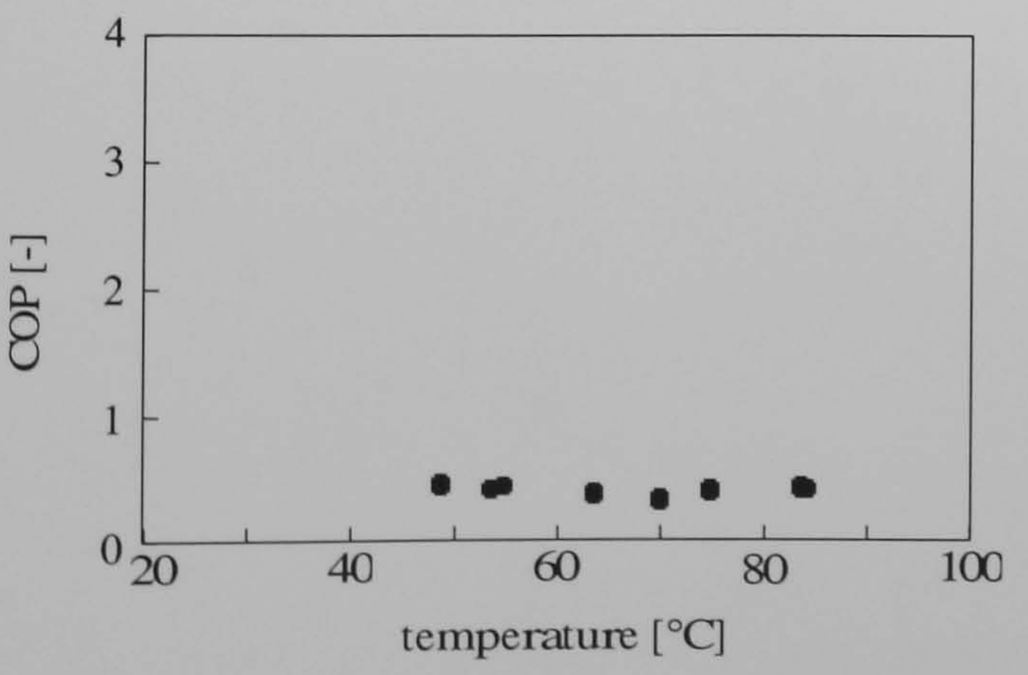

$\dot{V}_{\mathrm{R}}/\dot{V}_{\mathrm{P}} = 1.00,\ \dot{V}_{\mathrm{P}} = 2530m^3/h$

- $\eta_{\mathrm{sorp}} = 0.87 \pm 0.03$

Figure 4.12: Calculated COP from the test plant measurements

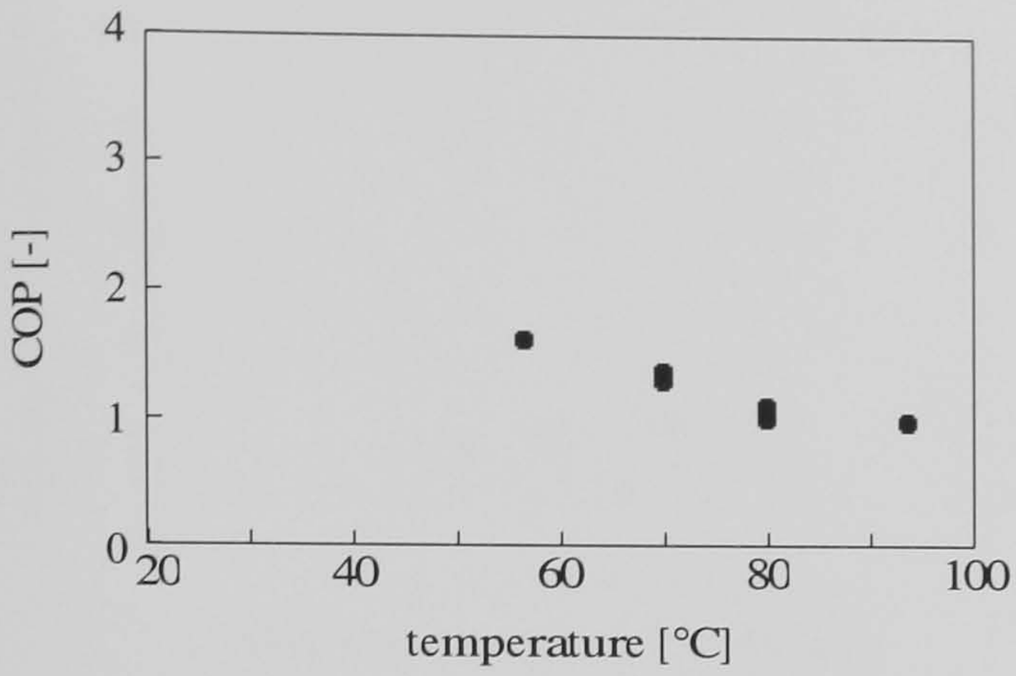

$\dot{V}_{\mathrm{R}}/\dot{V}_{\mathrm{P}} = 0.35,\ \dot{V}_{\mathrm{P}} = 2530m^3/h$

- $\eta_{\mathrm{sorp}} = 0.62 \pm 0.03$

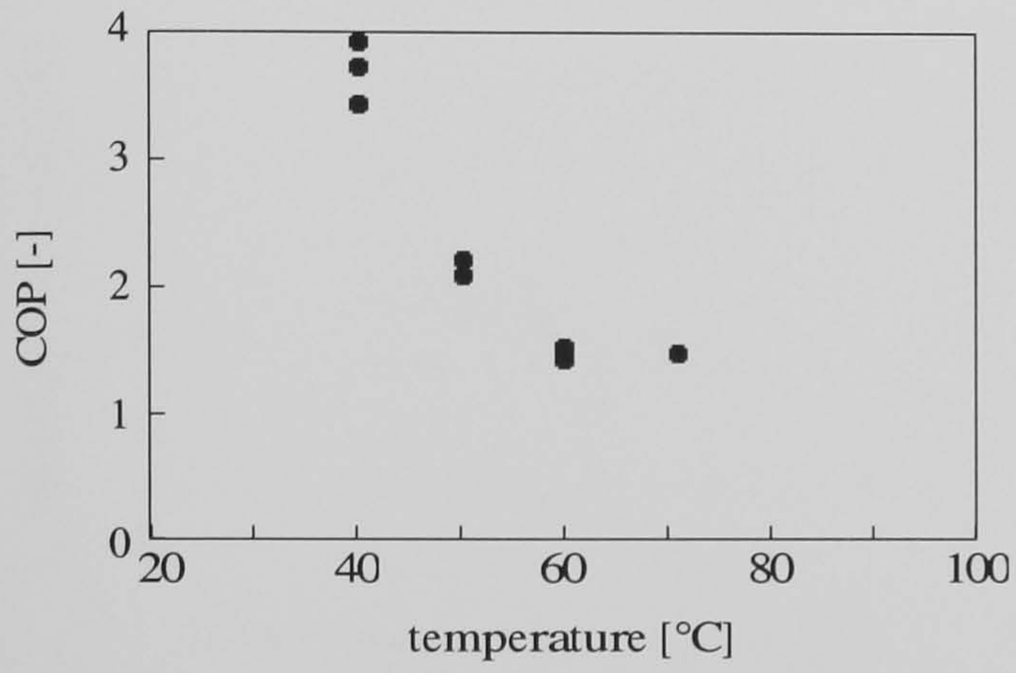

$\dot{V}_{\mathrm{R}}/\dot{V}_{\mathrm{P}} = 0.50,\ \dot{V}_{\mathrm{P}} = 2530m^3/h$

- $\eta_{\mathrm{sorp}} = 0.75 \pm 0.05$

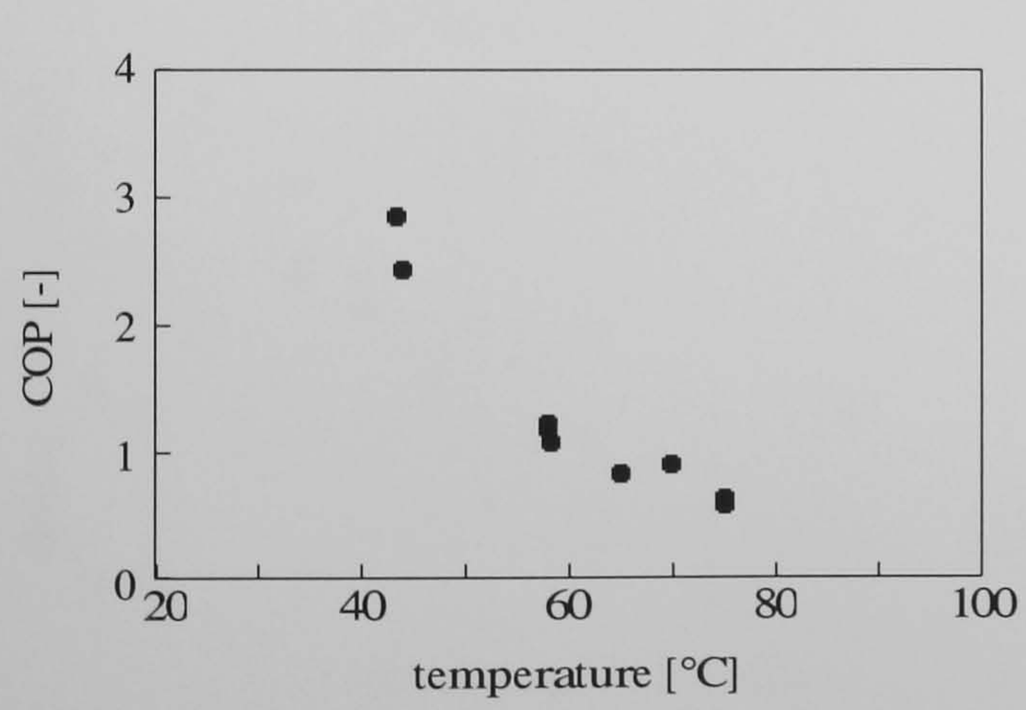

$\dot{V}_{\mathrm{R}}/\dot{V}_{\mathrm{P}} = 0.75,\ \dot{V}_{\mathrm{P}} = 2530m^3/h$

- $\eta_{\mathrm{sorp}} = 0.82 \pm 0.04$
- $\eta_{\mathrm{sorp}} = 0.79 \pm 0.02$
- $\eta_{\mathrm{sorp}} = 0.80 \pm 0.04$
- $\eta_{\mathrm{sorp}} = 0.85 \pm 0.02$

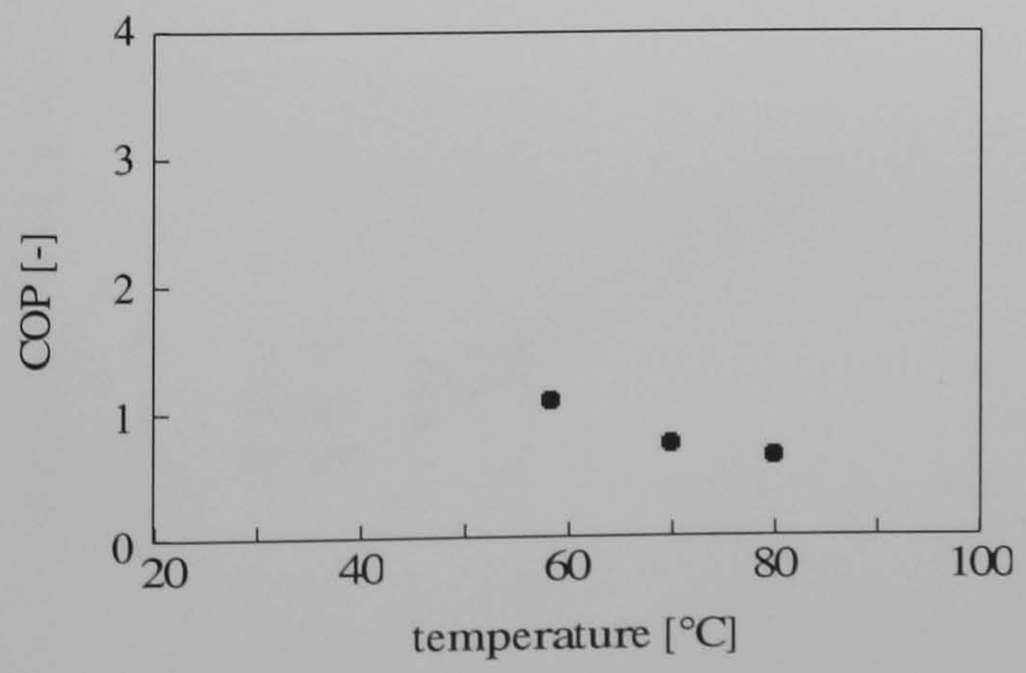

$\dot{V}_{\mathrm{R}}/\dot{V}_{\mathrm{P}} = 1.00,\ \dot{V}_{\mathrm{P}} = 2530m^3/h$

- $\eta_{\mathrm{sorp}} = 0.87 \pm 0.03$

Figure 4.13: Calculated COP from the measurements (ambient air regeneration)

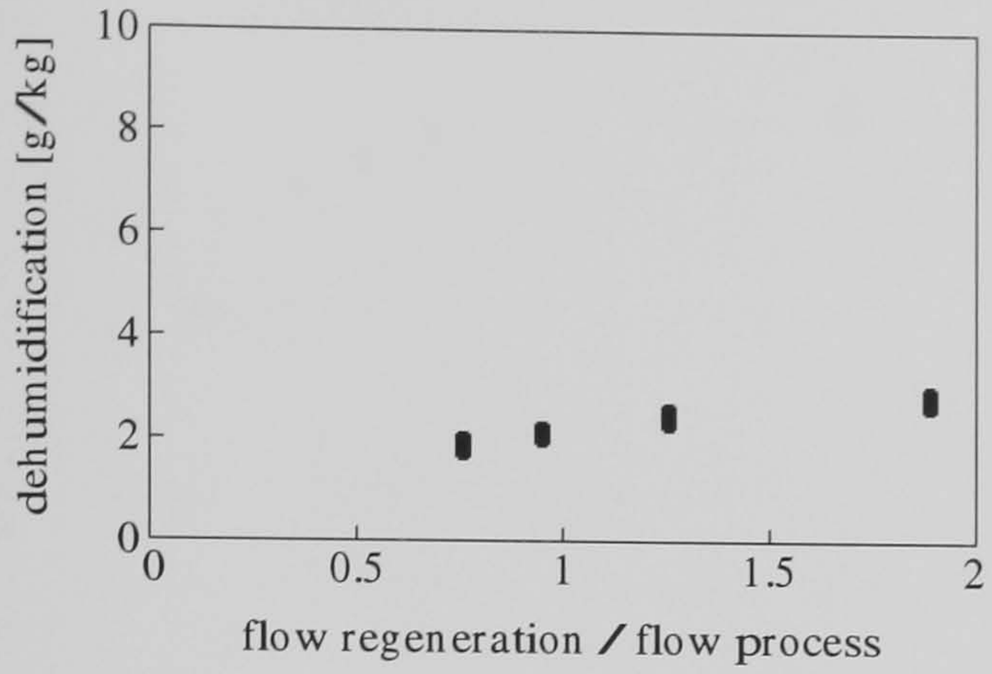

Figure 4.14a: Dehumidification [g/kg] dependent on decreasing process flow

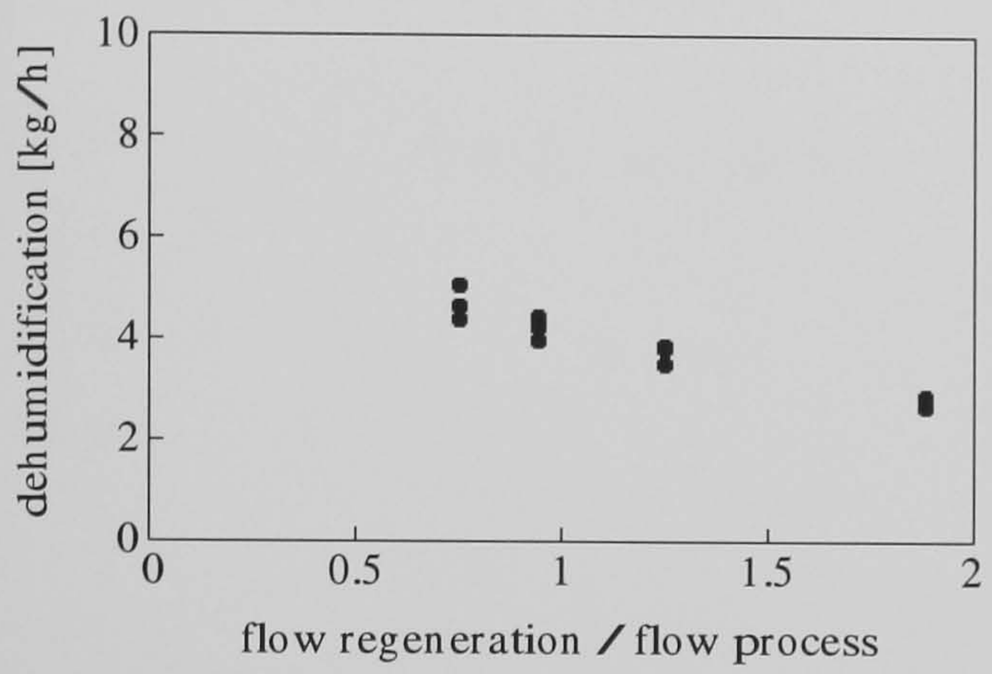

Figure 4.14b: Total dehumidification [kg/h] dependent on decreasing process flow

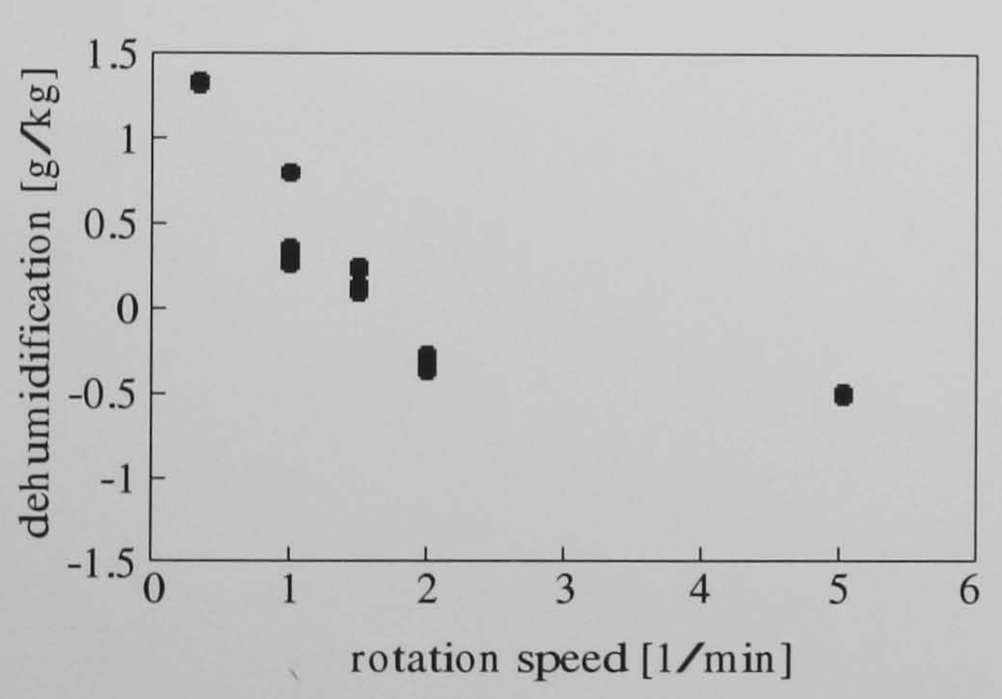

Figure 4.14c: Dehumidification [g/kg] dependent on rotation

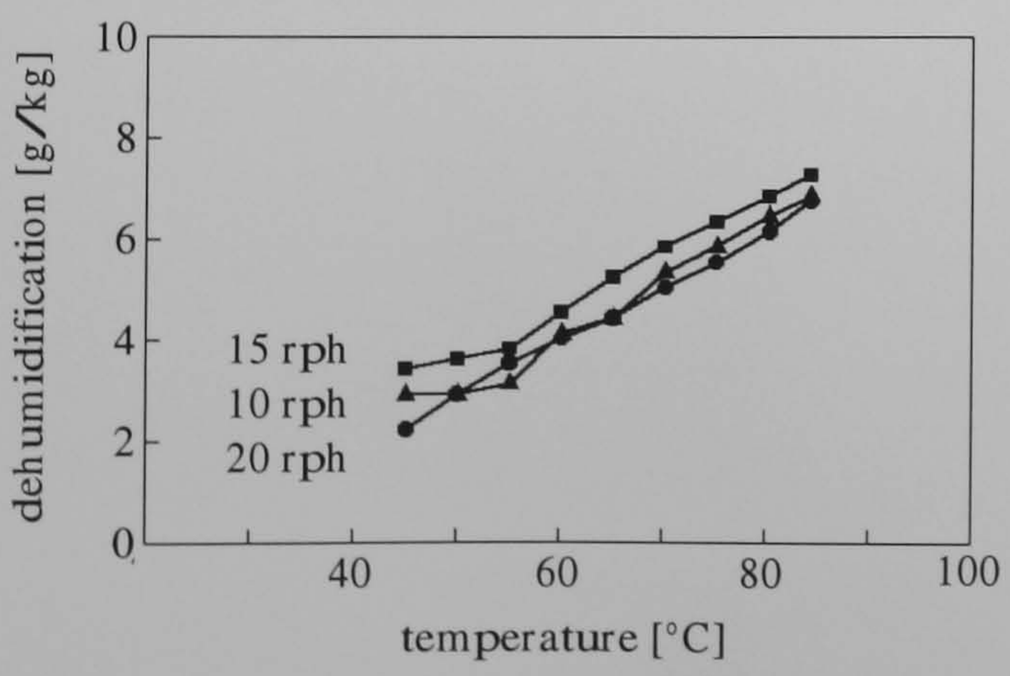

Figure 4.14d: Dehumidification [g/kg] dependent on rotation and temperature

Figure 4.14: Further measurement results of the dehumidifier

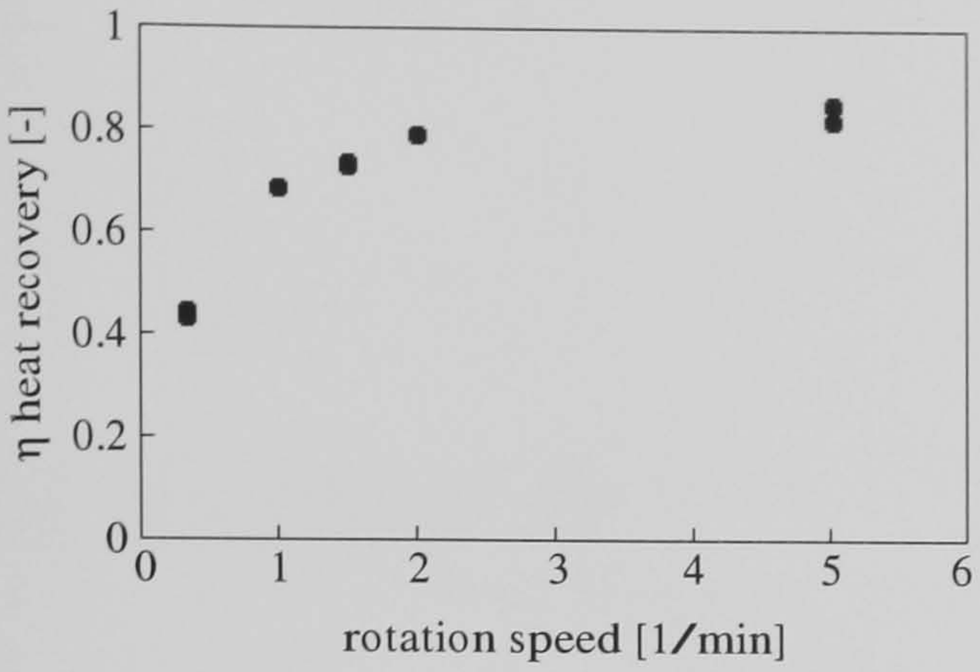

Figure 4.15a: Heat recovery efficiency of dehumidifier dependent on rotation

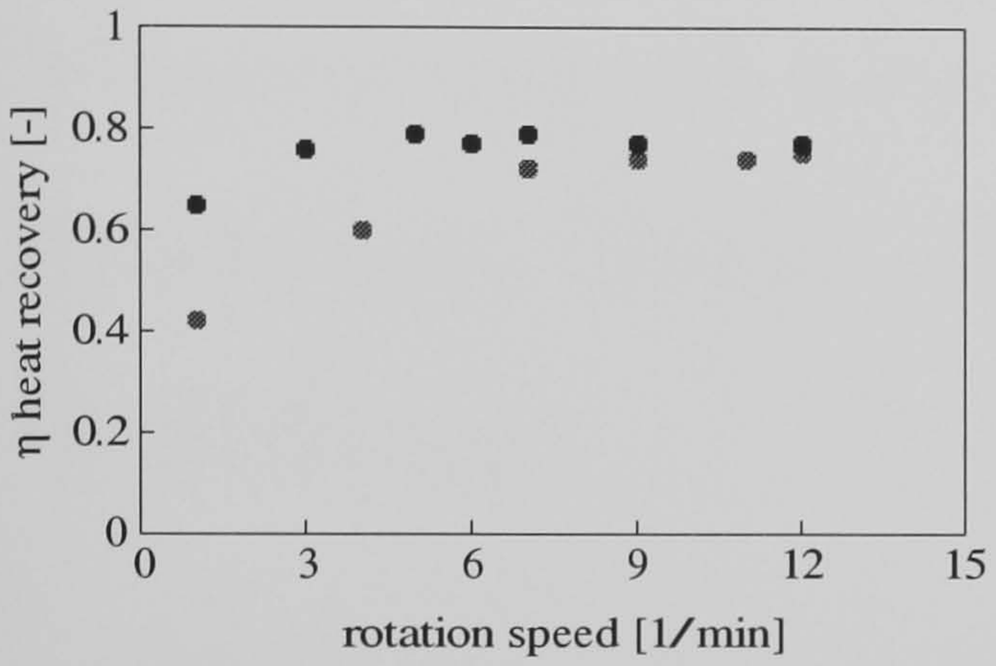

Figure 4.15b: Efficiency of heat recovery dependent on rotation

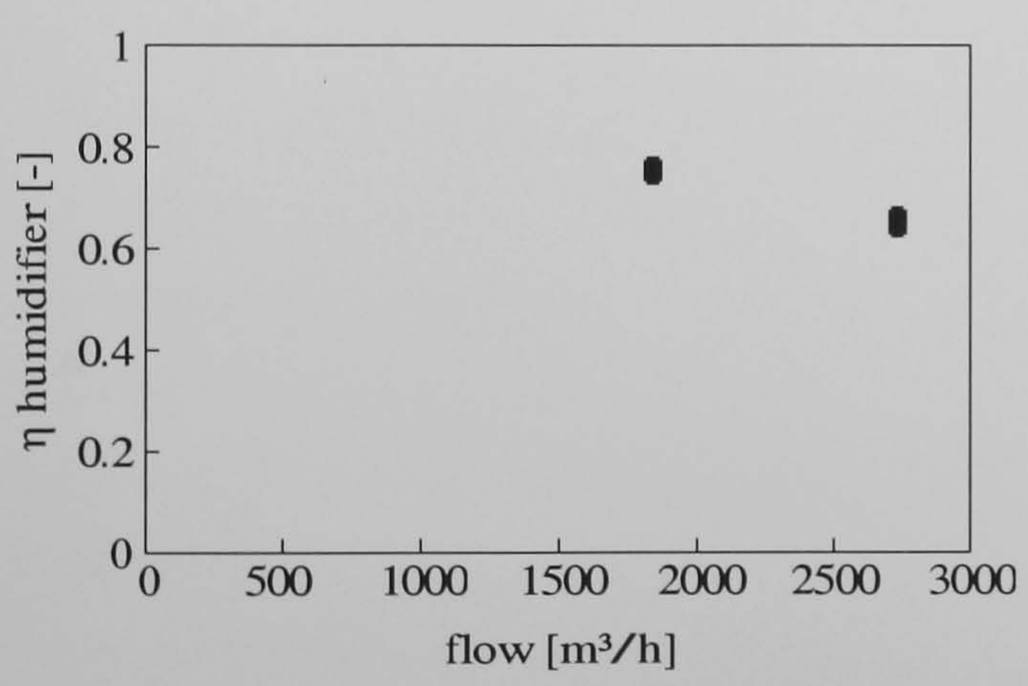

Figure 4.15c: Efficiency of humidifiers dependent on flow

Figure 4.15: Measurement results of test plant components

Chapter 5

Modelling of Desiccant Cooling Systems, Solar Collectors and Buildings

In the following chapter the modelling procedure for desiccant cooling systems, solar collectors and buildings will be described. Furthermore, the test building used will be described for which annual simulations were conducted. This test building and the adapted desiccant cooling systems with solar air collectors will be investigated for the climatic situations of Djakarta in Indonesia, Phoenix (Arizona) in the United States, Seville in Spain and Stuttgart in Germany. The target of these simulations is to obtain more information about the performance of desiccant cooling systems with solar air collectors which are connected to buildings in different climates. In particular, systems without thermal storage and their interaction with the dynamic thermal performance of the building will be investigated.

For the task of this work the program ESIMA, which is an abbreviation of "Energy Simulation in Mathematica" was developed in the environment of MATHEMATICA 1996. ESIMA is a modular simulation tool for dynamic thermal building simulations and for the simulation of heating, ventilation and air conditioning systems. It was developed to calculate the performance of buildings and HVAC plants and their interaction. The advantage of this tool is the ability to make quick changes in the source code which is important during development and to visualise results via graphical output without using additional programs.

5.1 Desiccant Cooling System

One of the main parameters describing the performance of an entire desiccant cooling system is the coefficient of performance abbreviated as COP. For the calculation of the COP it is usual to use enthalpy differences instead of temperature differences to show the influence of dehumidification. The thermal COP is calculated as

$$\mathrm{COP} = \frac{h_{\mathrm{amb}} - h_{\mathrm{in}}}{(1 - C_{\mathrm{bypass}}) \cdot \Delta h_{\mathrm{heater}}} \tag{5.1}$$

where C_{bypass} represents the amount of air streaming through the bypass and $\Delta h_{\mathrm{heater}}$ the enthalpy difference caused by a heater or solar collector. To calculate the enthalpies required for the calculation of the COP, each condition of air along the system must be evaluated. These conditions can only be calculated with the knowledge of component performance. The detailed calculation of a rotating dehumidifier has been described in chapter 3. For the heat recovery and the humidifiers the calculations will be provided in this chapter. Solar collectors will be described in detail in the next section.

In desiccant cooling systems a heat recovery with a high efficiency is required, as only this component is responsible for the decrease in enthalpy required for the desired inlet conditions. Rotating regenerators are effective in delivering high efficiencies with relatively small dimensions. The calculation of the heat recovery efficiency of these regenerators considering only sensible heat can be achieved with

$$\eta_{\mathrm{HR}} = \frac{\vartheta_{\mathrm{in},1} - \vartheta_{\mathrm{out},1}}{\vartheta_{\mathrm{in},1} - \vartheta_{\mathrm{in},2}}. \tag{5.2}$$

Equation 5.2 is only valid for balanced air flows; more precisely described balanced capacity flows in each section of the heat recovery. The efficiency depends on the velocity of the air flow and on the rotation speed of the wheel. By raising the rotation speed the rotational capacity and the efficiency increase. For unbalanced air flows in the heat recovery more detailed equations must be used.

The humidifiers in a desiccant cooling system are responsible for the cooling effect caused by evaporation. Hence it is necessary to employ humidification systems using liquid water to obtain a temperature drop during evaporation. Humidification systems using steam

are not appropriate for application in desiccant cooling systems. Detailed information on humidifiers are contained in HEINRICH and FRANZKE 1997. The calculation of the efficiency of a humidifier can be achieved by the following equation where X_s represents the absolute humidity at saturation.

$$\eta_{hum} = \frac{X_{out} - X_{in}}{X_s - X_{in}} \tag{5.3}$$

The modelling of conditions along the entire process of desiccant cooling must be carried out for multiple psychrometric calculation. Therefore, in the following, the relationships will be described for these calculation procedures.

GLÜCK 1991 specifies calculation procedures for calculating the saturation vapour pressure in Pa for the range of 0 °C to 100 °C with an error of $< 0.02\%$ with the following fit

$$\begin{aligned} P_{s,0\,°C-100\,°C} = 611 \cdot \exp(\, & 7.257 \cdot 10^{-2} \cdot \vartheta - 2.937 \cdot 10^{-4} \cdot \vartheta^2 \\ & +9.810 \cdot 10^{-7} \cdot \vartheta^3 - 1.901 \cdot 10^{-9} \cdot \vartheta^4) \end{aligned} \tag{5.4}$$

For the range of 100 °C to 200 °C the saturation vapour pressure can be calculated with an error of $< 0.03\%$ with

$$\begin{aligned} P_{s,100\,0\,°C-200\,0\,°C} = 611 \cdot \exp(\, & 7.142753 \cdot 10^{-2} \cdot \vartheta - 2.600931 \cdot 10^{-4} \cdot \vartheta^2 \\ & +6.432223 \cdot 10^{-7} \cdot \vartheta^3 - 7.410232 \cdot 10^{-10} \cdot \vartheta^4) \end{aligned} \tag{5.5}$$

The relative humidity describes the ratio of the existing vapour pressure P to the saturation vapour pressure P_s

$$rh = \frac{P}{P_s} \tag{5.6}$$

The absolute humidity X of humid air can be calculated with the knowledge of the gas constant of air $R_A = 287.1 J/(kg \cdot K)$, the gas constant of vapour $R_V = 461.4 J/(kg \cdot K)$ and the total atmospheric pressure which at sea level is $P_{tot} = 101325 Pa$.

$$X = \frac{R_A}{R_V} \cdot \frac{P}{P_{tot} - P} = 0.6222 \cdot \frac{P}{P_{tot} - P} \tag{5.7}$$

The enthalpy of humid air h, which is a value of the energy content of humid air, is the sum of the enthalpy of air h_A and the enthalpy of vapour h_V related to the reference temperature $\vartheta = 0\,°C$.

$$h_A = c_p \cdot \vartheta = 1.01 \cdot \vartheta \tag{5.8}$$

$$h_V = h_E + c_{p,V} \cdot \vartheta = 2501 + 1.86 \cdot \vartheta \tag{5.9}$$

$$h = h_A + X \cdot h_V \tag{5.10}$$

The conditions of humid air after a change of temperature and humidity can only be obtained by numerical solving methods using the previous equations. DEVRES 1994 therefore provides the solving procedures. The calculation procedure shown in Figure 5.1 for the psychrometric conditions in a desiccant cooling system of the ventilation type can be realised via the following:

1. Calculation of ambient air absolute humidity using equation 5.4, 5.6, 5.7 and enthalpy using equation 5.10 from climatic data of ambient air temperature and ambient air relative humidity.

2. Calculation of indoor air absolute humidity using equation 5.4, 5.6, 5.7 and enthalpy using equation 5.10 from data of indoor air temperature and indoor air relative humidity.

3. Calculation of absolute humidity after the outlet humidifier knowing the humidifier efficiency and using equation 5.3. The humidifier outlet temperature must be calculated by using numerical solving methods. The enthalpy is the same as the indoor air enthalpy.

4. Calculation of the regeneration temperature and calculation of the enthalpy and the relative humidity using numerical solving methods. The absolute humidity is the same as absolute humidity after the outlet humidifier. In the first run–through of this procedure the regeneration temperature should be estimated.

5. The dehumidifiers outlet conditions can be calculated knowing the dehumidification efficiency. The absolute humidity must be calculated using equation 3.9 and 3.11,

the enthalpy using equation 3.10, the temperature and the relative humidity using numerical analysis.

6. Calculation of the temperature after the heat recovery in the regeneration stream knowing the heat recovery efficiency and using equation 5.2.

7. Repetition of the last three steps until the regeneration temperature and the dehumidification does not change significantly.

8. Calculation of the temperature after the heat recovery in the process stream and using equation 5.2.

9. Calculation of absolute humidity after the inlet humidifier knowing the humidifier efficiency and using equation 5.3. The humidifier outlet temperature must be calculated by using numerical solving methods. The enthalpy is the same as after the heat recovery in the process stream.

For the calculation of desiccant cooling systems with ambient air regeneration the results can be obtained after one run–through of the procedure, as there is no interaction between regeneration temperature and dehumidification.

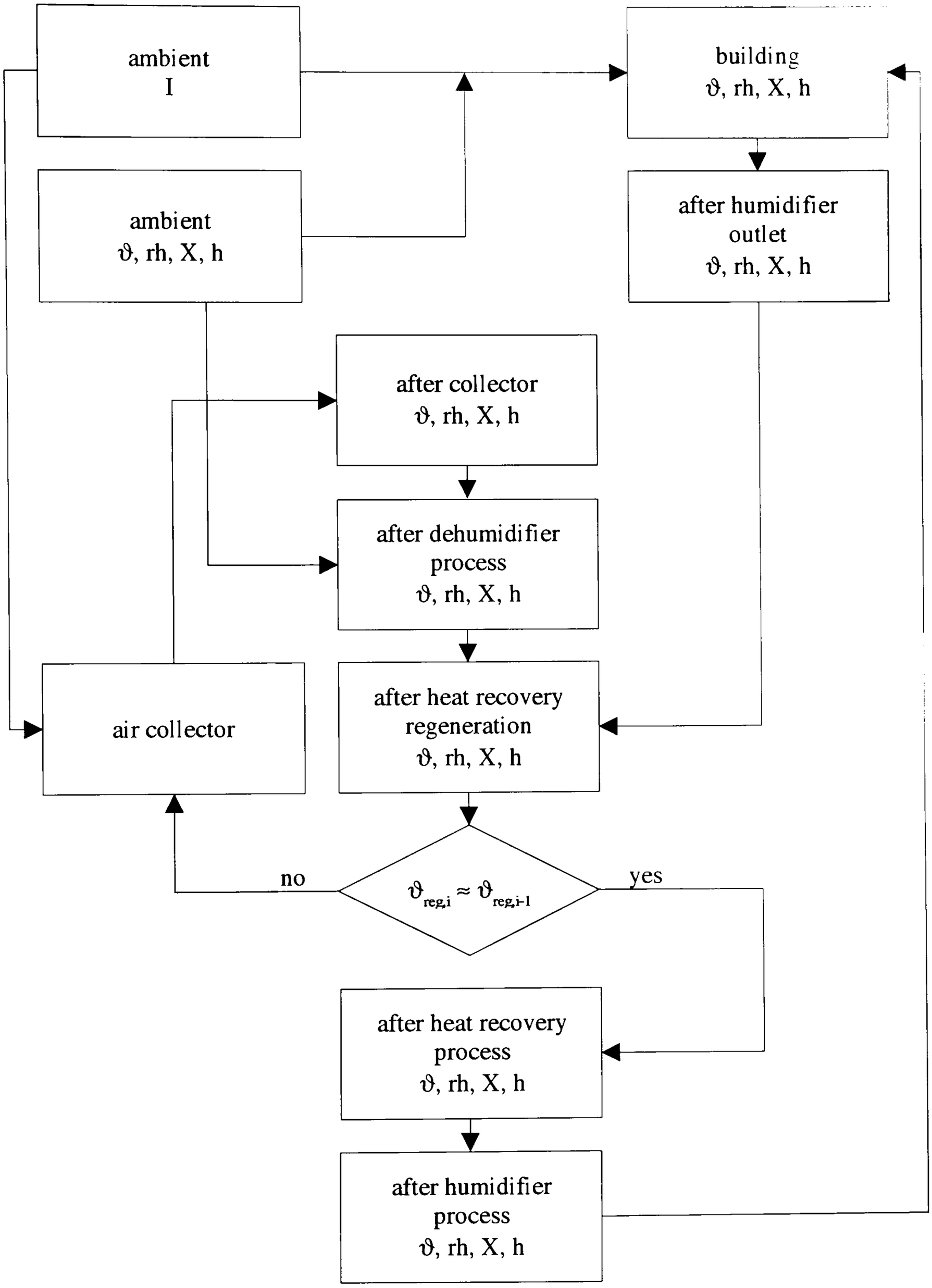

Figure 5.1: Flow chart of the calculation procedure for a DCS ventilation cycle with solar air collectors

5.2 Solar Collectors

Solar collectors are a special kind of heat exchanger that transform solar radiant energy into heat. However, solar collectors differ in some respects from conventional heat exchangers. In conventional heat exchangers, radiation is an unimportant factor, whereas the main parameter is the convective heat transfer coefficient. In solar collectors both phenomena are important. In the following, four collector types will be discussed, the flat–plate collector, the evacuated tube collector, the cpc–collector and the solar air collector. The question of which collector type is appropriate for desiccant cooling cannot be answered in general terms. The collector system must be chosen after consideration of the following aspects:

- What operating temperature must be reached by the collectors?
- What fluid must be heated up?
- How much space is available to install a collector field?

In most applications flat plate collectors and solar air collectors can provide the temperature levels required for desiccant cooling, hence they will be described in detail. In steady–state conditions the performance of a solar collector is described by an energy balance that indicates the distribution of incident solar energy into useful energy gain, thermal and radiant losses. A measure of collector performance is the collector efficiency η_{coll}

$$\eta_{\text{coll}} = \frac{\int Q_{\text{U}} dt}{\int G dt} \tag{5.11}$$

where Q_{U} is the useful energy gain per square metre and G the irradiation. The useful energy gain of a collector can be derived by

$$Q_{\text{U}} = A_{\text{coll}} \cdot (\tau \cdot \alpha \cdot G - U_{\text{coll}} \cdot (\vartheta_{\text{abs,m}} - \vartheta_{\text{amb}})) \tag{5.12}$$

where A_{coll} is the collector area, τ the transmission coefficient of the transparent cover, α the absorption coefficient of the absorber plate, U_{coll} the average U–value of the collector, $\vartheta_{\text{abs,m}}$ the mean absorber temperature and ϑ_{amb} the ambient temperature. A detailed

calculation of collector losses is rather complicated, but with some simplifications an estimation of collector losses can be handled easily. An empirical equation for the calculation of the U–value of the collectors top side U_{top} was developed by KLEIN 1979.

$$U_{\text{top}} = \frac{1}{\frac{n}{\frac{C}{T_{\text{abs,m}}} \cdot \left(\frac{T_{\text{abs,m}} - T_{\text{amb}}}{n+f}\right)^{e}} + \frac{1}{h_{\text{W}}}} + \frac{\sigma \cdot (T_{\text{abs,m}} + T_{\text{amb}}) \cdot (T_{\text{abs,m}}^2 + T_{\text{amb}}^2)}{\frac{1}{\epsilon_{\text{abs}} + 0.00591 \cdot n \cdot h_{\text{W}}} + \frac{2 \cdot n + f - 1 + 0.133 \cdot \epsilon_{\text{abs}}}{\epsilon_{\text{g}}} - n} \tag{5.13}$$

with

$$f = (1 + 0.0089 \cdot h_{\text{W}} - 0.1166 \cdot h_{\text{W}} \cdot \epsilon_{\text{abs}}) \cdot (1 + 0.07866 \cdot n)$$

$$C = \begin{cases} 520 \cdot (1 - 0.000051 \cdot \beta^2) & : \quad 0° < \beta < 70° \\ 390.052 & : \quad 70° < \beta < 90° \end{cases}$$

$$e = 0.43 \cdot \left(1 - \frac{100}{T_{\text{abs,m}}}\right)$$

where n is the number of glass covers, ϵ_g the emittance of glass, ϵ_{abs} is the emittance of the absorber, h_{W} the wind heat transfer coefficient and β the collector tilt angle. The values of the temperatures are in K. An example for top loss coefficients with $\beta = 45°$, $\vartheta_{\text{abs,m}} = 160°C$, $\vartheta_{\text{amb}} = 32°C$, $h_{\text{W}} = 10W/m^2K$, $\epsilon_g = 0.88$ and $\epsilon_{\text{abs}} = 0.95$ of a single covered collector is $U_{\text{top}} = 8.4W/m^2K$ and of a double covered collector $U_{\text{top}} = 5.0W/m^2K$. KLEIN 1979 describes an accuracy of this equation of $\pm 0.3W/m^2K$ for a temperature difference of $\vartheta_{\text{abs,m}} - \vartheta_{\text{amb}} = 200K$. The U–value of the collector can be derived with

$$U_{\text{coll}} = U_{\text{top}} + U_{\text{bottom}} + U_{\text{edges}} \tag{5.14}$$

The problem with equation 5.12 is that it is difficult to evaluate or measure the mean absorber temperature. For this reason the useful energy gain can be expressed in terms of the inlet fluid temperature $\vartheta_{\text{f,in}}$ and a parameter called the collector heat removal factor F_{R}, which can be evaluated analytically from basic principles. The equation can be written as

$$Q_{\text{U}} = A_{\text{coll}} \cdot F_{\text{R}} \cdot (\tau \cdot \alpha \cdot G - U_{\text{coll}} \cdot (\vartheta_{\text{f,in}} - \vartheta_{\text{amb}})) \tag{5.15}$$

To make a detailed analysis of F_R the temperature distributions must be known. The absorbed solar energy must be conducted along the plate to the region of the tubes. Thus the temperature level between the tubes will be higher than the temperature at the connection points of plate and tube. The transferred energy will heat the fluid and the temperature will rise along the flow direction. A mathematical description of each solving step is provided by DUFFIE and BECKMAN 1991. In the following only intermediate steps of the solution will be shown. In line with the fin theory the function F_{fin}, which is the standard fin efficiency, can be described with

$$F_{fin} = \frac{\tanh\left(\sqrt{\frac{U_{coll}}{\lambda \cdot x}} \cdot \frac{W-D}{2}\right)}{\sqrt{\frac{U_{coll}}{\lambda \cdot x}} \cdot \frac{W-D}{2}} \tag{5.16}$$

where λ is the heat conductivity of the absorber material, x the thickness of the plate, W the width between the tubes and D the tube diameter. Considering all resistances in the plate, the collector efficiency factor F' is

$$F' = \frac{\frac{1}{U_{coll}}}{W \cdot \left(\frac{1}{U_{coll}(D+(W-D)\cdot F_{fin})} + \frac{\gamma_{bond}}{\lambda_{bond} \cdot b_{bond}} + \frac{1}{\pi \cdot D_i \cdot h_{fi}}\right)} \tag{5.17}$$

where λ_{bond} is the bond thermal conductivity, γ_{bond} the average bond thickness, b_{bond} the bond width and h_{fi} the heat transfer coefficient between the fluid and the tube wall. The heat transfer coefficient h_{fi} covers a range from 100 W/m^2 (laminar flow) to 1000 W/m^2 (highly turbulent flow). Increasing h_{fi} beyond 1000 W/m^2 does not significantly increase F'. Taking the flow into consideration, the heat removal factor F_R is

$$F_R = \frac{\dot{m} \cdot c_p}{A_{coll} \cdot U_{coll}} \cdot \left(1 - \exp\left(-\frac{A_{coll} \cdot U_{coll} \cdot F'}{\dot{m} \cdot c_p}\right)\right) \tag{5.18}$$

It is convenient to define a collector flow factor F'' as the ratio of the heat removal factor to the collector efficiency factor.

$$F'' = \frac{F_R}{F'} \tag{5.19}$$

With all this information a collector can be described. If the outlet temperature is high, it will be especially necessary to know the critical radiation level I_{Tc} of a collector. This

is the value for which the absorbed radiation and the losses are equal:

$$I_{\mathrm{Tc}} = \frac{U_{\mathrm{coll}} \cdot (\vartheta_{\mathrm{f,in}} - \vartheta_{\mathrm{amb}})}{\tau \cdot \alpha} \tag{5.20}$$

Hence, it is possible to evaluate the mean temperature of the absorber plate, the mean temperature of the fluid and the fluid outlet temperature.

$$\vartheta_{\mathrm{abs,m}} = \vartheta_{\mathrm{f,in}} + \frac{(1 - F_{\mathrm{R}}) \cdot Q_{\mathrm{U}}}{A_{\mathrm{coll}} \cdot F_{\mathrm{R}} \cdot U_{\mathrm{coll}}} \tag{5.21}$$

$$\vartheta_{\mathrm{f,m}} = \vartheta_{\mathrm{f,in}} + \frac{(1 - F'') \cdot Q_{\mathrm{U}}}{A_{\mathrm{coll}} \cdot F_{\mathrm{R}} \cdot U_{\mathrm{coll}}} \tag{5.22}$$

$$\vartheta_{\mathrm{f,out}} = \vartheta_{\mathrm{f,in}} + \frac{Q_{\mathrm{U}}}{\dot{m} \cdot c_{\mathrm{p}}} \tag{5.23}$$

Solar air collectors as shown in Figure 5.2 are radiative heat exchangers which are essentially used at temperature levels below 100 °C in air heating and drying systems. The use of air as a heat transfer medium instead of water in solar collectors reduces the risks of corrosion and freezing and also helps to decrease the costs. The low density and low specific heat of air, however, require high volume flow rates that lead to high friction losses. Because of the low thermal conductivity, the temperature difference between the absorber and the fluid is much higher than in liquid collectors, and the thermal efficiency is reduced. Moreover, the ratio of additional energy required to move the fluid is much higher in air collectors than in liquid collectors. The design of the flow duct and heat transfer surface of solar air collectors should therefore be executed with the objectives of high heat transfer rates and low friction losses. In the literature, many different designs of solar air collectors are suggested. An important characteristic of the thermal behaviour is the flow path of the air. Two main types of design exist: Flow below the absorber plate; this includes a stagnant air layer between the absorber and the transparent cover; flow above or through the absorber in contact with the transparent cover. ALTFELD 1985 showed that the collector efficiency of the type having a stagnant air layer and flow below the absorber plate seems to be most promising in solar air collector design. To increase the collector efficiency factor F', additional fins under the absorber plate are required. The heat transfer coefficient h between the air and the duct walls is much more important than in liquid collectors. Therefore, it is useful to make a more detailed evaluation of the heat transfer coefficient. At first, the radiation heat transfer coefficient h_{r} would be

evaluated with

$$h_{\mathrm{r}} = \frac{4 \cdot \sigma \cdot T_{\mathrm{m}}^3}{\frac{1}{\epsilon_1} + \frac{1}{\epsilon_2} - 1} \tag{5.24}$$

where $\sigma = 5.67 \cdot 10^{-8} W/m^2 K^4$ is the radiation constant of Stefan and Boltzmann, T_{m} the mean radiation temperature in K, ϵ_1 and ϵ_2 are the emissivity coefficients of the reverse of the absorber plate and the bottom duct wall. In a first approximation, the radiation temperature can be assumed to be the mean fluid temperature. For the calculation of the convective heat transfer coefficient h_{c}, it can be assumed that it does not vary. In a first step the Reynolds number Re must be calculated with equation 3.17 and the Nusselt number Nu with the following correlation from the data of KAYS and CRAWFORD 1980.

$$Nu = 0.0158 \cdot Re^{0.8} \tag{5.25}$$

Since the length–to–diameter–ratio l/d_{h} is large and Re is greater than 2300, the flow is turbulent and fully developed. In flow situations where l/d_{h} is 10, the average Nu is approximately 16% higher than the given equation. If l/d_{h} equals 30, equation 5.25 still under–predicts by 5%. If l/d_{h} equals 100, the effect of the entrance region disappears. The convective heat transfer coefficient h_{c} can now be derived by equation 3.16. The collector efficiency factor F' for air collectors with the flow below the absorber plate and without any fins is

$$F' = \frac{1}{1 + \frac{U_{\mathrm{coll}}}{h_{\mathrm{c}} + \frac{1}{h_{\mathrm{c}}} + \frac{1}{h_{\mathrm{r}}}}}. \tag{5.26}$$

Having a solar air collector with fins the efficiency factor must be corrected to

$$F'_{\mathrm{fins}} = \frac{F'}{1 + \frac{1 - F'}{\frac{F'}{F_{\mathrm{plate}}} + \frac{W \cdot h_{\mathrm{plate}}}{2 \cdot W_2 \cdot h_{\mathrm{fin}} \cdot F_{\mathrm{fin}}}}} \tag{5.27}$$

where F_{plate} is the fin efficiency of the absorber plate and F_{fin} the fin efficiency of the fin. Now it is possible to derive F_{R} from equation 5.18, $\vartheta_{\mathrm{f,out}}$ from equation 5.23, $\vartheta_{\mathrm{abs,m}}$ from equation 5.21 and $\vartheta_{\mathrm{f,m}}$ from equation 5.22. The calculation must be made once more in

a further iteration step with a new average absorber plate temperature.

Next to the described flat–plate collectors, more sophisticated evacuated tube collectors are available. These collectors are long, narrow, flat absorbers which are mounted inside evacuated glass tubes. Convective heat losses from collectors are reduced or eliminated by evacuating the space between the absorber and the glass cover. As the pressure is reduced to a moderately low level, the convection ceases, but the heat conduction through the gas remains constant until the free path of the molecules has the order of the characteristic spacing. Most practical designs rely on evacuated tubes which provide the structural strength to withstand the pressure difference. The calculation of the collector parameters depends on the geometry of absorber and tube. A special type of evacuated tube collectors are compound parabolic concentrators, the so–called cpc–collectors, which have a parabolic mirror on the back of the glass tube. This collector type is appropriate for situations requiring a high temperature.

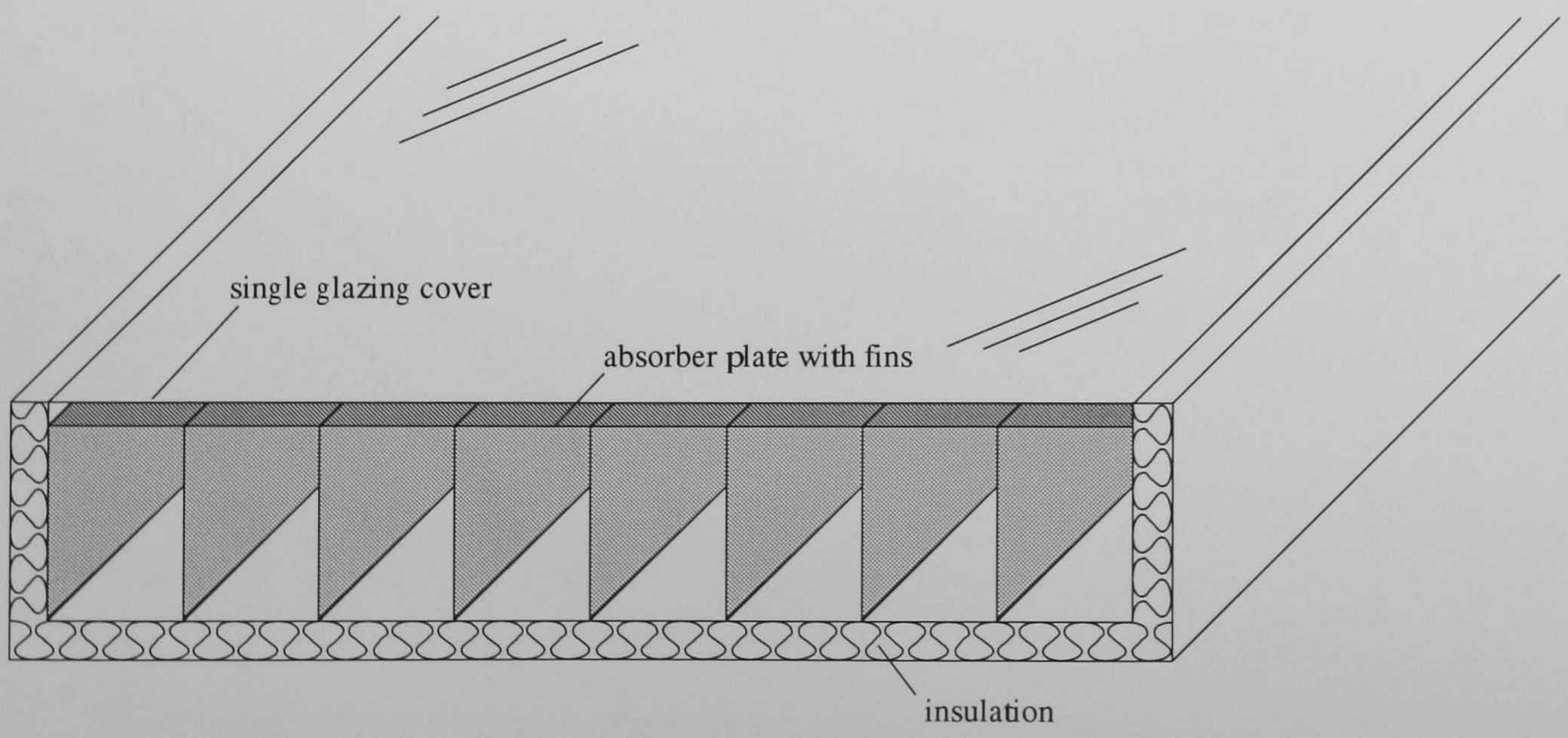

Figure 5.2: Schematic of an air collector

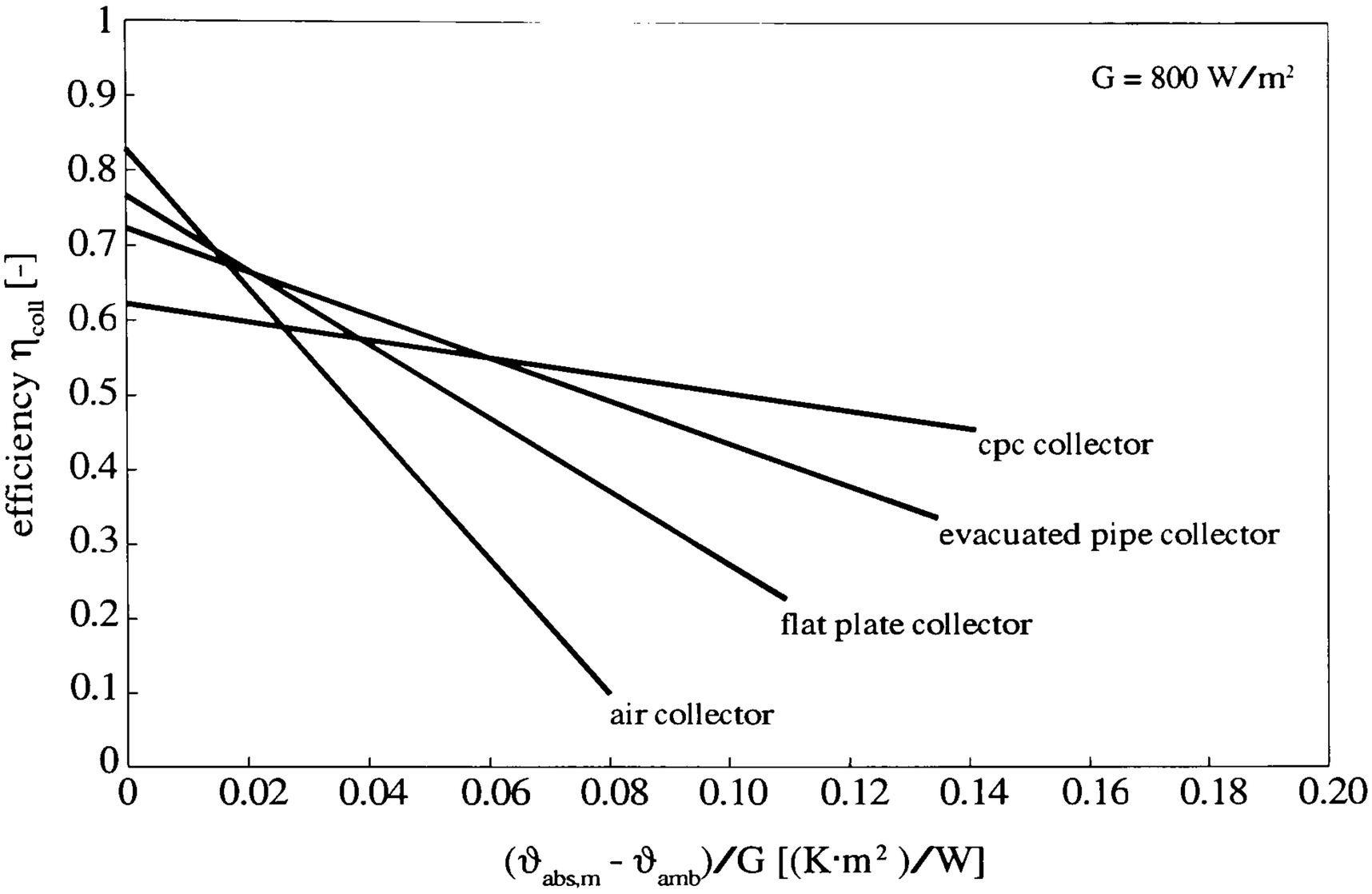

Figure 5.3: Efficiencies of different collectors

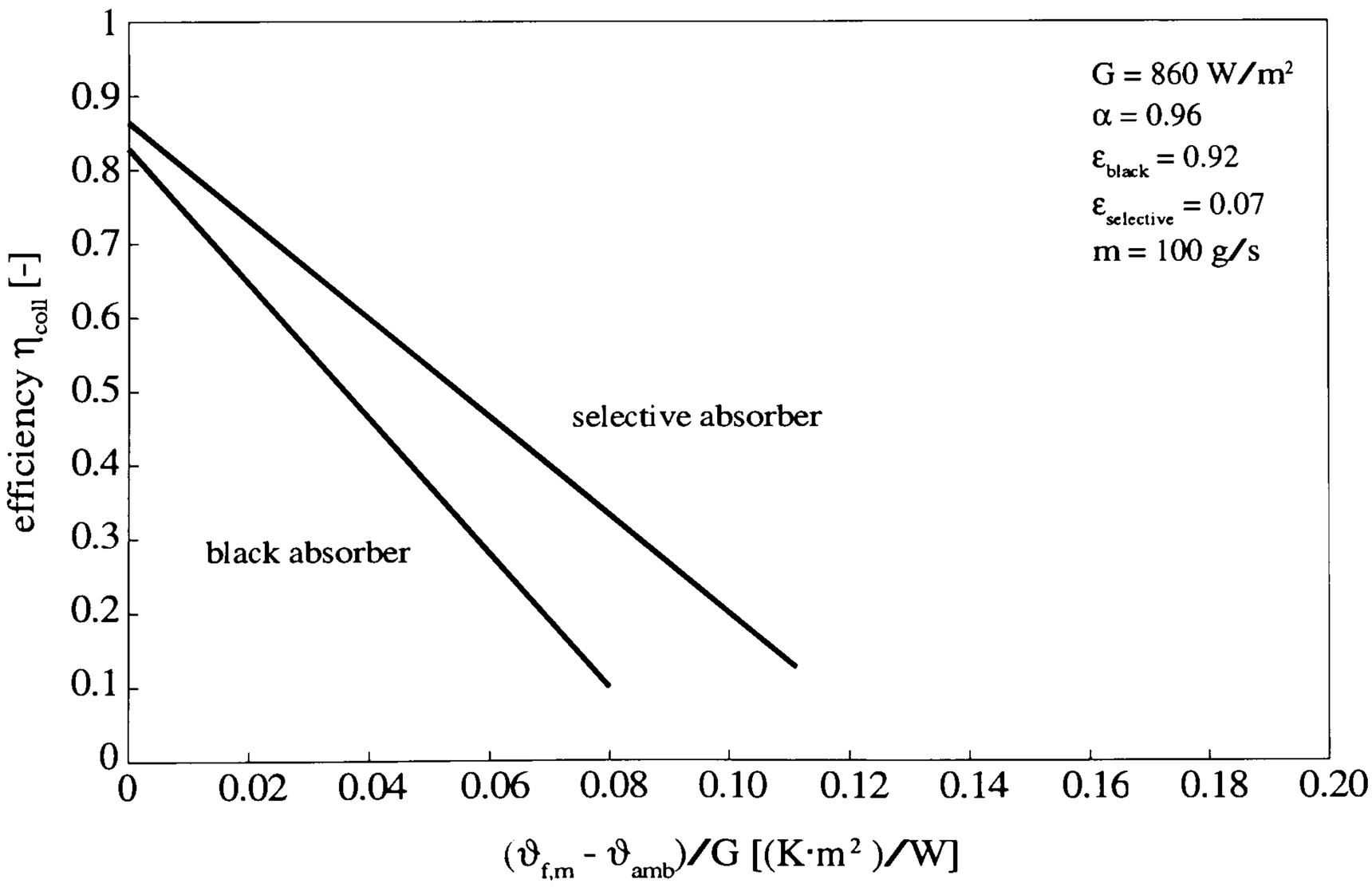

Figure 5.4: Efficiencies of different air collectors measured by MORHENNE and FIEBIG 1990

5.3 Building

The thermal performance of a building under dynamic boundary conditions must be calculated numerically. CLARKE 1985 and FEIST 1994 therefore gives an overview. In the following description the theoretical background for the building model is given. Starting from the Fourier heat conduction equation

$$\frac{\partial \vartheta}{\partial t} = a \cdot \frac{\partial^2 \vartheta}{\partial x^2} \tag{5.28}$$

where $a = \lambda/(\rho \cdot c)$ is the diffusivity, t the time step and x the thickness. For constructions with several layers and a non–infinite thickness, equation 5.28 must be solved numerically. A common method with a high numerical stability was suggested by Crank and Nicolson. Equation 5.28 was discretised with the Crank–Nicolson scheme combining explicit and implicit discretisation and guaranteeing numerical stability also for Fourier numbers of $P > 0.5$.

$$P = a \cdot \frac{\Delta t}{\Delta x^2} \tag{5.29}$$

The discretised heat conduction equation now allows the calculation of temperatures for each time step n from the previous time step $n-1$ at each location j of the construction. The main equation of layer 2 as a central layer surrounded by other layers for homogeneous materials is provided by SHIH 1984.

$$\vartheta_{1,\mathrm{n}} - \left(2 + \frac{2}{P}\right) \cdot \vartheta_{2,\mathrm{n}} + \vartheta_{3,\mathrm{n}} = -\vartheta_{1,\mathrm{n-1}} + \left(2 - \frac{2}{P}\right) \cdot \vartheta_{2,\mathrm{n-1}} - \vartheta_{3,\mathrm{n-1}} \tag{5.30}$$

This equation is only valid for homogeneous layers with constant thickness and diffusivity. For non–homogeneous layer combinations the equation must be formulated by introducing so–called virtual layers. The main equation of layer 2 for non–homogeneous materials is

$$\begin{gathered} -r_{12} \cdot \vartheta_{1,\mathrm{n}} + \left(\tfrac{1}{P} + 2 - r_{21} - r_{23}\right) \cdot \vartheta_{2,\mathrm{n}} - r_{32} \cdot \vartheta_{3,\mathrm{n}} \\ = \\ r_{12} \cdot \vartheta_{1,\mathrm{n-1}} + \left(\tfrac{1}{P} - 2 + r_{21} + r_{23}\right) \cdot \vartheta_{2,\mathrm{n-1}} + r_{32} \cdot \vartheta_{3,\mathrm{n-1}} \end{gathered} \tag{5.31}$$

with

$$r_{12} = \frac{1}{1+\frac{\lambda_2 \cdot \Delta x_1}{\lambda_1 \cdot \Delta x_2}} \quad r_{21} = \frac{1}{1+\frac{\lambda_1 \cdot \Delta x_2}{\lambda_2 \cdot \Delta x_1}} \quad r_{23} = \frac{1}{1+\frac{\lambda_3 \cdot \Delta x_2}{\lambda_2 \cdot \Delta x_3}} \quad r_{32} = \frac{1}{1+\frac{\lambda_2 \cdot \Delta x_3}{\lambda_3 \cdot \Delta x_2}}$$

where r are adaptation parameters of the introduced virtual layers. The heat transfer at the boundaries of the construction can be calculated by introducing a special Biot number Bi^* of GRIGULL and SANDNER 1979. This special Biot number considers the heat transfer at the surface as a fictitious heat conduction problem.

$$Bi^* = \frac{h}{\lambda} \cdot \frac{\Delta x}{2} \tag{5.32}$$

where h is the surface heat transfer coefficient. The resulting main equation of the boundary layer 1 for non–homogeneous materials is provided by

$$\begin{gathered} -\frac{2 \cdot Bi^*}{1+Bi^*} \cdot \vartheta_{\mathrm{L,n}} + \left(-\frac{1-Bi^*}{1+Bi^*} + \frac{2}{P} + 3 - 2 \cdot r_{12}\right) \cdot \vartheta_{1,\mathrm{n}} - 2 \cdot r_{21} \cdot \vartheta_{2,\mathrm{n}} \\ = \\ \frac{2 \cdot Bi^*}{1+Bi^*} \cdot \vartheta_{\mathrm{L,n-1}} + \left(\frac{1-Bi^*}{1+Bi^*} + \frac{2}{P} - 3 + 2 \cdot r_{12}\right) \cdot \vartheta_{1,\mathrm{n-1}} - 2 \cdot r_{21} \cdot \vartheta_{2,\mathrm{n-1}}. \end{gathered} \tag{5.33}$$

If there is an incident irradiance, it must be included in the boundary conditions. The matrix formulation of the problem can be written as

$$[A] = \begin{bmatrix} -\frac{1-Bi^*}{1+Bi^*} + \frac{2}{P_1} + 3 - 2 \cdot r_{12} & -2 \cdot r_{21} & 0 & \cdots & \cdots & 0 \\ -r_{12} & \frac{1}{P_2} + 2 - r_{21} - r_{23} & -r_{32} & & & \vdots \\ 0 & \ddots & & & & \vdots \\ \vdots & & & \ddots & & 0 \\ \vdots & & & -r_{45} & \frac{1}{P_5} + 2 - r_{54} - r_{56} & -r_{65} \\ 0 & \cdots & \cdots & 0 & -2 \cdot r_{56} & -\frac{1-Bi^*}{1+Bi^*} + \frac{2}{P_16} + 3 - 2 \cdot r_{65} \end{bmatrix}$$

$$[B] = \begin{bmatrix} \frac{1-Bi^*}{1+Bi^*} + \frac{2}{P_1} - 3 + 2 \cdot r_{12} & 2 \cdot r_{21} & 0 & \cdots & \cdots & 0 \\ r_{12} & \frac{1}{P_2} - 2 + r_{21} + r_{23} & r_{32} & & & \vdots \\ 0 & \ddots & & & & \vdots \\ \vdots & & & \ddots & & 0 \\ \vdots & & & r_{45} & \frac{1}{P_5} - 2 + r_{54} + r_{56} & r_{65} \\ 0 & \cdots & \cdots & 0 & 2 \cdot r_{56} & \frac{1-Bi^*}{1+Bi^*} + \frac{2}{P_16} - 3 + 2 \cdot r_{65} \end{bmatrix}$$

$$[BC] = \begin{bmatrix} \frac{2 \cdot Bi^*}{1+Bi^*} \cdot \left(\vartheta_{\mathrm{int,n}} + \vartheta_{\mathrm{int,n-1}}\right) + \frac{2}{h \cdot \left(1+\frac{1}{Bi^*}\right)} \cdot \left(I_{\mathrm{i,n}} + I_{\mathrm{i,n-1}}\right) \\ 0 \\ \vdots \\ 0 \\ \frac{2 \cdot Bi^*}{1+Bi^*} \cdot \left(\vartheta_{\mathrm{ext,n}} + \vartheta_{\mathrm{ext,n-1}}\right) + \frac{2}{h \cdot \left(1+\frac{1}{Bi^*}\right)} \cdot \left(I_{\mathrm{a,n}} + I_{\mathrm{a,n-1}}\right) \end{bmatrix}$$

$$
\begin{aligned}
[A] \cdot [\vartheta_{\mathrm{n}}] &= [B] \cdot [\vartheta_{\mathrm{n-1}}] + [BC] \\
[\vartheta_{\mathrm{n}}] &= [D] \cdot [\vartheta_{\mathrm{n-1}}] + [A]^{-1} \cdot [BC] \\
[D] &= [A]^{-1} \cdot [B]
\end{aligned} \tag{5.34}
$$

where $[A]$ and $[B]$ are the coefficient matrices and $[BC]$ the boundary conditions. For some cases analytical solutions of equation 5.28 are available. The numerical model can be validated by means of these analytical solutions only for special cases. The time dependence of heat conduction in a semi–infinite homogeneous material without a surface heat transfer coefficient can be identified with

$$
\vartheta(x,t) = \Delta\vartheta \cdot \mathrm{erf}\left(\frac{x}{2 \cdot \sqrt{a \cdot t}}\right) \tag{5.35}
$$

For layered constructions with a limited thickness the steady–state solutions are a possible way of checking. The programmed Crank–Nicolson scheme was tested in the way described. At the beginning of the check for the steady–state solution a constant temperature over the entire thickness of a construction was assumed. Afterwards the boundary conditions were set by using varying temperatures and surface heat transfer coefficients. The steady–state solution for the temperature distribution in the construction must be reached eventually. This check reproduced exactly the analytical solution.

For solar driven desiccant cooling systems, large collector areas are required. In this application it can be useful to design collector facades or collector roofs. Therefore, it is necessary to combine the algorithms for solar collectors and for dynamic heat transfer. In the special case of ventilated photovoltaic facades it is, moreover, necessary to eliminate the electric power from the heat balance. This can easily be done by substracting the power in the corresponding line of the boundary conditions BC in the equation 5.34. A more detailed description of solar facades is given by EICKER ET AL. 1998 B.

The International Energy Agency IEA initiated via Task 12 (solar heating and cooling programme) of Annex 21 (energy conservation in buildings and community systems) the BESTEST project (JUDKOFF and NEYMARK 1995) for the validation of detailed thermal simulation software. A method was developed for systematically testing this software and diagnosing the sources of predictive disagreement. The methodology consists of a

combination of empirical validation, analytical verification and comparative analysis techniques. The programs tested during the BESTEST project were BLAST, DOE2, ESP. SERIRES, S3PAS, TASE and TRNSYS. For this work the developed simulation software ESIMA was also tested using this prescribed procedure. The results for ESIMA are shown in Figure 5.6.

To simulate a building's performance it is necessary to have precise data for the incidence angle–dependent transmission and absorption of glazing. Therefore, the data of Pfrommer 1995 listed in the Tables 5.1, 5.2, 5.3 were used in this study.

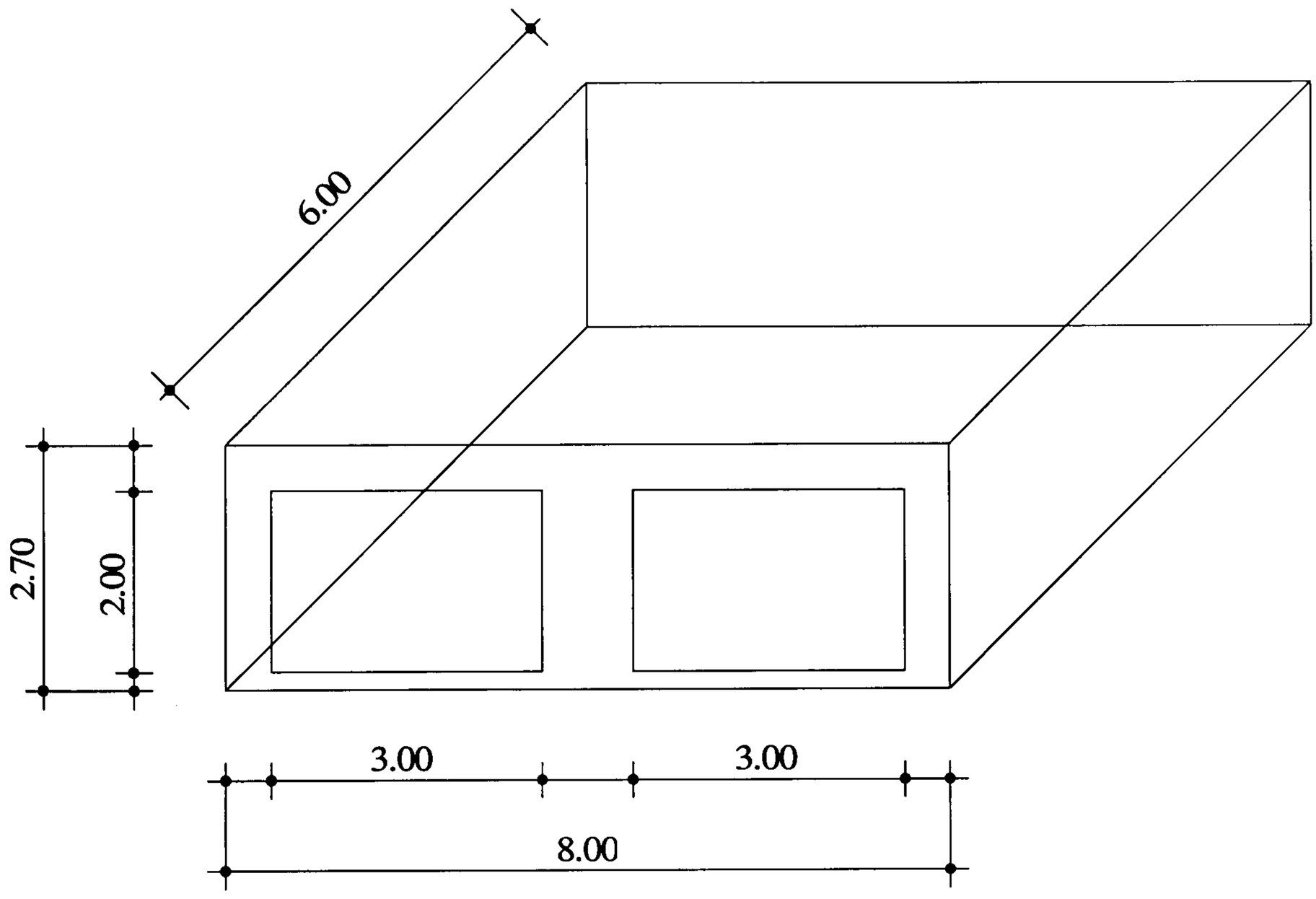

Figure 5.5: BESTEST building (Judkoff and Neymark 1995)

Table 5.1: Incidence–angle dependent transmission and absorption of clear single glazing

angle	0	10	20	30	40	50	60	70	80	90	diffuse
τ	0.764	0.763	0.761	0.755	0.744	0.722	0.675	0.571	0.343	0	0.673
α	0.166	0.167	0.170	0.174	0.180	0.186	0.192	0.192	0.174	0	0.180

Table 5.2: Incidence–angle dependent transmission and absorption of clear double glazing

angle	0	10	20	30	40	50	60	70	80	90	diffuse
τ	0.601	0.600	0.595	0.588	0.575	0.550	0.498	0.383	0.174	0	0.502
α	0.288	0.289	0.294	0.300	0.308	0.317	0.322	0.316	0.273	0	0.304

Table 5.3: Incidence–angle dependent transmission and absorption of low–ϵ double glazing

angle	0	10	20	30	40	50	60	70	80	90	diffuse
τ	0.504	0.503	0.501	0.495	0.484	0.462	0.417	0.318	0.143	0	0.421
α	0.310	0.311	0.315	0.321	0.329	0.337	0.341	0.332	0.283	0	0.323

Table 5.4: BESTEST cases used for validity checks of ESIMA and for simulations

BESTEST cases	description
Case 600	lightweight construction, south oriented window internal load 200 W, air change per hour 0.5 heating setpoint 20 °C, cooling setpoint 27 °C
Case 640	Case 600, setback 10 °C
Case 800	heavyweight construction, south oriented opaque window internal load 200 W, air change per hour 0.5 heating setpoint 20 °C, cooling setpoint 27 °C
Case 900	Case 800, south oriented window
Case 940	Case 900, setback 10 °C

Table 5.5: BESTEST constructions used for validity checks of ESIMA and for simulations

BESTEST constructions	Case 800 and 9xx	Case 6xx
walls	100 mm concrete 61.5 mm insulation 040 9 mm wood	12 mm plaster board 66 mm insulation 040 9 mm wood
roof	16 mm plaster board 118.5 mm insulation 040 19 mm wood	16 mm plaster board 118.5 mm insulation 040 19 mm wood
floor	80 mm concrete 1007 mm insulation 040	25 mm wood 1003 mm insulation 040
windows	double glazing $U = 3\,W/m^2K$	double glazing $U = 3\,W/m^2K$

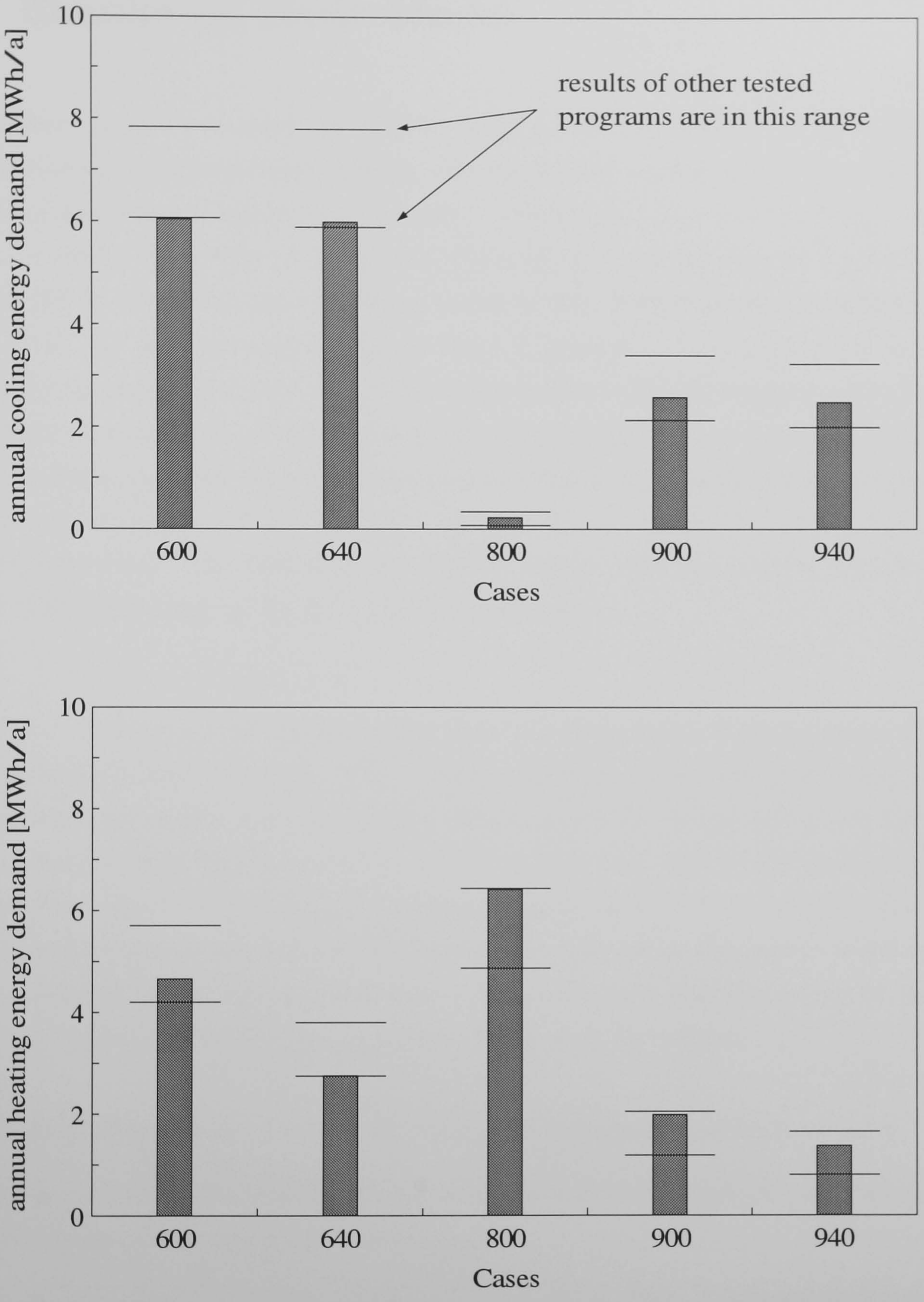

Figure 5.6: Results of ESIMA compared with BESTEST results

5.4 Simulation Basic Model

A simulation model was made in ESIMA with a building simular to BESTEST case 940, representing a heavyweight building, and for further studies according to BESTEST case 640 representing a lightweight building. This simple "shoe–box–building" shown in Figure 5.5 with a floor area of 48 m^2 was assumed to be occupied with 5 persons, each emitting 100 W of sensible heat and 30 g/h of moisture. Furthermore, an internal cooling load of 20 W/m^2 was assumed during the time of occupancy between 8 am to 6 pm. For all cases an air change per hour of 0.2 was estimated to consider leakages of the building. To limit the external loads of the building, a shading of the windows was considered which allows a maximum of 100 W/m^2 for transmitted irradiance. The indoor air temperatures were set to a minimum of 20 °C during occupancy time and were set back to 15 °C outside the occupancy time. The maximum permissible indoor air temperatures vary according to DIN 1946 depending on the ambient air temperature.

A desiccant cooling system programmed with the algorithm of the previous chapters was connected to this building. The constant parameters of this system were a heat recovery efficiency of 0.85 and a humidifier efficiency of 0.90. In one case study the bypass fraction changes from $\dot{V}_R/\dot{V}_P = 0.35$ to $\dot{V}_R/\dot{V}_P = 0.75$ and, hence, the dehumidification efficiency from $\eta_{sorp} = 0.62$ to $\eta_{sorp} = 0.82$ according to the measurement results presented previously. The system used in the simulations can operate in the modes listed in Table 5.7 depending on the indoor air conditions. Only in one case was the control by the room conditions disabled and the inlet temperature was used for control.

1. Mode 1: Heat recovery mode HR. Used for ventilation with heat recovery.
2. Mode 2: Ventilation mode V. Used only for ventilation without switching on any component of the system.
3. Mode 3: Adiabatic cooling mode AC. Used for cooling if dehumidification is not necessary or inlet temperatures are low enough, switching on the outlet humidifier and the heat recovery wheel.
4. Mode 4: Desiccant cooling mode DCS. Classic operating mode, switching on all components of the entire system.
5. Mode 5: Desiccant cooling mode DCS*. Used if indoor relative humidity exceeds 0.6. Classic operating mode, switching on all components except the inlet humidifier.

The heat supply of the desiccant cooling system is achieved only by using solar air collectors. For the simulations a maximum air velocity of 4 m/s in the collectors, a collector length of 15 m and a gap height of 95 mm are assumed. In a further study half of this collector area is used. According to the collectors of the test plant, in the simulations the first half of the collector area in the flow direction is black coated and the second half is selectively coated. The U–value of the collector is assumed to be constant. The use of solar air collectors means that no significant energy storage is available either in the desiccant cooling system or in the solar system. Thermal inertia is only provided by the mass of the building. The solar air collectors and their performance were evaluated according the equations on page 86 to page 90. All collectors were oriented facing the equator and were tilted at an angle equal to the latitude of their location to collect most of the beam radiation.

This test building and the adapted desiccant cooling systems with solar air collectors has been simulated for the climatic situations of Djakarta in Indonesia, Phoenix (Arizona) in the United States, Seville in Spain and Stuttgart in Germany. The climatic data sets for each location were produced with the program METEONORM 4.0 1999. A description of these different climates is provided in Table 5.6. All climates used are shown in psychrometric charts in the Figures 5.7 to 5.10 where each dot represents the climatic condition of one hour in the year.

Table 5.6: Description of the climates used in the simulations

site	latitude [°]	longitude [°]	altitude [m]	climate zone description by TROLL and PAFFEN 1980
Djakarta	-6.11	-106.44	5	tropical rain
Phoenix	33.26	112.01	347	desert and semi–arid, winters with frost
Seville	37.22	5.58	10	mediterrean, humid winters, dry summers
Stuttgart	48.50	-9.12	318	submaritime

5.5 Simulation Case Studies

In the following, all simulation case studies conducted for the four different climates are be described. The quantitative results are listed in the Tables 5.8 to 5.16. In the Figures in the appendix, the results are presented graphically for the entire year and for a three–day period with a high cooling load.

1. Desiccant cooling ventilation cycle (Figure 5.11) with $\dot{V} = 150\ m^3/h$ during occupation time. Adapted to a heavyweight building according to BESTEST case 940. The simulation results are presented in Table 5.8.

2. Desiccant cooling ventilation cycle (Figure 5.11) with $\dot{V} = 150\ m^3/h$ during occupation time and enforced night ventilation with $\dot{V} = 518\ m^3/h$ corresponding to 4 air changes per hour. Night ventilation through desiccant cooling system to enable cooling by humidifiers if appropriate. Adapted to a heavyweight building according to BESTEST case 940. The simulation results are presented in Table 5.9.

3. Desiccant cooling ventilation cycle (Figure 5.11) with $\dot{V} = 150\ m^3/h$ or $\dot{V} = 518\ m^3/h$ if additional cooling is required during occupation time and night ventilation with $\dot{V} = 518\ m^3/h$ corresponding to 4 air changes per hour. Night ventilation through desiccant cooling system to enable cooling by humidifiers if appropriate. Adapted to a heavyweight building according to BESTEST case 940. The simulation results are presented in Table 5.10.

4. Desiccant cooling ventilation cycle (Figure 5.11) with $\dot{V} = 150\ m^3/h$ during occupation time. Adapted to a heavyweight building according to BESTEST case 940. Half of the collector area is used compared to case 1. The simulation results are presented in Table 5.11.

5. Desiccant cooling ventilation cycle (Figure 5.11) with $\dot{V} = 150\ m^3/h$ during occupation time. Adapted to a lightweight building according to BESTEST case 640. The simulation results are presented in Table 5.12.

6. Desiccant cooling ventilation cycle with ambient air regeneration (Figure 5.12) and $\dot{V} = 150\ m^3/h$ during occupation time. Adapted to a heavyweight building according to BESTEST case 940. The simulation results are presented in Table 5.13.

7. Desiccant cooling ventilation cycle (Figure 5.11) with $\dot{V} = 150\ m^3/h$ during occupation time. Adapted to a heavyweight building according to BESTEST case 940. Not controlled by the room temperature and the indoor relative humidity.

Controlled to reach an inlet temperature close to 17 °C. The simulation results are presented in Table 5.14.

8. Desiccant cooling ventilation cycle (Figure 5.11) with $\dot{V} = 150\ m^3/h$ or $\dot{V} = 518\,m^3/h$ if additional cooling is required during occupation time and night ventilation with $\dot{V} = 518\ m^3/h$ corresponding to 4 air changes per hour. Night ventilation through desiccant cooling system to enable cooling by humidifiers if appropriate. $\dot{V}_R/\dot{V}_P$ variable between 0.35 and 0.75 dependent on regeneration temperature. Adapted to a heavyweight building according to BESTEST case 940. The simulation results are presented in Table 5.15.

9. Double stage desiccant cooling ventilation cycle (Figure 5.13) with $\dot{V} = 150\ m^3/h$ during occupation time. Same collector area as in case 1, divided in half for both dehumidifiers. Adapted to a heavyweight building according to BESTEST case 940. Simulations only for Djakarta's climate. The simulation results are presented in Table 5.16.

10. Double stage desiccant cooling ventilation cycle (Figure 5.13) with $\dot{V} = 150\ m^3/h$ or $\dot{V} = 518\ m^3/h$ if additional cooling is required during occupation time and night ventilation with $\dot{V} = 518\ m^3/h$ corresponding to 4 air changes per hour. Collector area divided in half for both dehumidifiers. Adapted to a heavyweight building according to BESTEST case 940. Simulations only for Djakarta's climate. The simulation results are presented in Table 5.16.

Table 5.7: Control of the desiccant cooling system in the simulations using room conditions

control mode	ϑ_i $[°C]$	rh_i $[-]$	η_{sorp}[1] $[-]$	η_{HR} $[-]$	$\eta_{h,in}$ $[-]$	$\eta_{h,out}$ $[-]$
HR	< 22	$0.00 \leq rh_i \leq 1.00$	0.00	0.85	0.00	0.00
V	$22 \leq \vartheta_i < 23$	$0.00 \leq rh_i \leq 1.00$	0.00	0.00	0.00	0.00
AC	$23 \leq \vartheta_i < 24$	$0.00 \leq rh_i \leq 1.00$	0.00	0.85	0.00	0.90
DCS	≥ 24	$0.00 \leq rh_i \leq 0.60$	$0.62 \leq \eta_{sorp} \leq 0.86$	0.85	0.90	0.90
DCS*	≥ 24	$0.60 < rh_i \leq 1.00$	$0.62 \leq \eta_{sorp} \leq 0.86$	0.85	0.00	0.90

[1]Varying dehumidification efficiencies in case study 8 with bypass control: If the regeneration temperature drops under $50°C$ by using $\dot{V}_R/\dot{V}_P = 0.75$, the bypass fraction is increased to 0.50 and if the regeneration temperature drops under $40°C$, the bypass fraction is increased to 0.65.

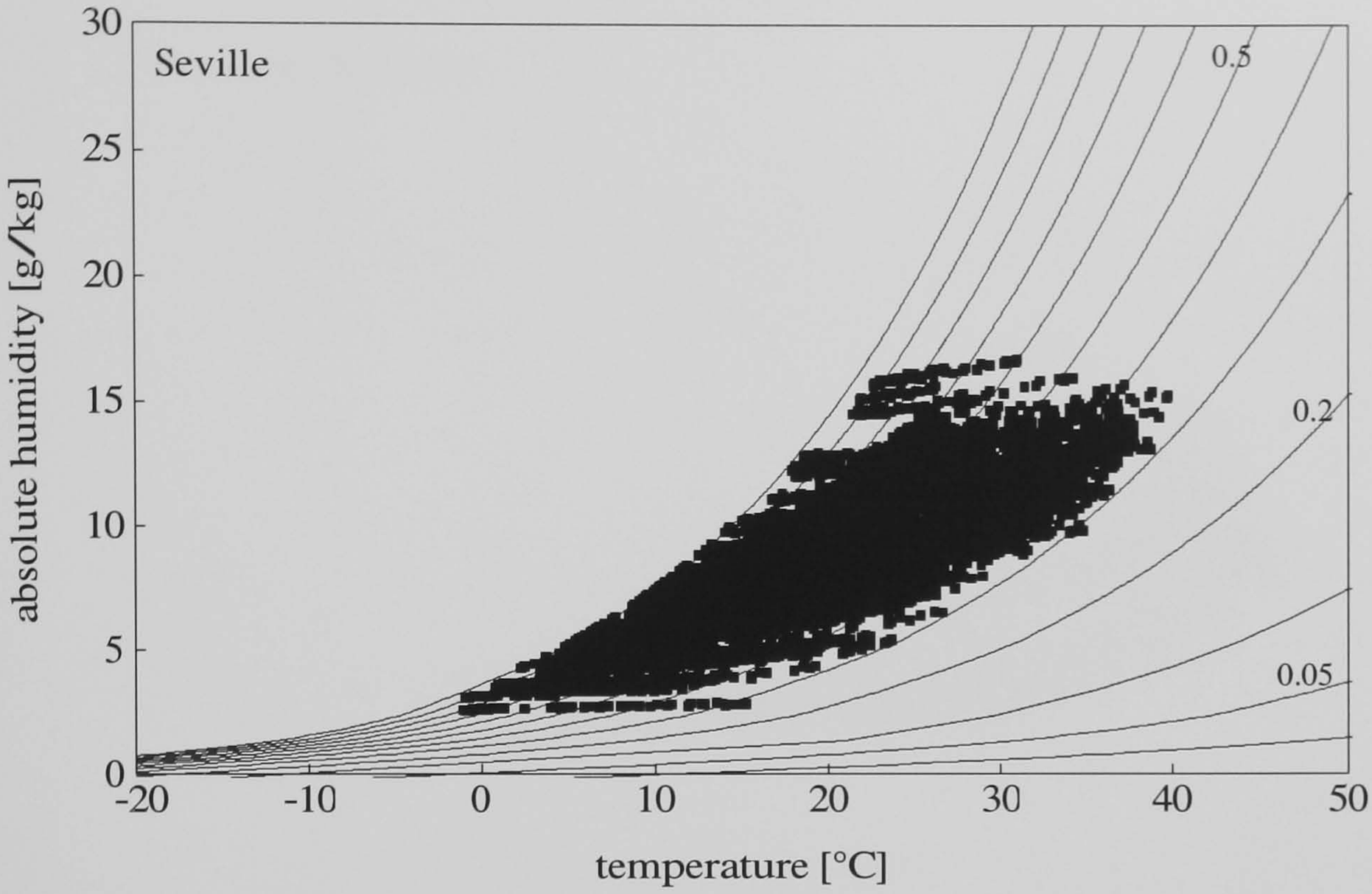

Figure 5.7: Psychrometric chart of Seville's climate

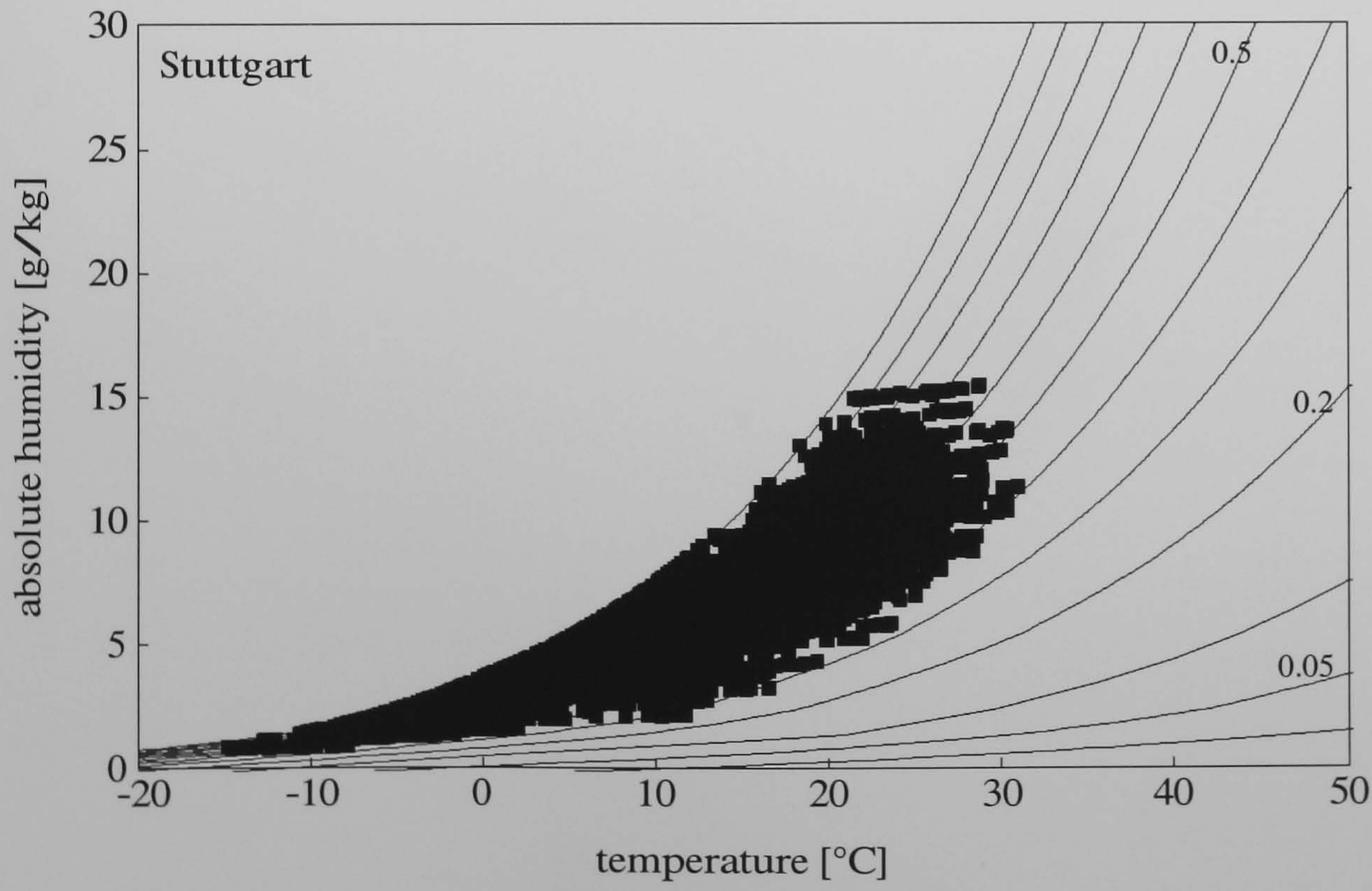

Figure 5.8: Psychrometric chart of Stuttgart's climate

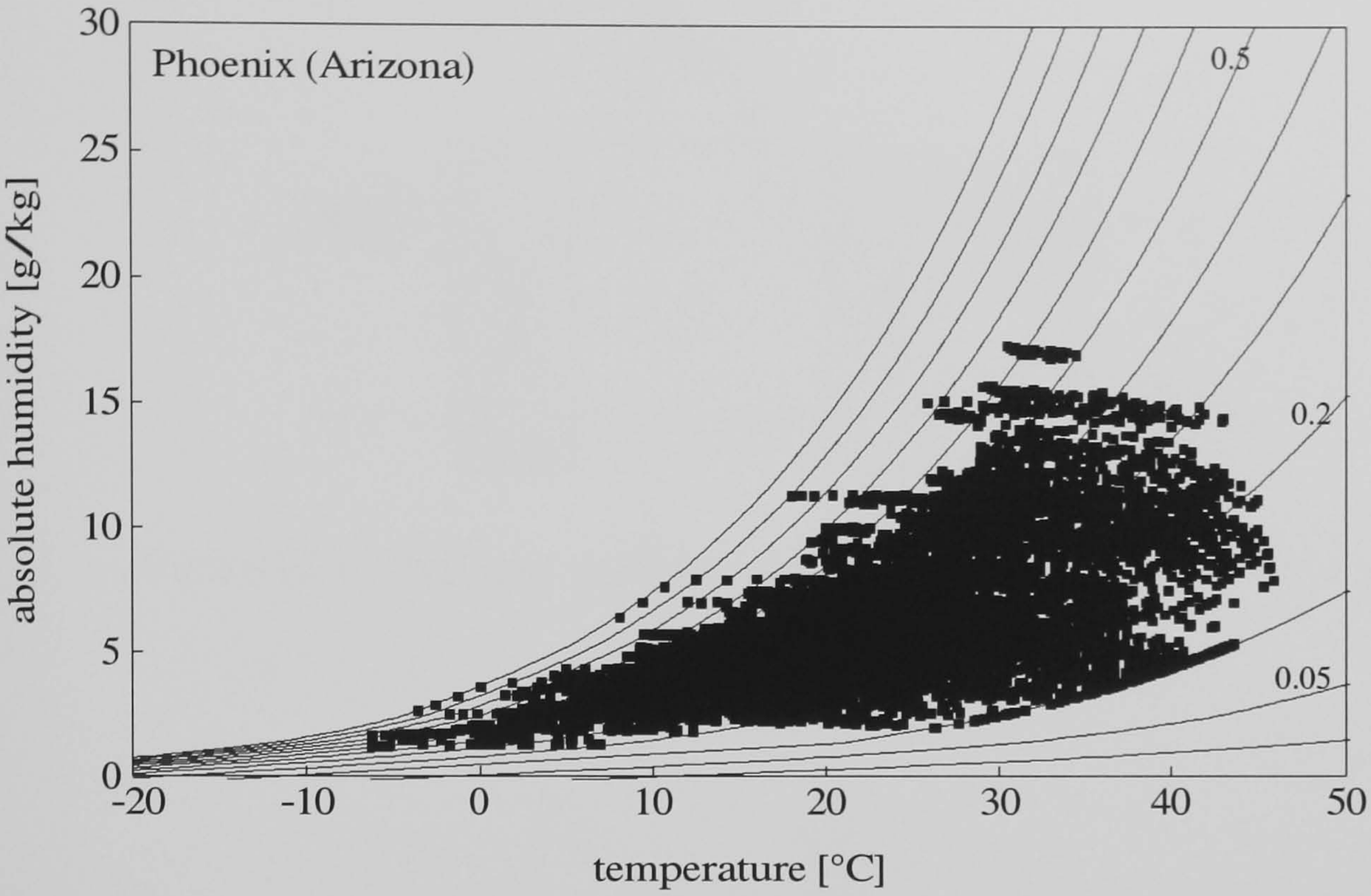

Figure 5.9: Psychrometric chart of Phoenix' climate

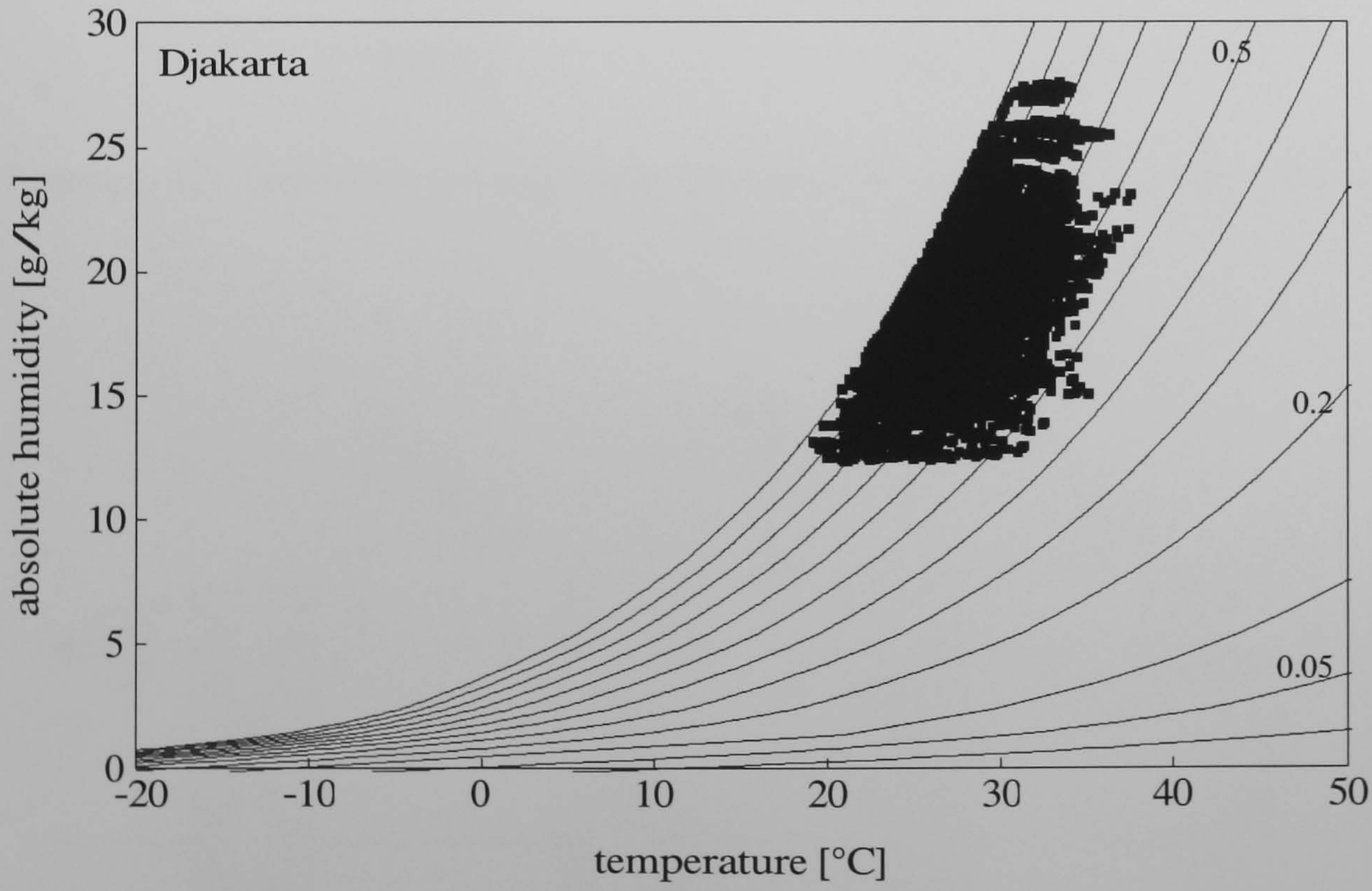

Figure 5.10: Psychrometric chart of Djakarta's climate

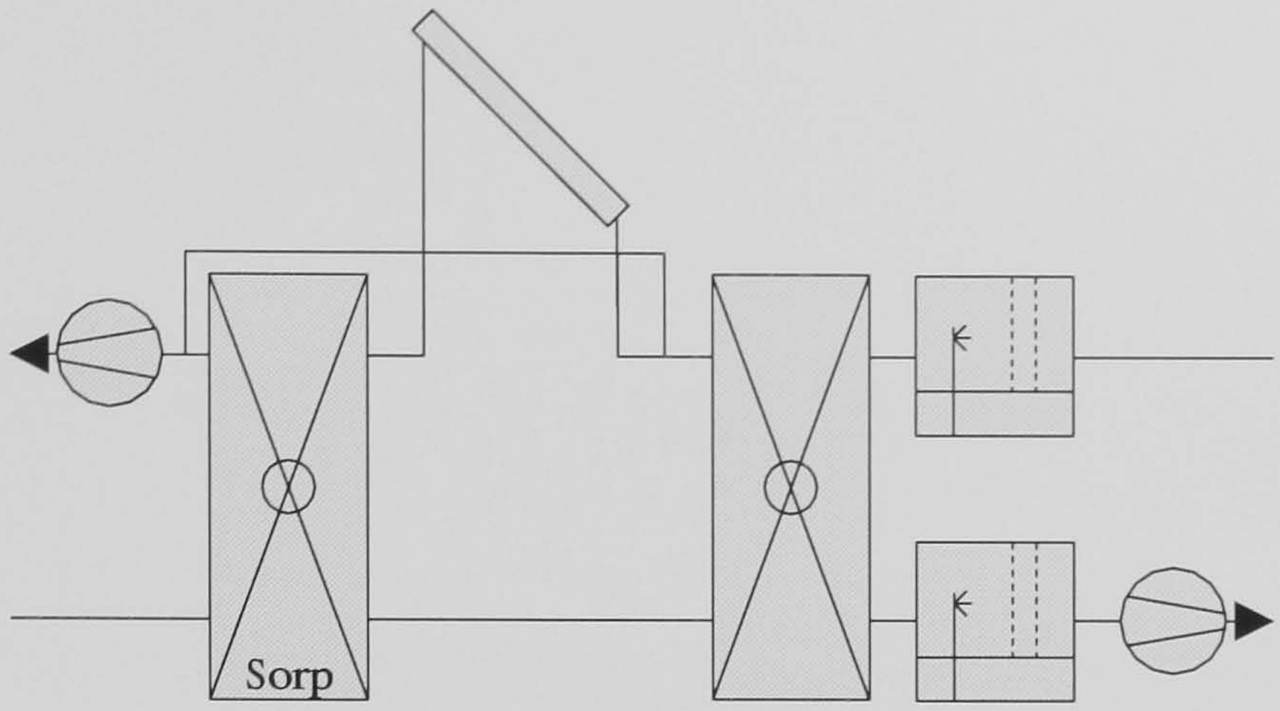

Figure 5.11: Desiccant cooling ventilation cycle used for the simulations

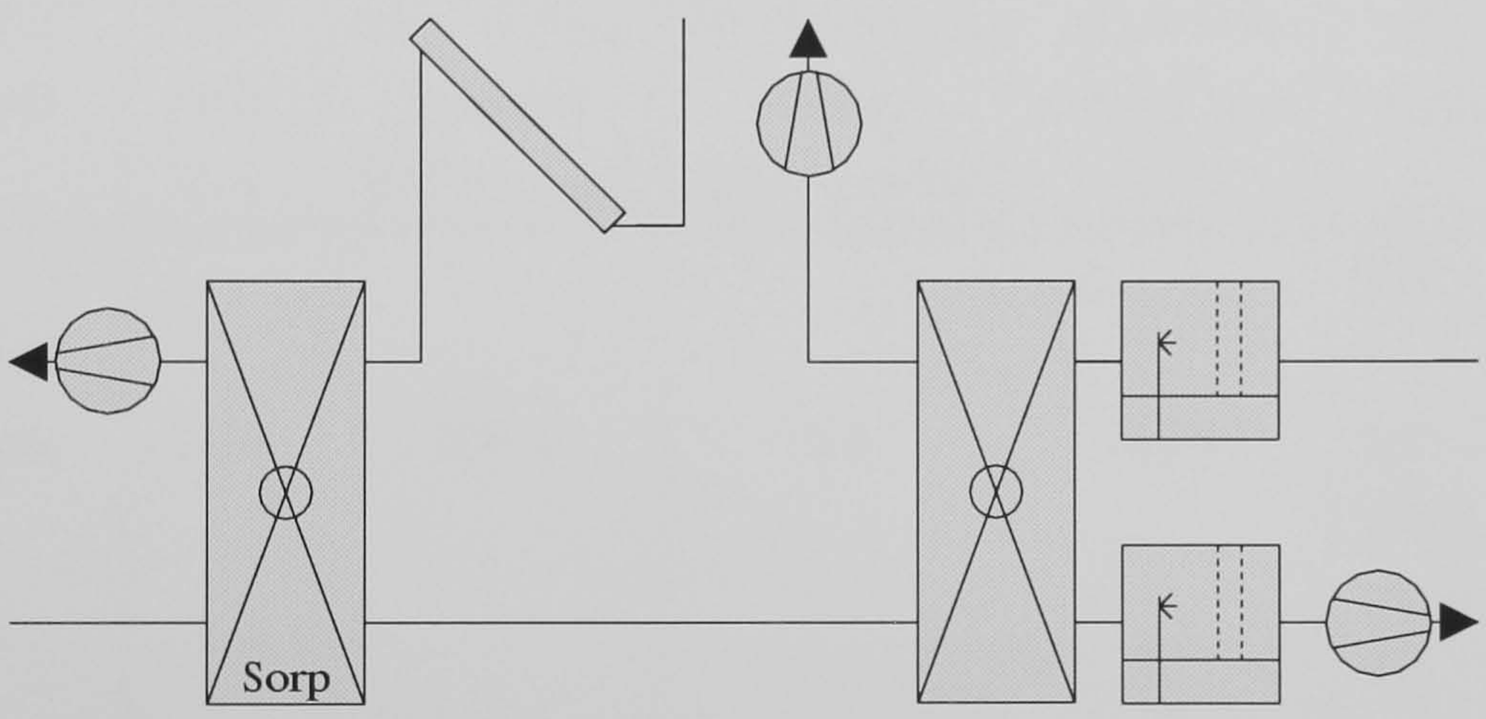

Figure 5.12: Desiccant cooling cycle (ambient air regeneration) used for the simulations

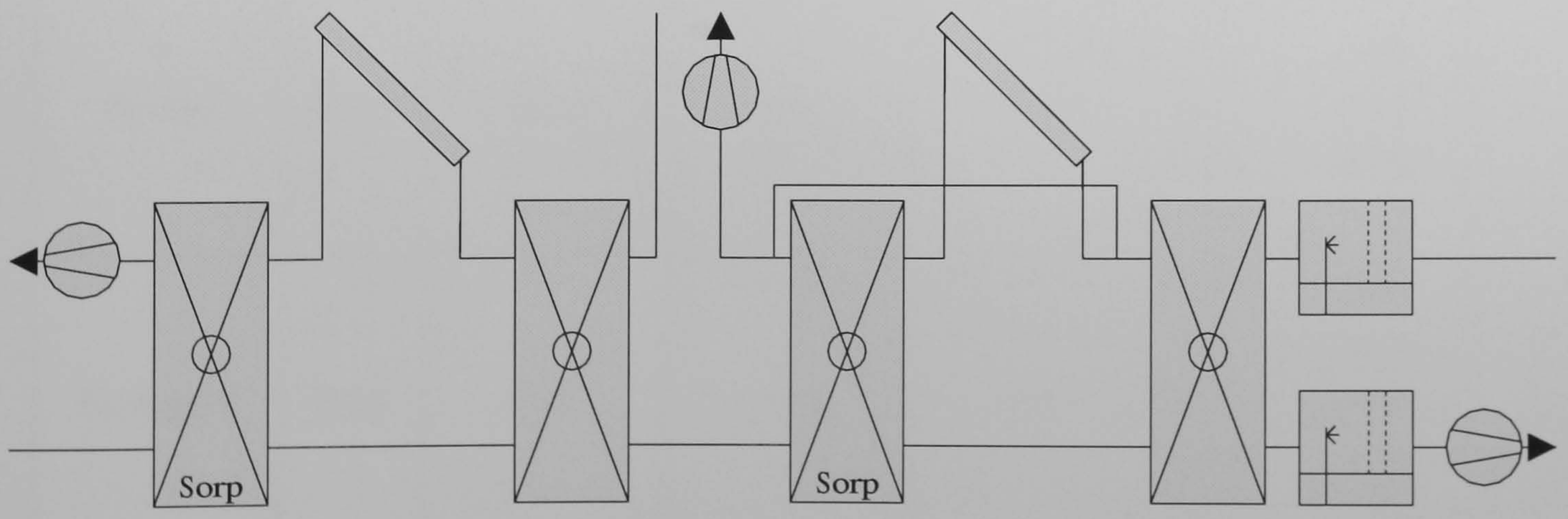

Figure 5.13: Double stage ventilation cycle used for the simulations

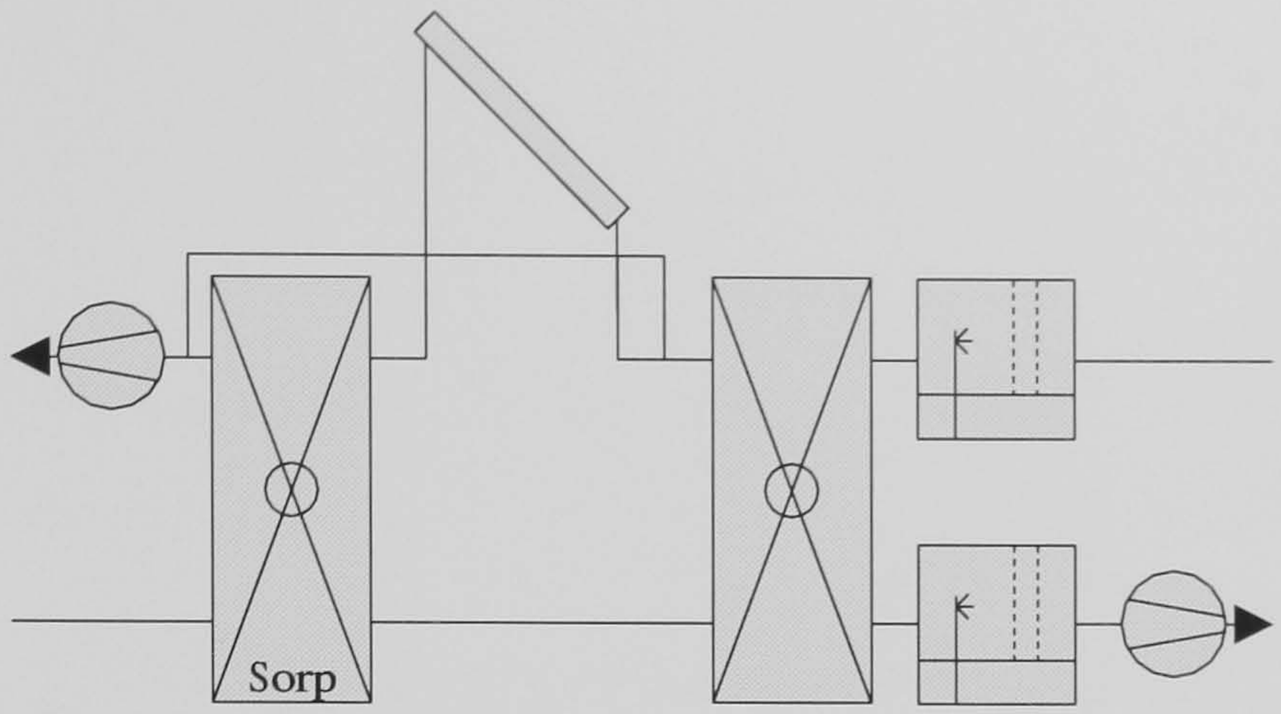

Table 5.8: Simulation results of case study 1 (heavyweight building, hygienic ventilation during occupation time). Detailed description on page 102. Discussion of the simulation results on page 117.

BESTTEST Case 940	$\overline{\text{COP}}$[1] DCS [–]	add. cooling demand $[kWh/m^2a]$	DCS cooling energy $[kWh/m^2a]$	$rh_i > 0.6$ during year [–]	control mode[2] during operation [–]	
Djakarta	2.26	206.3	5.3	0.83	HR V AC DCS DCS*	0.00 0.00 0.00 0.26 0.74
Phoenix	0.67	140.2	66.3	0.05	HR V AC DCS DCS*	0.01 0.02 0.02 0.88 0.07
Seville	0.72	95.2	54.2	0.08	HR V AC DCS DCS*	0.05 0.05 0.04 0.75 0.11
Stuttgart	0.52	26.9	37.2	0.01	HR V AC DCS DCS*	0.38 0.12 0.06 0.44 >0.00

[1] averaged COP of the DCS–mode and the DCS*–mode

[2] see Table 5.7

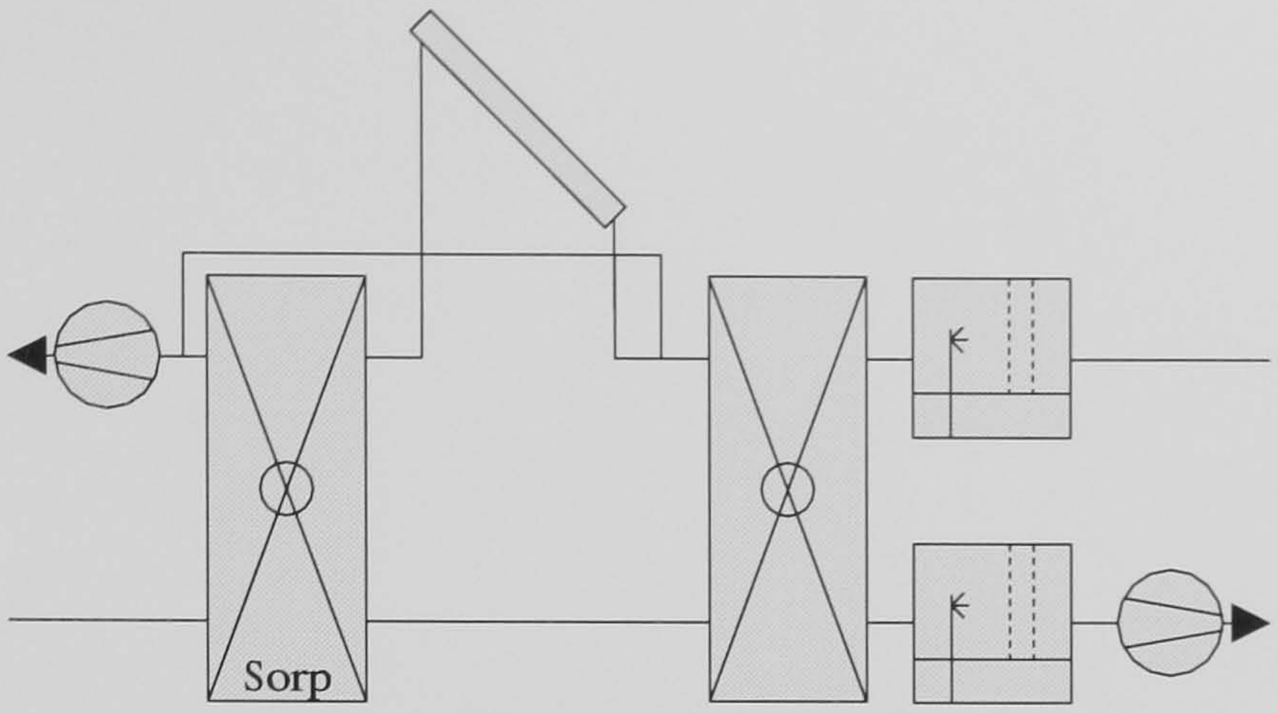

Table 5.9: Simulation results of case study 2 (heavyweight building, hygienic ventilation during occupation time, enhanced night ventilation with 4 air changes per hour). Detailed description on page 102. Discussion of the simulation results on page 118.

BESTTEST Case 940	$\overline{\text{COP}}$[1] DCS [–]	add. cooling demand $[kWh/m^2a]$	DCS cooling energy $[kWh/m^2a]$	$rh_\text{i} > 0.6$ during year [–]	control mode[2] during operation [–]	
Djakarta	2.18	211.5	0.1	0.84	HR	0.00
					V	0.00
					AC	0.00
					DCS	0.24
					DCS*	0.76
Phoenix	0.60	130.3	80.2	0.06	HR	0.01
					V	0.10
					AC	0.05
					DCS	0.79
					DCS*	0.06
Seville	0.73	87.1	65.3	0.09	HR	0.05
					V	0.11
					AC	0.07
					DCS	0.66
					DCS*	0.10
Stuttgart	0.53	23.6	41.7	0.01	HR	0.36
					V	0.16
					AC	0.08
					DCS	0.39
					DCS*	0.02

[1] averaged COP of the DCS–mode and the DCS*–mode

[2] see Table 5.7

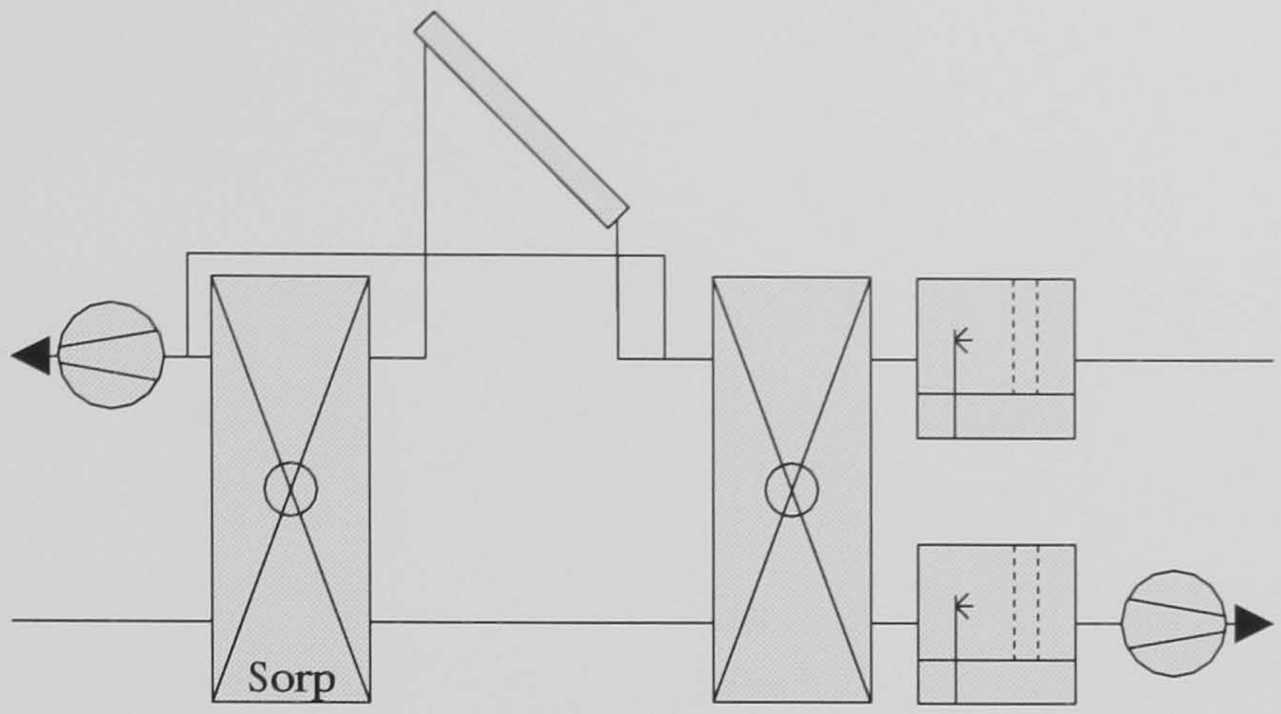

Table 5.10: Simulation results of case study 3 (heavyweight building, ventilation with maximum 4 air changes per hour, night ventilation). Detailed description on page 102. Discussion of the simulation results on page 119.

BESTTEST Case 940	$\overline{\text{COP}}$[1] DCS [–]	add. cooling demand $[kWh/m^2a]$	DCS cooling energy $[kWh/m^2a]$	$rh_i > 0.6$ during year [–]	control mode[2] during operation [–]	
Djakarta	4.04	218.4	2.6	0.88	HR	0.00
					V	0.00
					AC	0.00
					DCS	0.12
					DCS*	0.88
Phoenix	1.02	54.5	160.4	0.11	HR	0.01
					V	0.09
					AC	0.07
					DCS	0.70
					DCS*	0.13
Seville	1.12	34.9	121.7	0.16	HR	0.04
					V	0.11
					AC	0.07
					DCS	0.58
					DCS*	0.20
Stuttgart	0.57	6.9	58.0	0.02	HR	0.36
					V	0.16
					AC	0.09
					DCS	0.36
					DCS*	0.02

[1] averaged COP of the DCS–mode and the DCS*–mode

[2] see Table 5.7

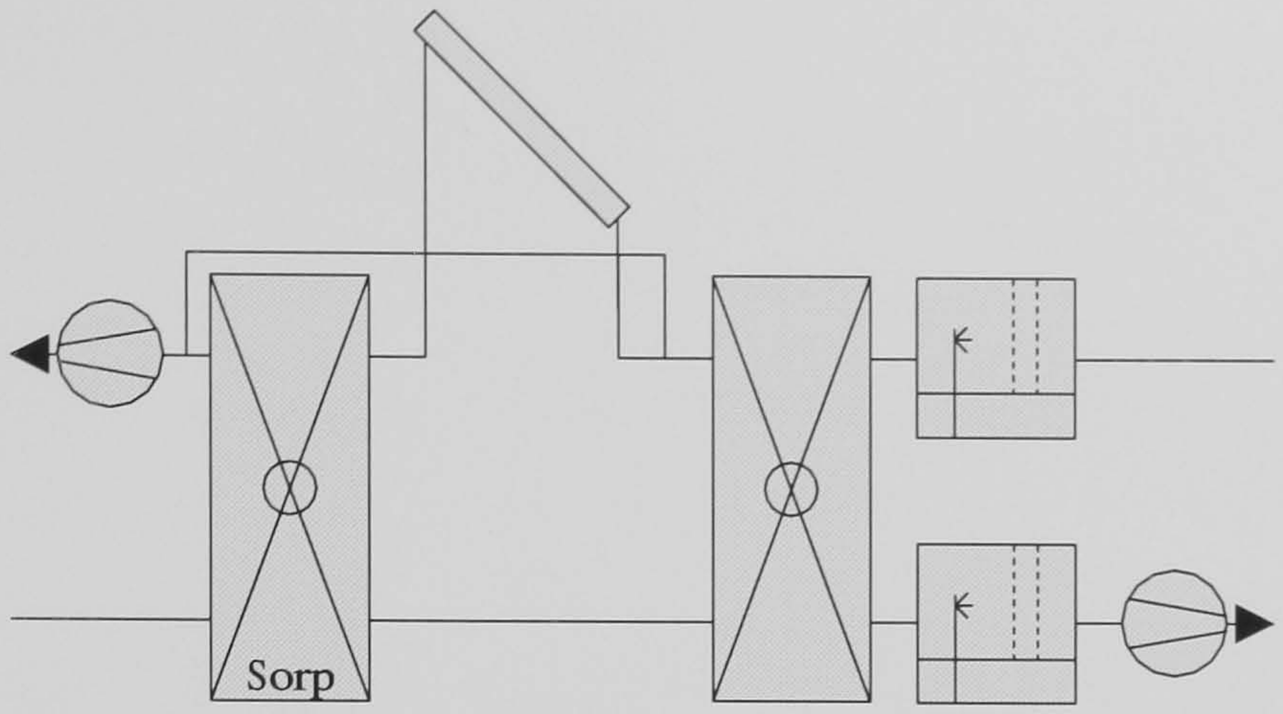

Table 5.11: Simulation results of case study 4 (heavyweight building, hygienic ventilation during occupation time, half collector area as in case study 1). Detailed description on page 102. Discussion of the simulation results on page 120.

BESTTEST Case 940	$\overline{\text{COP}}^1$ DCS [–]	add. cooling demand $[kWh/m^2a]$	DCS cooling energy $[kWh/m^2a]$	$rh_i > 0.6$ during year [–]	control mode[2] during operation [–]	
Djakarta	3.43	206.0	5.3	0.92	HR	0.00
					V	0.00
					AC	0.00
					DCS	0.08
					DCS*	0.92
Phoenix	0.96	135.6	71.8	0.08	HR	0.00
					V	0.06
					AC	0.05
					DCS	0.78
					DCS*	0.10
Seville	1.01	94.6	55.1	0.13	HR	0.04
					V	0.09
					AC	0.08
					DCS	0.62
					DCS*	0.17
Stuttgart	0.59	27.3	37.1	0.01	HR	0.39
					V	0.16
					AC	0.09
					DCS	0.39
					DCS*	0.02

[1] averaged COP of the DCS–mode and the DCS*–mode

[2] see Table 5.7

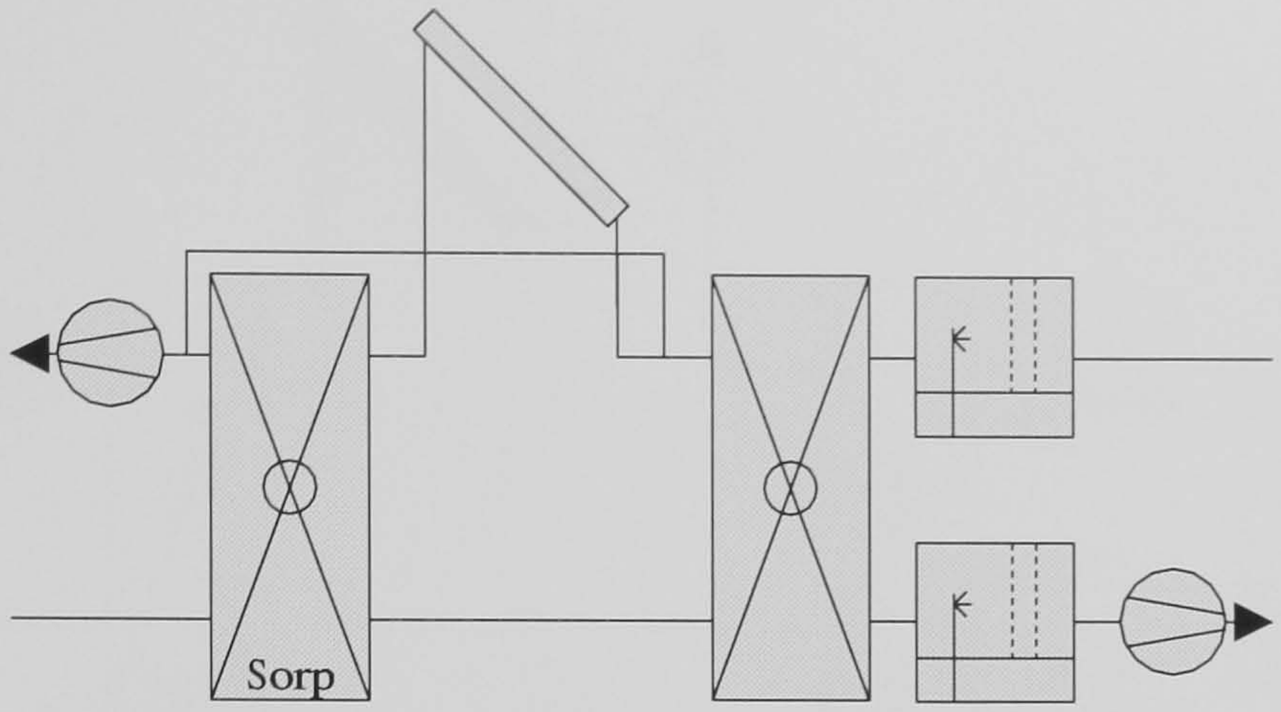

Table 5.12: Simulation results of case study 5 (lightweight building, hygienic ventilation during occupation time). Detailed description on page 102. Discussion of the simulation results on page 122.

BESTTEST Case 640	$\overline{\text{COP}}$[1] DCS [–]	add. cooling demand $[kWh/m^2a]$	DCS cooling energy $[kWh/m^2a]$	$rh_i > 0.6$ during year [–]	control mode[2] during operation [–]	
Djakarta	2.25	212.1	5.2	0.83	HR	0.00
					V	0.00
					AC	0.00
					DCS	0.26
					DCS*	0.74
Phoenix	0.67	165.2	63.9	0.05	HR	0.00
					V	0.02
					AC	0.02
					DCS	0.88
					DCS*	0.08
Seville	0.71	120.5	51.3	0.13	HR	0.08
					V	0.04
					AC	0.03
					DCS	0.77
					DCS*	0.08
Stuttgart	0.48	45.0	44.4	0.06	HR	0.29
					V	0.11
					AC	0.05
					DCS	0.55
					DCS*	>0.00

[1] averaged COP of the DCS–mode and the DCS*–mode

[2] see Table 5.7

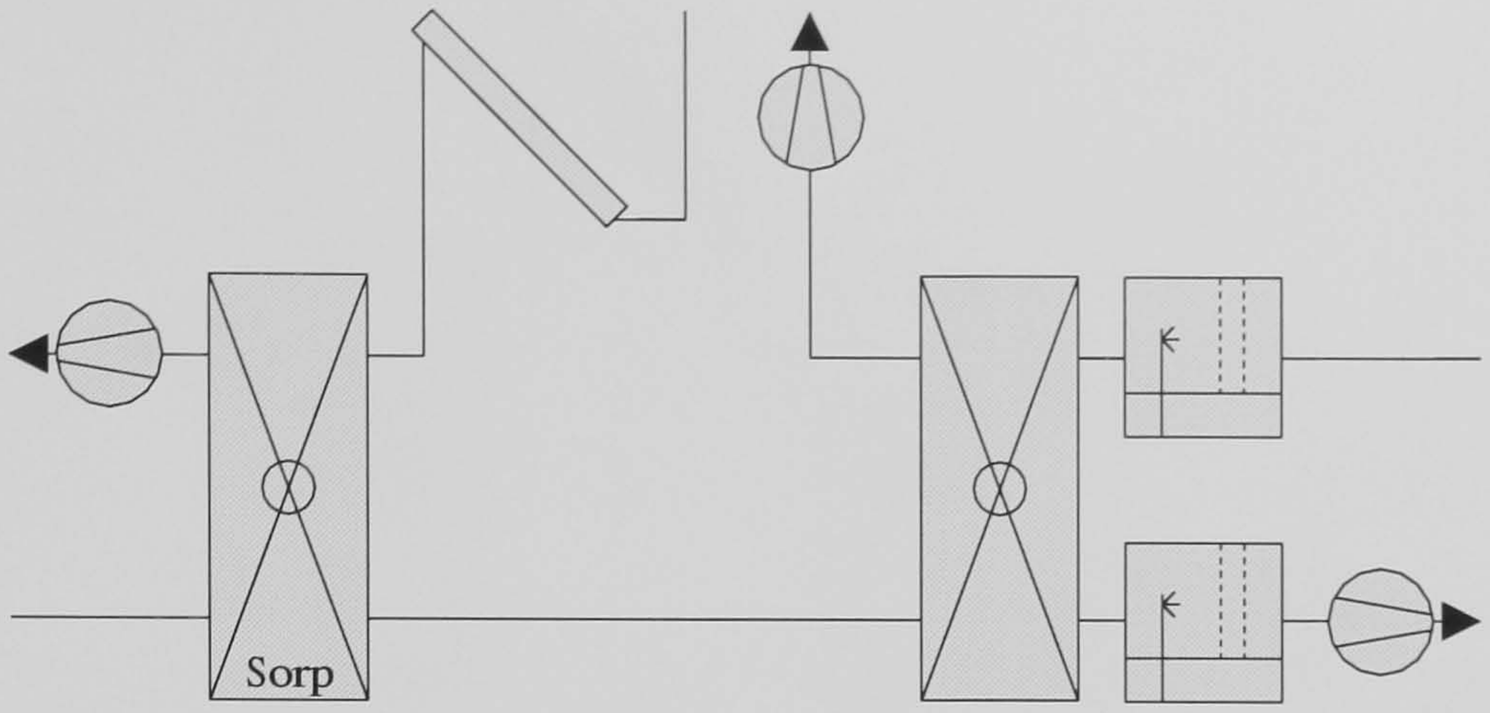

Table 5.13: Simulation results of case study 6 (heavyweight building, hygienic ventilation during occupation time, DCS with ambient air regeneration). Detailed description on page 102. Discussion of the simulation results on page 123.

BESTTEST Case 940	$\overline{\text{COP}}$[1] DCS [–]	add. cooling demand $[kWh/m^2a]$	DCS cooling energy $[kWh/m^2a]$	$rh_i > 0.6$ during year [–]	control mode[2] during operation [–]	
Djakarta	1.60	215.3	4.7	0.96	HR	0.00
					V	0.00
					AC	0.00
					DCS	0.06
					DCS*	0.94
Phoenix	1.40	137.8	69.1	0.03	HR	0.01
					V	0.02
					AC	0.02
					DCS	0.91
					DCS*	0.04
Seville	1.39	97.8	51.7	0.07	HR	0.05
					V	0.05
					AC	0.04
					DCS	0.78
					DCS*	0.08
Stuttgart	1.29	27.4	36.7	0.01	HR	0.38
					V	0.12
					AC	0.07
					DCS	0.43
					DCS*	>0.00

[1] averaged COP of the DCS–mode and the DCS*–mode

[2] see Table 5.7

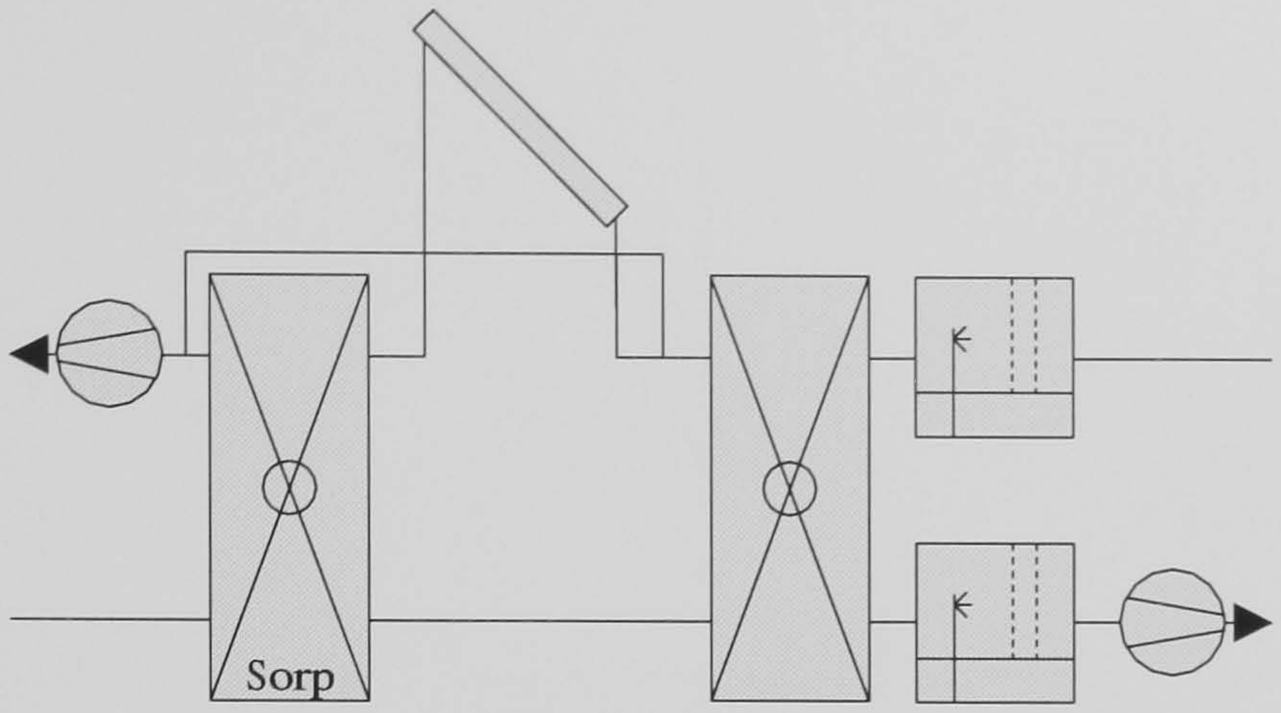

Table 5.14: Simulation results of case study 7 (heavyweight building, hygienic ventilation during occupation time, controlled to reach an inlet temperature close to 17 °C). Detailed description on page 102. Discussion of the simulation results on page 124.

BESTTEST Case 940	$\overline{\text{COP}}^1$ DCS [–]	add. cooling demand $[kWh/m^2a]$	DCS cooling energy $[kWh/m^2a]$	$rh_i > 0.6$ during year [–]	control mode[2] during operation [–]	
Djakarta	2.46	186.3	24.3	0.93	HR V AC DCS DCS*	0.00 0.02 0.14 0.84 –
Phoenix	1.42	155.1	53.1	0.10	HR V AC DCS DCS*	0.01 0.11 0.52 0.36 –
Seville	1.49	107.6	42.3	0.18	HR V AC DCS DCS*	0.03 0.06 0.53 0.38 –
Stuttgart	0.92	37.4	26.7	0.02	HR V AC DCS DCS*	0.33 0.08 0.52 0.07 –

[1] averaged COP of the DCS–mode and the DCS*–mode

[2] see Table 5.7

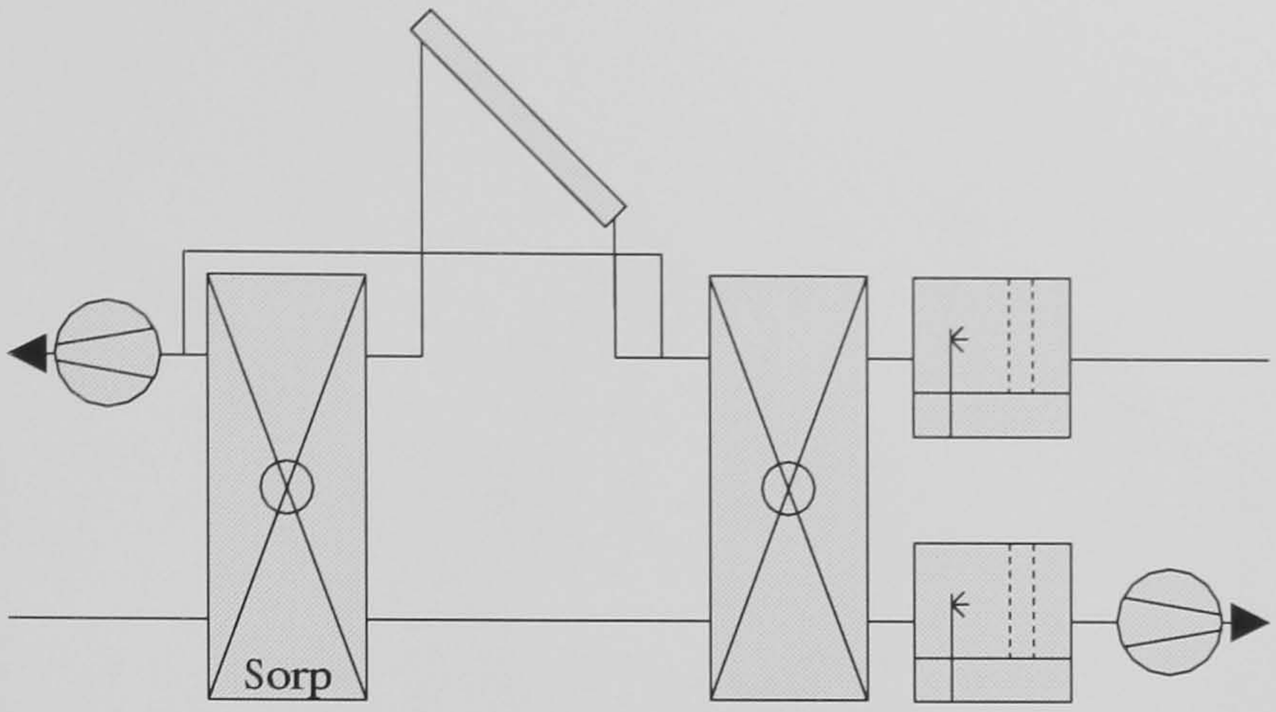

Table 5.15: Simulation results of case study 8 (heavyweight building, ventilation with maximum 4 air changes per hour, night ventilation, regeneration air flow controlled). Detailed description on page 103. Discussion of the simulation results on page 125.

BESTTEST Case 940	$\overline{\text{COP}}$[1] DCS [–]	add. cooling demand $[kWh/m^2a]$	DCS cooling energy $[kWh/m^2a]$	$rh_i > 0.6$ during year [–]	control mode[2] during operation [–]	
Djakarta	3.95	217.2	0.7	0.87	HR	0.00
					V	0.00
					AC	0.00
					DCS	0.13
					DCS*	0.87
Phoenix	1.42	50.3	161.4	0.09	HR	0.00
					V	0.09
					AC	0.12
					DCS	0.68
					DCS*	0.10
Seville	1.67	32.0	124.4	0.13	HR	0.03
					V	0.12
					AC	0.12
					DCS	0.57
					DCS*	0.15
Stuttgart	1.01	5.8	53.0	0.01	HR	0.31
					V	0.17
					AC	0.15
					DCS	0.35
					DCS*	0.01

[1] averaged COP of the DCS–mode and the DCS*–mode

[2] see Table 5.7

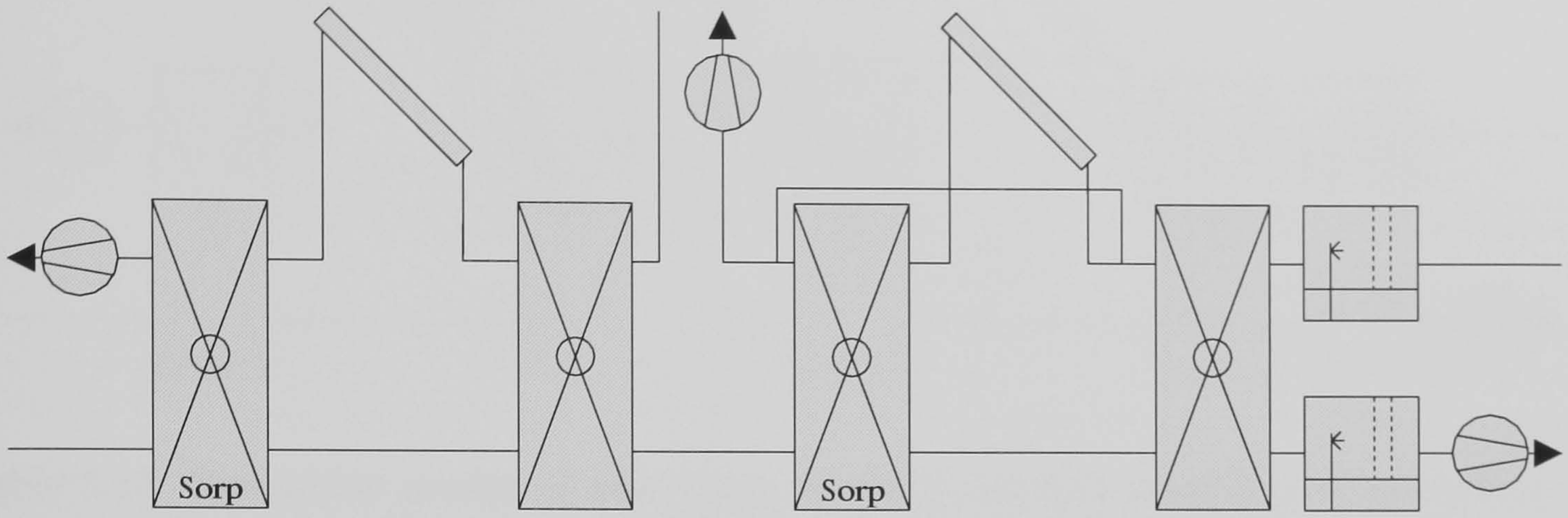

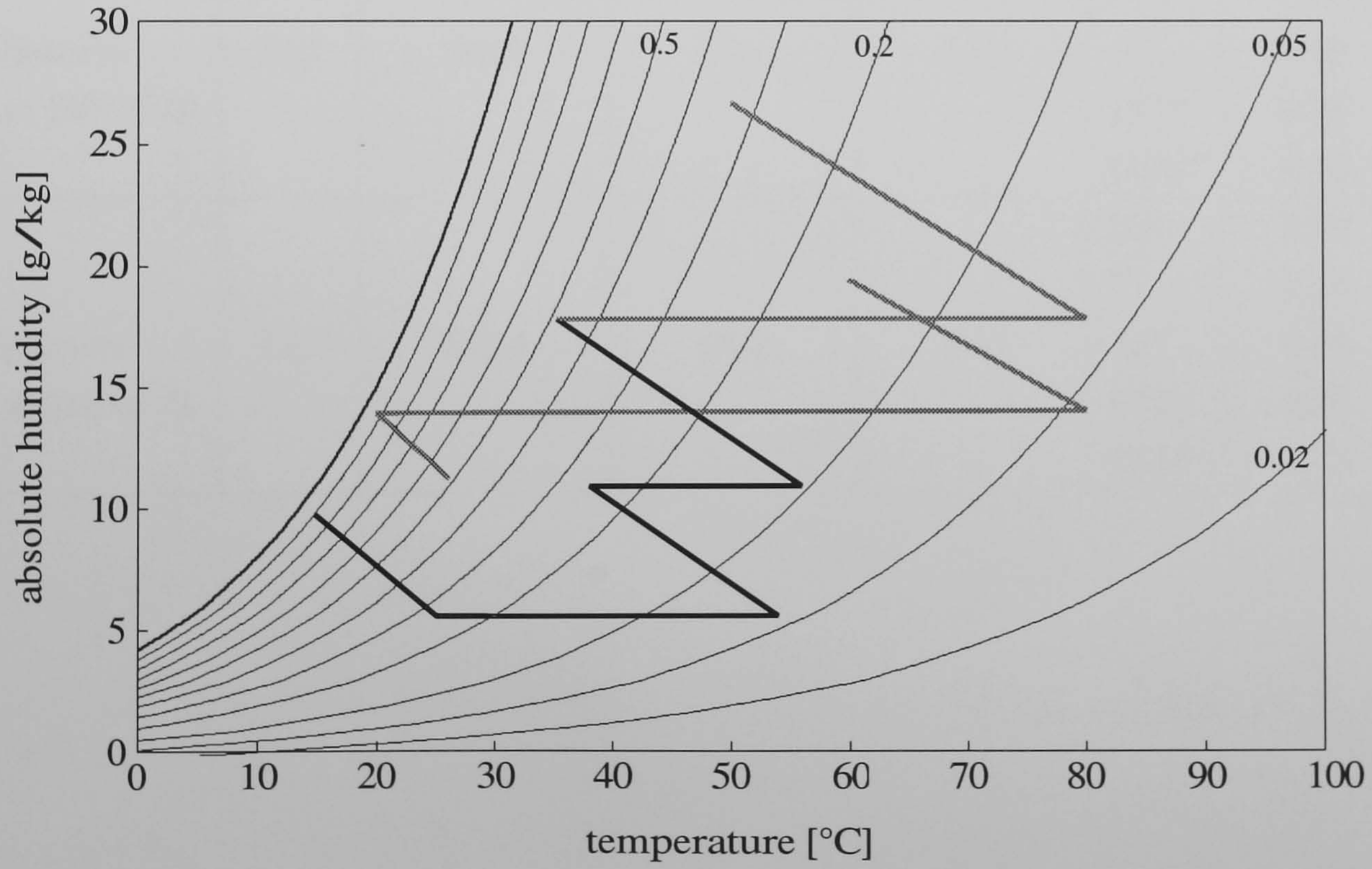

Figure 5.14: Double stage desiccant cooling ventilation cycle with solar air collectors for deep dehumidification

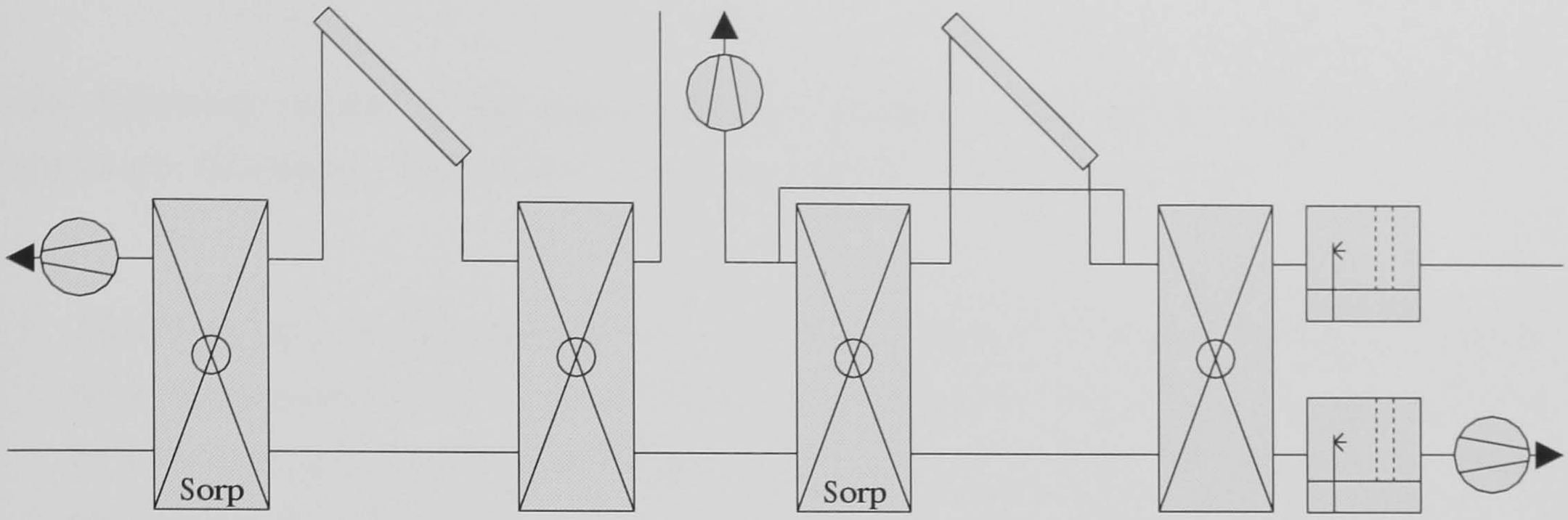

Table 5.16: Simulation results of case study 9 and 10 (double stage desiccant cooling system). Detailed description on page 103. Discussion of the simulation results on page 126.

BESTTEST Case 940	$\overline{\text{COP}}$[1] DCS [–]	add. cooling demand $[kWh/m^2a]$	DCS cooling energy $[kWh/m^2a]$	$rh_i > 0.6$ during year [–]	control mode[2] during operation [–]	
Djakarta $\dot{V}_{max} = 150\,m^3/h$	2.32	195.9	15.1	0.83	HR	0.00
					V	0.00
					AC	0.00
					DCS	0.26
					DCS*	0.74
Djakarta $\dot{V}_{max} = 518\,m^3/h$	2.65	153.3	62.2	0.73	HR	0.00
					V	0.00
					AC	0.00
					DCS	0.27
					DCS*	0.73

[1] averaged COP of the DCS–mode and the DCS*–mode

[2] see Table 5.7

5.6 Discussion of Simulation Results

In the following results of the simulation case studies conducted for the four different climates are discussed. The results were listed in the Tables 5.8 to 5.16.

1. This desiccant cooling ventilation cycle was designed with the minimum hygienic fresh air demand of $\dot{V} = 150m^3/h$ during occupation time. This cycle was adapted to a heavyweight building according to BESTEST case 940. The simulation results were listed in Table 5.8.

In Djakarta the desiccant cooling system powered only by solar energy is only capable of providing 3% of the annual cooling demand. The cause of this low value is the very high absolute humidity of the tropical climate. The rotating dehumidifier cannot remove enough water from the process air to keep the desiccant cooling system running in its initially desired mode. Because of the requirements of thermal comfort with a maximum wanted indoor relative humidity of 0.6 the inlet humidifier must be disabled for 74% of the operating hours. This results in an inlet temperature close to the indoor temperature in these cases. The relative humidity exceeded 0.6 for 83% of the year. However, the mean COP during the DCS–modes of 2.26 shows good system performance.

In Phoenix the system is capable of providing 32% of the annual cooling demand. It runs in its initially desired mode for 88% of operating hours. For 7% of the operating hours the rotating dehumidifier cannot remove enough water from the process resulting in a disabling of the inlet humidifier. The relative humidity exceeded 0.6 for 5% of the year. A mean COP during the DCS–modes of 0.67 was calculated.

In Seville the system is capable of providing 36% of the annual cooling demand. It runs in its initially desired mode for 75% of the operating hours. For 11% of the operating hours the rotating dehumidifier cannot remove enough water from the process resulting in a disabling of the inlet humidifier. The relative humidity exceeded 0.6 for 8% of the year. A mean COP during the DCS–modes of 0.72 was calculated.

In Stuttgart the system is capable of providing 58% of the annual cooling demand. It runs in the DCS–mode for 44% of the operating hours. If cooling is required

the rotating dehumidifier is able to remove enough water from the process in the occupation time resulting in a good performance of the inlet humidifier. A mean COP during the DCS–modes of 0.52 was calculated.

In all cases the system designed just for the minimum hygienic fresh air demand of 30 $m^3/(h \cdot \text{person})$ is too small to ensure thermal comfort requirements. In Stuttgart the system is able to remove all latent cooling loads, only additional sensible cooling must be provided. In Phoenix and Seville the dehumidification potential of a rotating dehumidifier is not enough for several hours in summer. This system applied in Djakarta does not accomplish the requirements of air conditioning at all, because of the low dehumidification potential. On the other hand, the COP reached in Stuttgart is the lowest and the COP reached in Djakarta is the highest. It can be shown that the COP reached by the desiccant cooling system increases with the ambient absolute humidity.

2. This desiccant cooling ventilation cycle was designed with the minimum hygienic fresh air demand of $\dot{V} = 150m^3/h$ during occupation time and enforced night ventilation with $\dot{V} = 518m^3/h$ corresponding to 4 air changes per hour. The night ventilation is used through the desiccant cooling system to enable cooling by humidifiers if appropriate. This cycle was adapted to a heavyweight building according to BESTEST case 940. The simulation results were presented in Table 5.9.

   In Djakarta the desiccant cooling system powered only by solar energy is never capable to remove sensible cooling loads. Night ventilation leads to an increase in the indoor humidity resulting in less running hours with the typical DCS–mode compared to the previous case without night ventilation. The inlet humidifier must be enabled for 76% of the operating hours. The relative humidity exceeded 0.6 for 84% of the year. However, the mean COP during the DCS–modes of 2.18 shows good system performance.

   In Phoenix the system is capable of providing 38% of the annual cooling demand. This value is 6% higher than without night ventilation. It runs in its initially desired mode for 79% of the operating hours, for 10% in the ventilation mode. For 6% of the operating hours the rotating dehumidifier cannot remove enough water from the process resulting in a disabling of the inlet humidifier. The relative humidity exceeded 0.6 for 6% of the year. A mean COP during the DCS–modes of 0.60 was

calculated.

In Seville the system is capable of providing 43% of the annual cooling demand. This value is 7% higher than without night ventilation. It runs in its initially desired mode for 66% of the operating hours, for 11% in the ventilation mode. For 10% of the operating hours the rotating dehumidifier cannot remove enough water from the process resulting in a disabling of the inlet humidifier. The relative humidity exceeded 0.6 for 9% of the year. A mean COP during the DCS–modes of 0.73 was calculated.

In Stuttgart the system is capable of providing 64% of the annual cooling demand. This value is 6% higher than without night ventilation. It runs in the DCS–mode for 39% of the operating hours, for 16% in the ventilation mode. For 2% of the operating hours the rotating dehumidifier cannot remove enough water from the process resulting in a disabling of the inlet humidifier. A mean COP during the DCS–modes of 0.53 was calculated.

In all cases the system designed just for the minimum hygienic fresh air demand of 30 $m^3/(h \cdot \text{person})$ is too small for thermal comfort requirements. However, the cooling demand was decreased by 6% to 7% by the use of night ventilation in Phoenix, Seville and Stuttgart. In Djakarta where the diurnal temperature swing is very low, the night ventilation does not have any energetic advantage.

3. This desiccant cooling ventilation cycle was designed with $\dot{V} = 150m^3/h$ or $\dot{V} = 518m^3/h$ if additional cooling is required during occupation time. Furthermore, night ventilation with $\dot{V} = 518m^3/h$ corresponding to 4 air changes per hour was enabled. The night ventilation is used through desiccant cooling system to enable cooling by humidifiers if appropriate. This cycle was adapted to a heavyweight building according to BESTEST case 940. The simulation results were presented in Table 5.10.

In Djakarta the desiccant cooling system powered only by solar energy is only capable of providing 1% of the annual cooling demand. The inlet humidifier must be enabled for 88% of the operating hours. Compared to case 1 these value show that the desiccant cooling system does not decrease the cooling demand, it increases due to the insufficient dehumidification. The relative humidity exceeded 0.6 for 88%

of the year. However, the mean COP during the DCS–modes of 4.04 shows good system performance.

In Phoenix the system is capable of providing 75% of the annual cooling demand. It runs in its initially desired mode for 70% of the operating hours, for 9% in the ventilation mode. For 13% of the operating hours the rotating dehumidifier cannot remove enough water from the process resulting in a disabling of the inlet humidifier. This is 7% more than in the case with only hygienic ventilation. The relative humidity exceeded 0.6 for 11% of the year. A mean COP during the DCS–modes of 1.02 was calculated. This value which is significantly higher than in the previous case studies caused by lower regeneration temperatures due to the same collector area used.

In Seville the system is capable of providing 78% of the annual cooling demand. It runs in its initially desired mode for 58% of the operating hours, for 11% in the ventilation mode. For 20% of the operating hours the rotating dehumidifier cannot remove enough water from the process resulting in a disabling of the inlet humidifier. Referring to the whole year this is 10% more than in the case with only hygienic ventilation. The relative humidity exceeded 0.6 for 16% of the year. A mean COP during the DCS–modes of 1.12 was calculated. This value which is significantly higher than in the previous case studies caused by lower regeneration temperatures due to the same collector area used.

In Stuttgart the system is capable of providing 89% of the annual cooling demand. It runs in the DCS–mode for 36% of the operating hours, for 16% in the ventilation mode. For 2% of the operating hours and of the entire year the rotating dehumidifier cannot remove enough water from the process resulting in a disabling of the inlet humidifier. A mean COP during the DCS–modes of 0.57 was calculated.

It is interesting that an increase of the air flow causes increased disabling of the inlet humidifiers, for all climates except of Stuttgart. With reference to the values with only hygienic ventilation, it is a doubling in time. In the case of Djakarta the higher value in the DCS*–mode compared to the previous simulations shows the insufficient dehumidification of the system once more.

4. This desiccant cooling ventilation cycle was designed with the minimum hygienic

fresh air demand of $\dot{V} = 150m^3/h$ during occupation time. This cycle was adapted to a heavyweight building according to BESTEST case 940. Compared to case 1 only half of the collector area is used. The simulation results were listed in Table 5.11.

In Djakarta the desiccant cooling system is only capable of providing 3% of the annual cooling demand. Because of the requirements of thermal comfort with a maximum desired indoor relative humidity of 0.6 the inlet humidifier must be disabled for 92% of the operating hours. This results in an inlet temperature close to the indoor temperature in these cases. The relative humidity exceeded 0.6 for 92% of the year. However, the mean COP during the DCS–modes of 3.43 shows good system performance.

In Phoenix the system is capable of providing 34% of the annual cooling demand. It runs in its initially desired mode for 78% of operating hours. For 10% of the operating hours the rotating dehumidifier cannot remove enough water from the process resulting in a disabling of the inlet humidifier. The relative humidity exceeded 0.6 for 8% of the year. A mean COP during the DCS–modes of 0.96 was calculated.

In Seville the system is capable of providing 37% of the annual cooling demand. It runs in its initially desired mode for 62% of the operating hours. For 17% of the operating hours the rotating dehumidifier cannot remove enough water from the process resulting in a disabling of the inlet humidifier. The relative humidity exceeded 0.13 for 83% of the year. A mean COP during the DCS–modes of 1.01 was calculated.

In Stuttgart the system is capable of providing 58% of the annual cooling demand. It runs in the DCS–mode for 39% of the operating hours. For 2% of the operating hours the rotating dehumidifier cannot remove enough water from the process resulting in a disabling of the inlet humidifier. A mean COP during the DCS–modes of 0.59 was calculated.

Compared to the simulations of case 1 with double the collector area it can be shown that nearly the same cooling loads can be removed. However, the indoor relative humidity more often reaches the critical value of 0.6 resulting in a disabling of the inlet humidifier. All calculated mean COPs are significantly higher compared

to case 1 which can be explained with the reduced amount of solar energy used for regeneration.

5. This desiccant cooling ventilation cycle was designed with the minimum hygienic fresh air demand of $\dot{V} = 150m^3/h$ during occupation time. This cycle was adapted to a lightweight building according to BESTEST case 640. The simulation results were presented in Table 5.12.

In Djakarta the desiccant cooling system powered only by solar energy is only capable of providing 2% of the annual cooling demand. The rotating dehumidifier cannot remove enough water from the process air to keep the desiccant cooling system running in its initially desired mode. The inlet humidifier must be disabled for 74% of the operating hours. The relative humidity exceeded 0.6 for 83% of the year. The mean COP during the DCS–modes of 2.25 shows good system performance. All simulated values are close to those of the simulations with the heavyweight building.

In Phoenix the system is capable of providing 28% of the annual cooling demand. It runs in its initially desired mode for 88% of the operating hours. For 8% of the operating hours the rotating dehumidifier cannot remove enough water from the process resulting in a disabling of the inlet humidifier. The relative humidity exceeded 0.6 for 5% of the year. A mean COP during the DCS–modes of 0.67 was calculated. The annual cooling demand has increased by 11% compared to the heavyweight building simulation.

In Seville the system is capable of providing 30% of the annual cooling demand. It runs in its initially desired mode for 77% of the operating hours. For 8% of the operating hours the rotating dehumidifier cannot remove enough water from the process resulting in a disabling of the inlet humidifier. The relative humidity exceeded 0.6 for 13% of the year. A mean COP during the DCS–modes of 0.71 was calculated. The annual cooling demand has increased by 15% compared to the heavyweight building simulation.

In Stuttgart the system is capable of providing 50% of the annual cooling demand. It runs in the DCS–mode for 55% of the operating hours. If cooling is required the rotating dehumidifier is able to remove enough water from the process at all times resulting in a good performance of the inlet humidifier. The relative humid-

ity exceeded 0.6 for 6% of the year. A mean COP during the DCS–modes of 0.48 was calculated. The annual cooling demand has increased by 39% compared to the heavyweight building simulation.

In all cases the system designed just for the minimum hygienic fresh air demand of 30 $m^3/(h \cdot person)$ is too small for thermal comfort requirements. A lightweight construction has no influence on the energetic demand and the performance of the desiccant cooling system in Djakarta. In spite of the fact that in Phoenix and Seville the cooling demand increases, the accumulated cooling energy of the desiccant cooling system decreases by 4% to 6%. The greatest influence of the lightweight construction occur in Stuttgart, where the annual cooling demand increases by 39%. Furthermore, the desiccant cooling system was able to remove 19% more cooling load from the building than in the heavyweight case.

6. This desiccant cooling ventilation cycle with ambient air regeneration was designed with the minimum hygienic fresh air demand of $\dot{V} = 150m^3/h$ during occupation time. This cycle was adapted to a heavyweight building according to BESTEST case 940. The simulation results were presented in Table 5.13.

In Djakarta the application of a desiccant cooling cycle with ambient air regeneration leads to the requirements that for 94% of the operating time the inlet humidifier must be disabled. The relative humidity exceeded 0.6 for 96% of the year.

In Phoenix the system is capable of providing 33% of the annual cooling demand. It runs in its initially desired mode for 91% of the operating hours. For 4% of the operating hours the rotating dehumidifier cannot remove enough water from the process resulting in a disabling of the inlet humidifier. This is half of the time compared with the common ventilation cycle. The relative humidity exceeded 0.6 for 3% of the year. The cooling energy provided by the desiccant cooling system increases by 4%.

In Seville the system is capable of providing 35% of the annual cooling demand. It runs in its initially desired mode for 78% of the operating hours. For 8% of the operating hours the rotating dehumidifier cannot remove enough water from the process resulting in a disabling of the inlet humidifier. The relative humidity exceeded 0.6 for 7% of the year. The cooling energy provided by the desiccant cooling

system drops by 5%.

In Stuttgart the system is capable of providing 57% of the annual cooling demand. It runs in its initially desired mode for 43% of the operating hours. If cooling is required the rotating dehumidifier is able to remove enough water from the process at every time resulting in a good performance of the inlet humidifier. The cooling energy provided by the desiccant cooling system drops by 1%.

Interesting in this case study is that the cooling energy provided by the desiccant cooling system drops in Stuttgart and in Seville. On the other hand, the cooling energy provided increases by 4% in Phoenix. The main outcome of this study is, however, that the inlet humidifier must not be disabled as often as with the conventional ventilation cycle in these climates. An exception is the climate of Djakarta, where the absolute humidity after the outlet humidifier is lower than the ambient–air absolute humidity resulting in a higher percentage of the DCS*–mode. Except of Djakarta, the mean COP calculated is greater than in the other studies, because the lower absolute humidity of the regeneration air leads to a significant higher dehumidification at low regeneration temperatures.

7. This desiccant cooling ventilation cycle was designed with the minimum hygienic fresh air demand of $\dot{V} = 150m^3/h$ during occupation time. This cycle was adapted to a heavyweight building according to BESTEST case 940. Compared to case 1 another control strategy is used. The room temperature and the indoor relative humidity are not considered. The system is controlled to reach an inlet temperature close to 17 °C. The simulation results were listed in Table 5.14.

   Neglecting the humidity limits of the thermal comfort requirements, the desiccant cooling system is capable of providing 12% of the annual cooling demand in Djakarta. Nonetheless, the relative humidity exceeded 0.6 for 93% of the year. The mean COP during the DCS–modes of 2.46 shows good system performance.

   In Phoenix the system is capable of providing 26% of the annual cooling demand. It runs in the DCS–mode for 36% of operating hours, for 52% in the adiabatic cooling mode. Nonetheless, the relative humidity exceeded 0.6 for 10% of the year. A mean COP during the DCS–modes of 1.42 was calculated.

In Seville the system is capable of providing 29% of the annual cooling demand. It runs in the DCS–mode for 38% of operating hours, for 53% in the adiabatic cooling mode. Nonetheless, the relative humidity exceeded 0.6 for 18% of the year. A mean COP during the DCS–modes of 1.49 was calculated.

In Stuttgart the system is capable of providing 42% of the annual cooling demand. It runs in the DCS–mode for 7% of operating hours, for 52% in the adiabatic cooling mode. The relative humidity exceeded 0.6 for 2% of the year. A mean COP during the DCS–modes of 0.92 was calculated.

Compared to the simulations of case 1 considering the room conditions, the relative humidity exceeds 0.6 more often resulting in uncomfortable room conditions. The desired inlet temperature of 17 °C can be reached in Phoenix, Seville and Stuttgart in half of the time with the adiabatic cooling mode. However, the dehumidifier is often disabled when indoor relative humidity is too high. The calculated mean COP's are significantly higher than in case 1 with the other control strategy.

8. This desiccant cooling ventilation cycle was designed with $\dot{V} = 150m^3/h$ or $\dot{V} = 518m^3/h$ if additional cooling is required during occupation time. To obtain a better system performance $\dot{V}_R/\dot{V}_P$ is variable between 0.35 and 0.75 dependent on regeneration temperature. Furthermore night ventilation with $\dot{V} = 518m^3/h$ corresponding to 4 air changes per hour was enabled. The night ventilation is used through desiccant cooling system to enable cooling by humidifiers if appropriate. This cycle was adapted to a heavyweight building according to BESTEST case 940. The simulation results were listed in Table 5.15.

In Djakarta the desiccant cooling system powered only by solar energy is only capable of providing less than 1% of the annual cooling demand. The inlet humidifier must be enabled for 87% of the operating hours. Comparing to case 3 these value show that the desiccant cooling system does not decrease the cooling demand, it increases it caused by the insufficient dehumidification. The relative humidity exceeded 0.6 for 87% of the year. However, the mean COP during the DCS–modes of 3.95 shows good system performance.

In Phoenix the system is capable of providing 76% of the annual cooling demand. This is 1% more than in the comparable case 3. It runs on its initially desired mode

in 68% of the operating hours, for 12% in the adiabatic cooling mode and in 9% in the ventilation mode. For 10% of the operating hours the rotating dehumidifier cannot remove enough water from the process, resulting in a disabling of the inlet humidifier. The relative humidity exceeded 0.6 for 9% of the year. A mean COP during the DCS–modes of 1.42 was calculated. This value is significantly higher than in case 3 without a bypass control.

In Seville the system is capable of providing 80% of the annual cooling demand. This is 2% more than in the comparable case 3. It runs on its initially desired mode for 57% of the operating hours, for 12% in the adiabatic cooling mode and in the ventilation mode. For 15% of the operating hours the rotating dehumidifier cannot remove enough water from the process, resulting in a disabling of the inlet humidifier. Referring to case 3 this is 5% less. The relative humidity exceeded 0.6 for 13% of the year. A mean COP during the DCS–modes of 1.67 was calculated. This value is significantly higher than in case 3 without a bypass control.

In Stuttgart the system is capable of providing 90% of the annual cooling demand. This is 1% more than in the comparable case 3. It runs on the DCS–mode for 35% of the operating hours, for 15% in the adiabatic cooling mode and for 17% in the ventilation mode. For 1% of the operating hours and of the entire year the rotating dehumidifier cannot remove enough water from the process, resulting in a disabling of the inlet humidifier. A mean COP during the DCS–modes of 1.01 was calculated. This value is significantly higher than in case 3 without a bypass control.

As expected, the mean COP of the desiccant cooling system increases if the regeneration air flow is decreased. However, it is interesting that the provided cooling energy of the desiccant cooling system with a bypass control also increases, because higher regeneration temperatures occur by a lower regeneration air flow. Reduced dehumidification efficiencies and higher regeneration temperatures are more useful for the performance of the dehumidifier than high dehumidification efficiencies but low regeneration temperatures. Compared to the other cases without a bypass control, more dehumidification is achieved in hours with only poor irradiation. This results in less hours in which the inlet humidifier must be disabled.

9. This double stage desiccant cooling ventilation cycle was designed with the minimum hygienic fresh air demand of $\dot{V} = 150 m^3/h$ during occupation time. The collector area was divided in half for both dehumidifiers. This cycle was adapted

to a heavyweight building according to BESTEST case 940. The simulation results were presented in Table 5.16 and were carried out only for Djakarta's climate.

In Djakarta the double stage desiccant cooling system powered only by solar energy is capable of providing 7% of the annual cooling demand. The cause of this low value is the very high absolute humidity of the tropical climate. However, this is more than twice that of the system in case 1. The rotating dehumidifiers cannot remove enough water from the process air to keep the desiccant cooling system running in its initially desired mode. Because of the requirements of thermal comfort with a maximum desired indoor relative humidity of 0.6, the inlet humidifier must be disabled for 74% of the operating hours. This results in an inlet temperature close to the indoor temperature in these cases. The relative humidity exceeded 0.6 for 83% of the year. This high value occurs because a natural air change of 0.2 per hour is considered. However, the mean COP during the DCS–modes of 2.32 shows good system performance.

10. This double stage desiccant cooling ventilation cycle was designed with the minimum hygienic fresh air demand of $\dot{V} = 150m^3/h$ or $\dot{V} = 518m^3/h$ if additional cooling is required during occupation time and night ventilation with $\dot{V} = 518m^3/h$ corresponding to 4 air changes per hour. The collector area was divided in half for both dehumidifiers. This cycle was adapted to a heavyweight building according to BESTEST case 940. The simulation results were presented in Table 5.16 and were carried out only for Djakarta's climate.

In Djakarta the double stage desiccant cooling system powered only by solar energy is capable of providing 29% of the annual cooling demand. This is 4.1 times more than in the previous study, although the air flow is increased by the factor 3.5. Because of the requirements of thermal comfort with a maximum desired indoor relative humidity of 0.6, the inlet humidifier must be disabled for 73% of the operating hours. This results in an inlet temperature close to the indoor temperature in these cases. The relative humidity exceeded 0.6 for 73% of the year. This high value occurs, because a natural air change of 0.2 per hour is considered. However, the mean COP during the DCS–modes of 2.65 shows good system performance. The higher COP compared to the previous case study can be explained with the more efficient working outlet humidifier during the DCS–modes due to the lower indoor humidity.

Chapter 6

Suggestions for the Design of Desiccant Cooling Systems

In the following chapter general suggestions for the design of solar driven desiccant cooling systems will be given. These suggestions have been developed from the experience gained with the desiccant cooling test plant and from the interpretations of the simulation case studies. Appropriate solar driven desiccant cooling systems for the different climates investigated in this work will be given and the special features of plants, collector systems and buildings will be illustrated. In those cases in which a solar driven desiccant cooling system cannot ensure the desired thermal comfort, suggestions for appropriate combinations with different air conditioning systems will be given. In these selections the energy efficiency will be of greatest interest. After the general description of the systems detailed information on the required components will be provided and criteria for the control strategies in the different applications will be given.

6.1 General Suggestions for Desiccant Cooling with Solar Energy

Due to the type of construction of desiccant cooling systems with only air as a the cooling medium, the cooling capacity is linearly dependent on the volume flow for steady-state room conditions and for the same regeneration temperatures. Desiccant cooling systems in general and all air conditioning systems using the entering air as the cooling medium

are energetically interesting if the cooling loads can be removed from the building with no more than the fresh air demand required for health and hygiene. In cases where sensible cooling loads dominate, air systems are often not the appropriate choice due to the energy demand of the fans. Normally, it is more energy saving to use a liquid medium, as for example with chilled ceilings, to avoid an energy consuming high air flow. Hence, modern cooling concepts focus on the separation of cooling and ventilation where possible. As a result, desiccant cooling systems as complete air conditioning systems are mainly appropriate for applications with a high fresh air demand, as for example assembly rooms, lecture halls and offices for a large number of people.

Desiccant cooling ventilation cycles shown in Figure 5.11 provide dehumidification, cooling and the required ventilation to accomplish the fresh air demand of people. They are the common manner of configuration of a desiccant cooling system. However, for special applications it is convenient to use modified cycles.

An advantage of the desiccant cooling ventilation cycle with ambient air regeneration as shown in Figure 5.12 is that the returning air need not be carried to the intake of the solar collectors. This is an important feature, because with the use of solar air collector facades constructive problems appear with the need of carrying the air to the bottom of a facade. A further advantage is that leaks in the solar air collector facade do not influence the system's performance in the same way as in the common cycles, where the returning air flow and, hence, the cooling capacity of the heat recovery and the outlet humidifier will be decreased. However, this system configuration has disadvantages. It requires a third fan and consequently more electrical energy. A further disadvantage is that the heat of adsorption after the dehumidifier will not be recovered for the regeneration process.

Desiccant cooling recirculation cycles as shown in Figure 2.6 are appropriate for use in applications where latent loads dominate, for example in industrial processes. Here, where dehumidification is needed and the fresh air demand is not high, the advantage of a recirculation cycle compared to a ventilation cycle is that the cooling capacity is equal to the cooling load of the building, because the ambient air need not be cooled down and dried to the desired indoor air conditions. However, if mainly sensible cooling loads must be removed, an air system is questionable because of the high energy demand of fans. Furthermore, the fresh air demand must be provided by another ventilation system.

In desiccant cooling systems, flat–plate collectors, vacuum tube collectors and solar air collectors can all be used. Due to the maximum regeneration temperature requirements of around 80 °C, vacuum tube collectors which can provide higher temperatures are not necessary. If the cooling load is well correlated, in time, with the irradiance, solar air collectors are appropriate for providing the required regeneration heat in desiccant cooling systems. The advantages of solar air collectors in desiccant cooling systems are the ability to avoid a heat exchanger, the easy building integration and the reduced costs compared to flat–plate collectors. The area demand of solar air collectors should be determined with detailed calculations. To provide a provisional value the specific area used in the simulations was in the cases with 4 air changes per hour, 8.8% of the floor area (case studies 2, 3, 8 and 10). Furthermore, the specific area was 8.3 m^2 per 1000 m^3/h of air flow. Assuming an inlet temperature of 10 K below the room temperature the area demand results in 2.4 m^2/kW of removed cooling load. Using flat–plate collectors with storage systems, higher fractions can be appropriate, because these systems can facilitate cooling during hours with no sunshine. A significant decrease of the COP of desiccant cooling systems with solar air collectors can occur if they are not leak–tight. Ambient air will be sucked in through the small gaps at the flanges resulting in a reduced air flow from the building. This unbalanced air flow leads to an insufficient temperature reduction in the process air flow at the heat recovery. Furthermore, the cooling capacity of the outlet humidifier is reduced. Particularly interesting for desiccant cooling systems with solar air collectors are the ventilation cycles with ambient air regeneration as mentioned above. Leaks at the solar air collectors will not influence the COP of the system in such a major way as in the common ventilation cycle. However, these investigations have shown that regeneration is possible with a significantly reduced regeneration air flow.

6.2 Control of Desiccant Cooling Systems with Solar Energy

Desiccant cooling systems must be controlled to reach optimum performance and high COPs. One possibility for the control is the use of the inlet temperature as the control parameter. The desiccant cooling system will be switched into different possible modes (see page 100) to achieve an inlet temperature which should be close to a specified value, for example 17 °C. This automatically results, during winter, in the use of the heat recovery mode, in spring and autumn in the use of the ventilation mode and in summer

in the use of the adiabatic cooling mode and the desiccant cooling modes. The advantage of this control strategy is that the inlet temperature is maintained within a small band, allowing good planning for the air distribution system. In all climates investigated high COPs can be reached because the system operates approximately half the time in the adiabatic cooling mode, which means that the dehumidifier, the inlet humidifier and the solar collectors are not needed. In Stuttgart such a temperature control, neglecting the indoor humidity can provide comfortable conditions 99% of the time. In the other climates which are more humid the indoor relative humidity often exceeds the maximum permissible value. However, the dehumidifier is often disabled when indoor relative humidity is too high, because this value is not part of the control. To avoid ignoring such indoor conditions, a control strategy depending on the room conditions is suggested in Table 5.7. By controlling the desiccant cooling system dependent on the room conditions, which can be measured in the outlet air flow, the interaction with the building can be taken into account. When using solar energy, the control of desiccant cooling systems must be adapted to solar operation to achieve high solar fractions. In contrast to desiccant cooling systems in which the regeneration energy must be paid for and should be minimized, the solar energy should be used at all times when available.

Using a variable air flow dependent on the solar irradiation decreases the demand of electrical energy for the fans. Furthermore, with a variable regeneration air flow, the mean COP of the desiccant cooling system can be increased. However, the cooling energy provided by the desiccant cooling system with a bypass control to achieve the variable regeneration air flow also increases because higher regeneration temperatures occur with a lower regeneration air flow. As the measurements and the simulations showed reduced dehumidification efficiencies and a higher regeneration temperatures are more useful for the performance of the dehumidifier than high dehumidification efficiencies but low regeneration temperatures. Hence, enabling a bypass control leads to more dehumidification at times with only poor irradiation. This results in fewer hours in which the inlet humidifier must be disabled. To achieve thermal comfort with this control strategy in which the inlet temperature is not controlled, high inductive air inlet systems should be used to avoid draught because low inlet temperatures may occur. A further suggestion is to use controlled inlet humidifiers to avoid exceedingly low inlet temperatures.

Rotary dehumidifiers in solar driven desiccant cooling systems with fluctuating regeneration temperatures can be run at variable rotation speed. Particularly when high regeneration temperatures occur, the dehumidification decreases due to the heat retention. A

control strategy for an optimum dehumidifier rotation was presented in EICKER ET AL. 1998 A. The temperature in the exhaust air stream will be measured directly behind the sorption wheel and shortly before the process section is entered. The performance of the desorption process is evident from the difference between this temperature and the regeneration temperature. Having a small temperature difference at high regeneration temperatures shows that the desorption process is still completed and the desiccant will be unnecessarily heated. This results in a decreased dehumidification in the adsorption section of the dehumidifier, because the desiccant must first be cooled down to temperatures at which an adsorption is possible. In such a case, the control may increase the rotation speed. Figure 6.1 shows the arrangement of the control sensors for this approach.

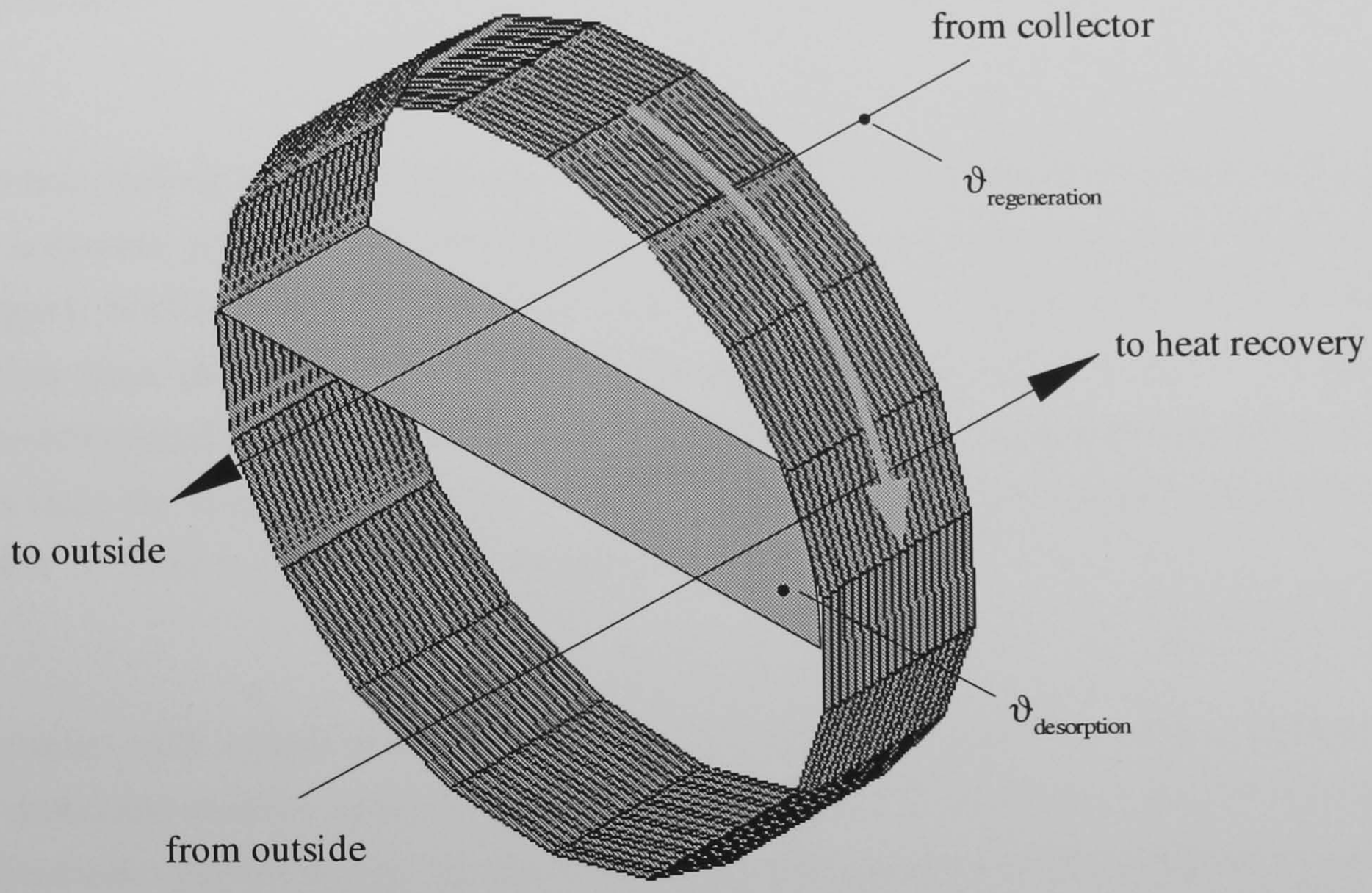

Figure 6.1: Control of rotation fluctuating regeneration temperatures

6.3 Desiccant Cooling in Different Climates

In the following the results of the simulations will be concluded to give design suggestions for the application of desiccant cooling systems in different climates. The locations used for the simulations can also be used as examples for similar climates.

As the simulations show it is only possible in climates like Stuttgart to ensure thermal comfort for most of the year with a desiccant cooling system driven only by solar energy from air collectors. In the climates of Seville and Phoenix (Arizona) additional cooling and dehumidification are required. One possibility for providing cooling during hours with no irradiation is to store solar thermal energy. Here, systems with flat–plate collectors and storage systems may be appropriate. Due to the advantages with regard to the building integration of solar air collectors, a combination with solar liquid collectors is also possible.

Desiccant cooling ventilation cycles with ambient air regeneration as shown in Figure 5.12 show a system performance comparable to the common ventilation cycle in climates like Stuttgart, Seville and Phoenix. Only in Djakarta, where the ambient absolute humidity is higher than the humidity after the outlet humidifier, this system shows a poor performance compared to the common cycle. In climates where the ambient absolute humidity is less than the humidity after the outlet humidifier, lower regeneration temperatures are possible to achieve the same dehumidification.

In climates with a high absolute humidity like the investigated climate of Djakarta, common desiccant cooling systems with rotating dehumidifiers cannot ensure enough dehumidification. Nevertheless, in these climates the sorptive dehumidification provides a main energetic advantage compared to the dehumidification by surface coolers. For these cases desiccant cooling systems with a cooled dehumidification process meet the requirements. However, these systems are not in such a marketable commodity as the systems with the rotating dehumidifiers. A suggestion is to create a double stage desiccant cooling cycle as shown in Figure 5.14 by adding a second rotating dehumidifier and a second heat recovery to the common desiccant cooling ventilation cycle. This additional part must be regenerated by ambient air.

Furthermore, hybrid systems combining conventional compressor cooling technology and desiccant cooling technology can provide a good contribution for energy–efficient air conditioning systems. Possible configurations of desiccant cooling systems with compression chillers are shown in Figure 6.2 and Figure 6.3. Solar assisted systems are shown in Figure 6.4 and Figure 6.5. Using compressor cooling technology in combination with desiccant cooling systems leads to high overall COPs (see Table 2.1) because the condenser heat of the compressor is used for the regeneration. This results in a significantly smaller area demand for the solar collectors. Moreover, smaller or in some cases no cooling towers will be required. The system configuration shown in Figure 6.4 is appropriate in climates where the absolute humidity of the ambient air does not exceed values of 20 g/kg. Hence, it is a solution for the presented climates of Seville, Phoenix and Stuttgart. In tropical climates like Djakarta the system configuration shown in Figure 6.5 is appropriate if only one dehumidifier should be used. Nevertheless, the appropriate system combination must be investigated by simulations.

Today's air conditioning concepts often use the combination of chilled ceilings and displacement ventilation. To run these systems, cold water temperatures of around 15 °C for the chilled ceilings and inlet air temperatures of around 22 °C must be provided. These two requirements appear unachievable with desiccant cooling systems because they are pure air handling units and the idea is to achieve low inlet temperatures to remove a large amount of the cooling load from the building. However, by the use of a compressor for the cold water circuit a part of the regeneration heat for a desiccant cooling system can be provided by the condenser. Also, by the use of a controlled inlet humidifier with a variable humidification efficiency the required inlet temperatures for displacement ventilation can be accomplished. If only a small amount of water is evaporated by the inlet humidifier the indoor–air relative humidity decreases, resulting in a lower dew point temperature of the air. This makes it possible to allow lower temperatures of the chilled ceiling without condensation, resulting in a higher cooling capacity.

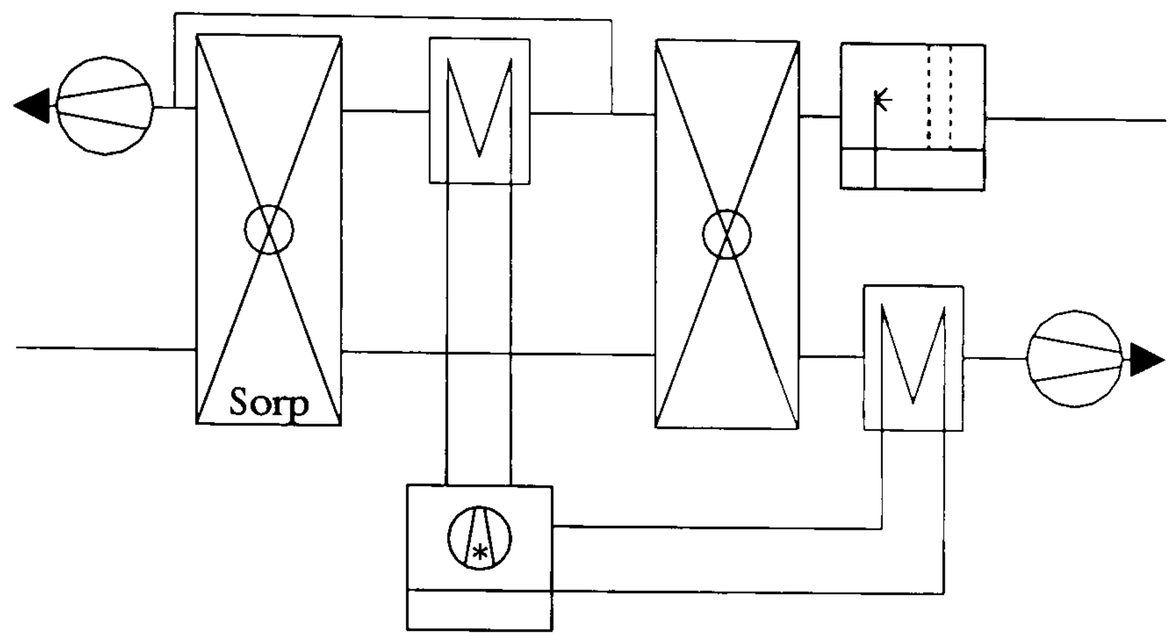

Figure 6.2: Combination of a desiccant cooling system with a compression chiller without using solar energy (Inlet humidifier is replaced by the surface cooler)

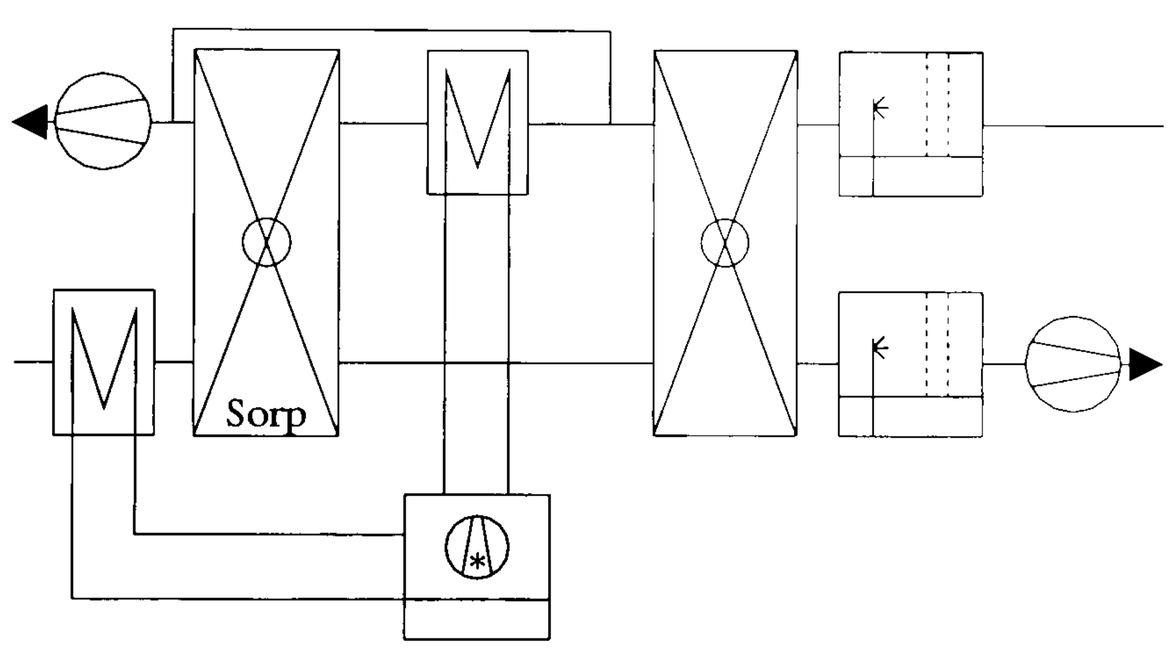

Figure 6.3: Combination of a desiccant cooling system with a compression chiller without using solar energy (Surface cooler in front of the dehumidifier to achieve deep dehumidification)

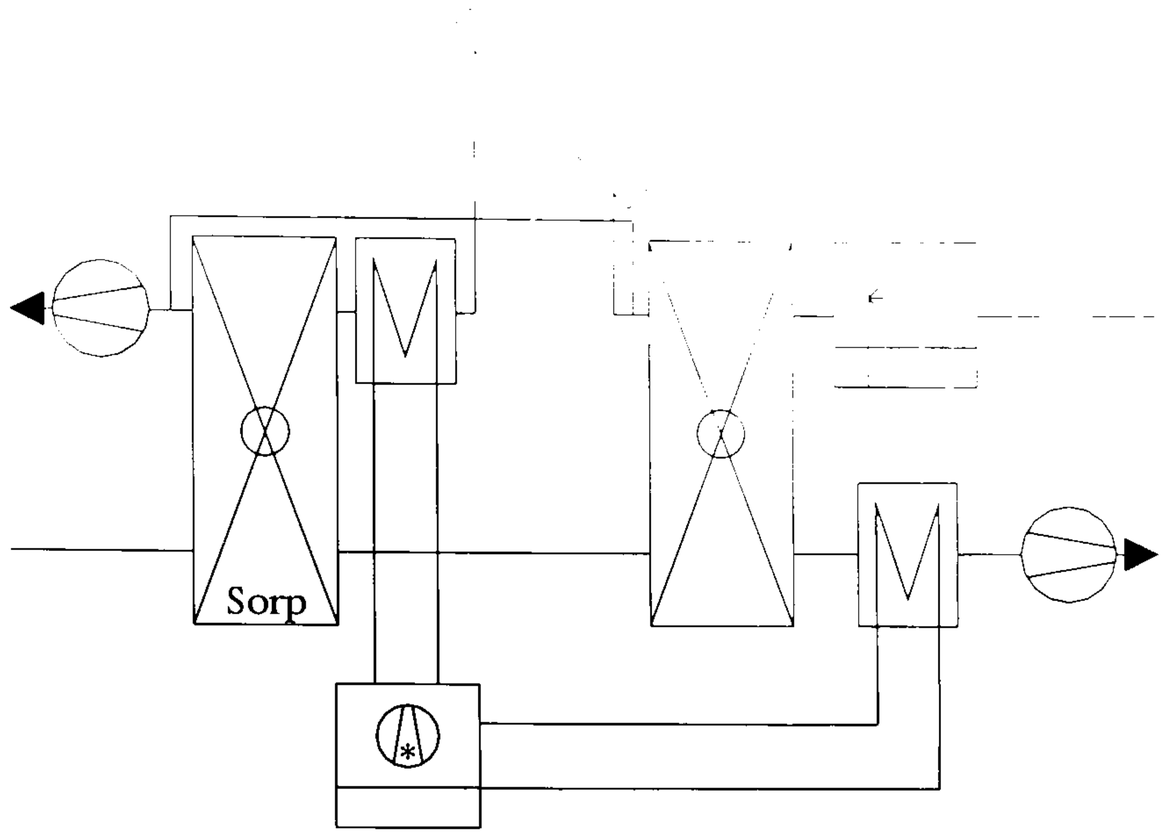

Figure 6.4: Solar assisted desiccant cooling system with a compression chiller (Inlet humidifier is replaced by the surface cooler)

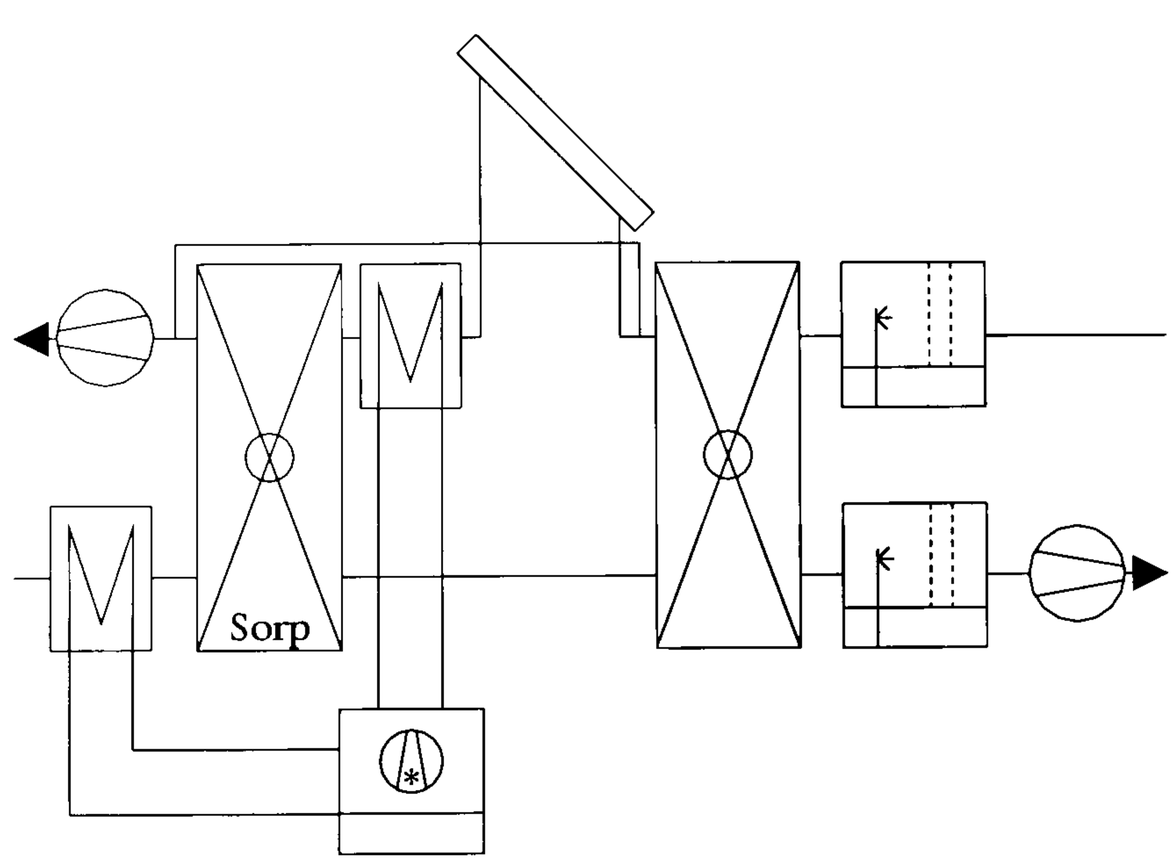

Figure 6.5: Solar assisted desiccant cooling system with a compression chiller (Surface cooler in front of the dehumidifier to achieve deep dehumidification)

6.4 Current Economical Aspects of Desiccant Cooling Systems

In the following a rough economical comparison of desiccant cooling systems with conventional air conditioning systems with compression chillers will be given. Furthermore, the main parameters for a detailed economical analysis will be presented to carry out comparisons for different boundary conditions. On this basis possible energy savings and the reduction of running costs can be calculated by detailed simulation programs. At the moment, the investment costs for desiccant cooling systems without solar components are close to those of conventional air conditioning systems with compression chillers. In dependence of the costs for the regeneration heat, the running costs can be 1/3 lower than for the conventional system according to HEINRICH and FRANZKE 1997. The main variables for possible investment and running cost reductions for desiccant cooling systems compared with conventional air conditioning systems with compression chillers are:

- Cooling tower is not necessary
- Cost reduction in the building construction by the use of collector facades and collector roofs
- Possibility to use waste heat or to get cheap heat at the required temperature level
- Consideration of the reduction of the electrical peak load
- Costs and quality of the fresh water, which must be prepared for the use in the humidifiers
- Full–year running time must be considered and the reduction of the energy demand in winter due to the high efficient working enthalpy recovery and heat recovery

Compared to conventional air conditioning systems the following components must be installed additionally and lead to an increase of the investment costs:

- Dehumidifier
- Solar collectors
- Complex control system especially for solar driven systems

EICKER gives an example for the cost distribution of a current project where a solar assisted desiccant cooling system with solar air collectors is installed the costs can be assigned to 60% for the desiccant cooling system, 8% for the ductwork of the air distribution system, 12% for the solar air collectors. 7% for the installation of the solar air collectors and 13% for the connecting ductwork of the solar air collectors. In this project, approximately 1/3 of investments were needed for the solar components. In future, it can be assumed that especially the costs for the control system of a solar powered desiccant cooling system will decrease because these systems are, obviously, in a pilot phase.

Generally, the amount of electrical energy needed for the fans is higher in desiccant cooling systems, compared with conventional systems, due to the additional pressure losses at the dehumidifier. Furthermore, significant pressure losses can occur in the solar air collectors. In Table 6.1 the pressure losses of an air conditioning system with compression chiller, heat recovery and two humidifiers, of a desiccant cooling system with solar air collectors and of a desiccant cooling system with solar air collectors and ambient air regeneration are listed exemplary. The pressure losses were assumed to be constant 200 Pa for all inlet and outlet ductwork. Only for the desiccant cooling system with ambient air regeneration where the outlet ducts are separated from the regeneration ducts the pressure losses were assumed to be 150 Pa for each. It can be shown in this example that the overall pressure losses of a desiccant cooling system were 18% greater than the pressure losses of the corresponding air conditioning system without a dehumidifier and without solar air collectors. The desiccant cooling system with ambient air regeneration leads to overall pressure losses which are 26% higher. To avoid an increase in the demand for electrical energy for the fans, the velocities chosen should be smaller than in other systems. This also leads to higher component efficiencies.

The savings of primary energy which can be expected with solar assisted desiccant cooling systems must be evaluated by detailed thermal simulations. According to the investigations presented on page 42 around 60% of primary energy savings can be achieved in Germany assuming a solar fraction of 90%. A conventional air conditioning systems with compression chillers and heat recovery is considered as the reference system.

Table 6.1: Examples of pressure losses in different air conditioning systems

air conditioning system	components	$\Delta P[Pa]$	
air conditioning system	heat recovery	150	
with heat recovery	heat exchanger (cooling, dehumidification)	150	
and humidifier	heat exchanger (heating)	150	
$v_{in} = v_{out} = 3m/s$	humidifier	100	
	ducts, muffler, filter	200	
	humidifier	100	
	heat recovery	150	
	ducts, muffler, filter	200	$\Sigma P_i = 1200$
desiccant cooling system	dehumidifier	210	
with solar air collectors	heat recovery	150	
$v_{in} = v_{out} = 3m/s$	humidifier	100	
$\dot{V}_{\mathrm{R}}/\dot{V}_{\mathrm{P}} = 0.75$	ducts, muffler, filter	200	
	humidifier	100	
	heat recovery	150	
	solar air collectors	150	
	dehumidifier	150	
	ducts, muffler, filter	200	$\Sigma P_i = 1410$
desiccant cooling system	dehumidifier	210	
with solar air collectors	heat recovery	150	
(ambient air regeneration)	humidifier	100	
$v_{in} = v_{out} = 3m/s$	ducts, muffler, filter	200	
$\dot{V}_{\mathrm{R}}/\dot{V}_{\mathrm{P}} = 0.75$	humidifier	100	
	heat recovery	150	
	ducts, muffler, filter	150	
	solar air collectors	150	
	dehumidifier	150	
	ducts, muffler, filter	150	$\Sigma P_i = 1510$

Chapter 7

Conclusions

The aim of this work was the detailed investigation of the performance of desiccant cooling systems driven only by warm air from solar air collectors. These solar air collectors have not been implemented in desiccant cooling systems yet and seem to be appropriate for the implementation of solar energy, because desiccant cooling systems are air handling units requiring warm air for the regeneration process. Therefore, a test plant has been installed. Parametric studies, particularly of the dehumidifier, have been undertaken.

One of the main results is the fact that the dehumidification efficiency decreases only by 6% while the air flow is reduced from $\dot{V}_R/\dot{V}_P = 0.75$, which is a usual operating mode, to $\dot{V}_R/\dot{V}_P = 0.50$. An air flow ratio of $\dot{V}_R/\dot{V}_P = 0.35$ would decrease the dehumidification efficiency by 19% using the same reference. A reduction of the regeneration air flow is important for saving energy, as the energy input for regeneration is linearly dependent on the regeneration air flow. A reduced regeneration air flow enables desiccant cooling systems to run with high COPs.

The results of the measurements were used as input parameters for a new dynamic simulation program, which was specifically developed for the purpose of assessing the potential for desiccant cooling systems under different climatic conditions. This modular simulation tool allows dynamic thermal building simulations and the simulation of heating, ventilation and air conditioning systems and their interaction.

The simulations were executed for a desiccant cooling system with solar air collectors con-

nected to a test building and using climatic data of Stuttgart, Phoenix (Arizona), Seville and Djakarta. The use of solar air collectors signifies that no energy storage is available either in the desiccant cooling system or in the solar system. Thermal inertia is only provided by the mass of the building. As the simulations show, it is almost possible in climates like Stuttgart to ensure thermal comfort with a desiccant cooling system driven only by solar air collectors nearly all the time. In the investigated climates of Seville and Phoenix additional cooling and dehumidification are required.

The simulation results for a system, which can provide an air flow of 4 air changes per hour, show that in heavyweight buildings the use of solar energy alone without any storage system can cover 89% of the cooling demand in Stuttgart, 78% of the cooling demand in Seville, 75% of the cooling demand in Phoenix and only 1% of the cooling demand in Djakarta. In the tropical climate of Djakarta or during humid periods in Phoenix and Seville, it is necessary to disable the function of the inlet humidifier, resulting in an inlet air temperature close to the room conditions. Hence, the cooling capacity of the system is very low. On the other hand, the simulations show that in humid climates the COPs obtained of the desiccant cooling systems are high and reach values significantly greater than 1. This shows that it is extremely useful to install desiccant cooling systems working only for sorptive dehumidification, which is less energy–consuming than dehumidification in common air conditioning systems, where the air must be cooled below or close to the dew point temperature.

Next to the common desiccant cooling ventilation cycle, a cycle with ambient air regeneration was investigated. It shows a system performance comparable to the common ventilation cycle. An advantage of this desiccant cooling ventilation cycle with ambient air regeneration is that the returning air need not be carried to the intake of the solar collectors. A further advantage is that leaks in the solar air collectors do not influence the system's performance in the same way as in the common cycles, where the returning air flow and, hence, the cooling capacity of the heat recovery and the outlet humidifier will be decreased. In climates where the ambient absolute humidity is less than the humidity after the outlet humidifier, lower regeneration temperatures are possible to achieve the same dehumidification.

For the requirements of deep dehumidification in tropical climates, an additional component for dehumidification is necessary. Therefore, a double stage desiccant cooling cycle

with a second rotating dehumidifier and a second heat recovery is suggested. A desiccant cooling system with this configuration can cover 29% of the cooling demand in Djakarta using the same study as before where only 1% were achieved.

Desiccant cooling systems are also appropriate for system combinations as for example with compression chillers. Using compressor cooling technology in combination with desiccant cooling systems leads to high overall COPs because the condenser heat of the compressor can be used for the regeneration of the dehumidifier. This results in a significantly smaller area demand for the solar collectors.

The mean COP of the desiccant cooling system increases by using a variable regeneration air flow. However, the provided cooling energy of the desiccant cooling system with a bypass control also increases, because higher regeneration temperatures occur with a lower regeneration air flow. Reduced dehumidification efficiencies and higher regeneration temperatures are more useful for the performance of the dehumidifier than high dehumidification efficiencies but low regeneration temperatures.

By controlling the desiccant cooling system in dependence on the room conditions, which can be measured in the outlet air flow, the interaction with the building is taken into account. When using solar energy, the control of desiccant cooling systems must be adapted to solar operation to achieve high solar fractions. In contrast to desiccant cooling systems in which the regeneration energy must be bought and should be saved, the solar energy should be used at all times when it is available. Therefore, future work should focus on the development of control strategies especially when different cooling technologies should be combined to achieve synergistic effects.

References

ALTFELD, K. 1985: Exergetische Optimierung flacher solarer Lufterhitzer. Exergetic optimization of flat solar air heaters. Ruhr-Universität Bochum, Dissertation.

ARBEITSGEMEINSCHAFT FÜR SPARSAMEN UND UMWELTFREUNDLICHEN ENERGIEVERBRAUCH E.V. ASUE 1996: Wärme macht Kälte – Absorptionskälteerzeugung in der Praxis. Heat makes cold – Absorption cooling in practice. Band 17. Vulkan–Verlag Essen.

ATKINS, P.W. 1988: Physikalische Chemie. Physical chemistry. VCH Weinheim.

BÄCKSTRÖM, M.; EMBLIK, E. 1965: Kältetechnik. Cooling technology. Verlag G. Braun, Karlsruhe.

BANKS, P.J.; CLOSE, D.J.; MACLAINE-CROSS, I.L. 1970: Coupled heat and mass transfer in fluid flow through porous media – An analogy with heat transfer. Heat transfer, proceedings of the 4th international heat transfer conference, Versailles.

BANKS, P.J.; CLOSE, D.J. 1972: Coupled equilibrium heat and single adsorbate transfer in fluid flow through a porous medium. Predictions for a silica gel air dryer using characteristic chart. Chemical Engineering Science 27:1157-1169.

BEGGS, C.B.; WARWICKER, B. 1998: Desiccant cooling: parametric energy study. Proceedings of CIBSE A: 19(2).

BEHNE, M. 1997: Alternativen zur Kompressionskältenutzung in Bürogebäuden. Alternatives to compressor cooling in office buildings. HLH 46 – 48.

BROWN, M. 1990: The thermal mass of buildings in reducing energy consumption. ASME Journal of Solar Energy Engineering, Vol. 112.

BRUNAUER, S.; EMMET, P.; TELLER, E. 1938: Adsorption of gases in multimolecular layers. Journal Am. Chem. Soc. 60.

BUSWEILER, U. 1984: Nichtisotherme Ad- und Desorptionskinetik an Einzelkörnern technischer Adsorbentien am Beispiel der Wasserdampfadsorption an Silicagel und Moleku-

larsieb. Non–isothermal adsorption and desorption kinetics on granules of technical adsorbens with an example of the vapour adsorption of silica gel and molecular sieve. Dissertation, Technische Hochschule Darmstadt.

BUSWEILER, U. 1995: Klimatisieren mit Desiccant Cooling im praktischen Einsatz. Air conditioning with desiccant cooling in practice. In: Solar unterstützte Klimatisierung von Gebäuden mit Niedertemperaturverfahren. FhG–ISE Tagungsband. Freiburg.

BUSWEILER, U.; GÖBEL, U. 1997: Desiccant cooling – ein wirtschaftlicher Vergleich. Desiccant cooling – an economic comparison. Ki Luft– und Kältetechnik.

CLARKE, J.A. 1985: Energy simulation in building design. Adam Hilger Ltd Bristol.

CRANK, J. 1975: The mathematics of diffusion. Clarendon Press Oxford.

CURRAN, H.,M. 1993: Active solar systems – Mechanical systems and components. Massachusetts Institute of Technology.

DEVRES, Y.O. 1994: Psychrometric properties of humid air: calculation procedures. Applied Energy 48.

DIN 1946 Teil 2 1994: Raumlufttechnik – Gesundheitstechnische Anforderungen. Indoor air technology – health–related requirements. Beuth Verlag Berlin.

DREHER, H. 1979: Gleichgewicht und Kinetik bei der Adsorption mehrerer Komponenten aus der Gasphase in einem isothermen Adsorber am Beispiel der Systeme Wasser – Benzol – Methanol – Silicagel. Equilibrium and kinetics of multiple–components adsorption from the gas phase in an isothermal adsorber with an example of the systems water – benzol – methanol – silica gel. Dissertation, Technische Hochschule Darmstadt.

DUFFIE, J.A.; BECKMAN, A.B. 1991: Solar engineering of thermal processes. John Wiley & Sons, New York.

EICHENGRÜN, S. 1993: Theoretische und experimentelle Untersuchung des dynamischen Verhaltens von periodisch arbeitenden Sorptionsaggregaten. Theoretical and experimental investigations of the dynamic performance of periodically working sorption aggregates. Dissertation, Technische Universität München.

EICKER, U.; HÖFKER, G. 1996: Kühlen mit Solarenergie. Cooling with solar energy. In: Proceedings of Bauphysikertreffen 1996, Fachhochschule Stuttgart – Hochschule für

Technik.

EICKER, U.; HÖFKER, G.; SEEBERGER, P. 1998: Offene solare Sorptionskühlung mit Luftkollektoren. Open cycle desiccant cooling with air collectors. Achtes Symposium Thermische Solarenergie, OTTI Staffelstein.

EICKER, U.; HÖFKER, G.; SEEBERGER, P.; FUX, V.; INFIELD. D. 1998: Building integration of PV and solar air heaters for optimised heat and electricity production. 2nd World Conference and Exhibition on Photovoltaic Solar Energy Conversion, Vienna.

ERPENBECK, T. 1999: Sorptionsgestützte Klimatisierung – Experimentelle und theoretische Analyse von Potential und Systemverhalten. Desiccant Cooling – Experimental and analytical analysis of the potential and system performance. Dissertation, Universität Karlsruhe.

FEIST, W. 1994: Thermische Gebäudesimulation. Verlag C.F. Müller.

FRANZKE, U. 1989: Ein Beitrag zum Wärme- und Stoffaustausch in rotierenden Speichermaterialien. A contribution to the heat and mass transfer in rotating storing materials. Dissertation, Technische Universität Karl-Marx-Stadt (Chemnitz).

FRANZKE, U. 1995: Chancen der solar unterstützten Klimatisierung in Deutschland. Chances of solar cooling in Germany. In: Solar unterstützte Klimatisierung von Gebäuden mit Niedertemperaturverfahren, FhG-ISE Tagungsband, Freiburg.

FRANZKE, U. 1998: Market situation on cooling and air conditioning systems. Presentation at the 2nd workshop of the project definition phase of IEA task 25, Palermo.

GASSEL, A. 2000: Betriebserfahrungen mit einer solar beheizten Adsorptionskältemaschine. Practical experience with a solar driven adsorption chiller. Dresdner Kolloquium "Solare Klimatisierung", ILK Dresden.

GLÜCK, B. 1991: Zustands– und Stoffwerte Wasser, Dampf, Luft, Verbrennungrechnung. Condition and material values, water, vapour, air, calculation of combustion. Verlag für Bauwesen Berlin.

GRIGULL, U.; SANDNER, H. 1979: Wärmeleitung. Heat conduction. Springer Verlag Berlin.

GUTERMUTH, W. 1980: Untersuchungen der gekoppelten Wärme– und Stoffübertragung

in Sorptionsregeneratoren. Investigation on the coupled heat and mass transfer in sorption regenerators. Dissertation, Technische Hochschule Darmstadt.

HEINRICH, G.; FRANZKE U. 1997: Sorptionsgestütze Klimatisierung. Desiccant cooling. C.F. Müller Verlag Heidelberg.

HENNING, H.–M. 1993: Regenerierung von Adsorbentien mit solar erzeugter Prozeßwärme. Regeneration of adsorbens with solar–produced process heat. Dissertation, Universität Oldenburg, VDI Fortschrittsberichte Verfahrenstechnik 350.

HENNING, H.–M. 1995: Auslegung von solar unterstützten Desiccant Cooling Systemen - Ergebnisse von Systemsimulationen. Design of solar powered desiccant cooling systems - Results of system simulations. In: Solar unterstützte Klimatisierung von Gebäuden mit Niedertemperaturverfahren, FhG–ISE Tagungsband, Freiburg.

HENNING, H.–M. 1998: Short report on the US solar cooling programme in the 1970s and 1980s. Presentation at the 2nd workshop of the project definition phase of IEA task 25, Palermo.

HENNING, H.–M.; HINDENBURG, C.; PAULUSSEN, S. 1998: Study on the economy of solar assisted cooling systems for buildings. Presentation at the 2nd workshop of the project definition phase of IEA task 25, Palermo.

HETTIG, C. 1995: Möglichkeiten und Verfahren zum Kühlen mit Sonnenenergie. Possibilities and methods of solar cooling. Hochschule für Technik Stuttgart, Diplomarbeit im Studiengang Bauphysik.

HOLLEMANN, A.F.; WIBERG, E. 1995: Lehrbuch der anorganischen Chemie. Textbook of the anorganic chemistry. Walter de Gruyter Berlin, Auflage 101.

IHLE, C. 1996: Klimatechnik mit Kältetechnik. Air conditioning technology. Schriftenreihe "Der Heizungsingenieur" Band 4, 3. Auflage. Werner Verlag Düsseldorf.

JOKISCH, F. 1975: Über den Stofftransport im hygroskopischen Feuchtebereich kapillarporöser Stoffe am Beispiel des Wasserdampftransportes in technischen Adsorbentien. On the mass transfer in the hygroscopic field of capillary–porous materials with an example of the water–vapour transport in technical adsorbens. Dissertation, Technische Hochschule Darmstadt.

JUDKOFF, R.; NEYMARK, J. 1995: International Energy Agency building energy simu-

lation test (BESTEST) and diagnostic method. National Renewable Energy Laboratory Golden Colorado.

JURINAK, J.J. 1982: Open cycle solid desiccant cooling - Component models and system simulations. PhD thesis, University of Wisconsin–Madison.

KAST, W.; JOKISCH, F. 1972: Überlegungen zum Verlauf von Sorptionsisothermen und zur Sorptionskinetik an porösen Feststoffen. Considerations of the course of sorption isothermes and of the sorption kinetics of porous media. Chemie–Ingenieur–Technik 44 Nr. 8.

KAST, W. 1988: Adsorption aus der Gasphase. Adsorption out of the gas phase. VCH Verlagsgesellschaft Weinheim.

KAVIANY, M. 1991: Principles of heat transfer in porous media. Springer Verlag New York Berlin Heidelberg.

KAYS, W.M.; CRAWFORD,M.E. 1980: Convective heat and mass transfer. 2nd edition, Mc Graw Hill New York.

KESSLING, W. 1997: Luftentfeuchtung und Energiespeicherung mit Salzlösungen in offenen Systemen. Dehumidification of air and energy storage with salt solutions in open systems. Dissertation, Universität Freiburg, VDI Fortschrittsberichte Verfahrenstechnik 509.

KESSLING, W.; LÄVEMANN, E. 1995: Klimatisierung über Sorption: Neuartiger Entfeuchter für DEC-Systeme. Air conditioning with desiccant cooling systems: New dehumidifier for desiccant cooling systems. In: Solar unterstützte Klimatisierung von Gebäuden mit Niedertemperaturverfahren, FhG–ISE Tagungsband, Freiburg.

KHELIFA, N. 1984: Das Adsorptionspaar Silicagel – Wasserdampf. Anwendung als solares Klimatisierungssystem. The adsorption pair silica gel – vapour. Application as a solar air conditioning system. Dissertation, Universität München.

KLEIN, S.A. 1979: Calculation of flat–plate loss coefficients. In: Solar energy, 17, 79.

KRISCHER, O.; KAST, W. 1978: Die wissenschaftlichen Grundlagen der Trocknungstechnik. The scientific fundamentals of desiccation. Springer–Verlag Berlin.

LÄVEMANN, E.; SIZMANN, R. 1992: Energy storage in open cycle desiccant cooling sys-

tems – comparison of solid and liquid desiccants. Solid Sorption Refrigeration Symposium Paris.

LAMP, P. 1995: Einsatz von Sorptionskältemaschinen zur solar unterstützten Klimatisierung. Application of sorption chillers for solar assisted air conditioning. In: Solar unterstützte Klimatisierung von Gebäuden mit Niedertemperaturverfahren, FhG–ISE Tagungsband, Freiburg.

LAMP, P.; ZIEGLER, F. 1997: Solar cooling with closed sorption systems – Introduction in the technology. In: Solar sorptive cooling, DLR–Workshop Forschungsverbund Sonnenenergie.

MACLAINE-CROSS, I.L. 1974: A theory of combined heat and mass transfer in regenerators. PhD thesis, Monash University Clayton, Victoria, Australia.

MATHEMATICA 3.0 1996: Wolfram Research Inc. Champaign Illinois.

METEONORM 4.0 1999: Global meteorological database for solar energy and applied climatology. Meteotest Bern.

MOFFAT, A.; SCHILLER, M. 1981: Landscape design, how to save energy. William and Narrow, New York.

MORHENNE, J., FIEBIG, M. 1990: Entwicklung und Erprobung einer Baureihe von optimierten, modularen Solarlufterhitzern für Heizung und Trocknung. Development and testing of a series of optimised modular solar air heaters for heating and drying. Projekt 0335003E6 Institut für Thermo- und Fluiddynamik, Lehrstuhl für Wärme– und Stoffübertragung, Universität Bochum.

MÜLLER, M. 1980: Handbuch ausgewählter Klimastationen der Erde. Handbook of selected climatic stations on earth. Gerold Richter, Universität Trier.

MUNTERS, C.G. 1968: Inorganic, fibous, gas–conditioning packing for heat and moisture transfer. Technical report, U.S. patent 3377225.

PFEIFFER, S. 1986: Sorptionsprozesse Klimatechnik. Sorption processes in air conditioning technology. Fachbericht 22/1236 VEB Kombinat Luft– und Kältetechnik Dresden.

PFROMMER, P. 1995: Thermal modelling of highly glazed spaces. PhD thesis, De

Montfort University Leicester.

POLANYI, M. 1916: Adsorption von Gasen (Dämpfen) durch ein festes nichtflüssiges Adsorbens. Adsorption of gas (vapour) by a solid non–liquid adsorbens. Deutsche Physikalische Gesellschaft 18.

RECKNAGEL,H.; SPRENGER, E.; SCHRAMEK, E.–R. 1994: Taschenbuch für Heizung + Klimatechnik 94/95. Handbook of heating and air conditioning technology 94/95. Oldenbourg Verlag München.

ROMMEL, M. 1995: Kollektoren für die solare Klimatisierung. Collectors for solar cooling. In: Solar unterstützte Klimatisierung von Gebäuden mit Niedertemperaturverfahren, FhG–ISE Tagungsband, Freiburg.

SCHWEIGLER, C.; HELLMANN, H.–M.; PREISSNER, M.; DEMMEL, S.; ZIEGLER, F. 1997: Operation and performance of a 350 kW (100 RT) single–effect/double–lift absorption chiller. In: Solar sorptive cooling, DLR–Workshop Forschungsverbund Sonnenenergie.

SHIH, T.M. 1984: Numerical heat transfer. Springer Verlag Berlin.

SPAHN, H.; GNIELINSKI, V. 1971: Wärme– und Stoffaustausch in einem Sorptionsrotor. Heat and mass transfer in a sorption regenerator. Verfahrenstechnik 5 Mainz.

SZOKOLAY, S. 1984: Passive and low energy design for thermal and visual comfort. Passive and low energy ecotechniques. 3rd International PLEA Conference, Mexico City, Pergamon Press Oxford.

TROLL, C.; PAFFEN, K. 1980: Jahreszeitenklimate der Erde. Seasonal climates of the earth. Berlin.

UHLMANN, H.-J. 1976: Untersuchung der adiabaten Festbettadsorption am System Silicagel – Wasserdampf. Investigations of the adiabatic bed sorption of the system silica gel – water vapour. Dissertation, Universität Stuttgart.

WAGNER, W. 1998: Wärmeübertragung. Heat transfer. Vogel Buchverlag Würzburg.

WEISCHEDEL, R. 1996: Experimentelle Untersuchungen an einer sorptionsgestützen Klimaanlage. Experimental investigations in a desiccant cooling system. Hochschule für Technik Stuttgart, Diplomarbeit im Studiengang Bauphysik.

WILLMES, A. 1992: Taschenbuch Chemische Substanzen. Handbook chemical substances. Verlag Harri Deutsch Frankfurt am Main.

ZIEGLER, F. 1997: Kompressions– und Absorptionsanlagen, um Kälte und Wärme bereitzustellen. Compressor and absorption systems for providing cold and heat. http://www.cip.physik.tu.muenchen.de.

Appendix A

In the following graphs the simulation results of case 1, 3, 7 and 8 will be shown in exemplary fashion. The results are presented for the hottest 3–day–period evaluated in case study 1 and for the entire year of case study 8 for the climates of Seville, Stuttgart and Phoenix (Arizona).

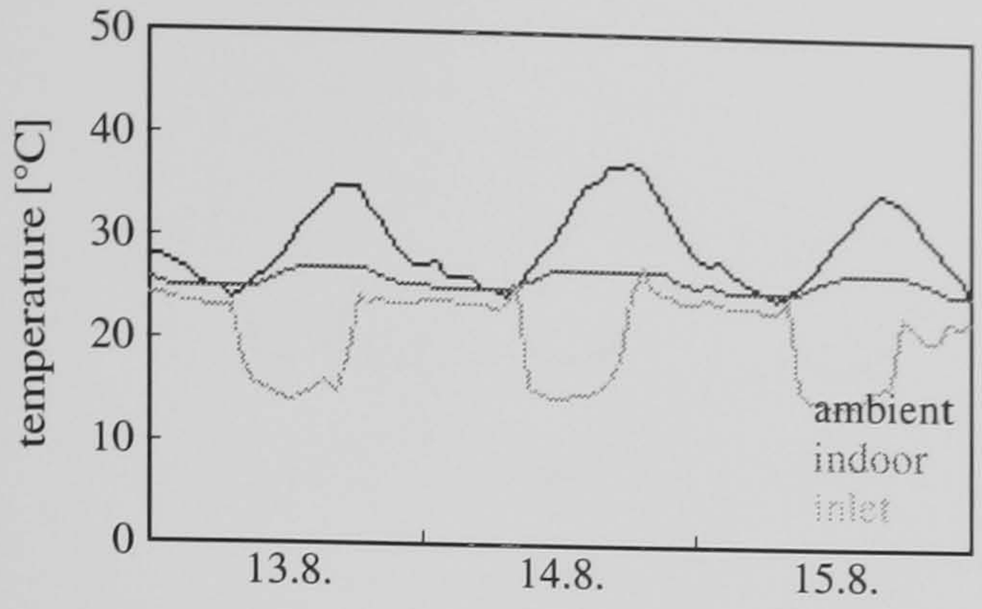

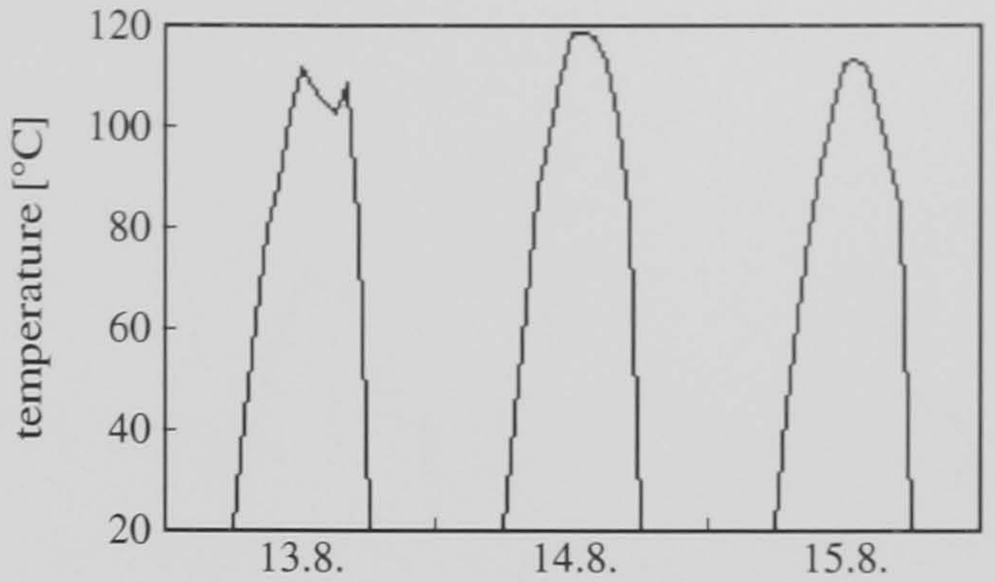

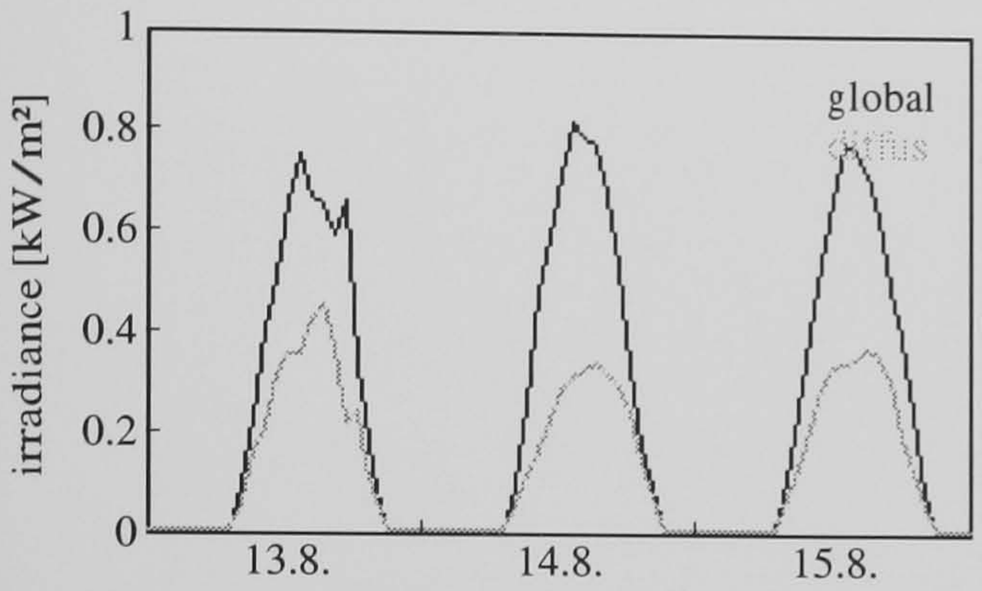

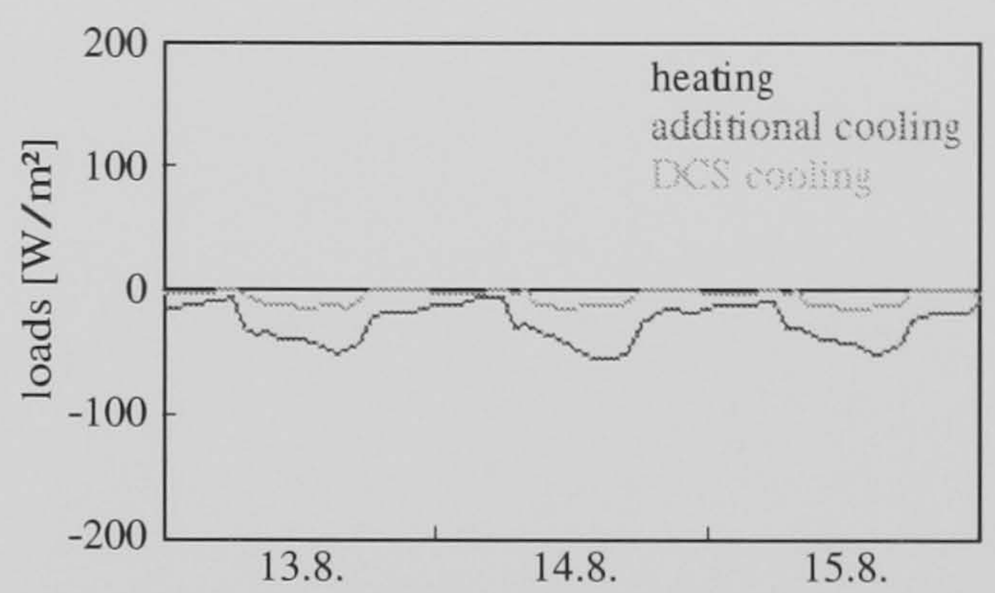

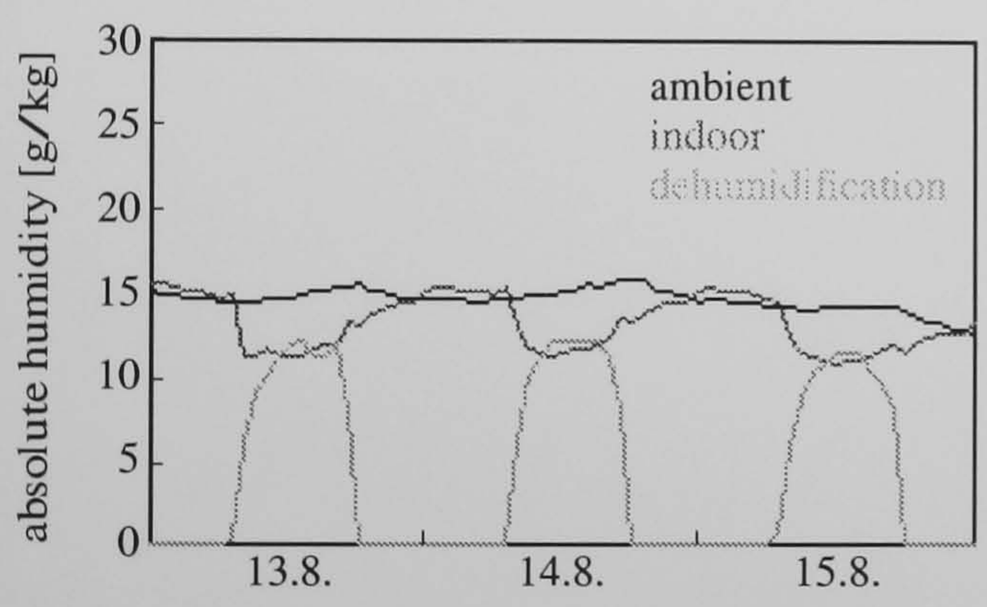

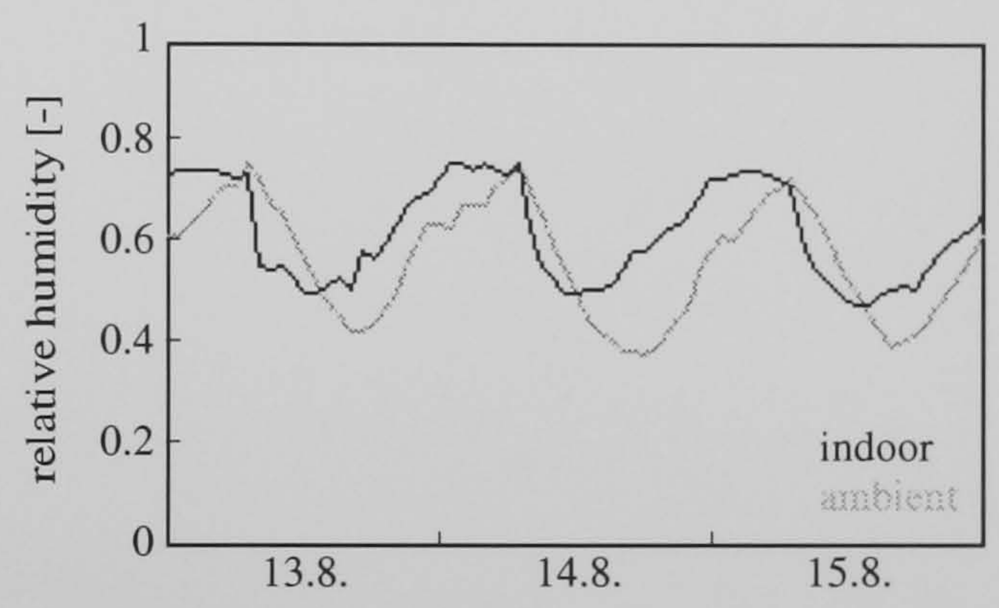

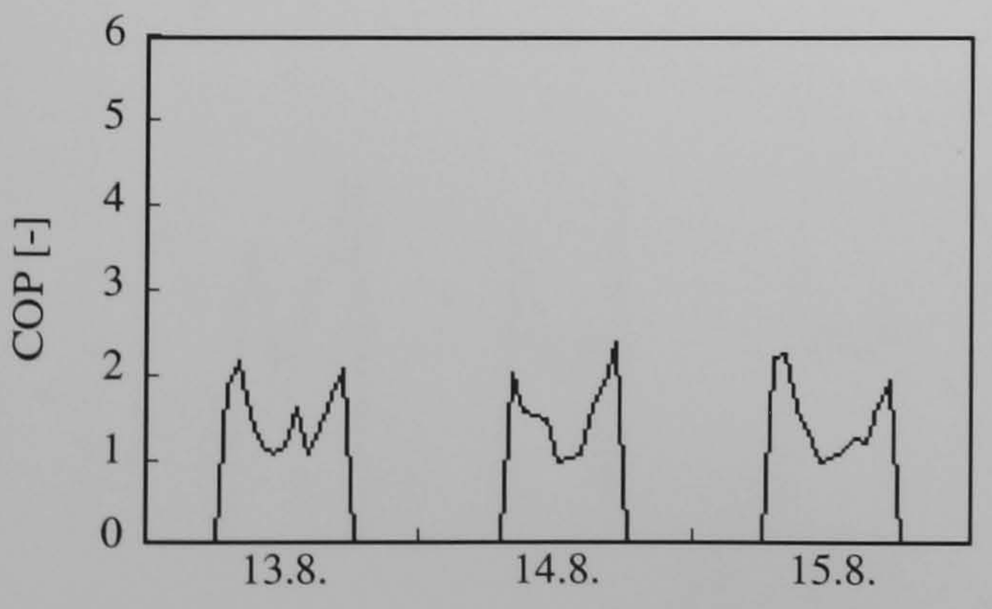

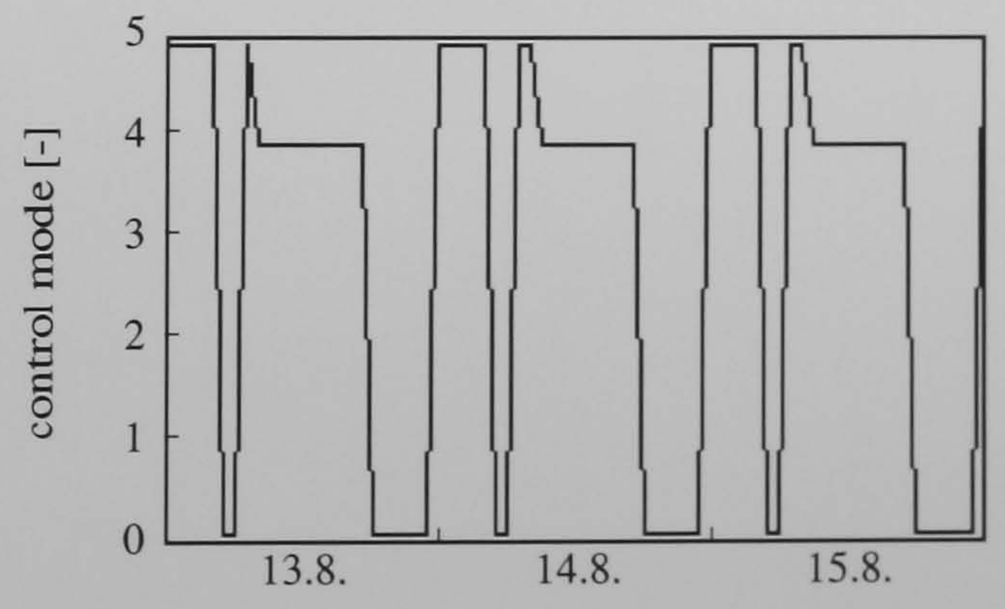

Figure A.1: Seville: Simulation results of case study 1 (heavyweight building, hygienic ventilation during occupation time). Detailed description on page 102. Discussion of the simulation results on page 117.

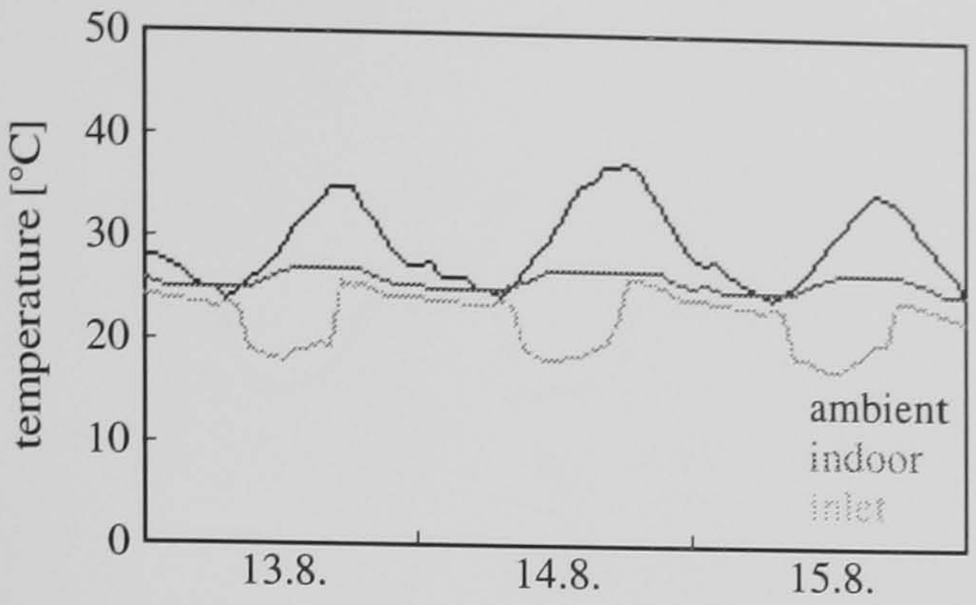

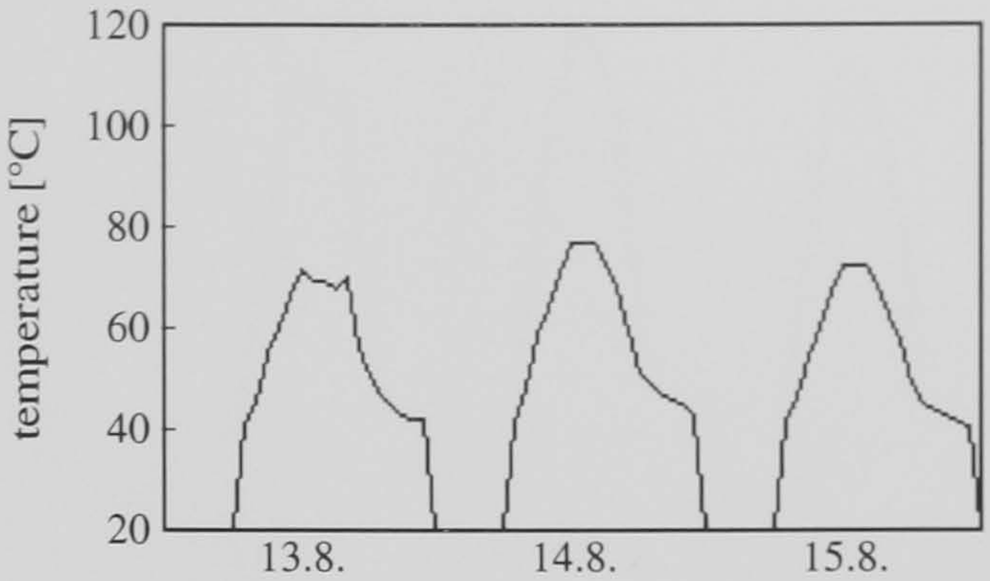

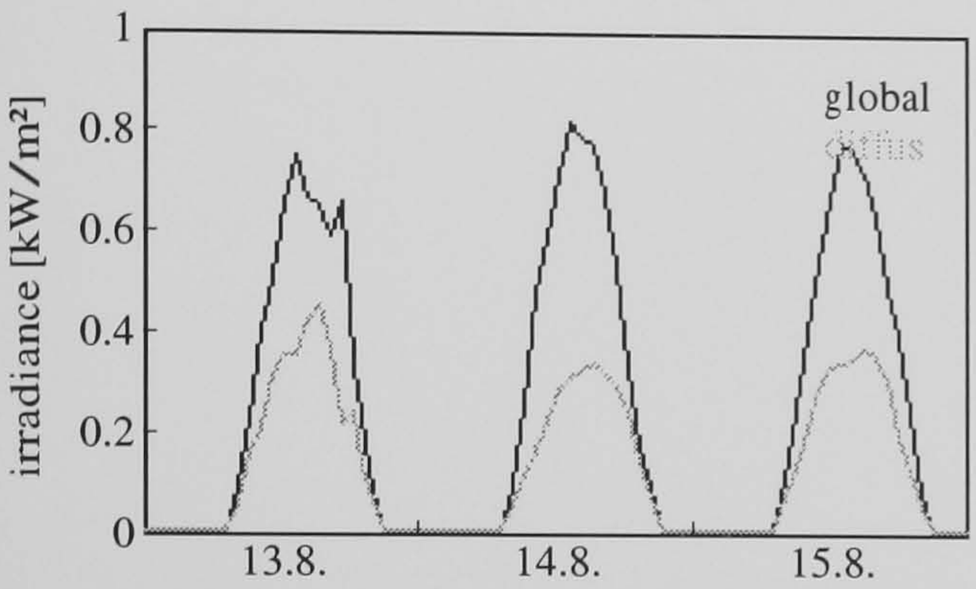

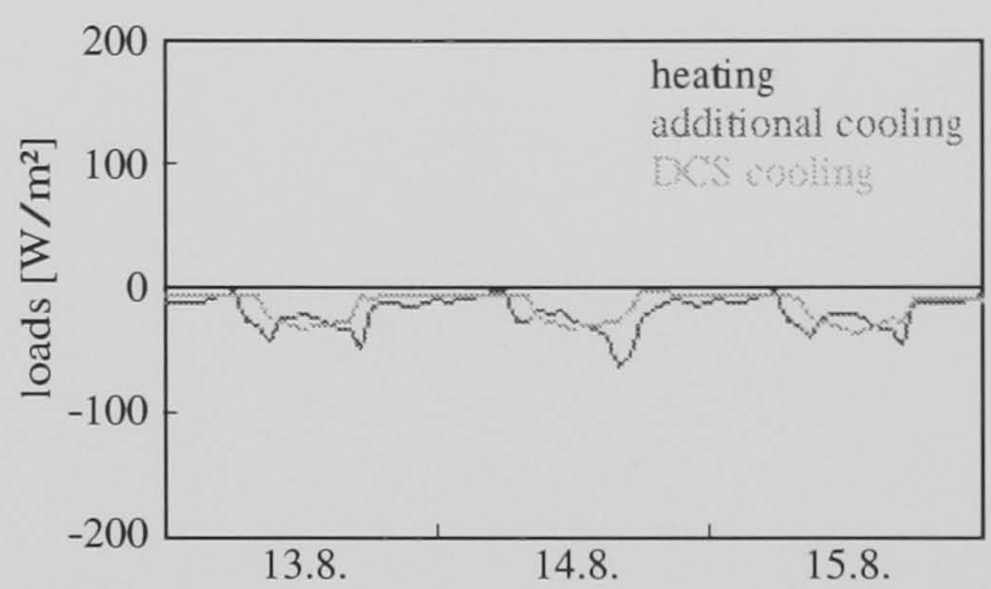

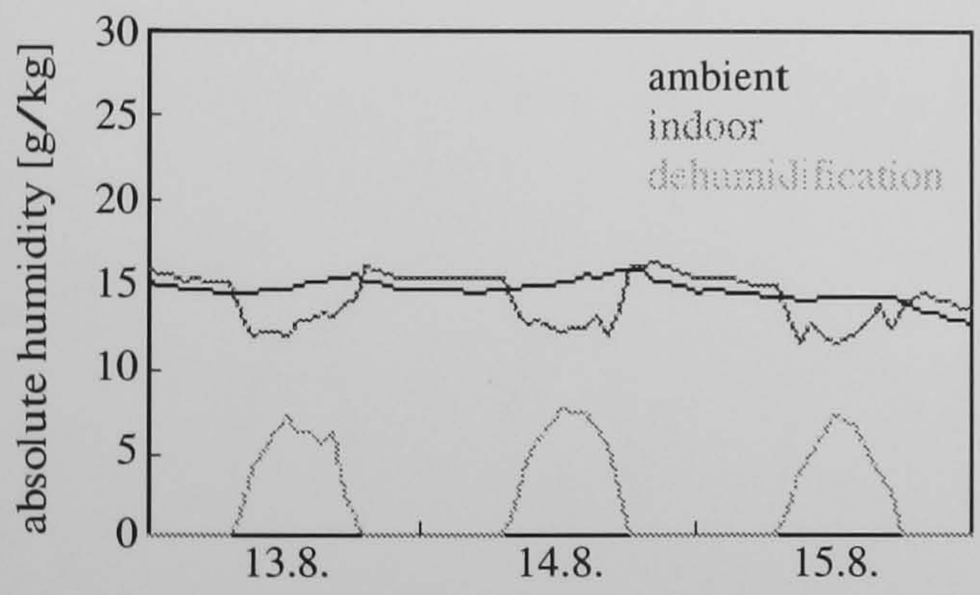

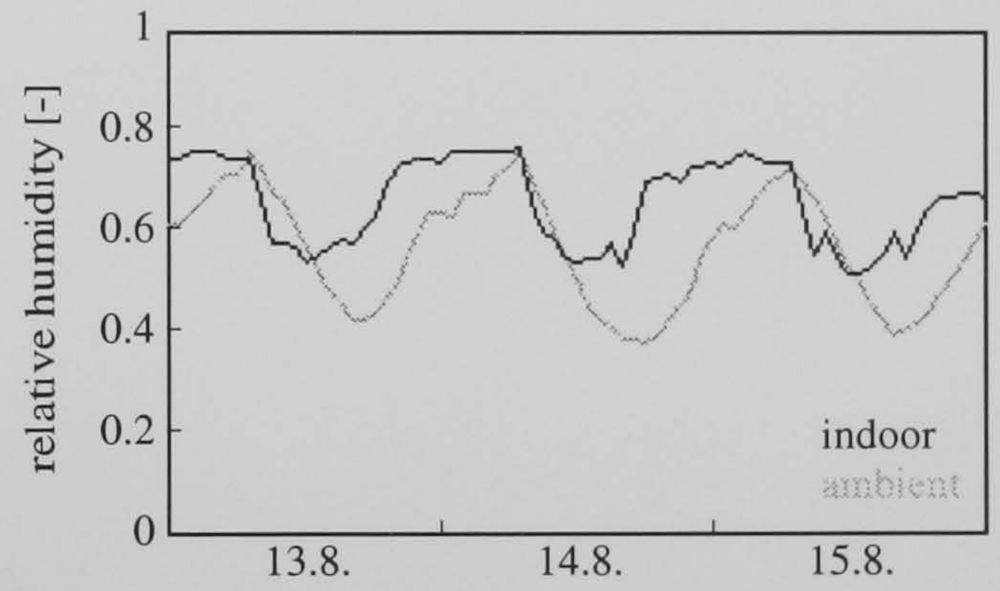

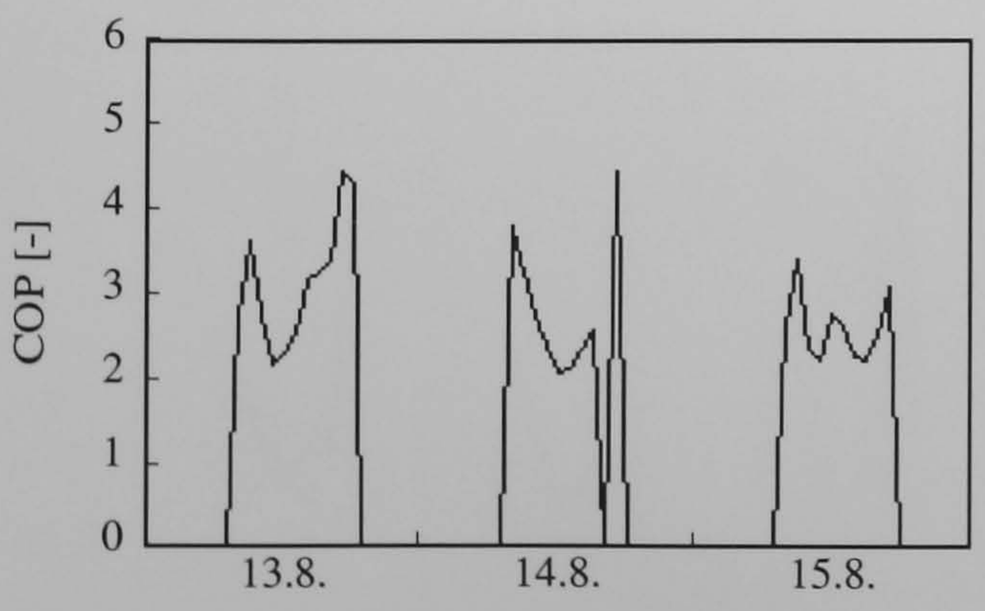

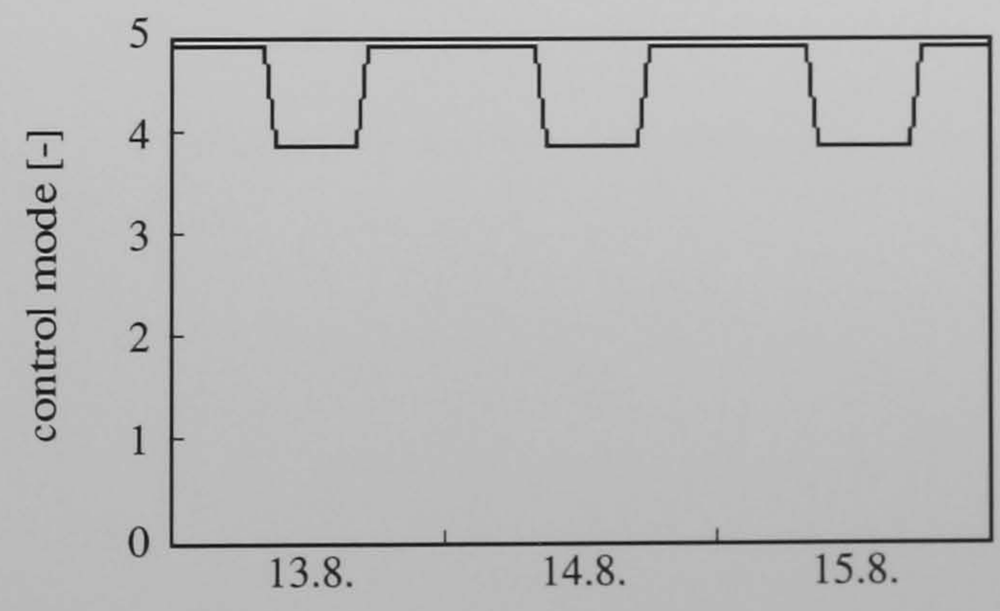

Figure A.2: Seville: Simulation results of case study 3 (heavyweight building, ventilation with maximum 4 air changes per hour, night ventilation). Detailed description on page 102. Discussion of the simulation results on page 119.

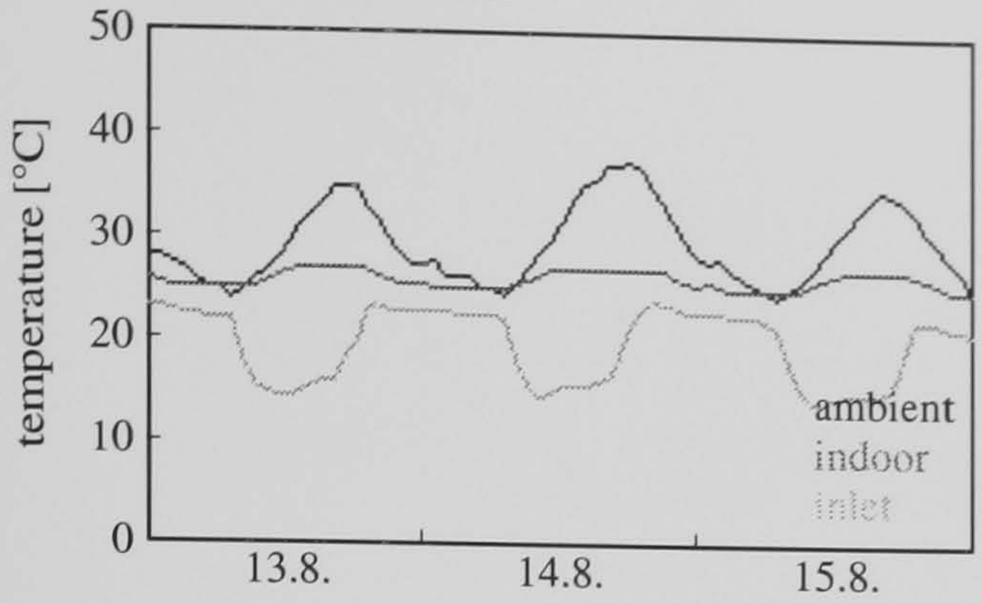

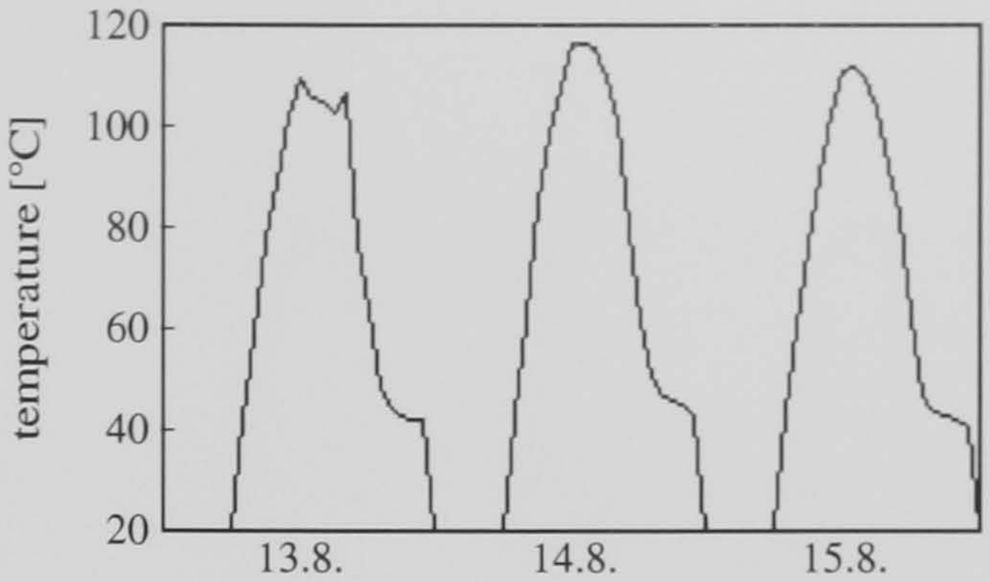

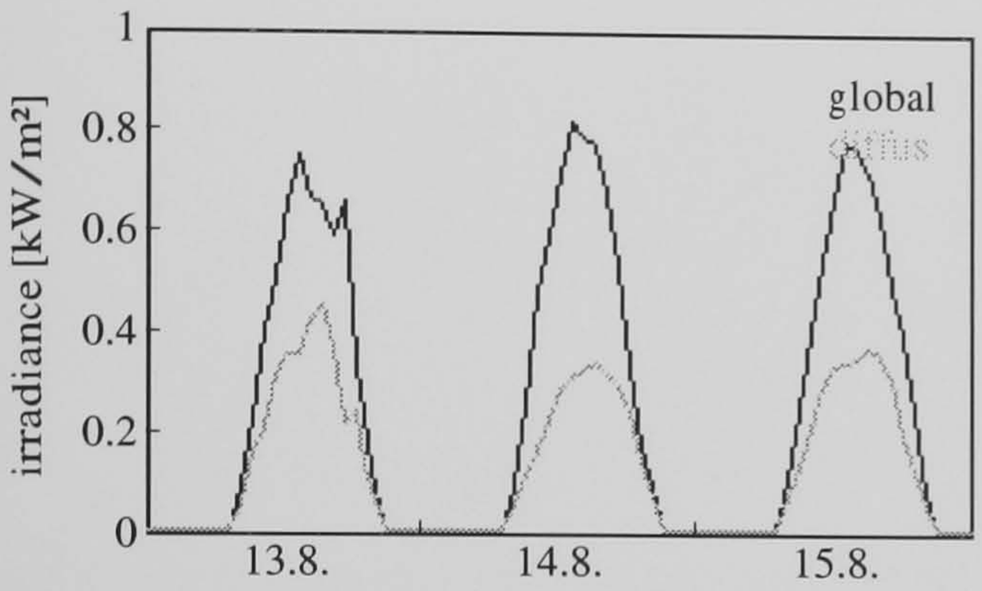

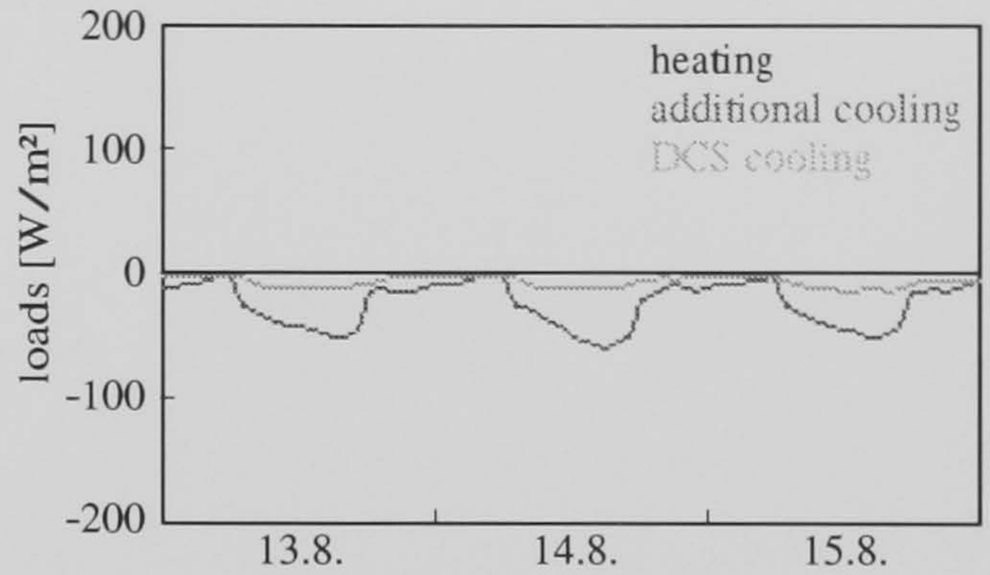

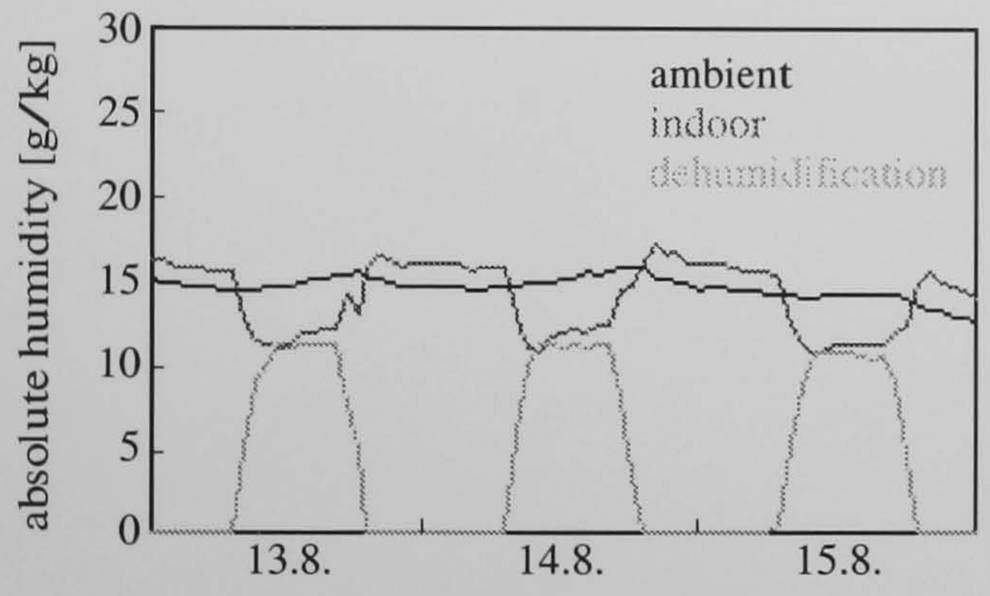

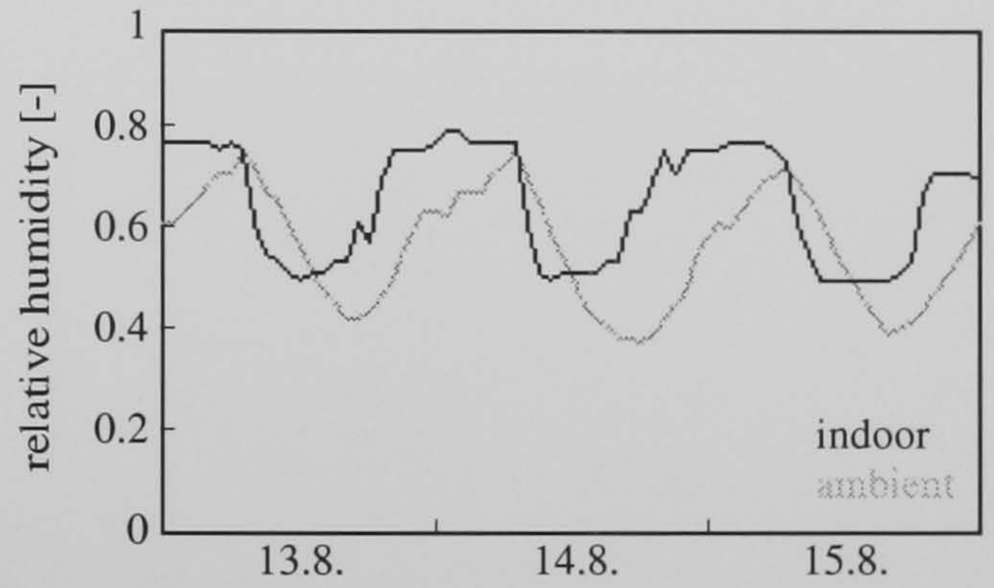

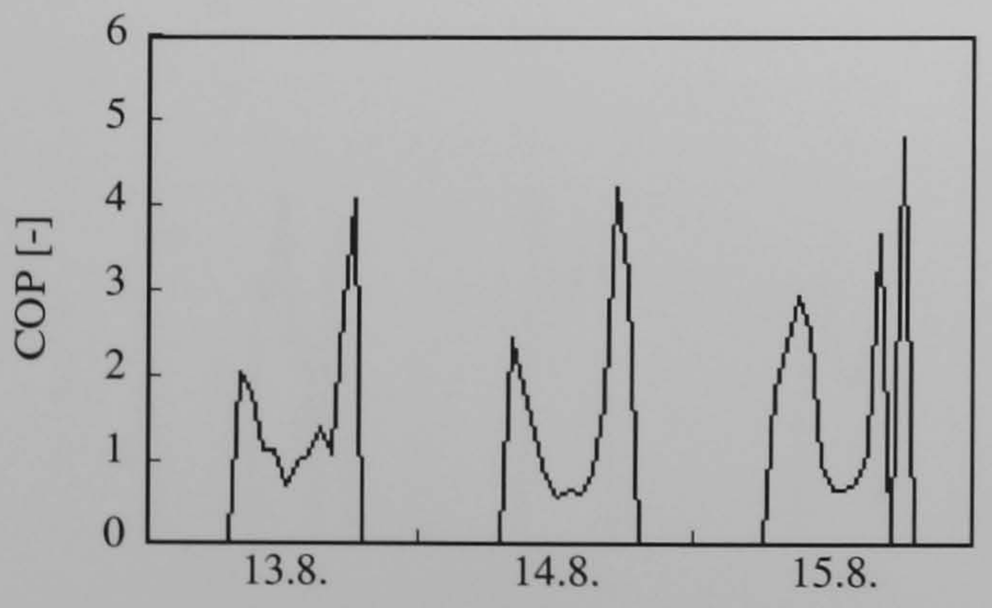

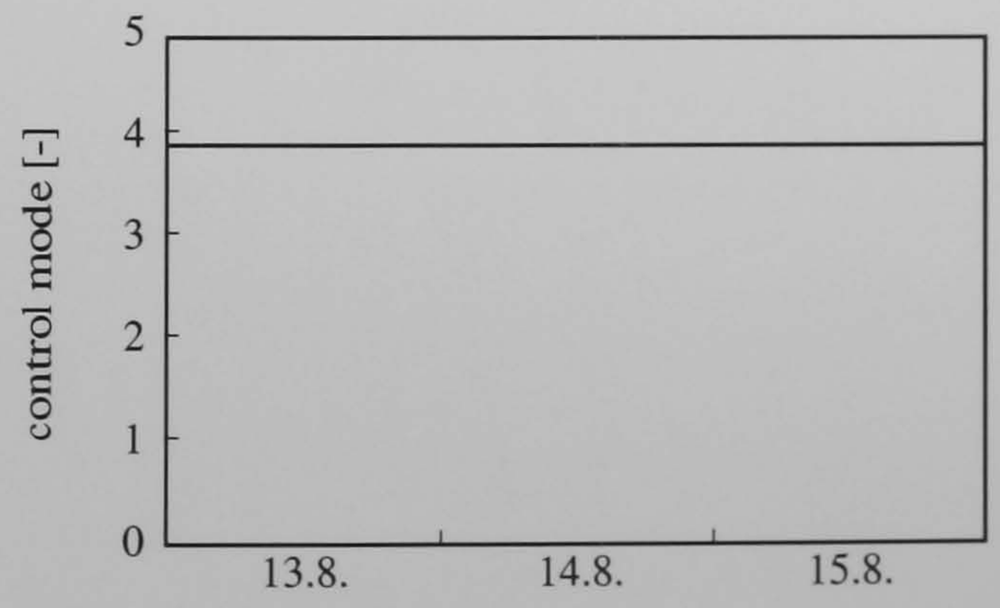

Figure A.3: Seville: Simulation results of case study 7 (heavyweight building, hygienic ventilation during occupation time, controlled to reach an inlet temperature close to 17 °C). Detailed description on page 102. Discussion of the simulation results on page 124.

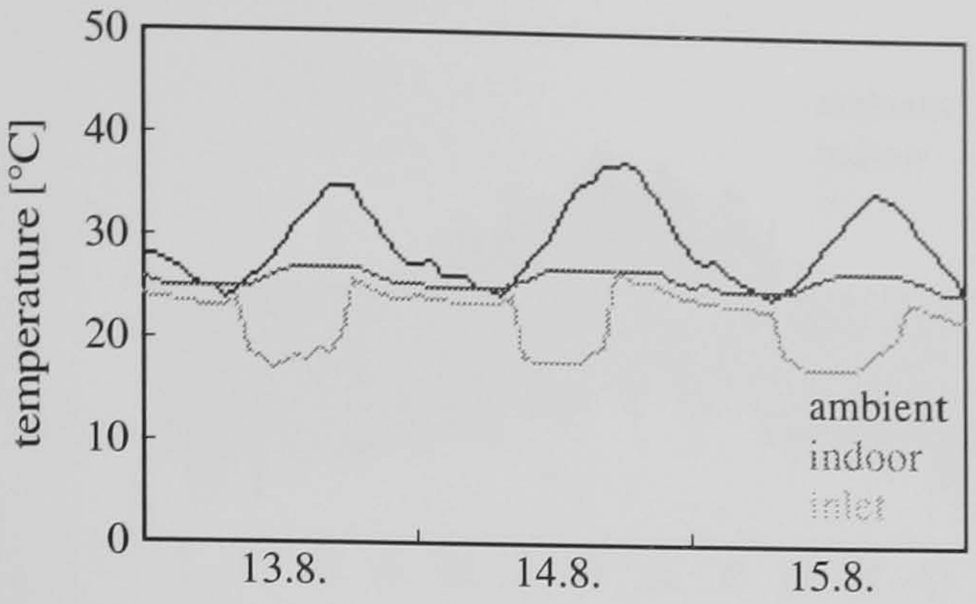

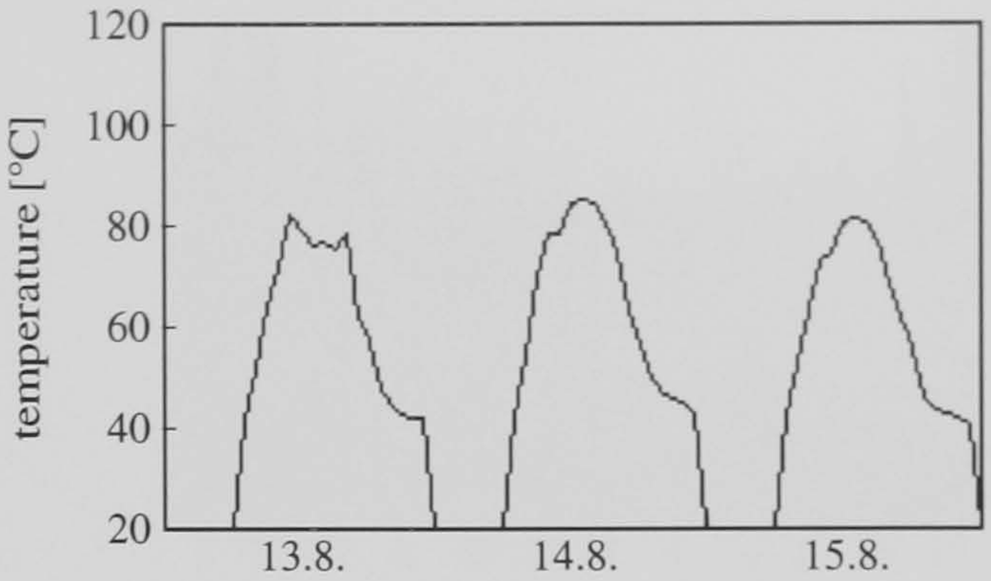

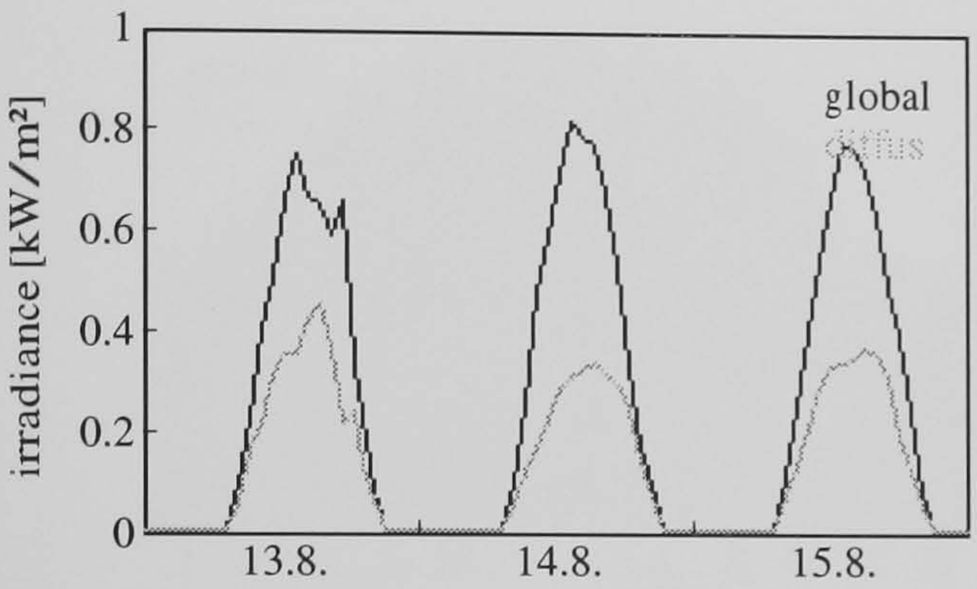

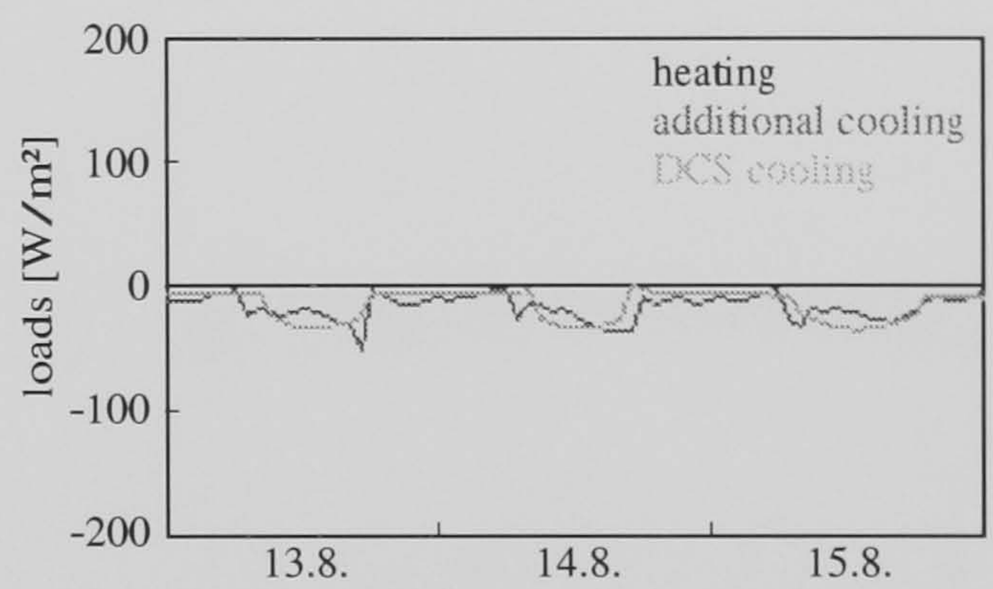

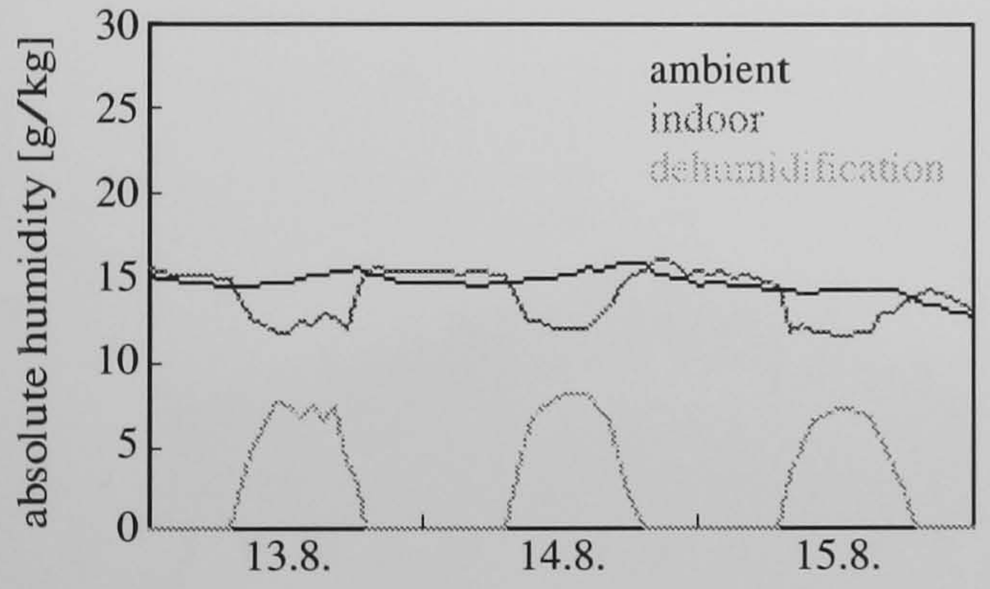

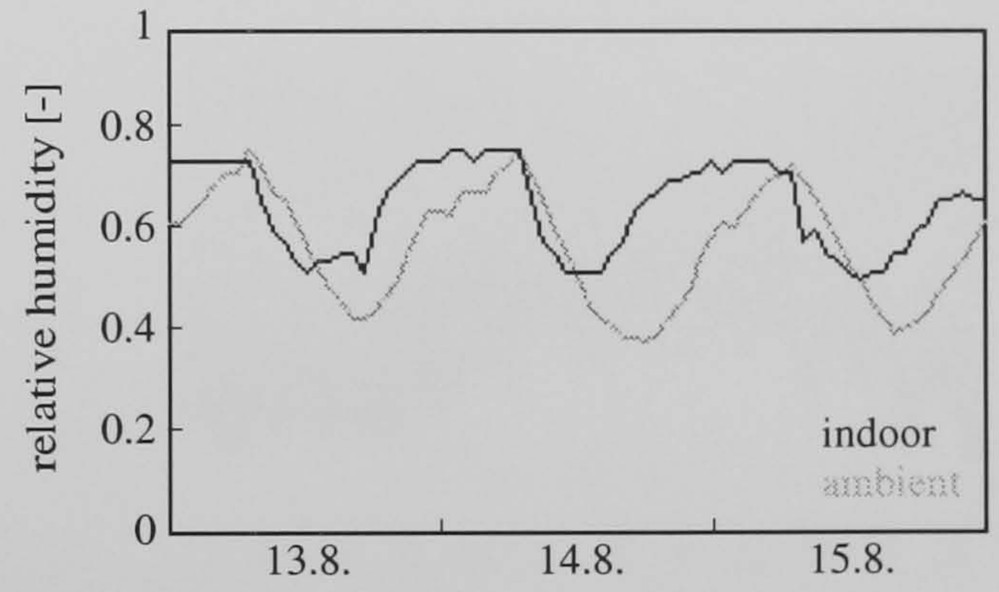

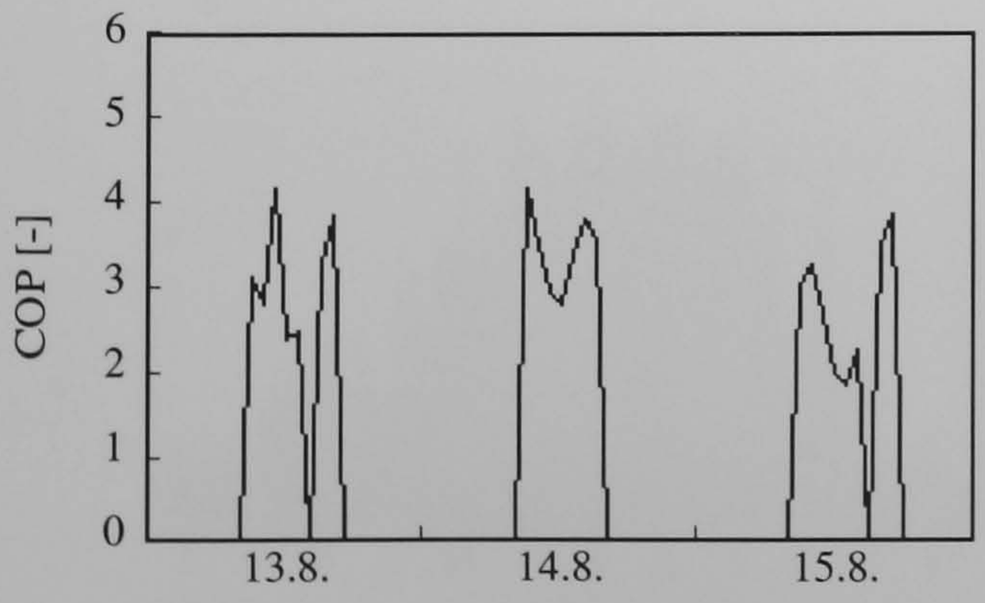

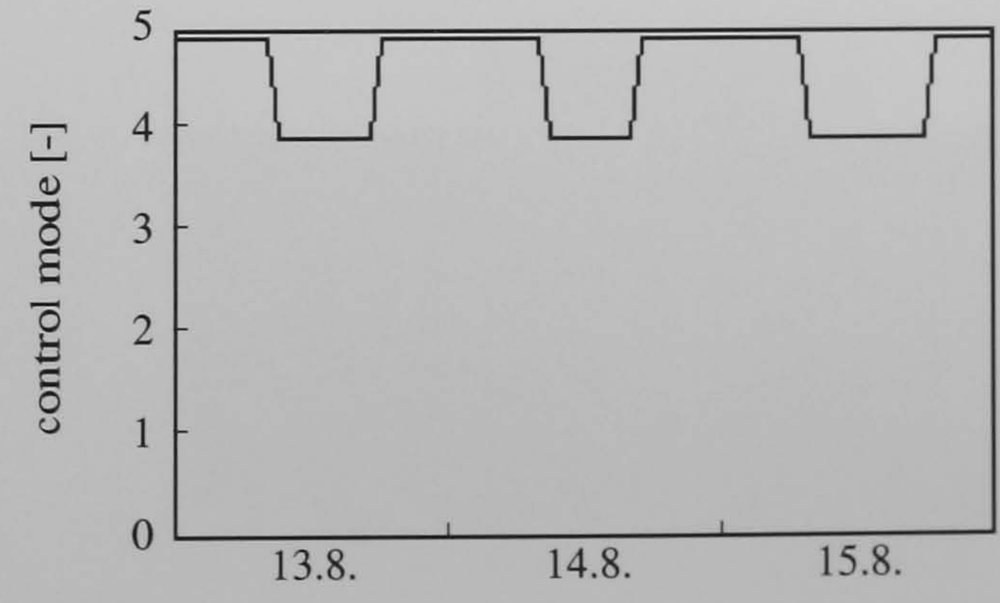

Figure A.4: Seville: Simulation results of case study 8 (heavyweight building, ventilation with maximum 4 air changes per hour, night ventilation, regeneration air flow controlled). Detailed description on page 103. Discussion of the simulation results on page 125.

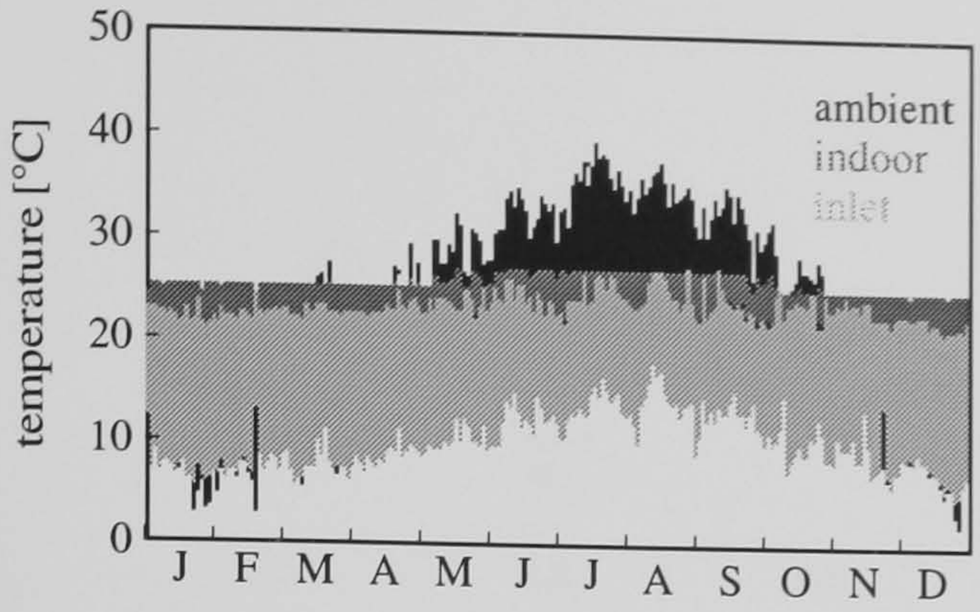

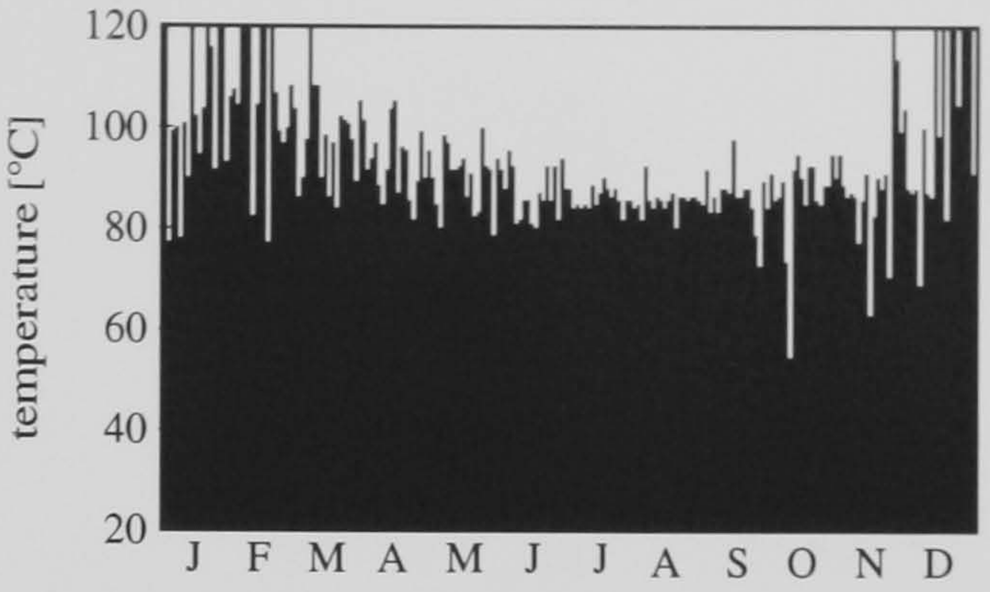

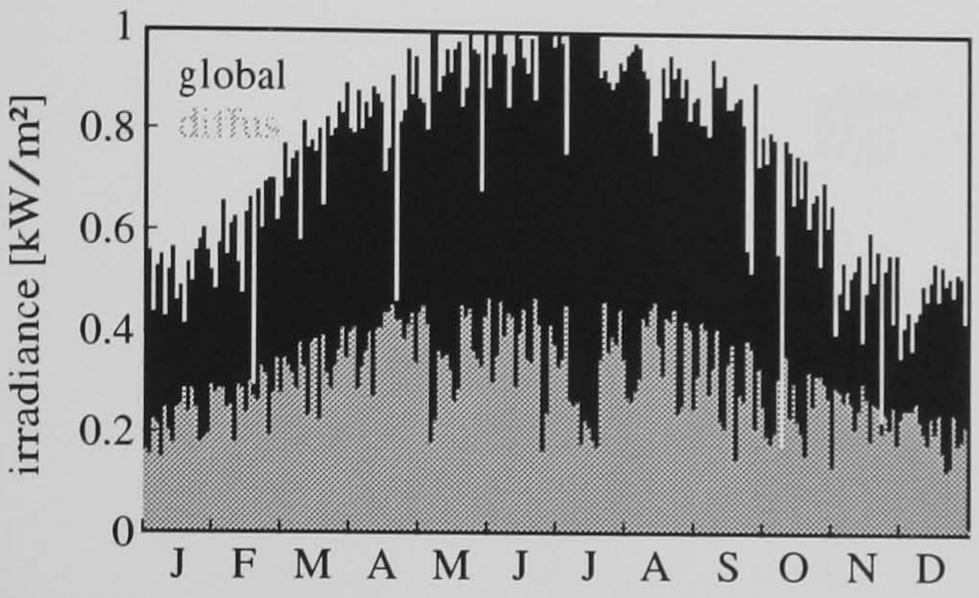

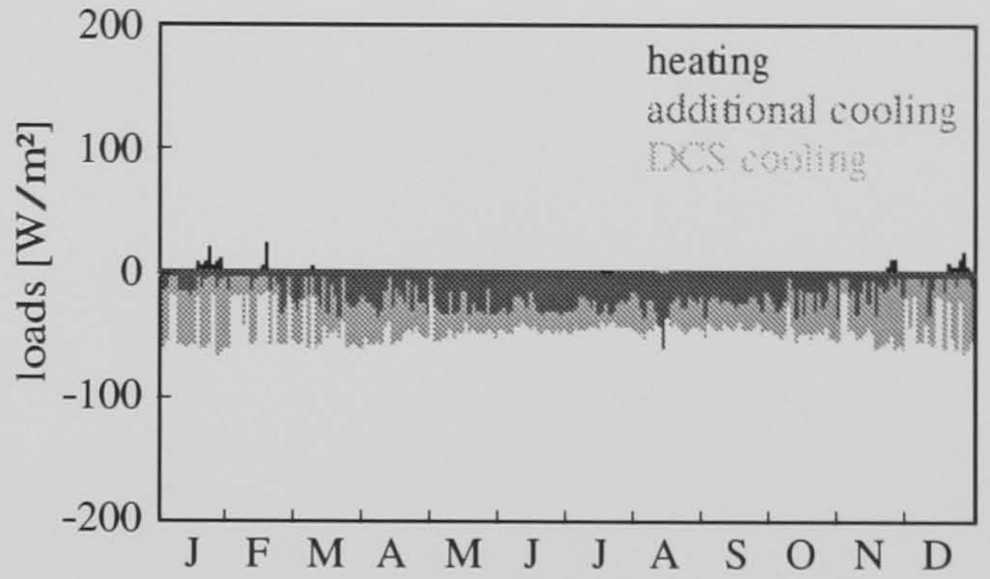

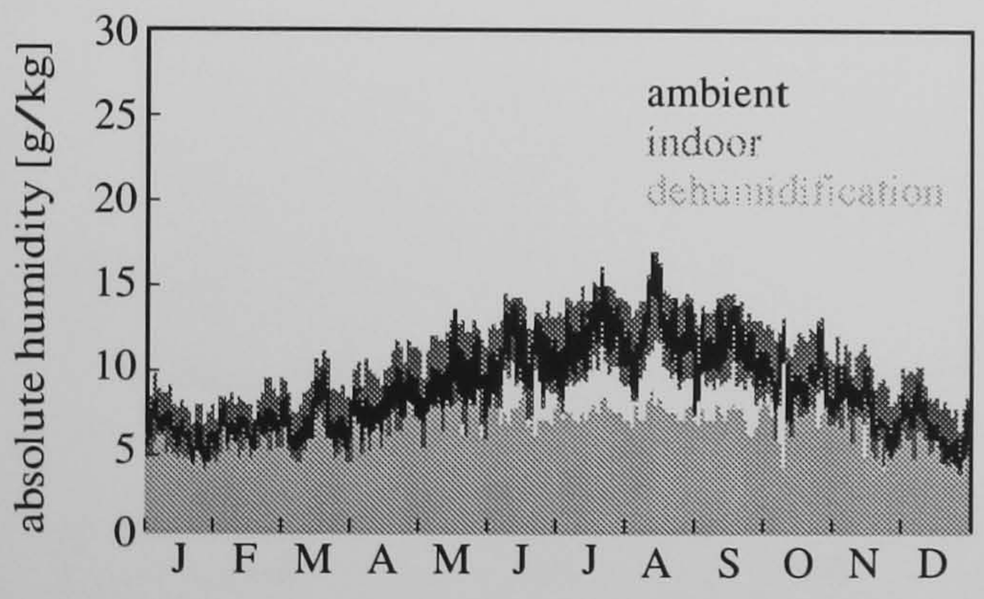

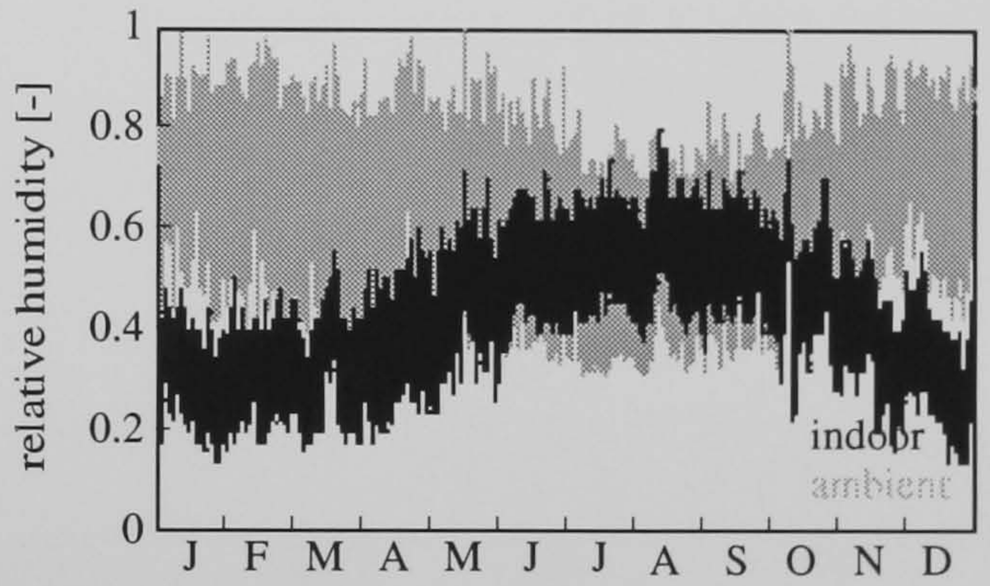

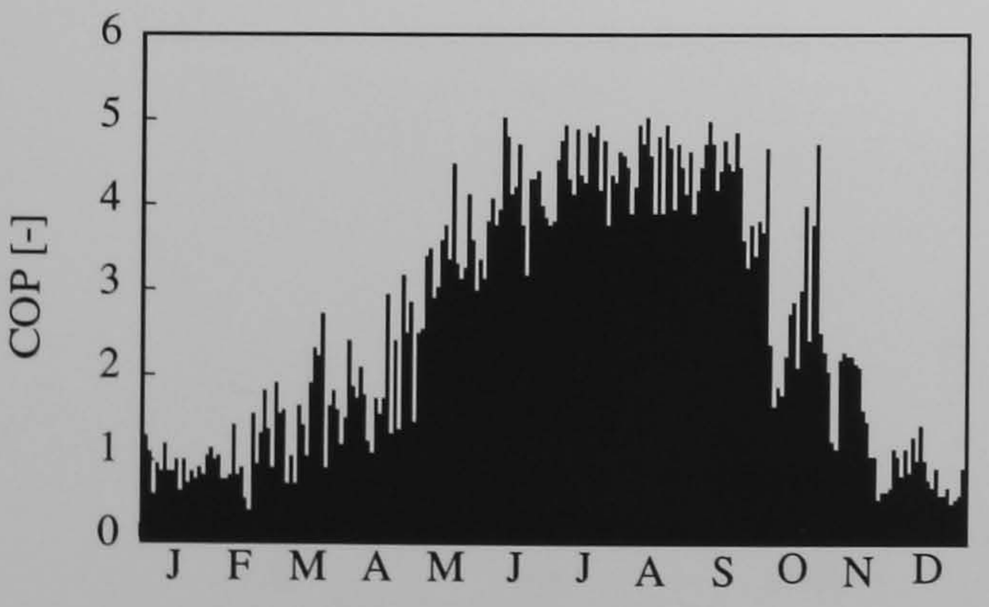

Figure A.5: Seville: Simulation results of case study 8 (heavyweight building, ventilation with maximum 4 air changes per hour, night ventilation, regeneration air flow controlled). Detailed description on page 103. Discussion of the simulation results on page 125.

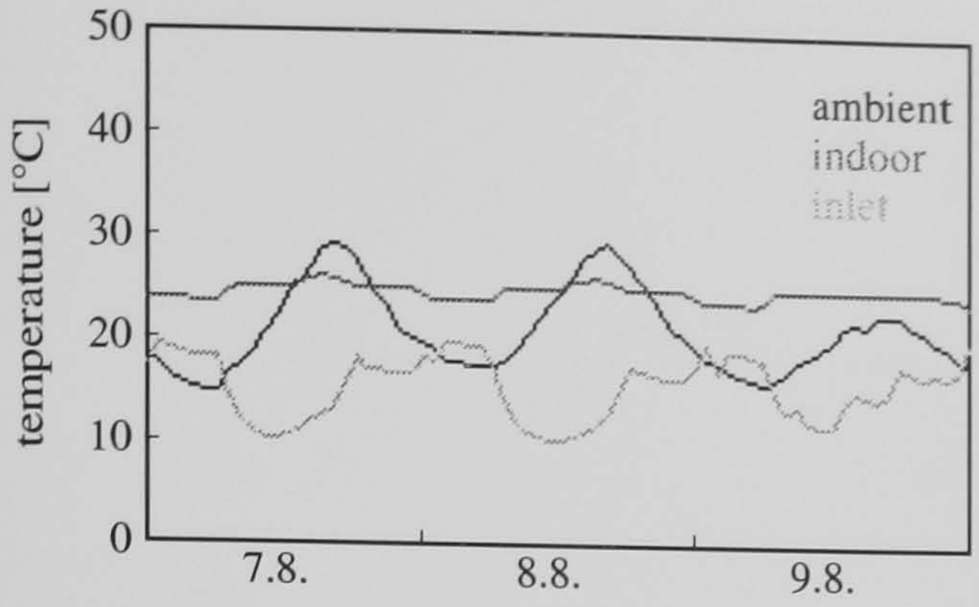

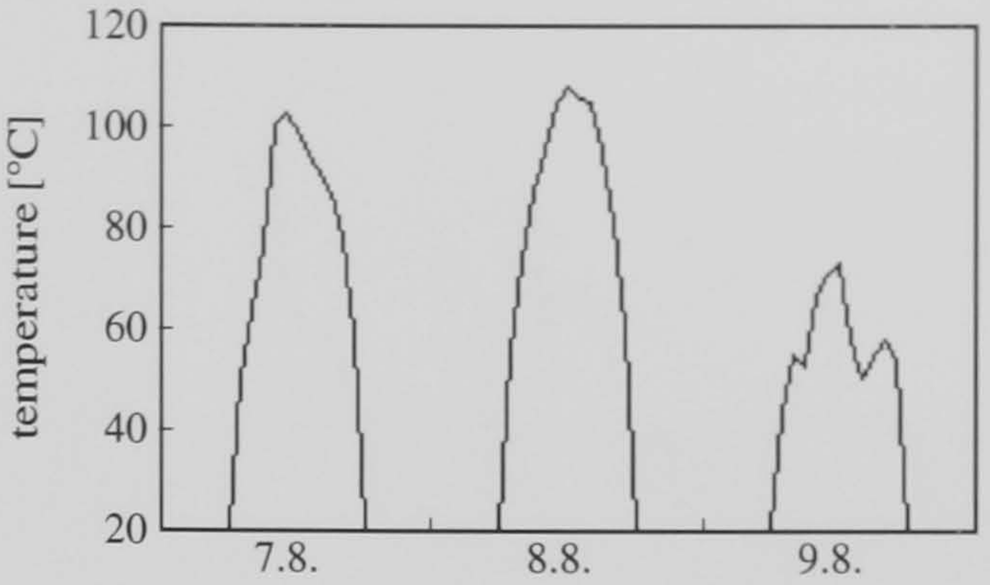

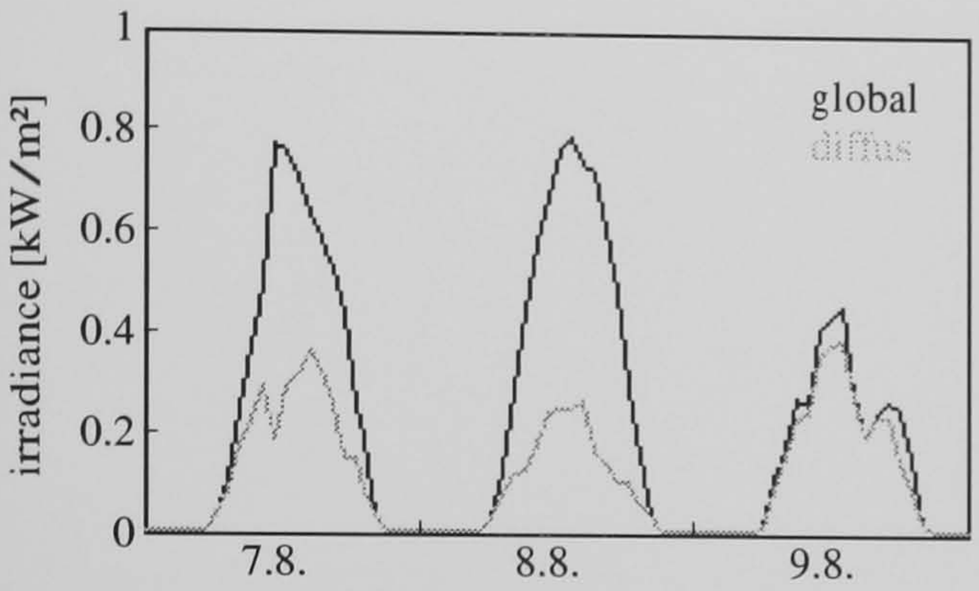

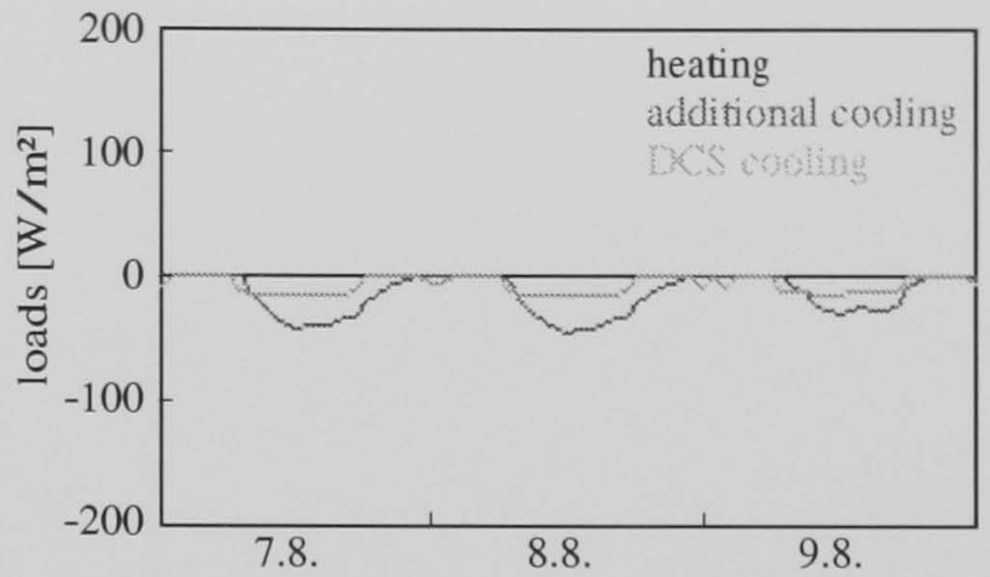

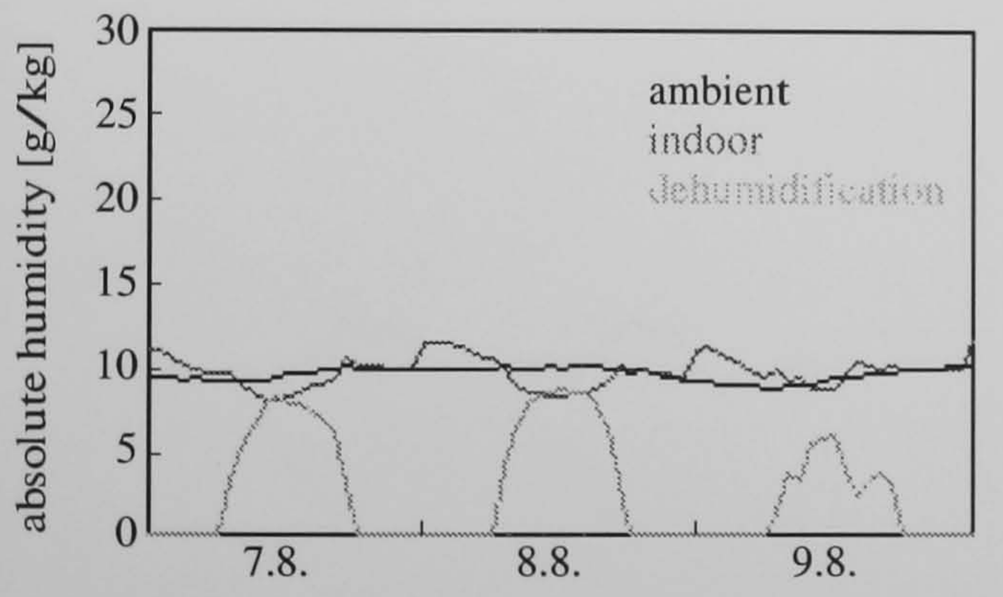

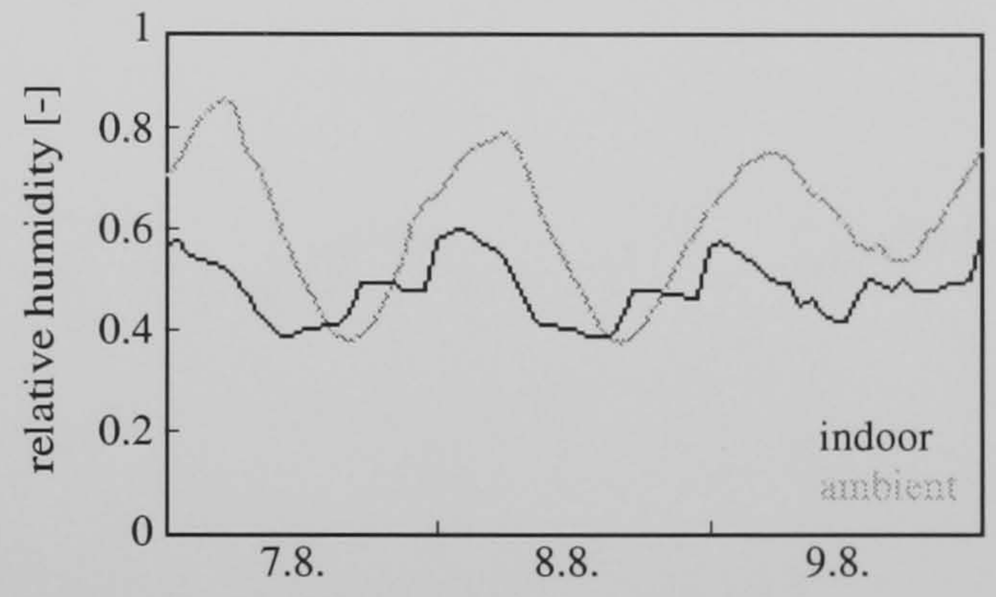

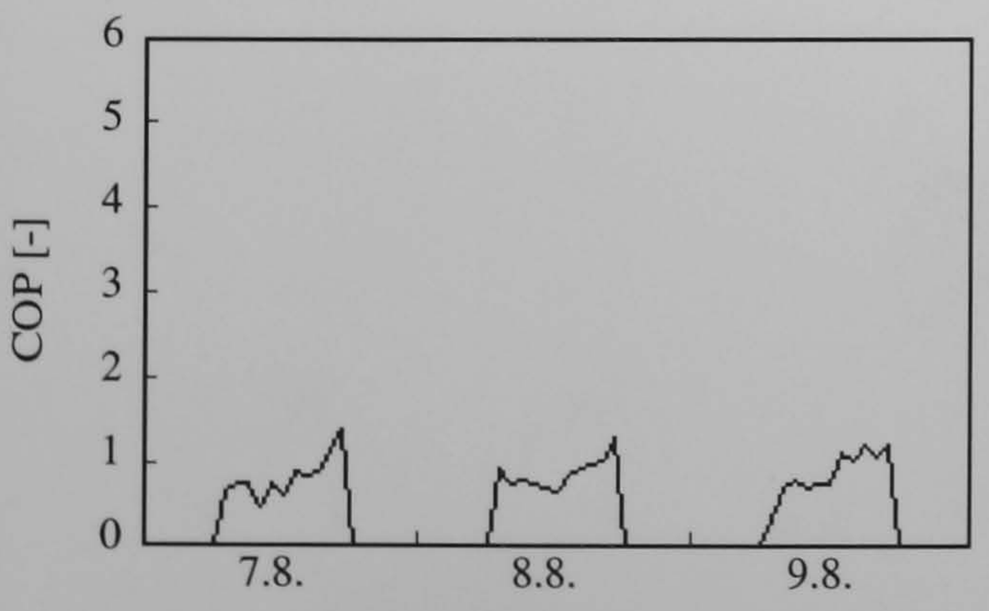

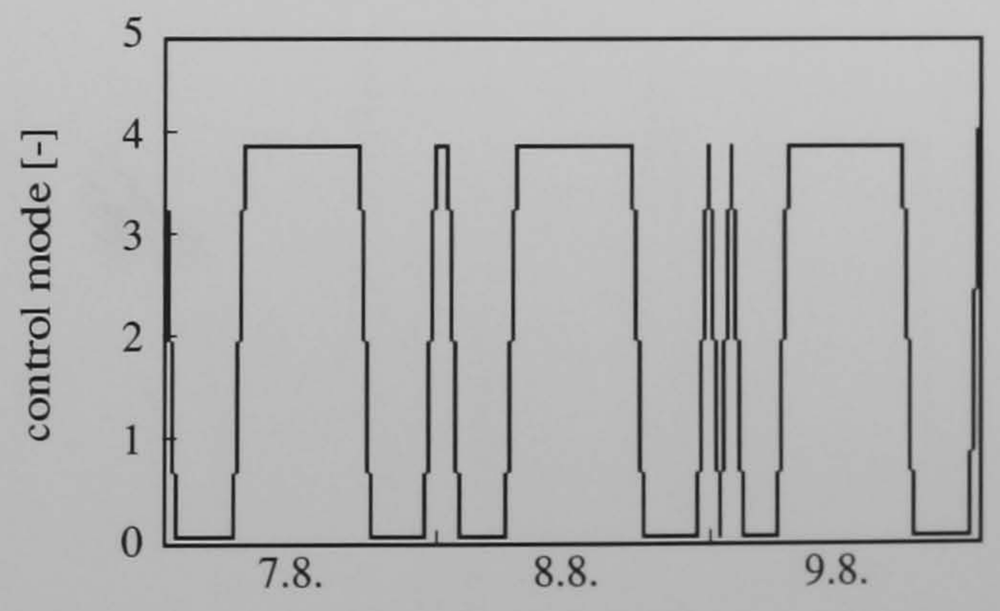

Figure A.6: Stuttgart: Simulation results of case study 1 (heavyweight building, hygienic ventilation during occupation time). Detailed description on page 102. Discussion of the simulation results on page 117.

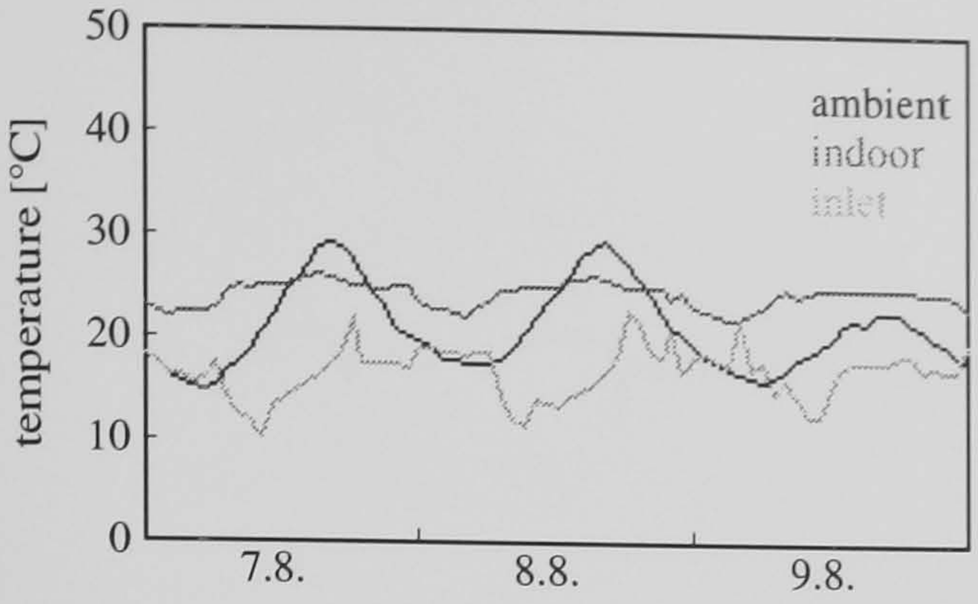

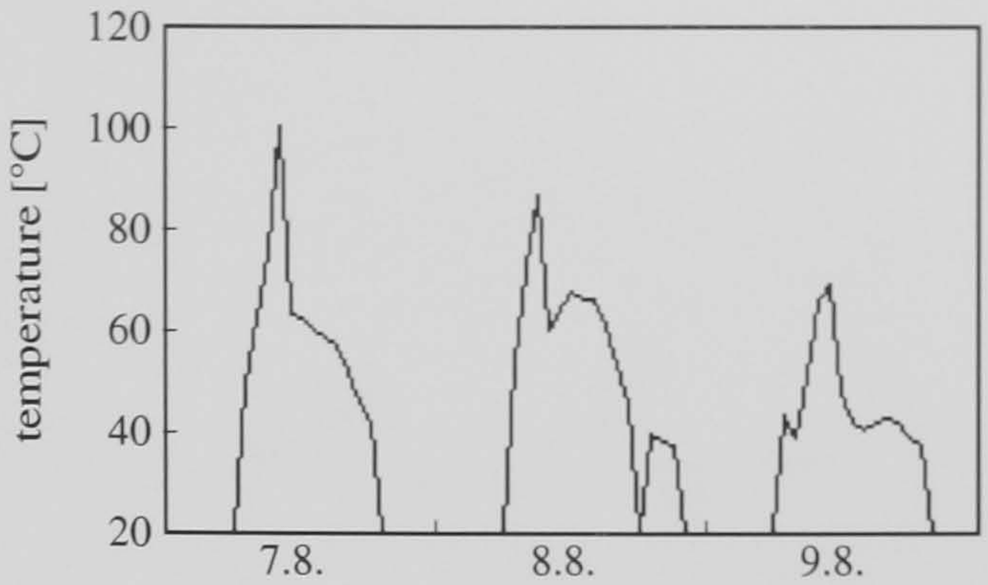

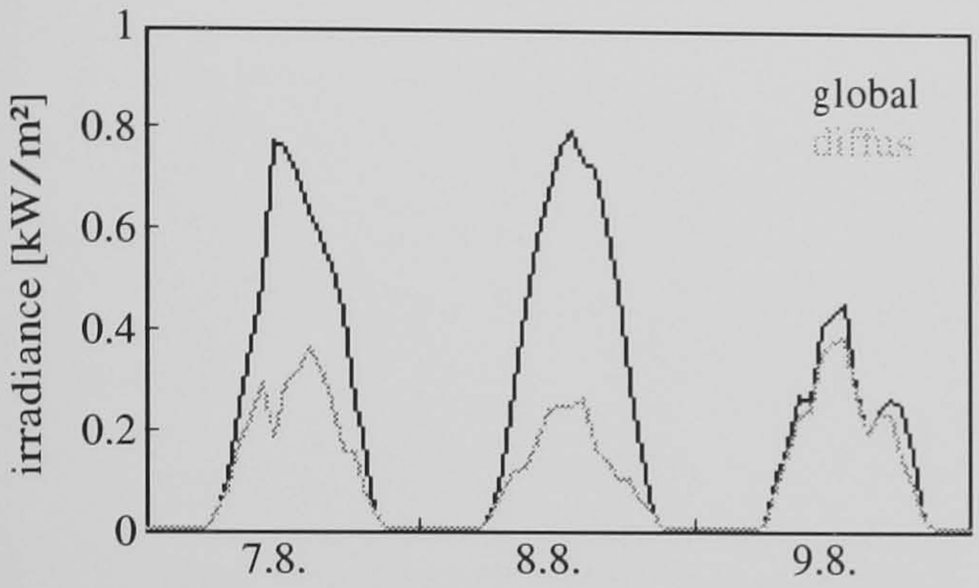

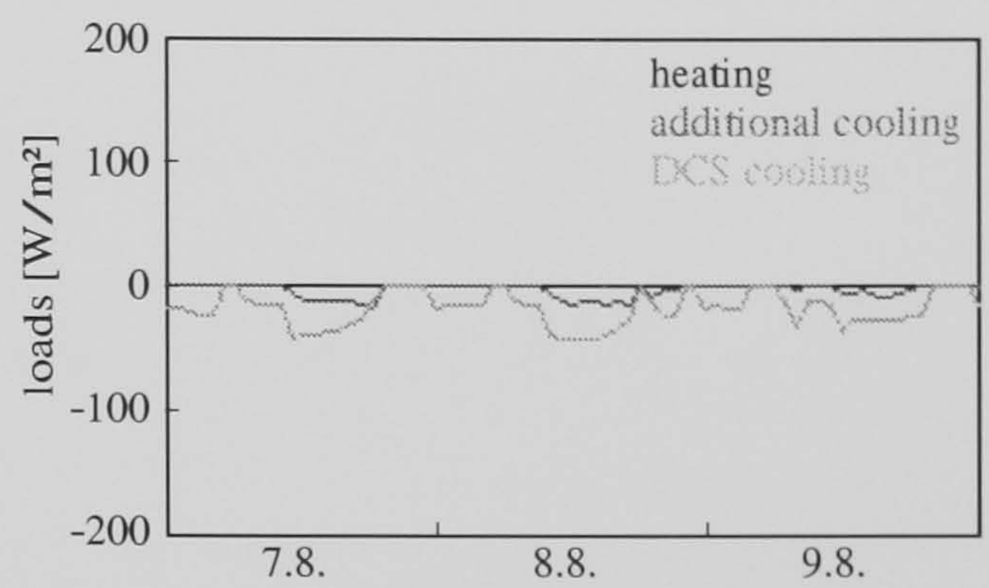

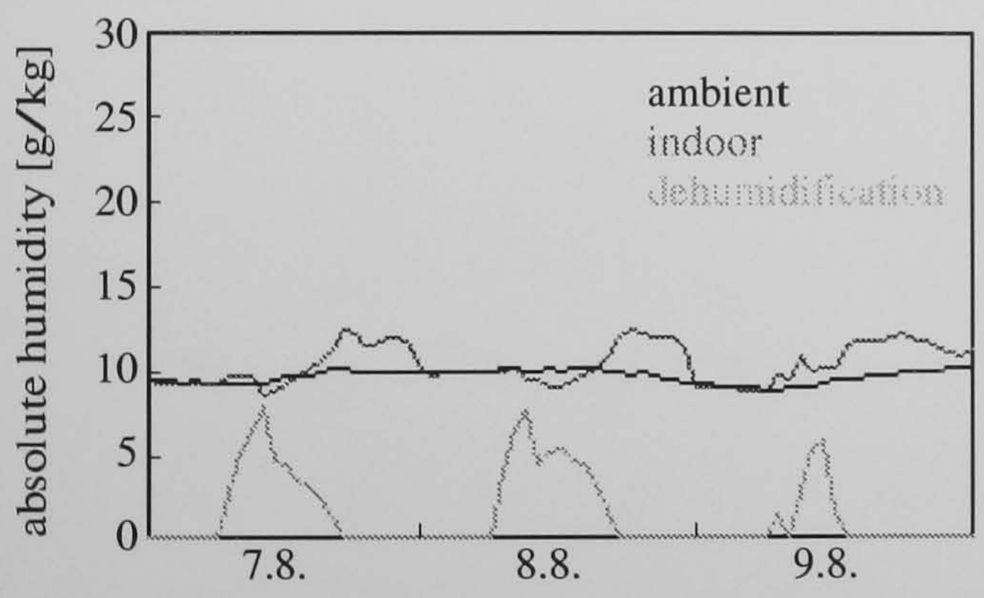

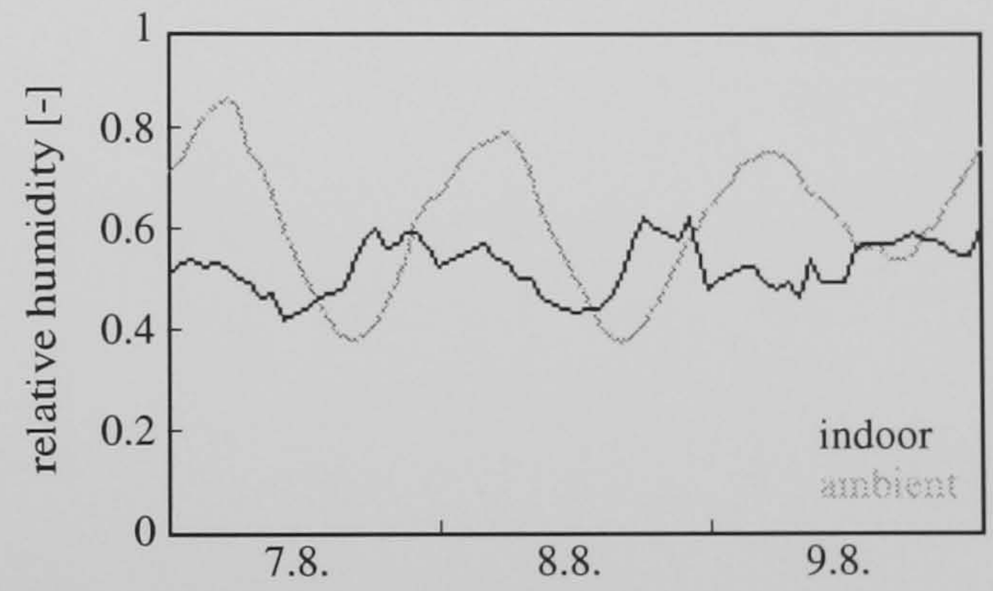

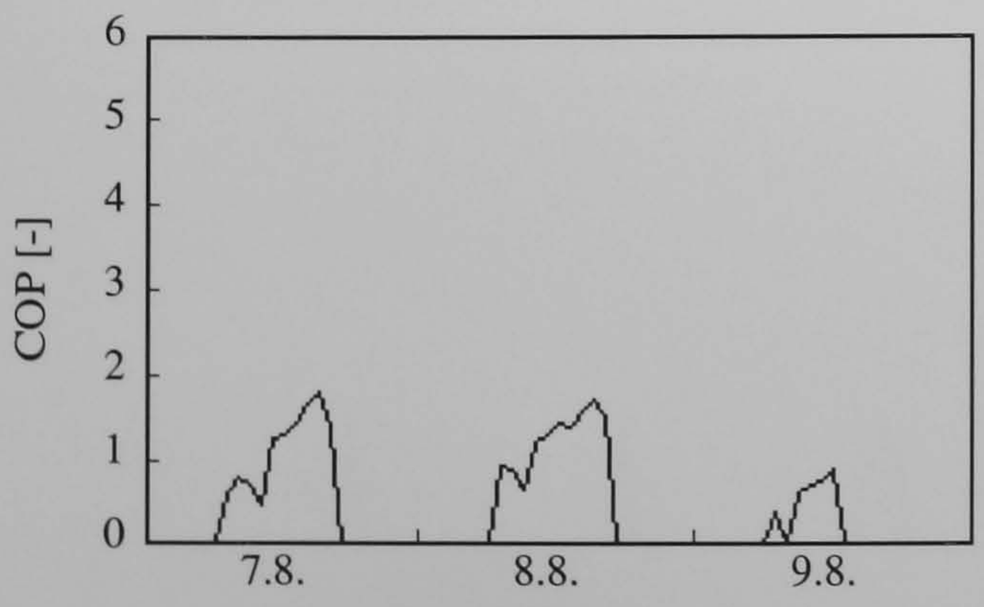

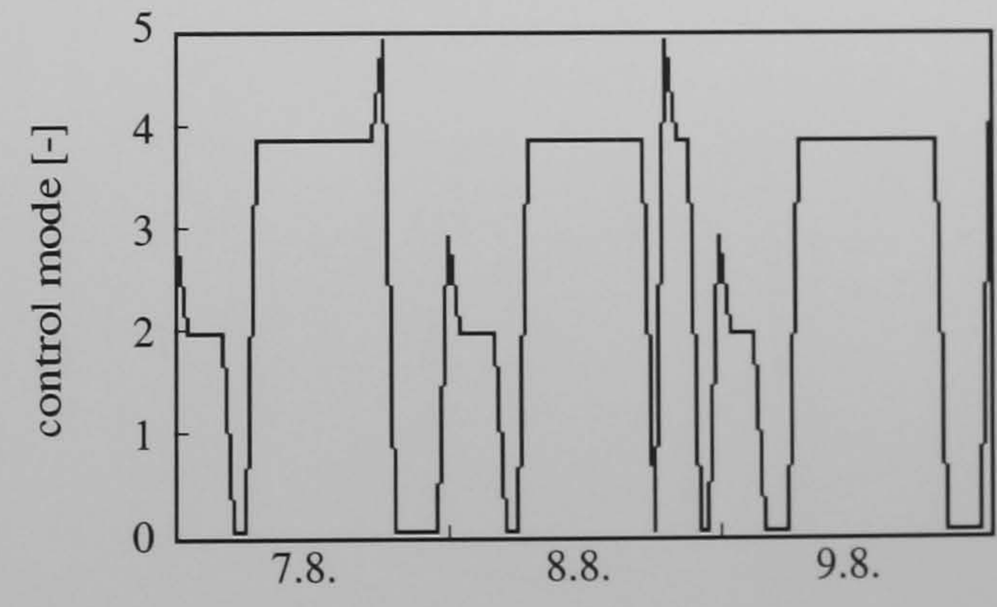

Figure A.7: Stuttgart: Simulation results of case study 3 (heavyweight building, ventilation with maximum 4 air changes per hour, night ventilation). Detailed description on page 102. Discussion of the simulation results on page 119.

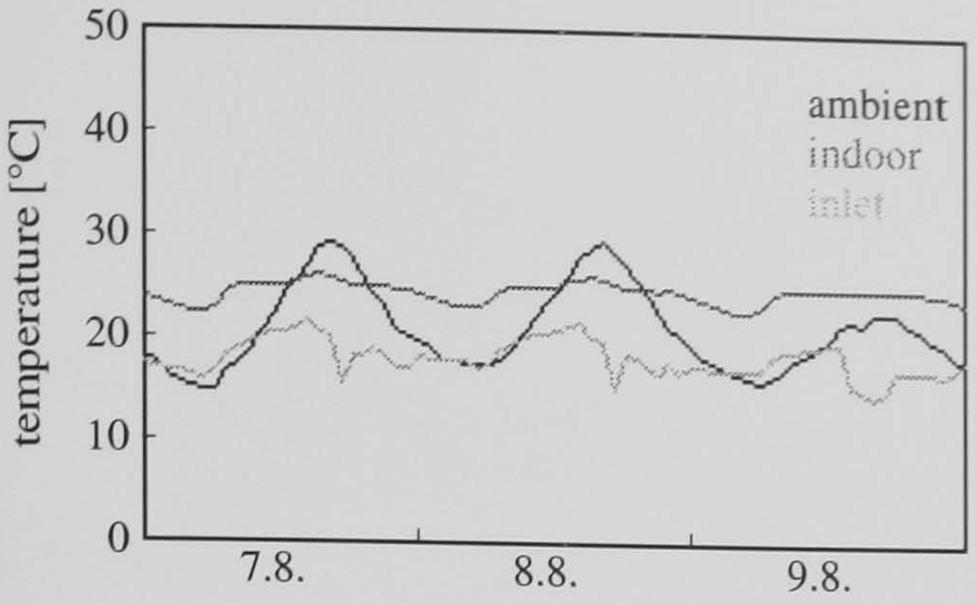

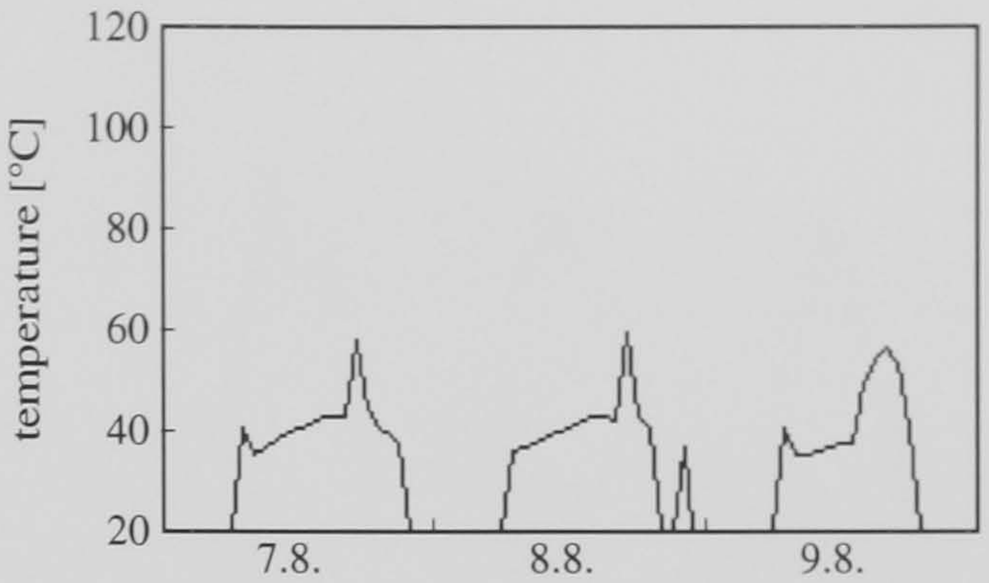

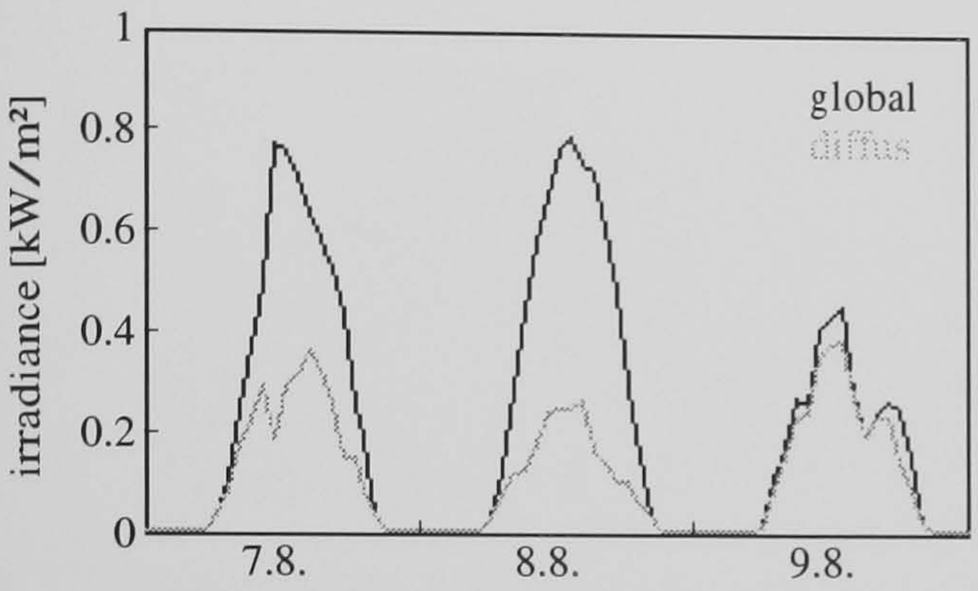

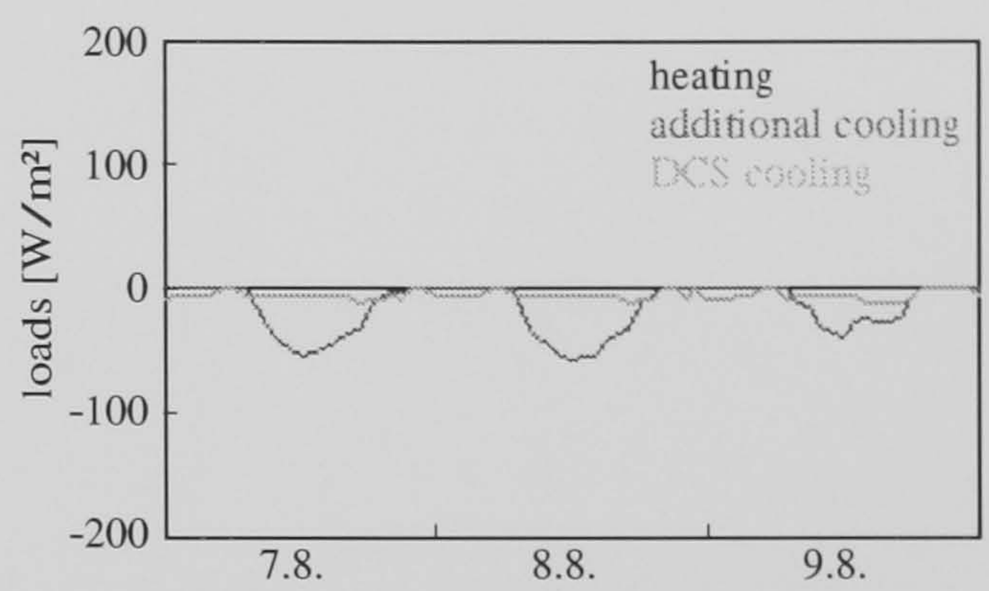

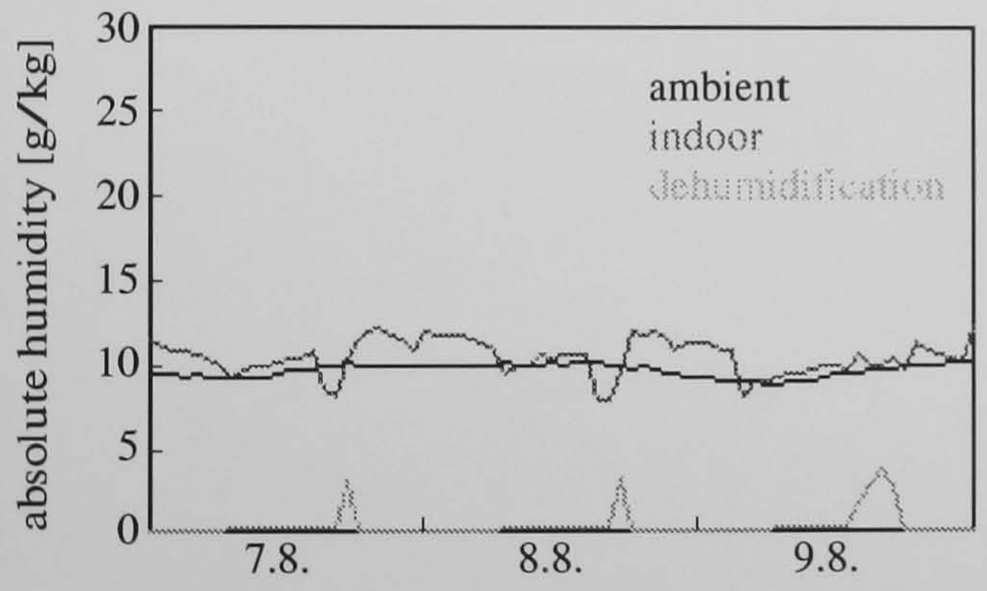

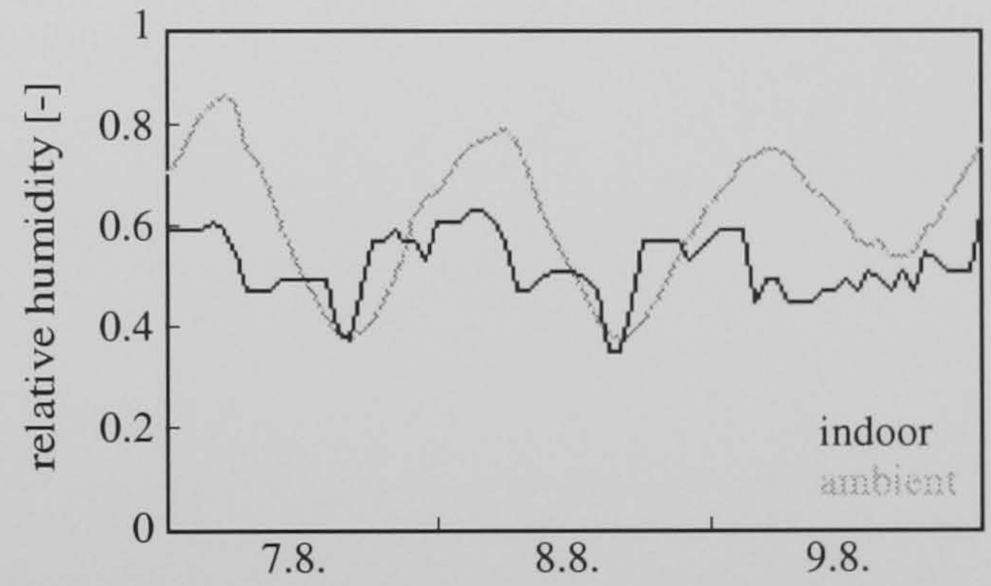

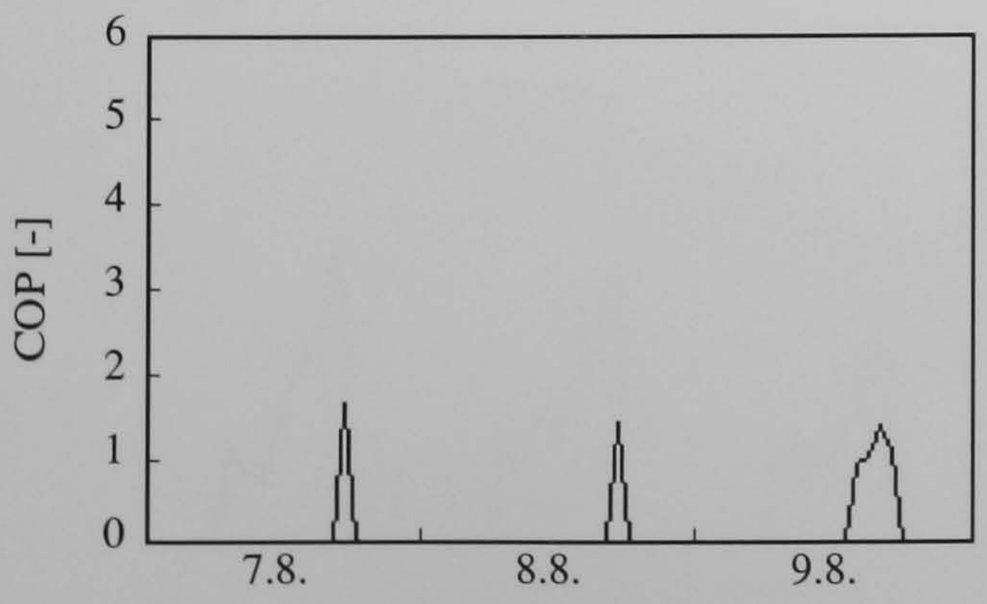

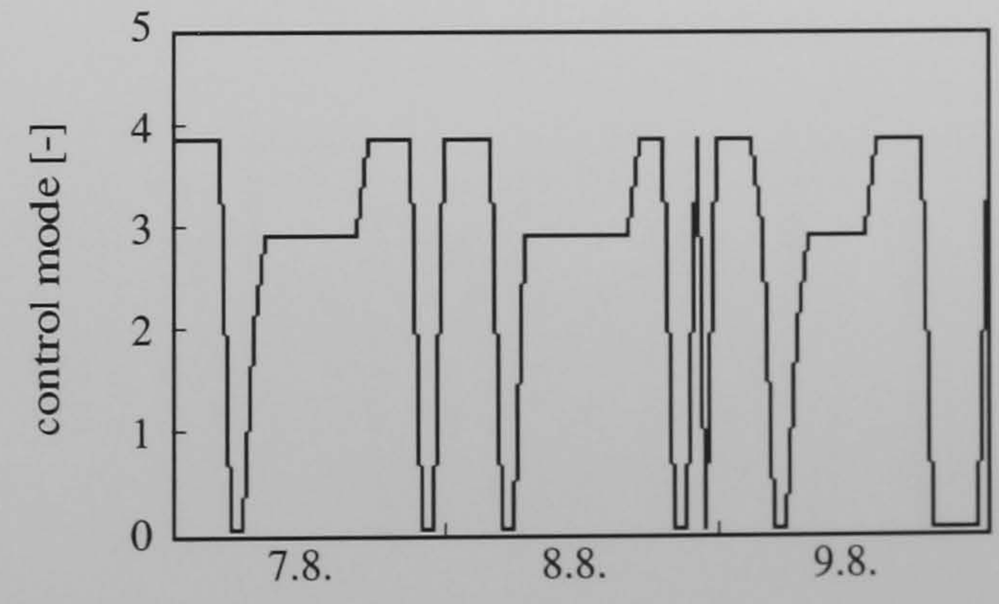

Figure A.8: Stuttgart: Simulation results of case study 7 (heavyweight building, hygienic ventilation during occupation time, controlled to reach an inlet temperature close to 17 °C). Detailed description on page 102. Discussion of the simulation results on page 124.

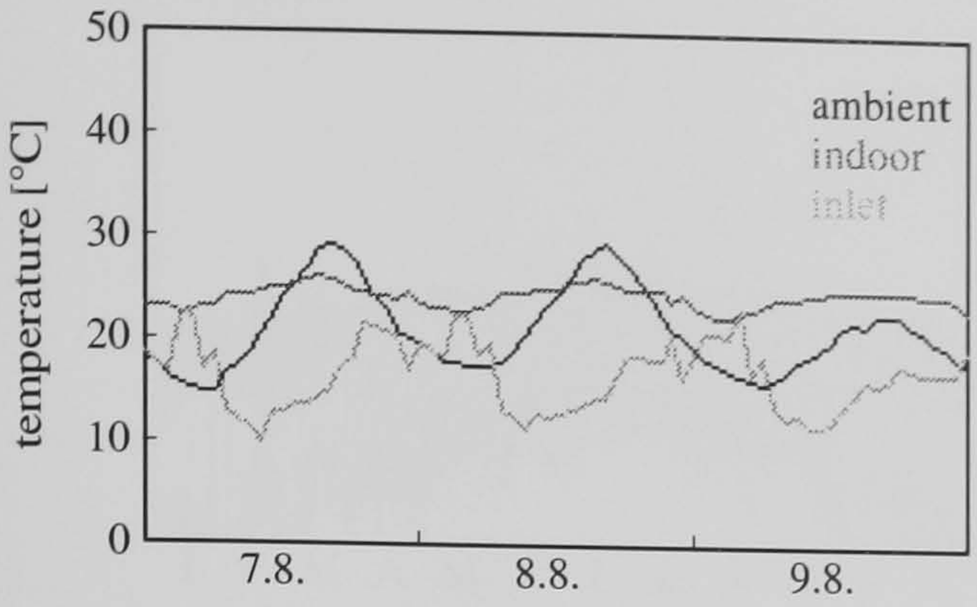

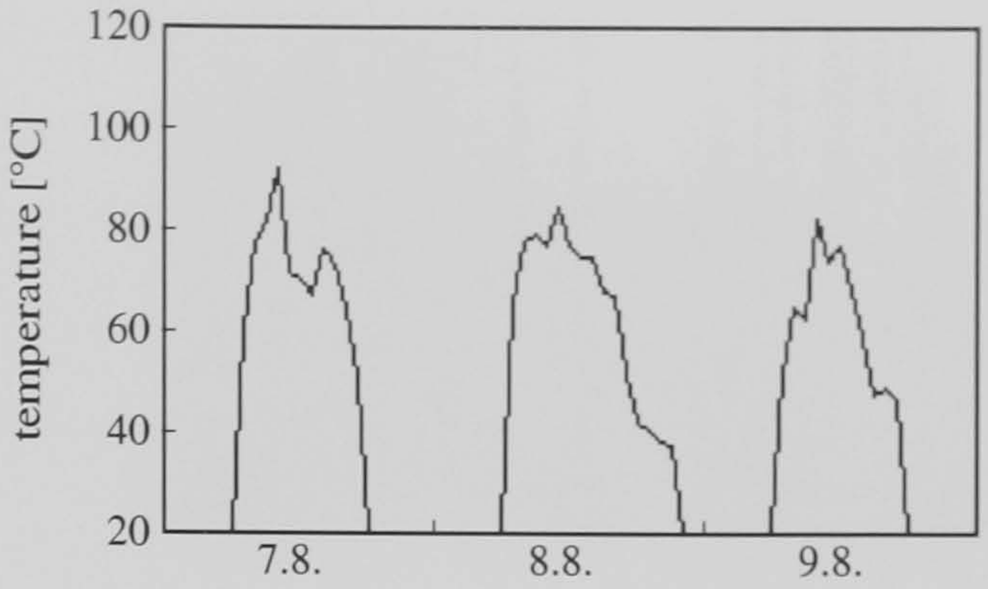

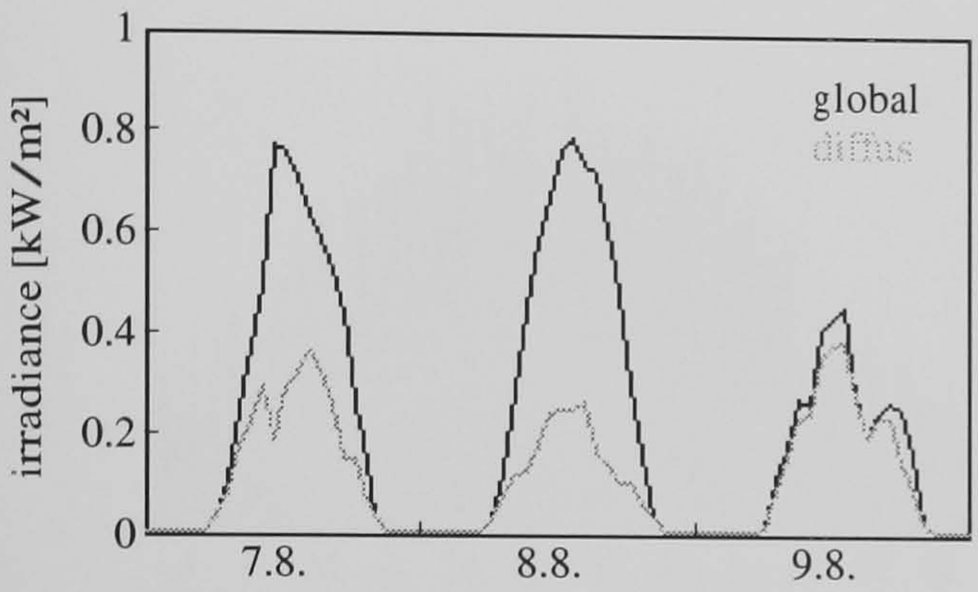

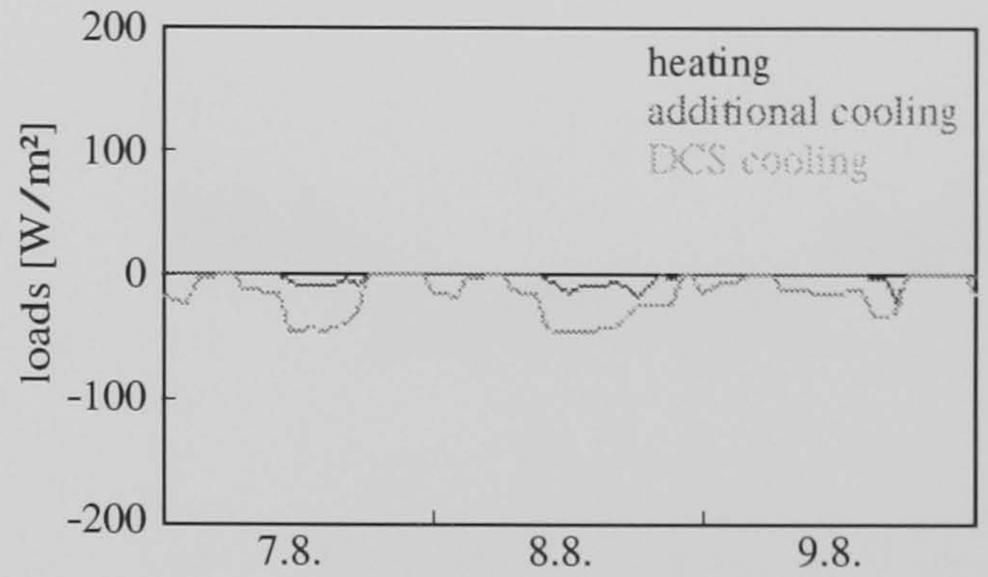

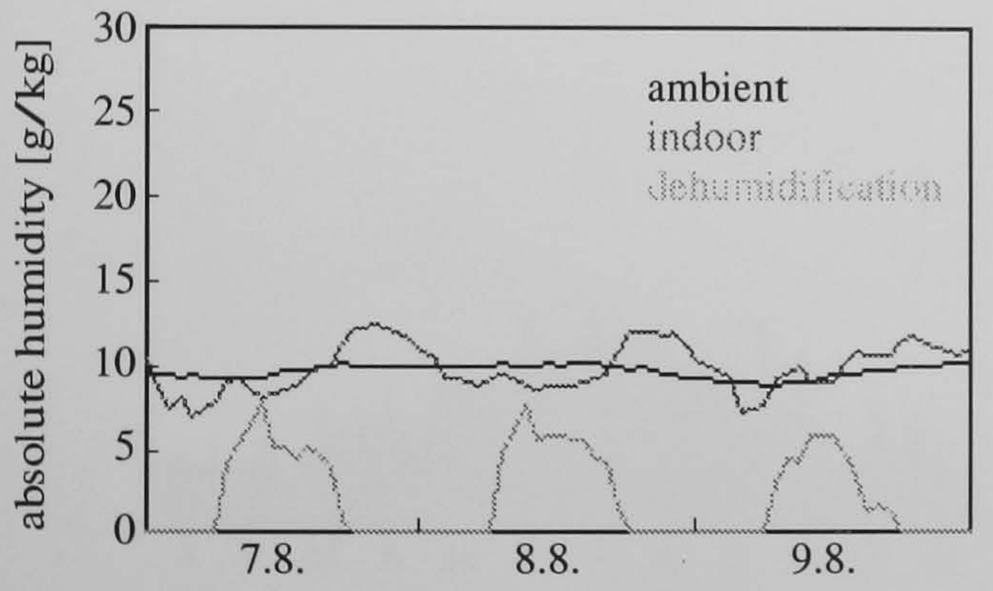

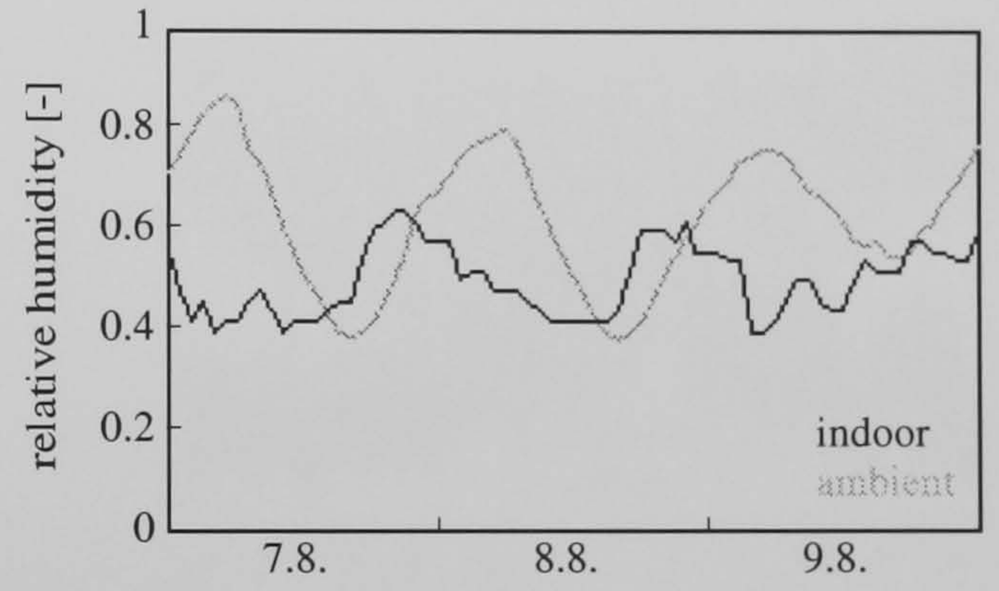

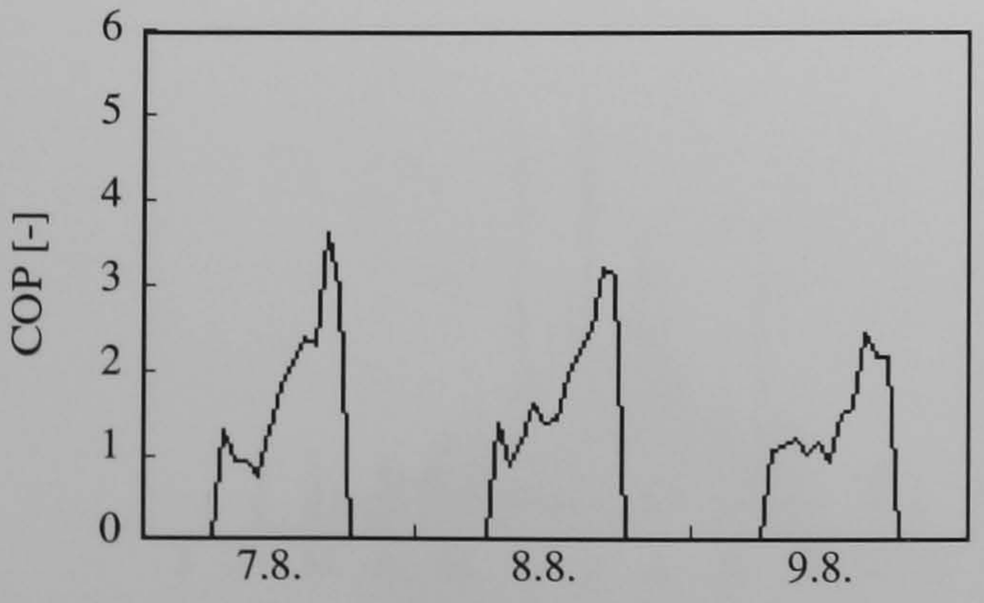

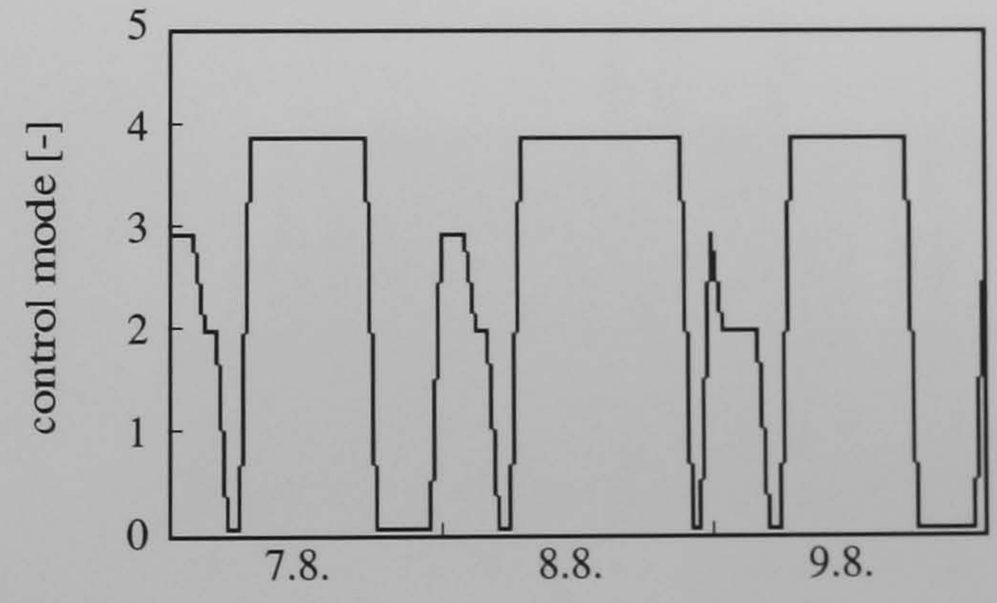

Figure A.9: Stuttgart: Simulation results of case study 8 (heavyweight building, ventilation with maximum 4 air changes per hour, night ventilation, regeneration air flow controlled). Detailed description on page 103. Discussion of the simulation results on page 125.

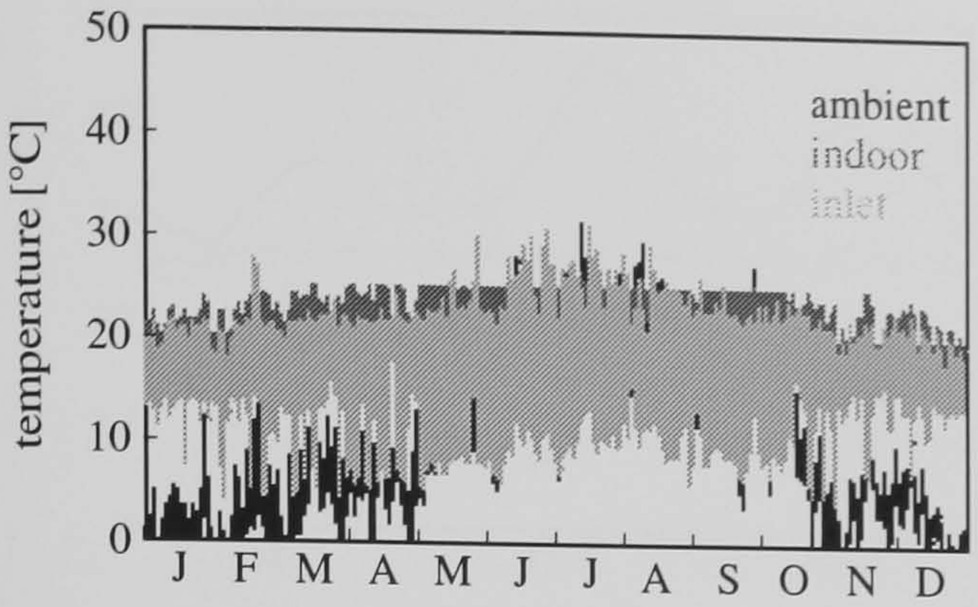

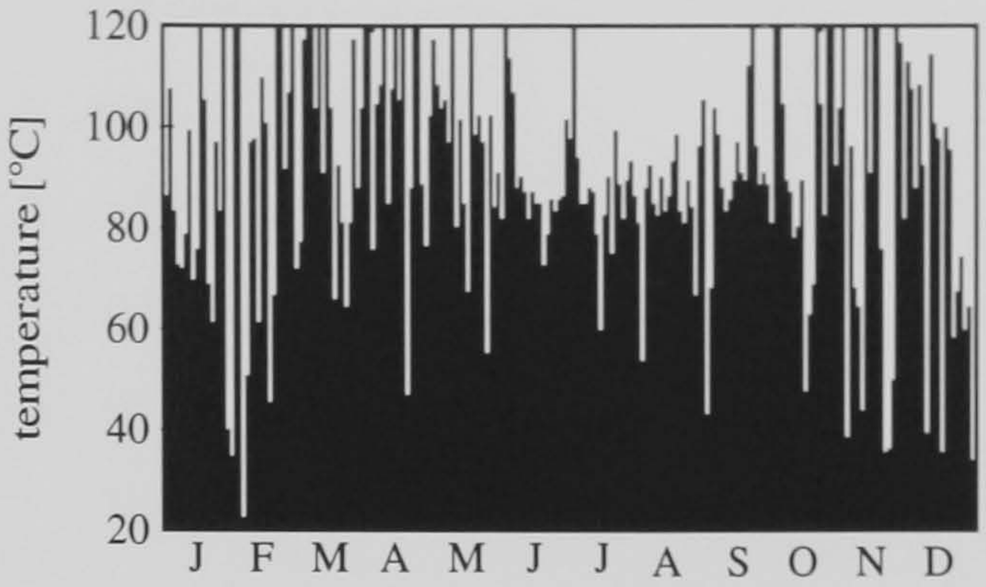

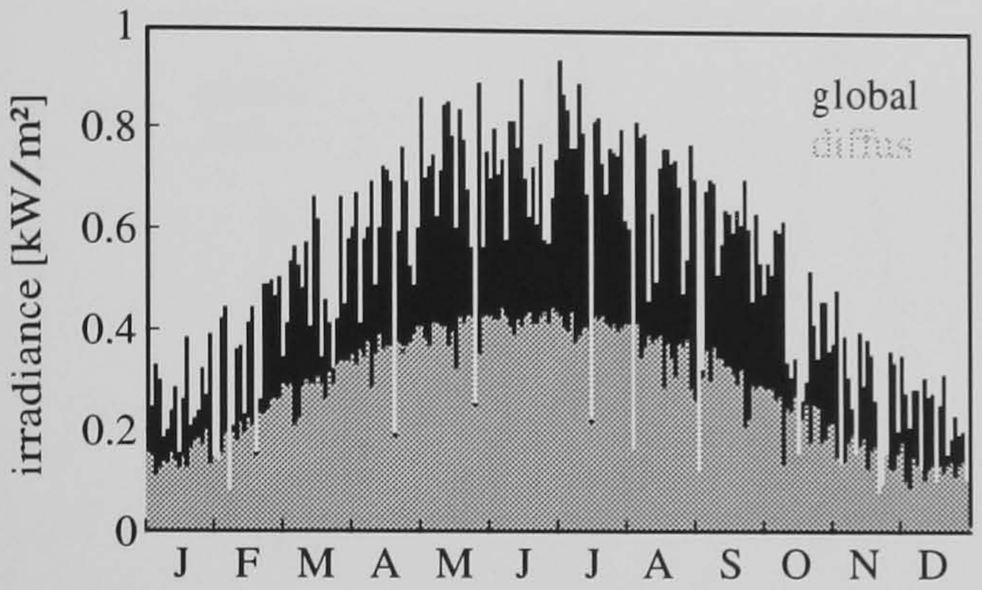

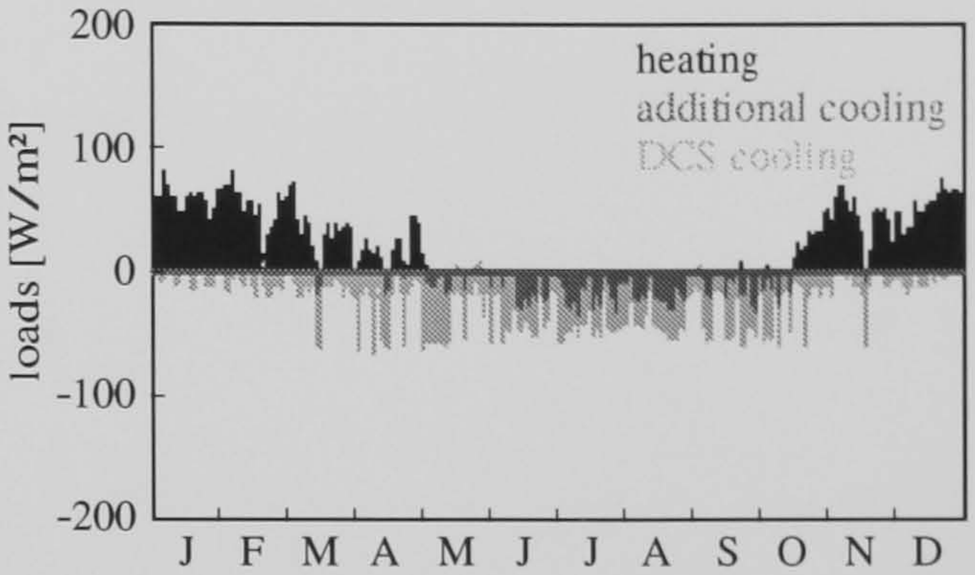

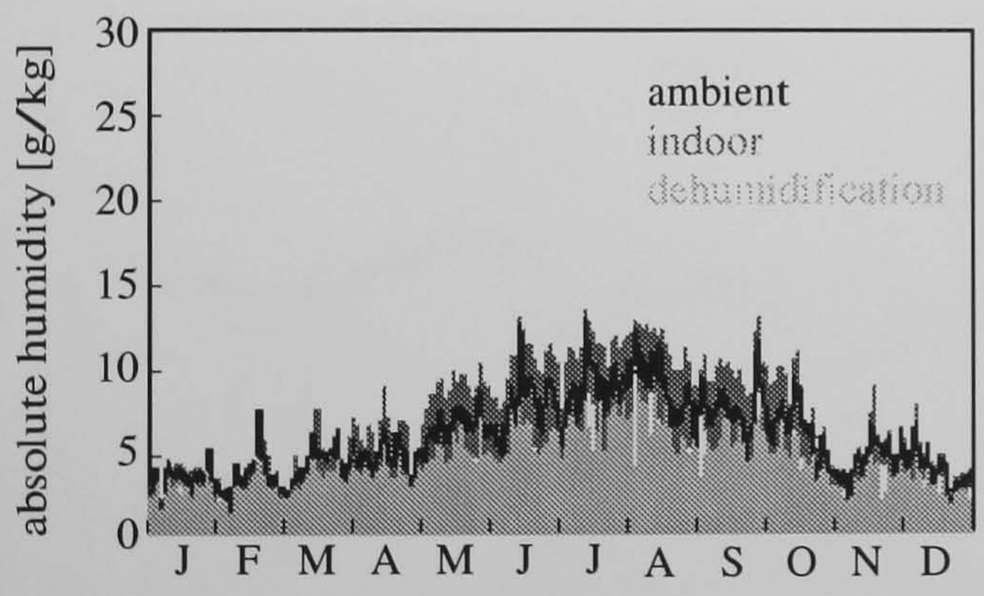

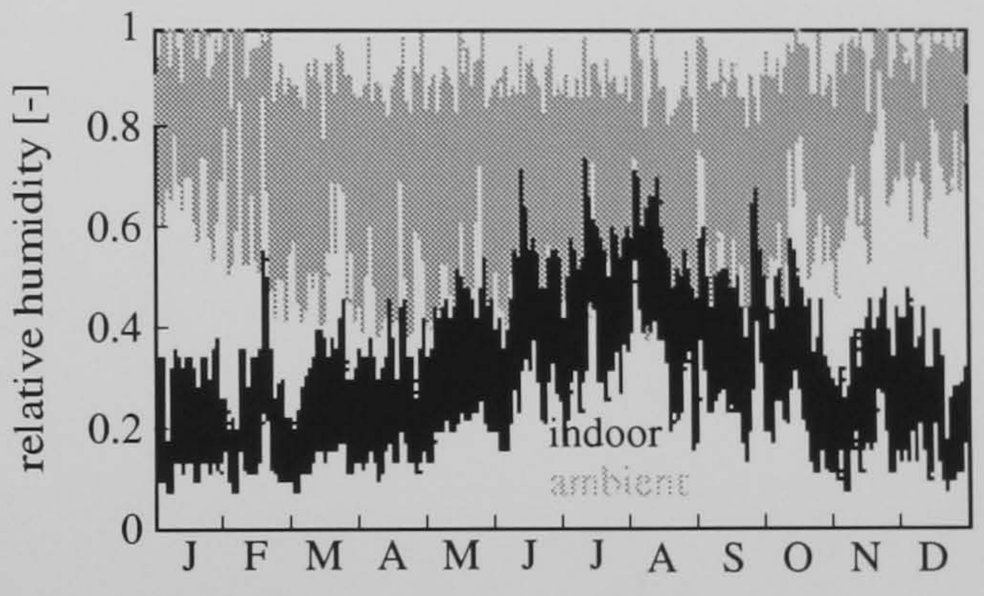

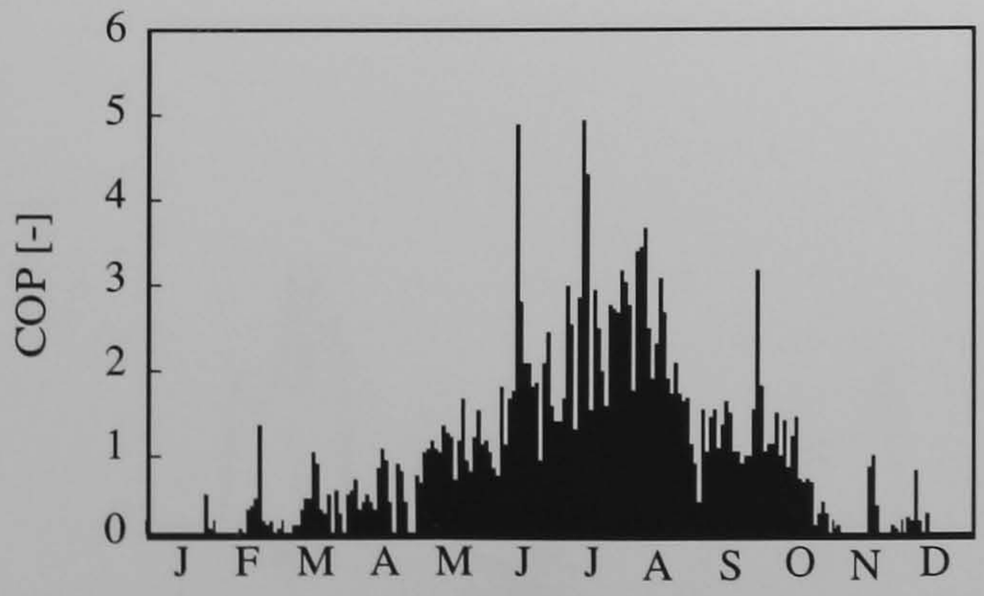

Figure A.10: Stuttgart: Simulation results of case study 8 (heavyweight building, ventilation with maximum 4 air changes per hour, night ventilation, regeneration air flow controlled). Detailed description on page 103. Discussion of the simulation results on page 125.

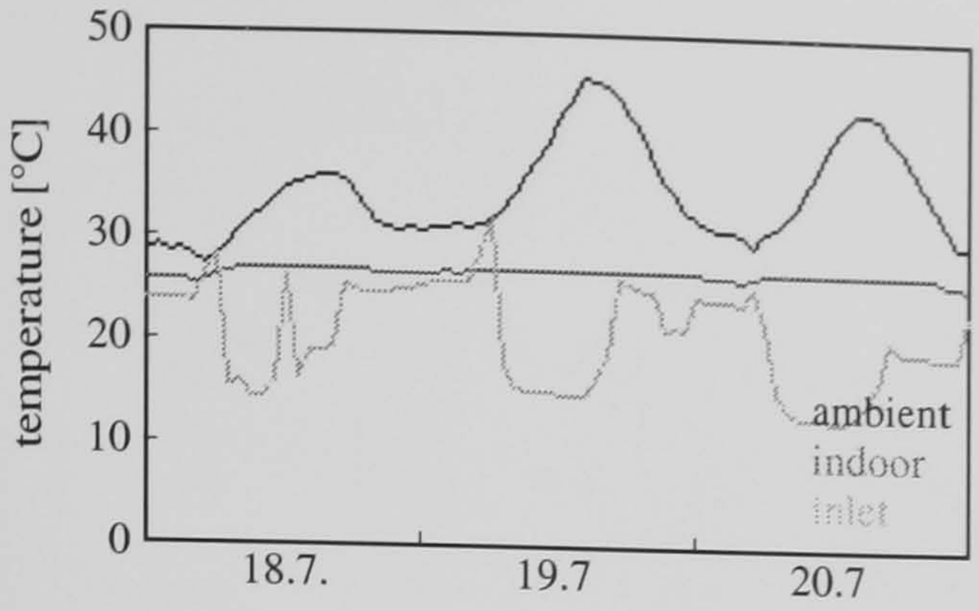

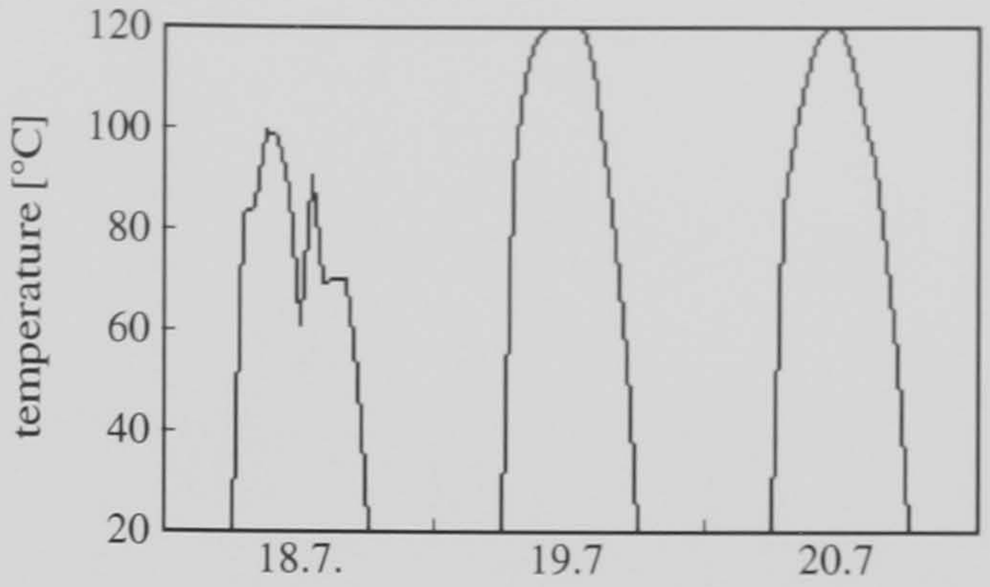

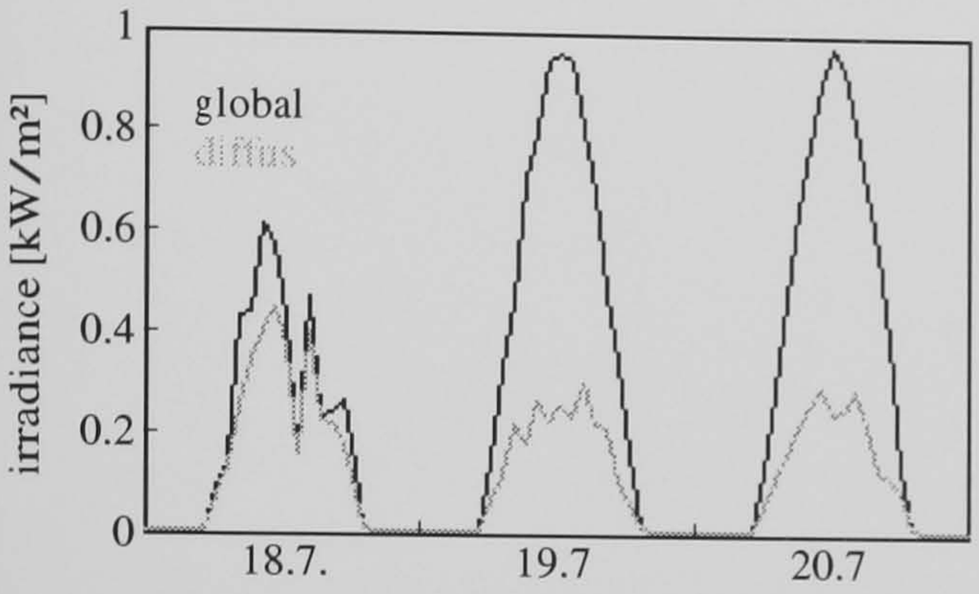

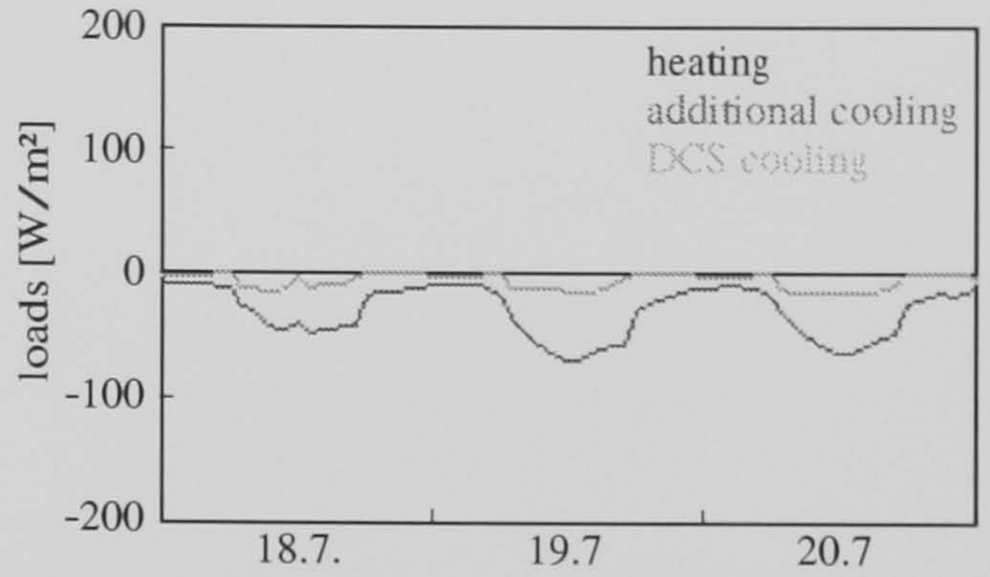

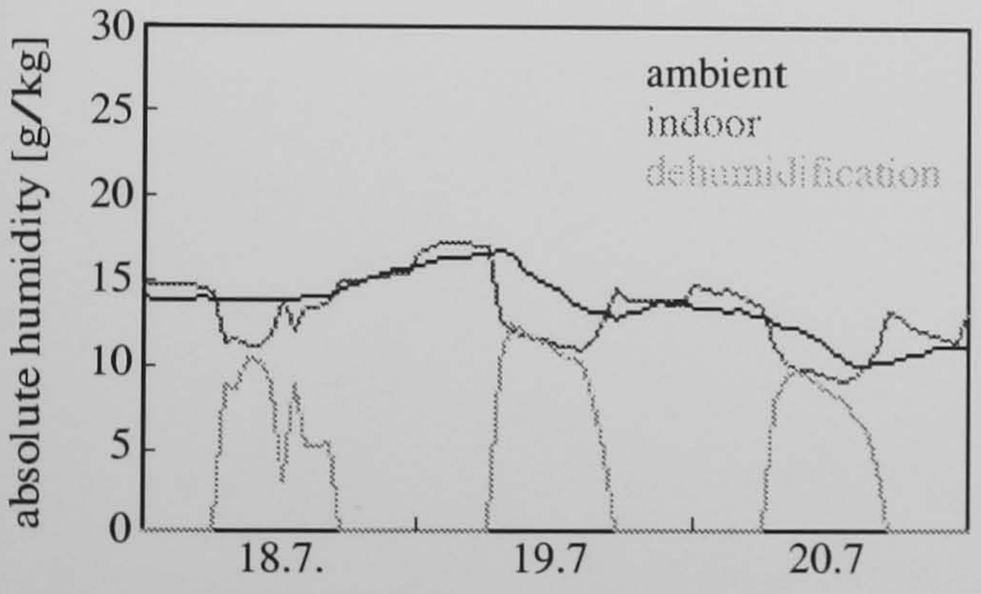

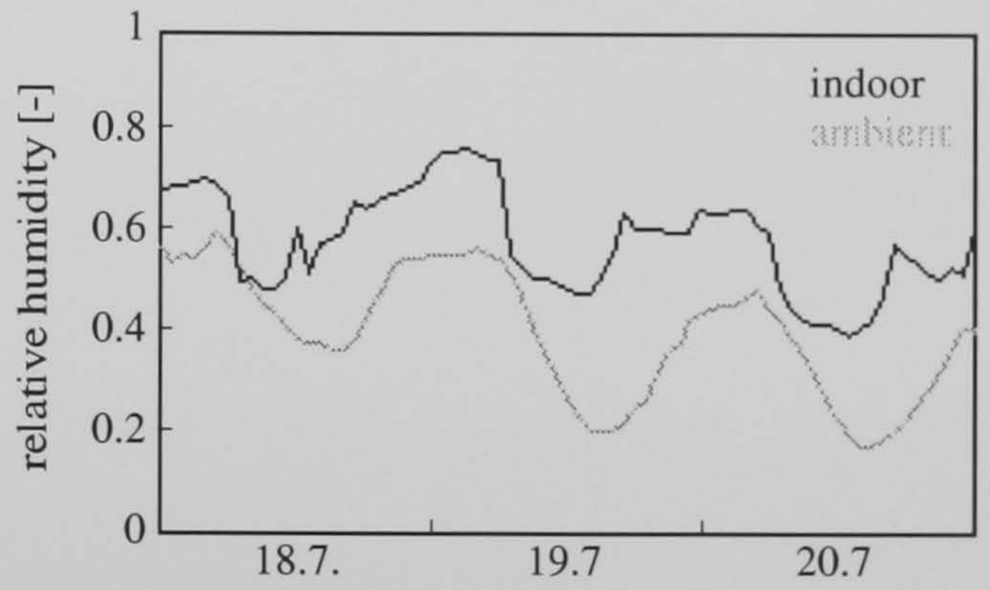

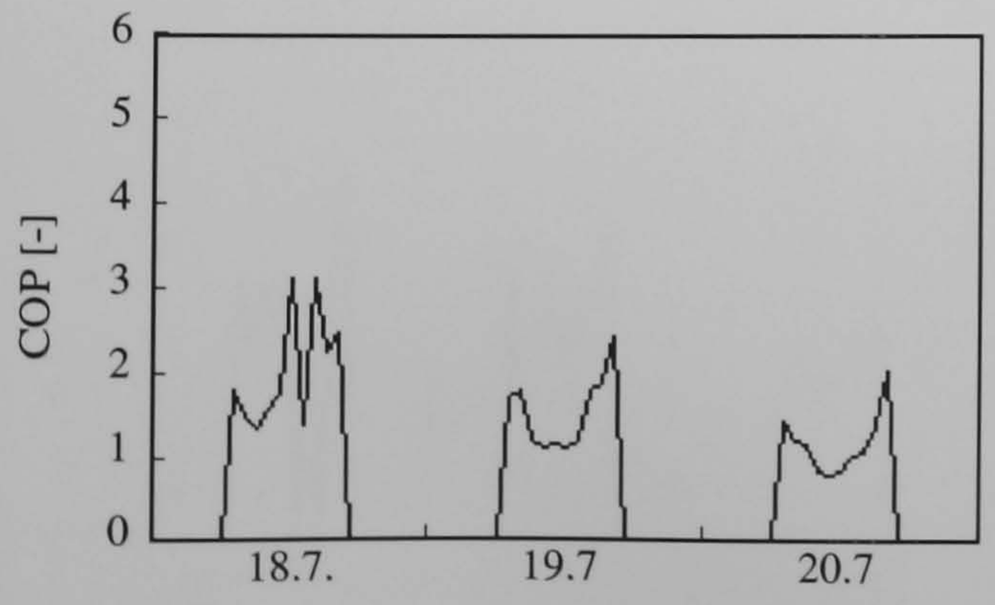

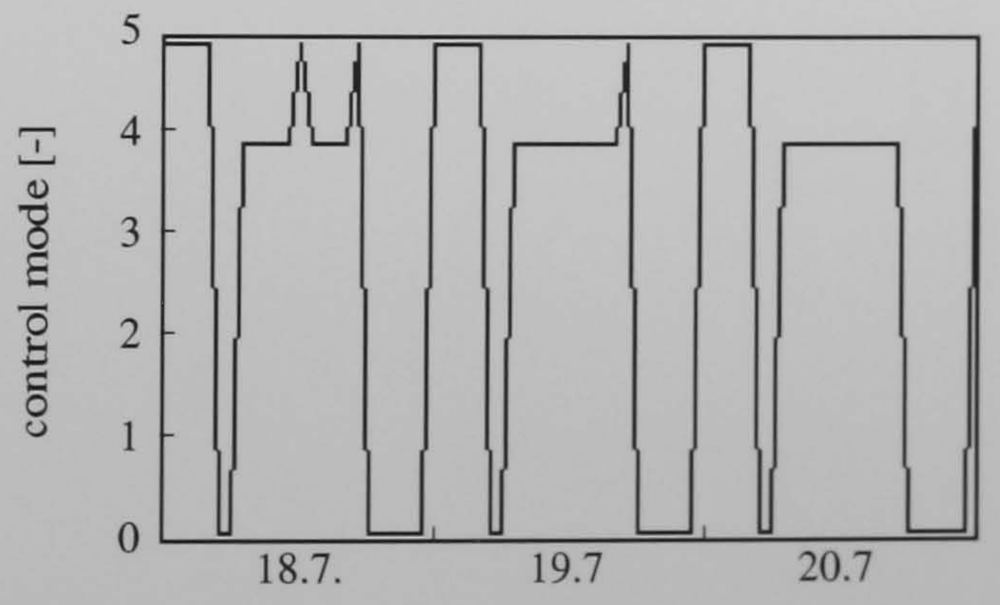

Figure A.11: Phoenix: Simulation results of case study 1 (heavyweight building, hygienic ventilation during occupation time). Detailed description on page 102. Discussion of the simulation results on page 117.

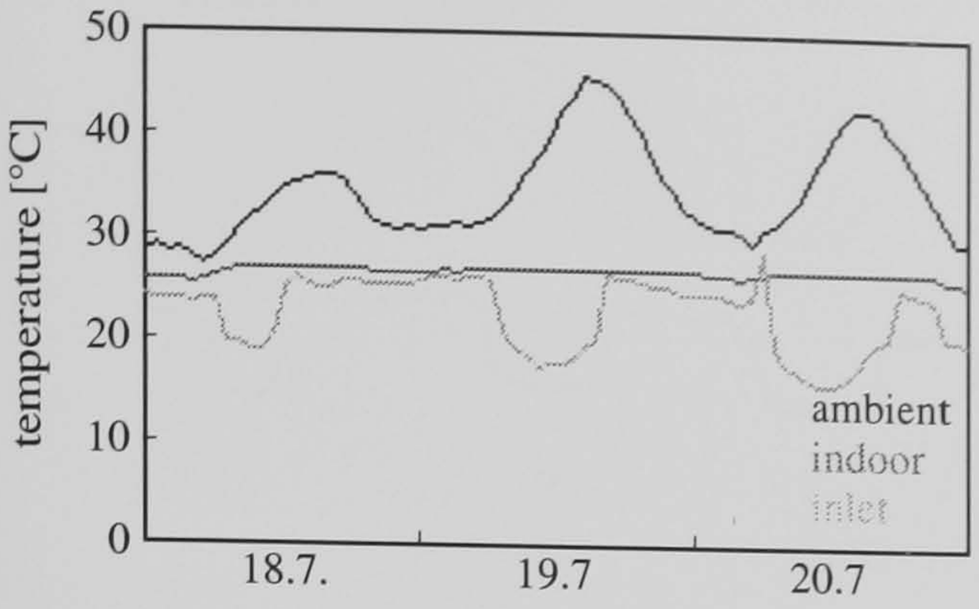

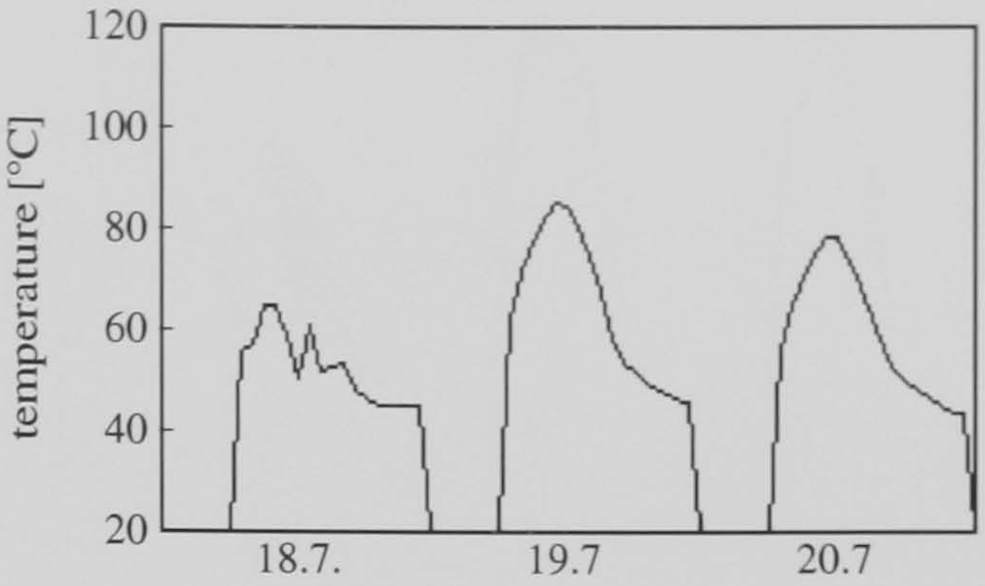

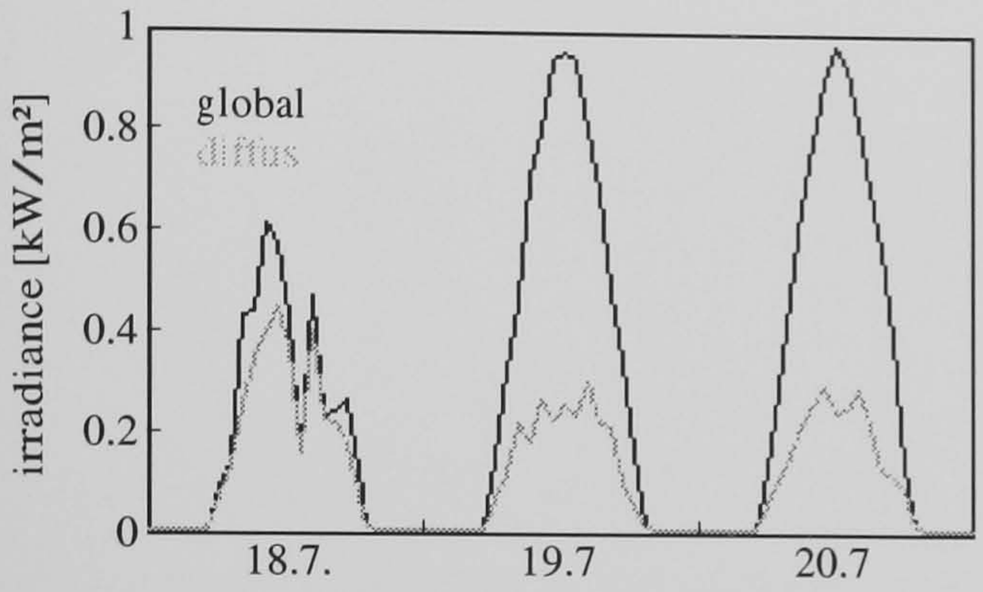

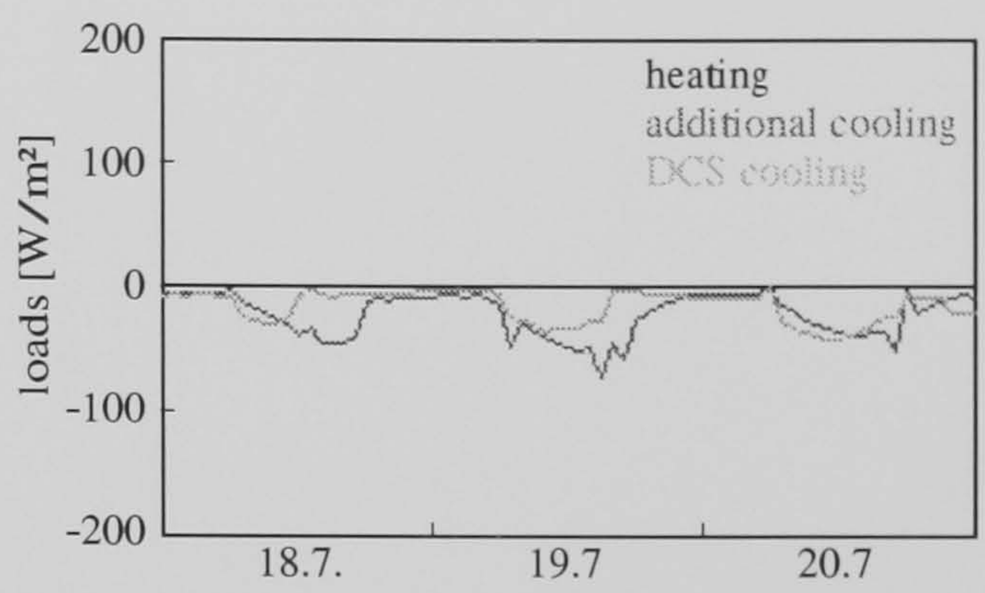

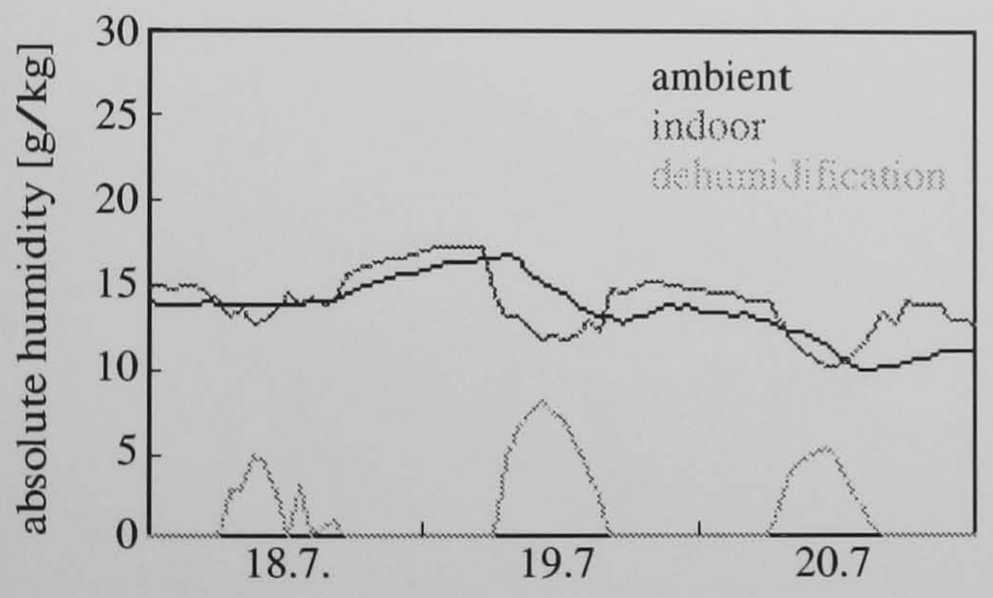

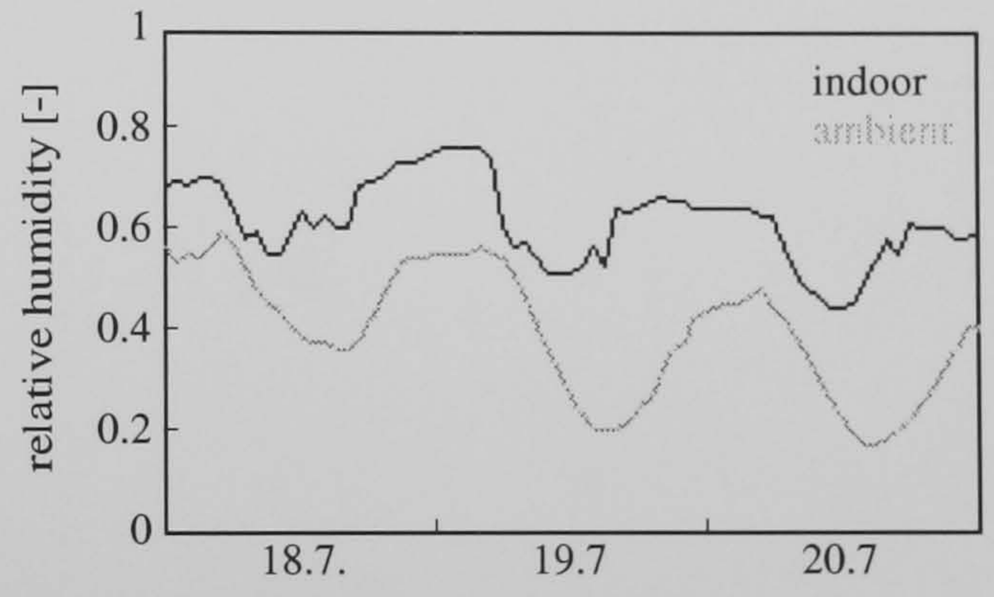

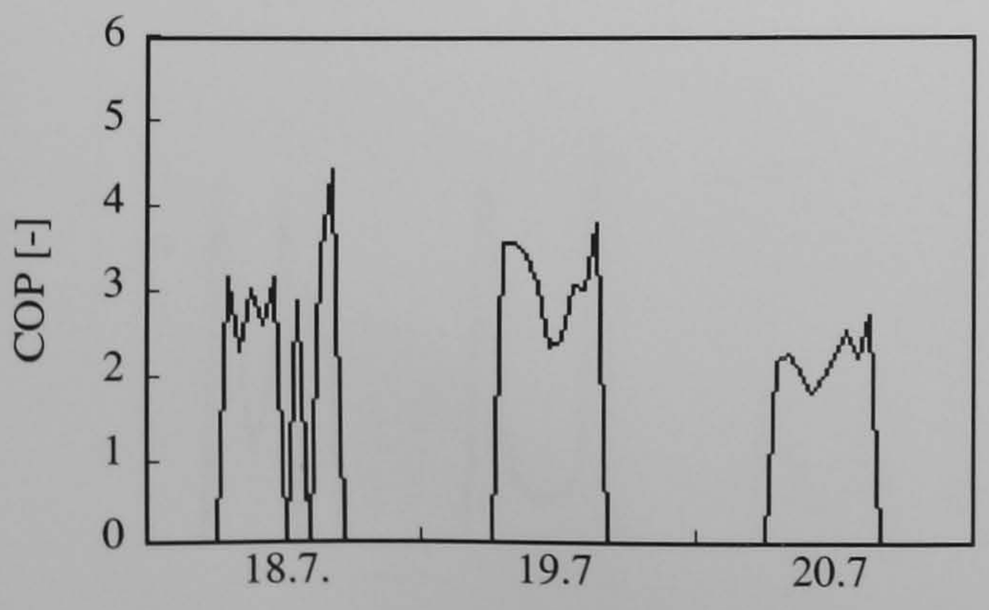

Figure A.12: Phoenix: Simulation results of case study 3 (heavyweight building, ventilation with maximum 4 air changes per hour, night ventilation). Detailed description on page 102. Discussion of the simulation results on page 119.

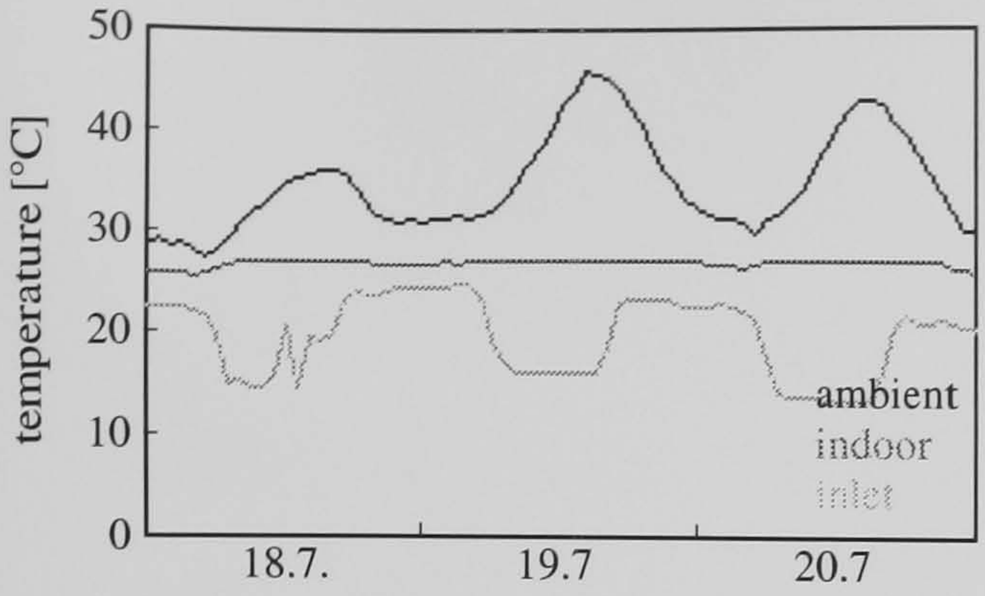

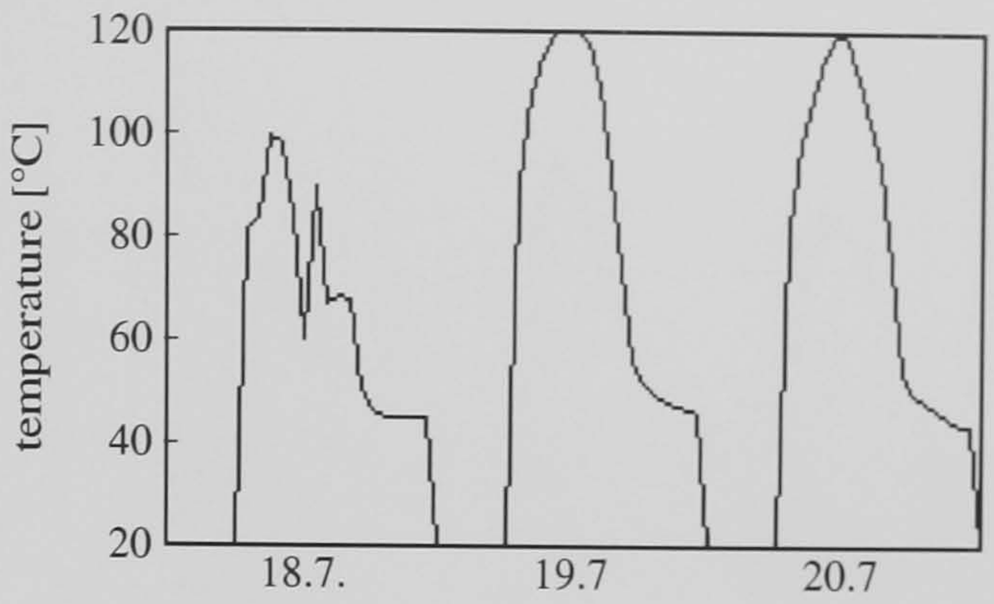

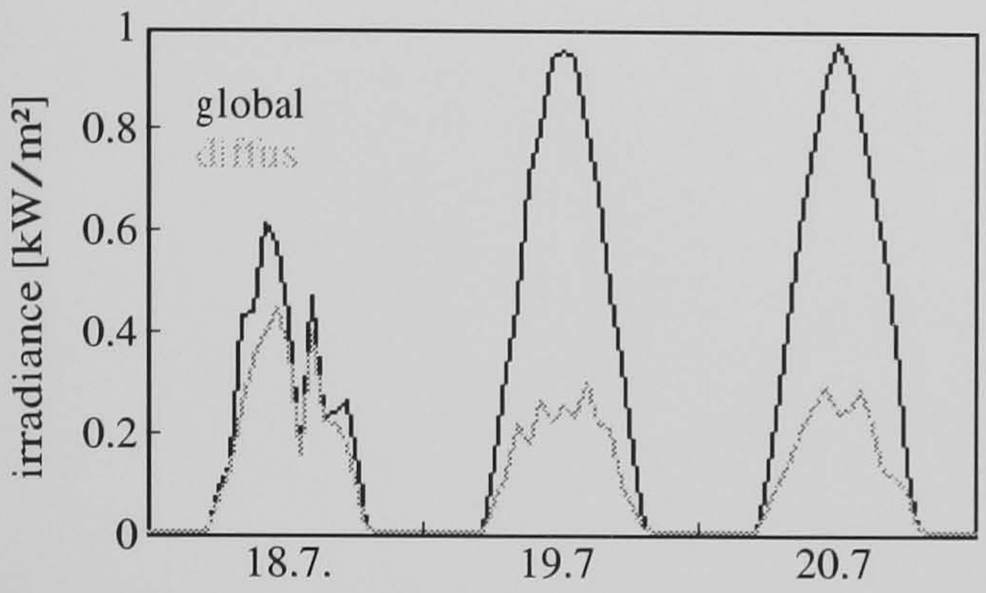

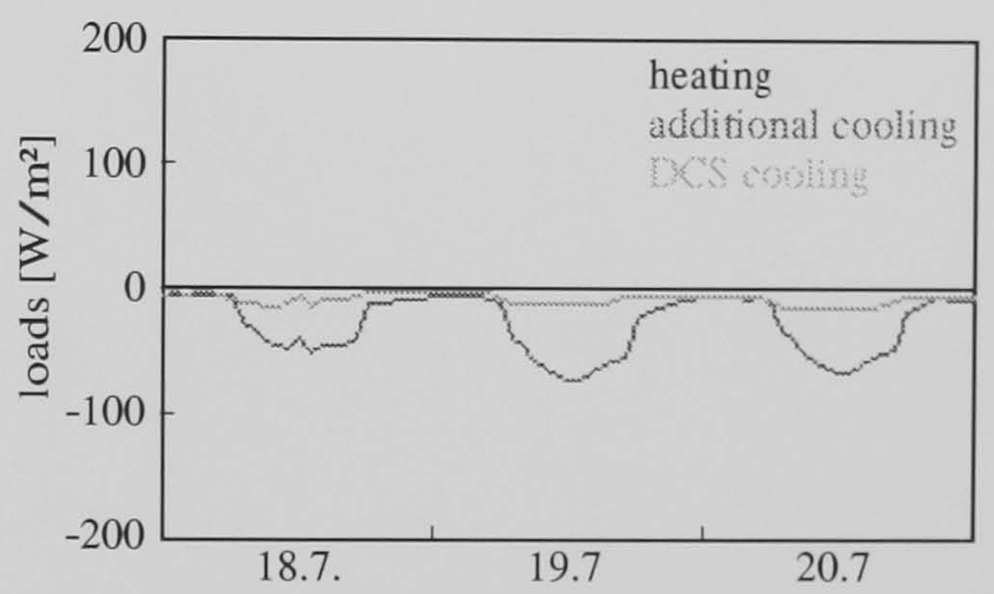

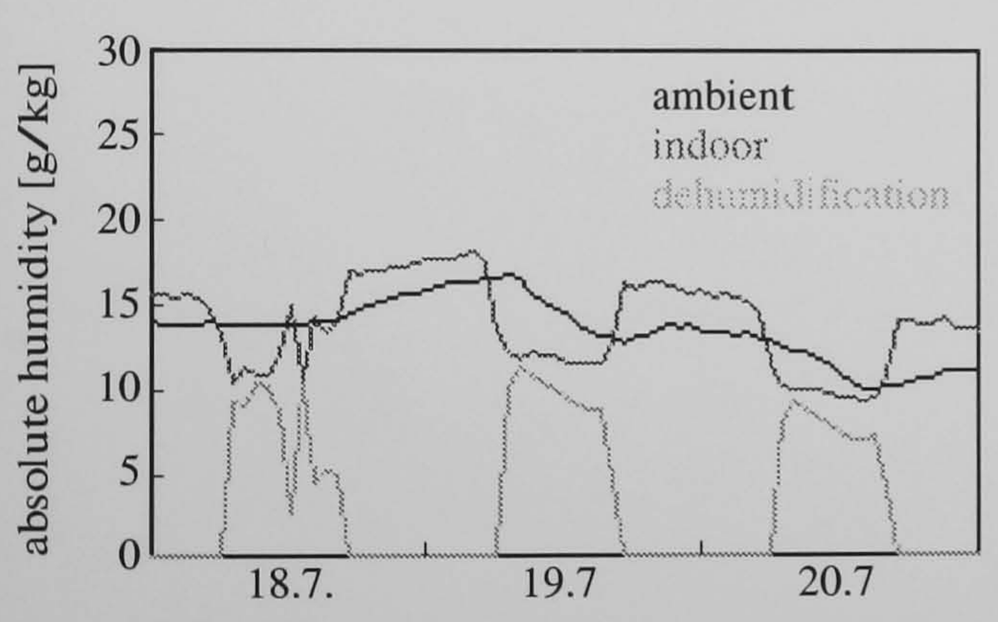

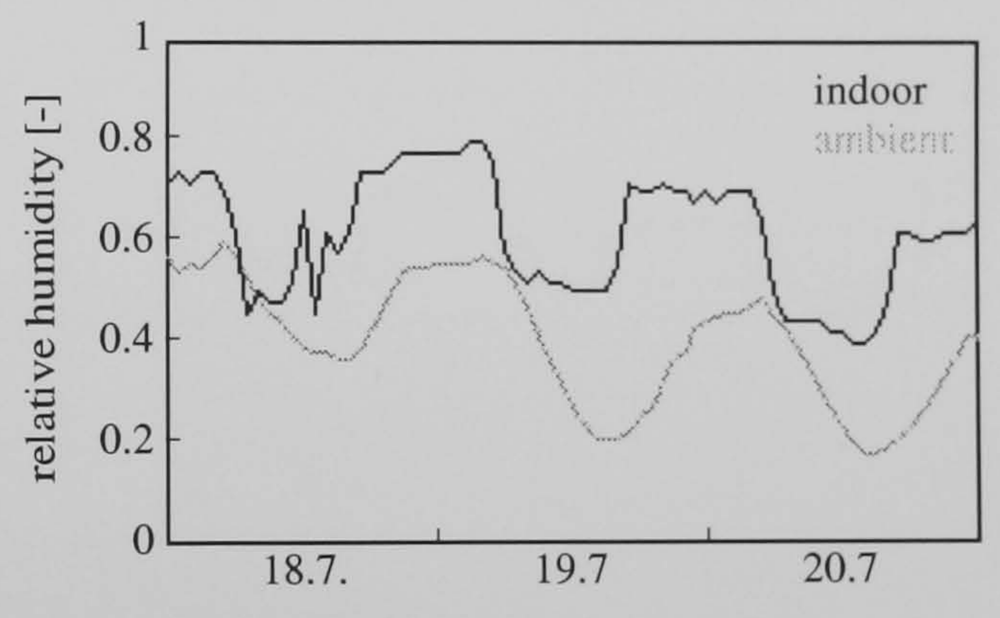

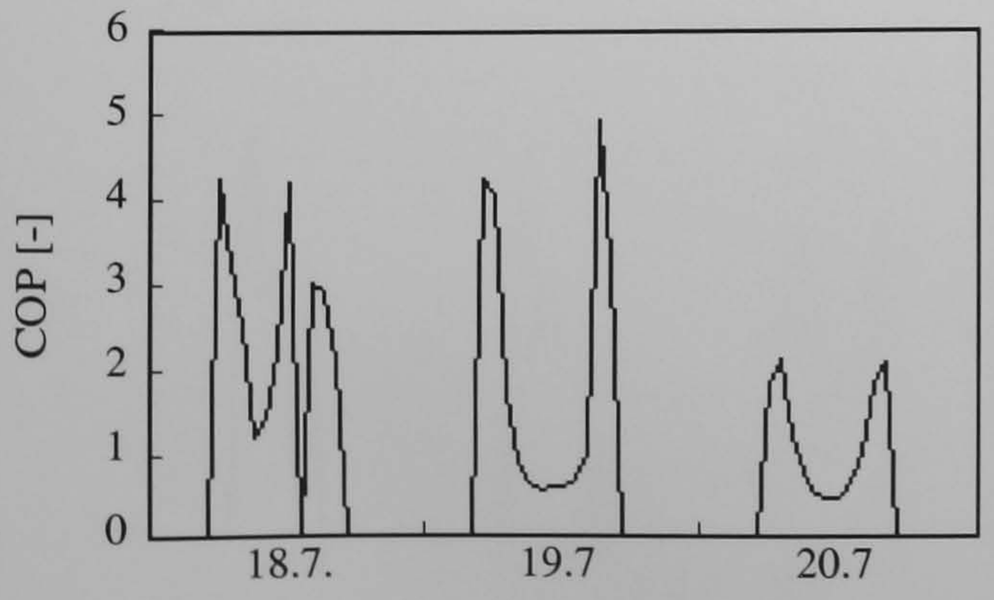

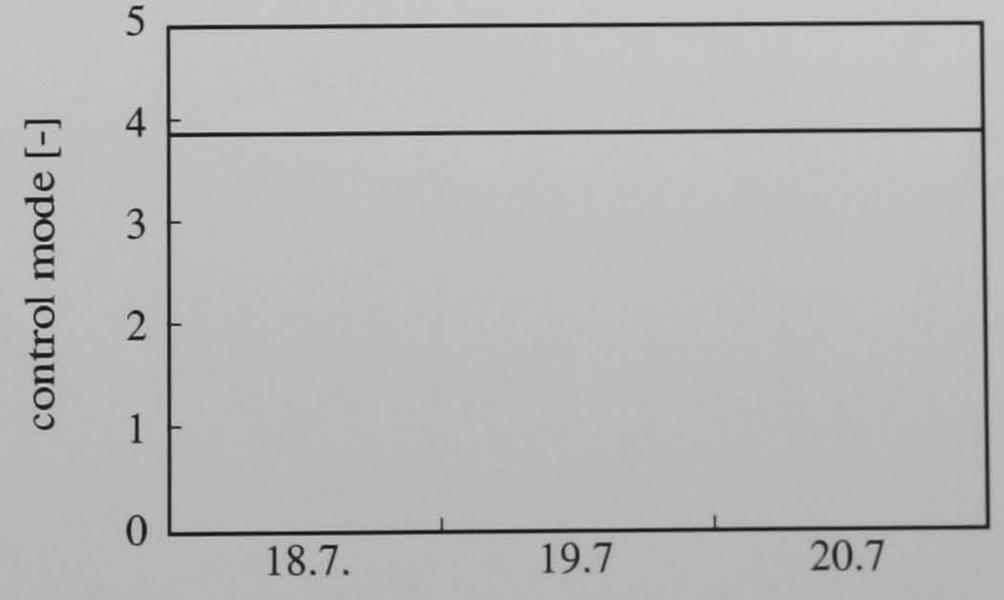

Figure A.13: Phoenix: Simulation results of case study 7 (heavyweight building, hygienic ventilation during occupation time, controlled to reach an inlet temperature close to 17 °C). Detailed description on page 102. Discussion of the simulation results on page 124.

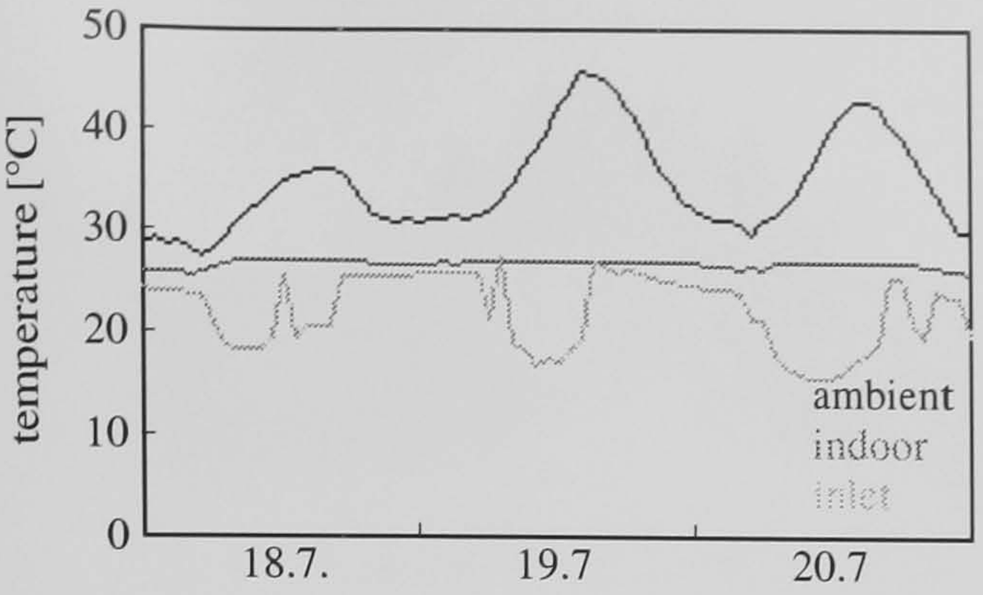

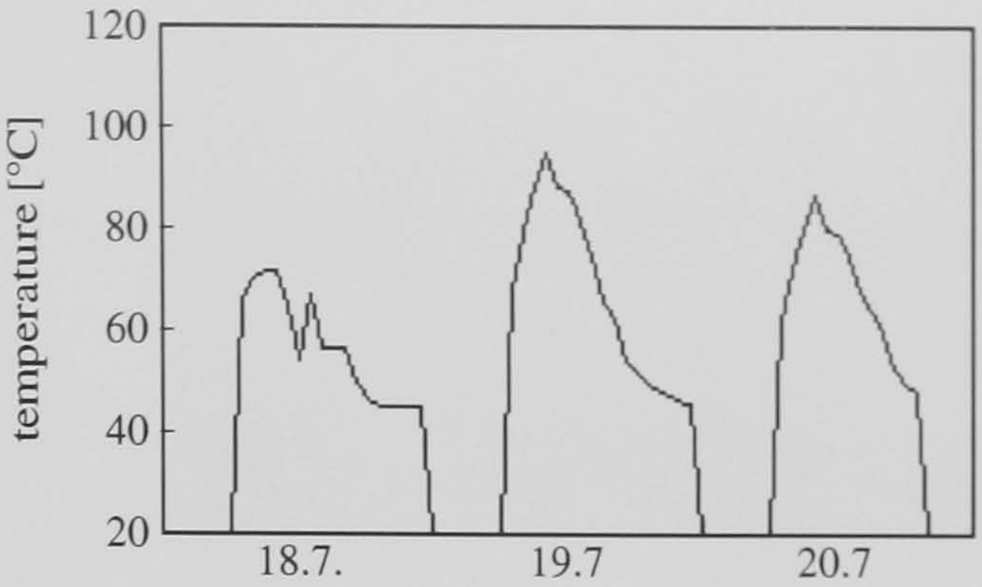

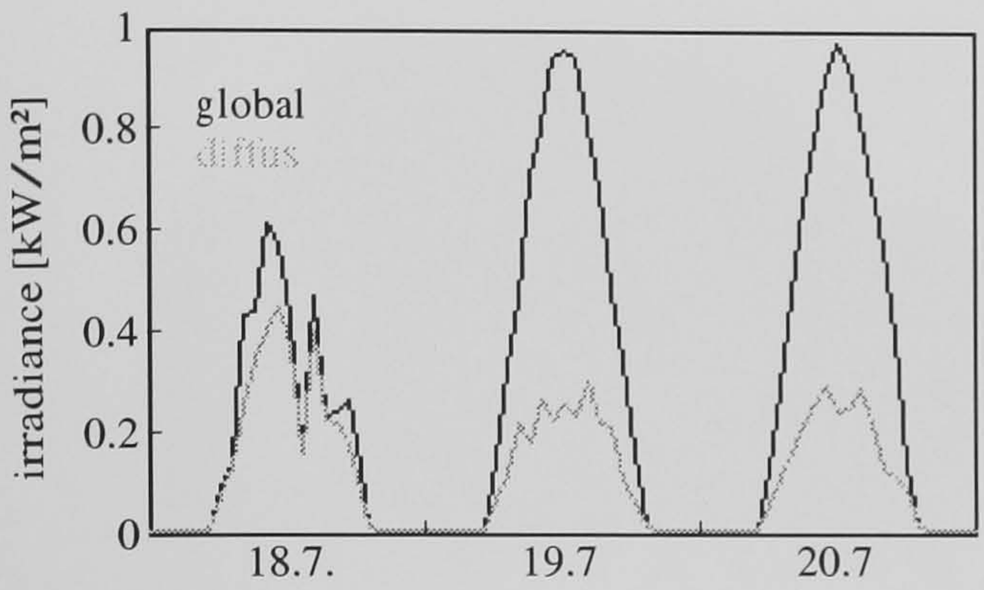

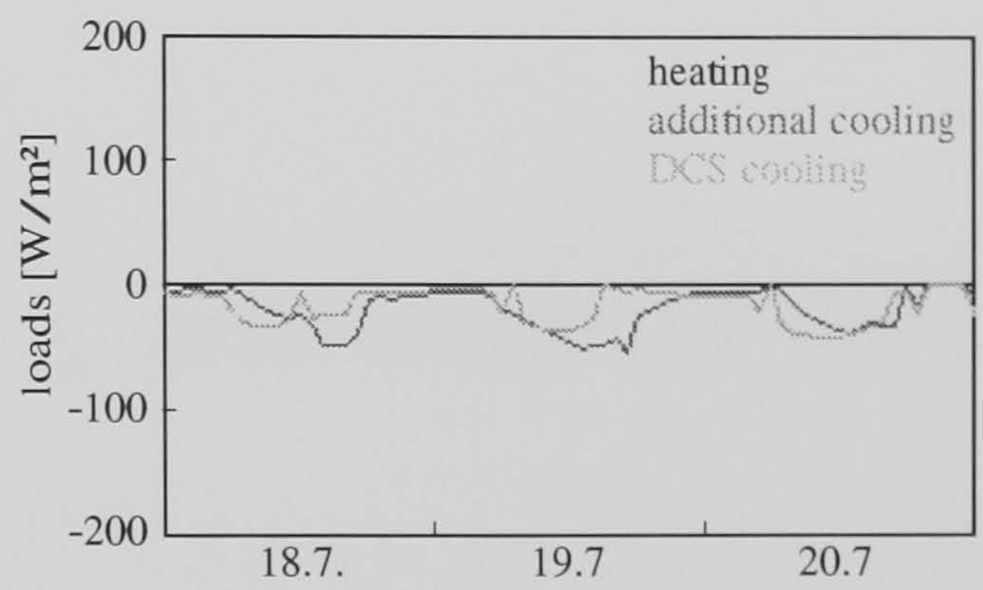

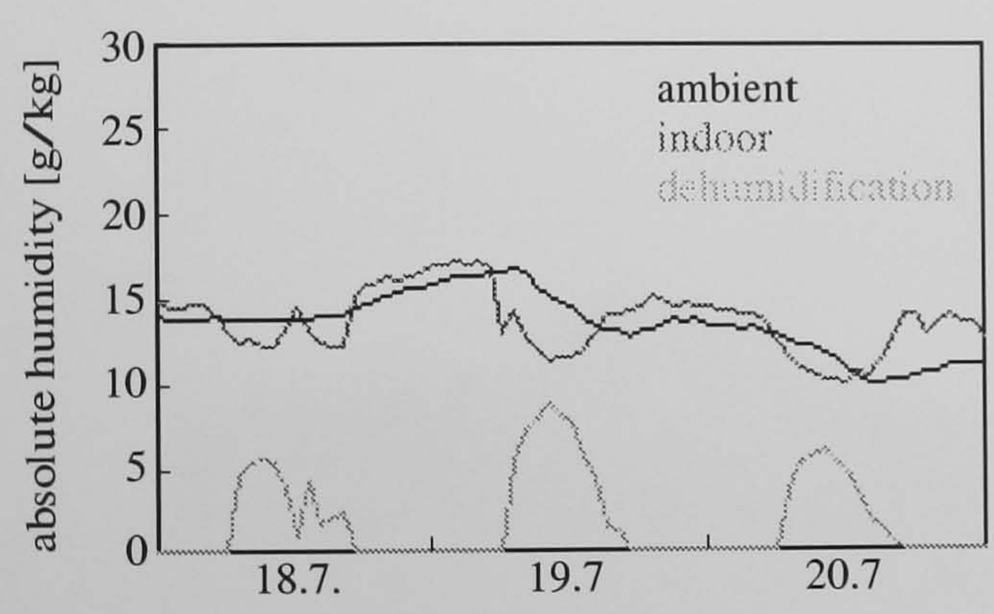

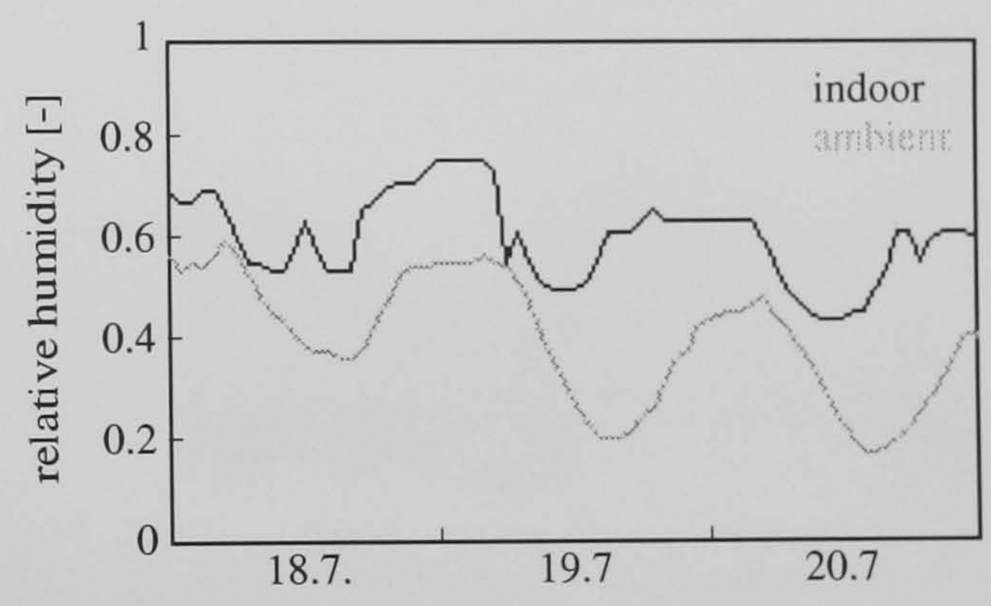

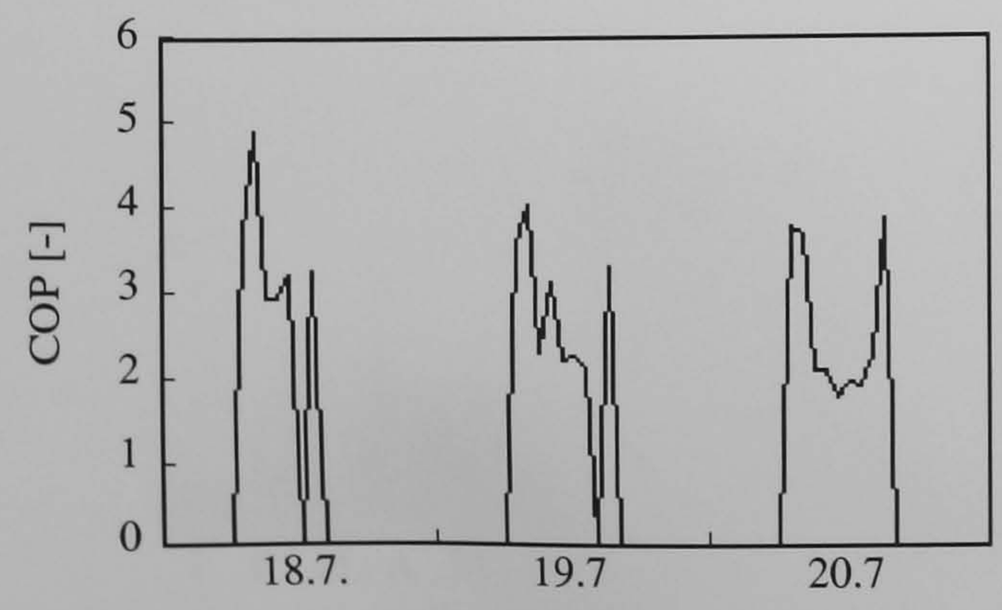

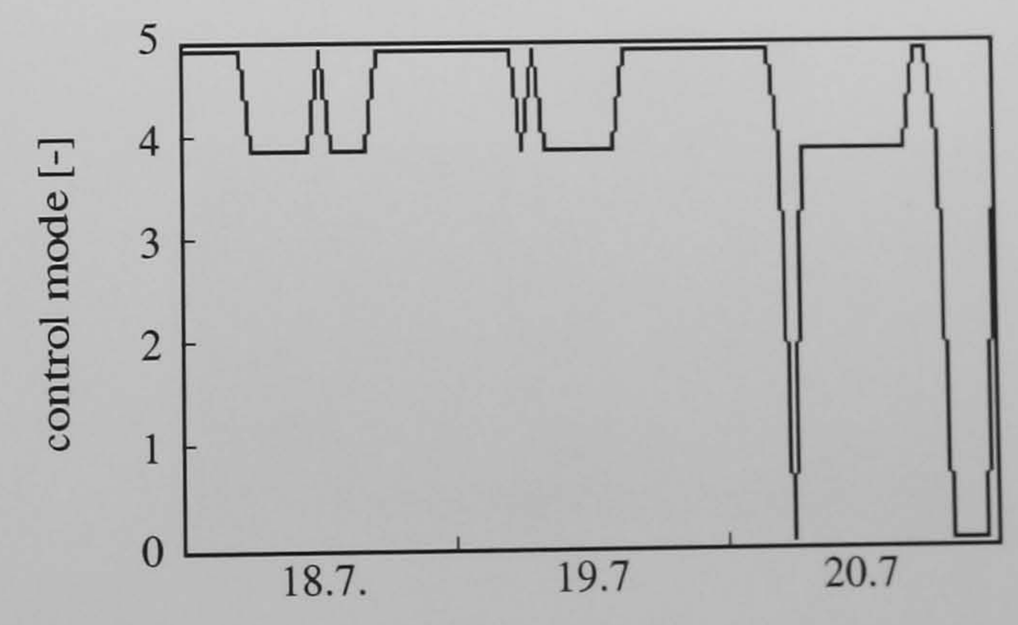

Figure A.14: Phoenix: Simulation results of case study 8 (heavyweight building, ventilation with maximum 4 air changes per hour, night ventilation, regeneration air flow controlled). Detailed description on page 103. Discussion of the simulation results on page 125.

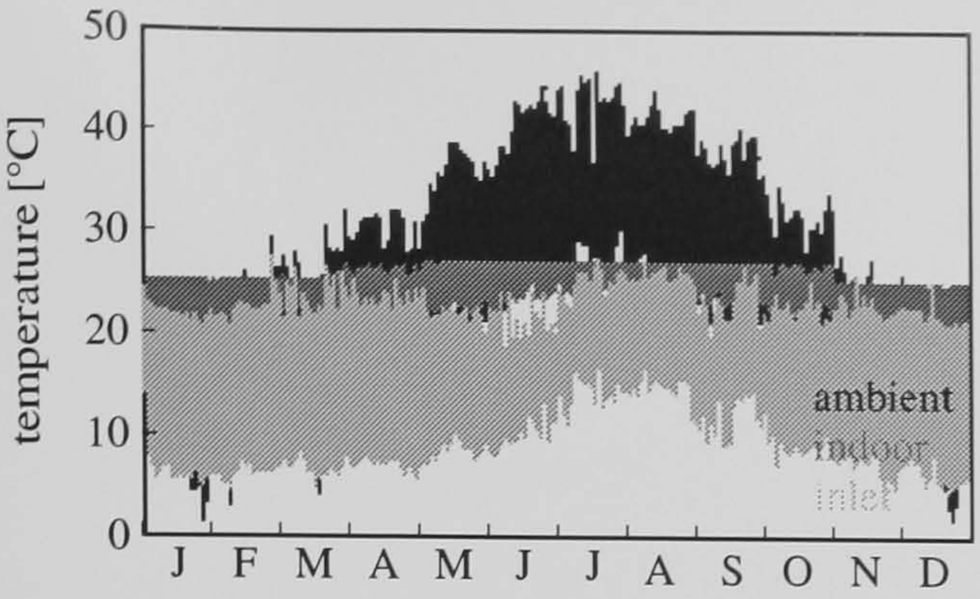

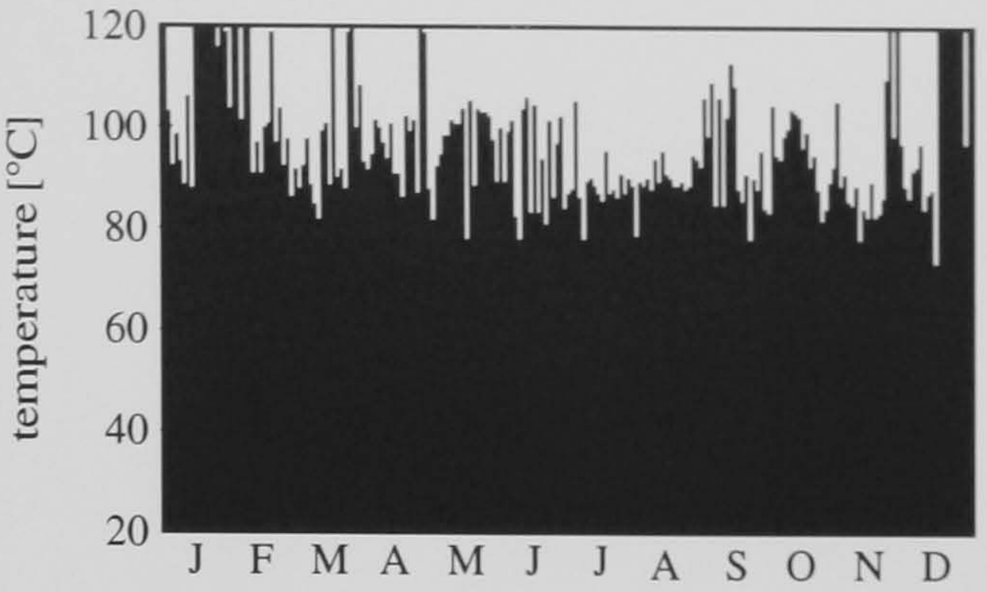

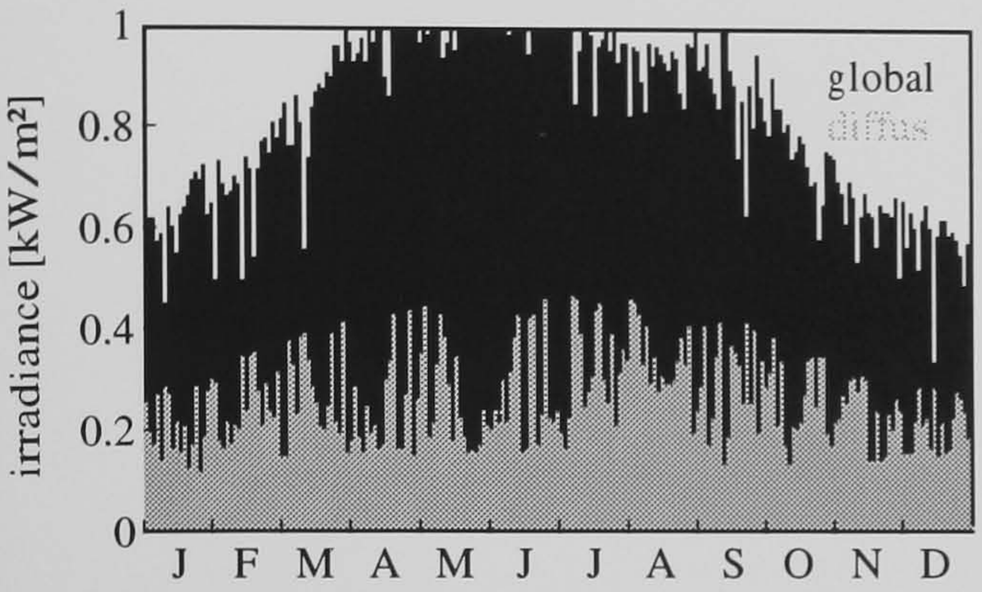

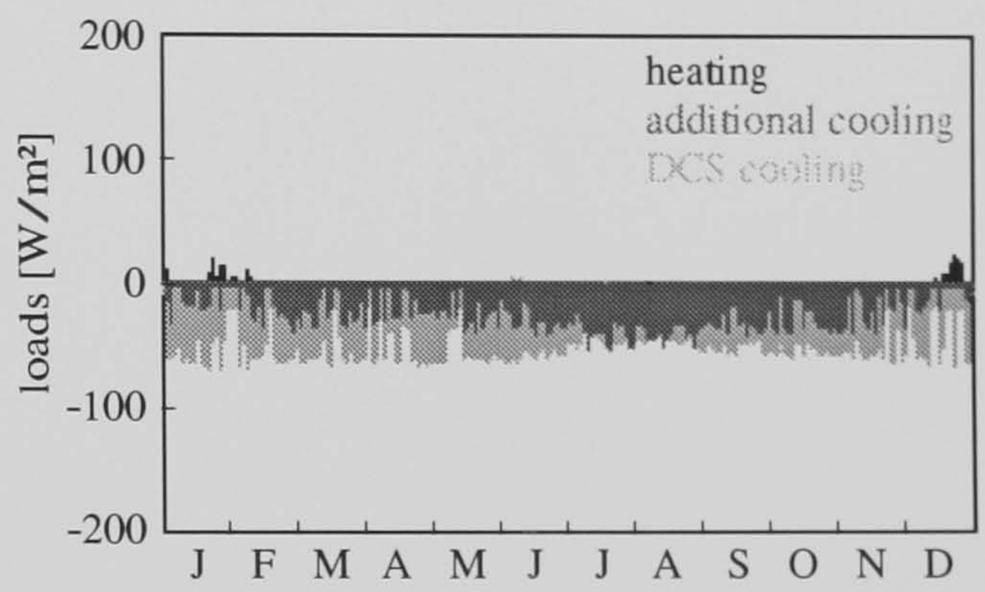

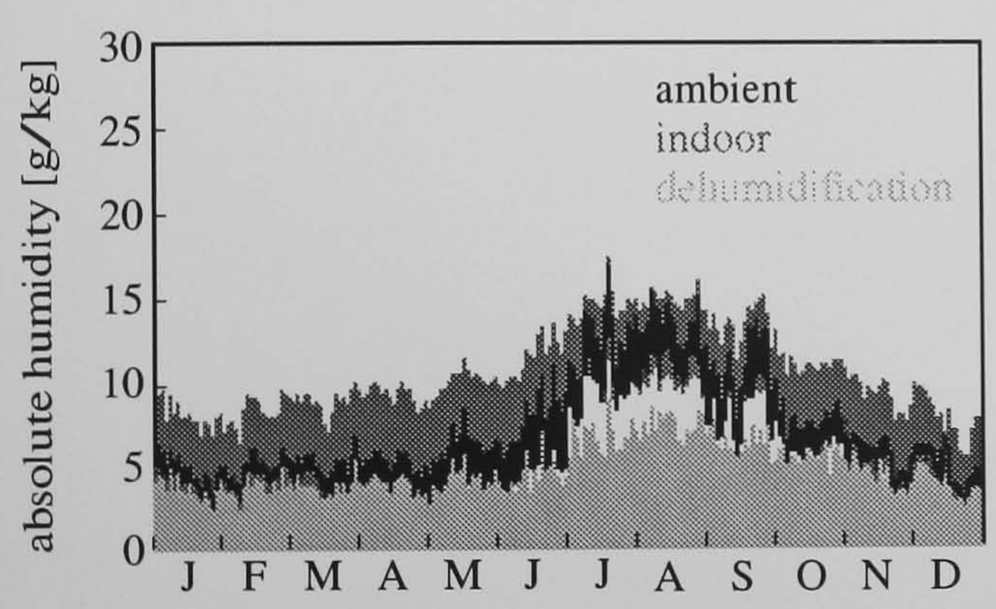

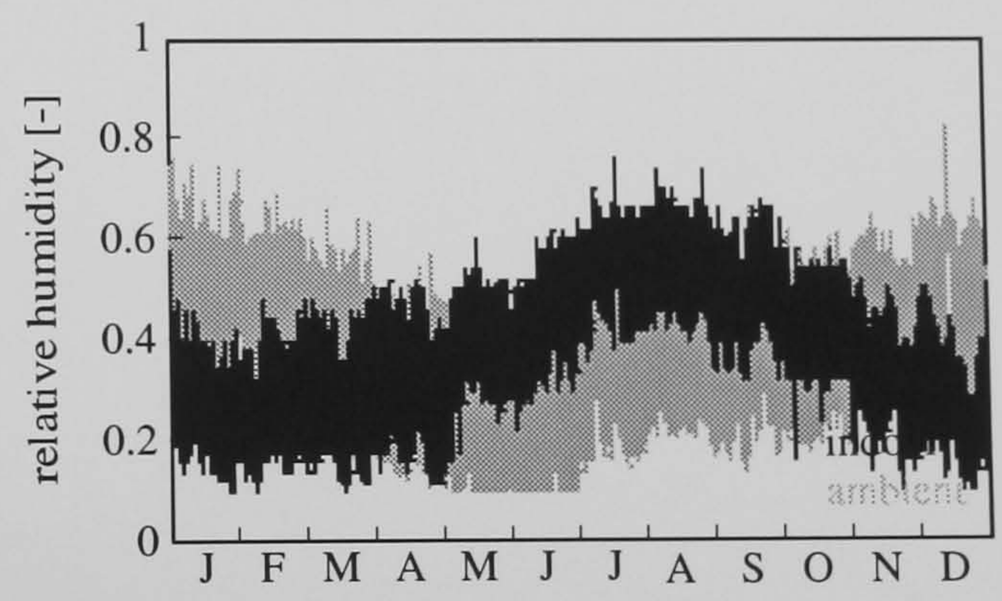

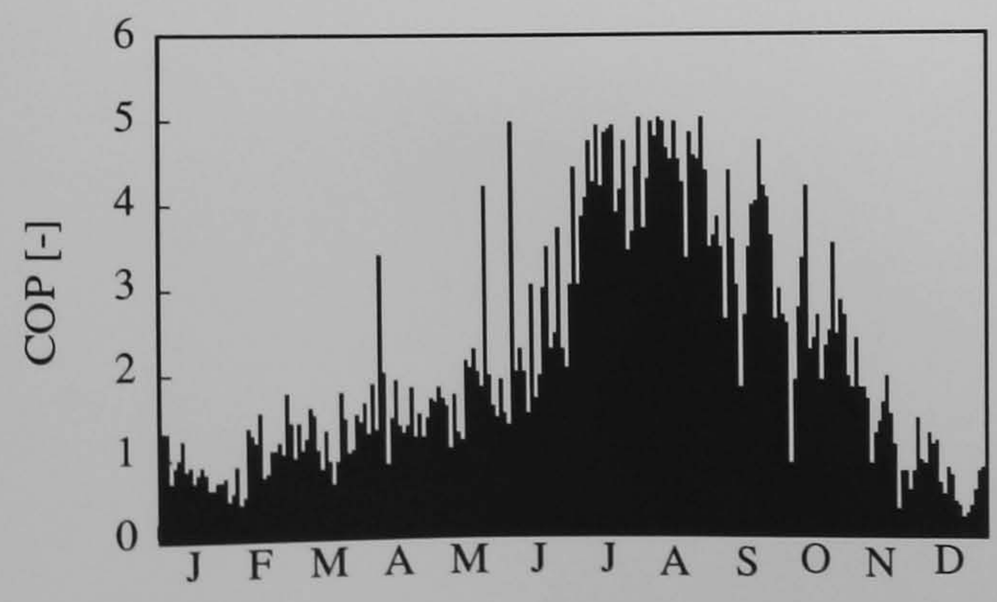

Figure A.15: Phoenix: Simulation results of case study 8 (heavyweight building, ventilation with maximum 4 air changes per hour, night ventilation, regeneration air flow controlled). Detailed description on page 103. Discussion of the simulation results on page 125.